MULTI-TRACER APPROACHES FOR GROUNDWATER DISCHARGE AND ANTHROPOGENIC POLLUTION IN THE PACIFIC

A DISSERTATION SUBMITTED TO THE GRADUATE DIVISION OF
THE UNIVERSITY OF HAWAIʻI AT MĀNOA IN PARTIAL FULFILLMENT
OF THE REQUIREMENTS FOR THE DEGREE OF

DOCTOR OF PHILOSOPHY

IN

GEOLOGY AND GEOPHYSICS

December 2020

By: Trista McKenzie

Dissertation Committee:
Henrietta Dulai, Chairperson
Brian Popp
Chip Fletcher
Scott Rowland
Jonghyun Harry Lee

Keywords: submarine groundwater discharge, radon, radium, contaminants of emerging concern, tracers, wastewater, sea level rise, groundwater inundation, Hawaiʻi, Australia

ACKNOWLEDGEMENTS

The culmination of this dissertation would not have been possible without the help and support from others. First, and foremost, I want to thank my advisor, Henrietta Dulai, for her guidance throughout this process. Henrietta has constantly motivated and encouraged me to to seek out opportunities, to approach science rigorously and innovatively, and to challenge myself. I owe much of what I've learned as a scientist to her inspiring and supportive advising, from when I started working in her lab as an undergraduate, through today. I also want to ackowledge my dissertation committee – Brian Popp, Chip Fletcher, Scott Rowland, and Harry Lee – for their expertise, time, and encouragement throughout this process. I also want to thank Bridget Smith-Konter for being on my comprehensive exam committee and Robert Whittier who was on my Master's commitee and was very helpful for the Chapter 2 of this dissertation.

I am immensely thankful to everyone who has assisted with field or lab work in Hawai'i, including Eric Welch, Jennet Chang, Michael Mathioudakis, Daniel Dores, Shellie Habel, Catherine Hudson, Natalie Wallsgrove, Alex Santos, Saki Katazakai, Brytne Okuhata, Sierra Stammer, Kristina Remple, Diamond Tachera, Orit Sivan, Danny Lucudine, and Warren McKenzie. The research in this PhD was only successful because of the people here who helped – most of whom *volunteered* to assist with fieldwork in polluted environments carrying heavy gear over long, hard days in the hot sun.

I also want to acknowledge everyone in Australia – particularly Isaac Santos – for not only supporting the project, but also integrating me within the lab group for the two months I was there and ensuring a successful project. The fieldwork was a breeze because we had such an industrious, knowledgeable, and collaborative crew – I thank Ceylena Holloway, James Tucker, Ryo Sugimoto, Toshimi Nakajima, and Kana Harada for making it easy. Additional thanks to Ceylena for helping with additional lab work and inviting me to practice with your outrigger canoe team, making me feel at home (despite paddling at 5am in near freezing temperatures)! I also want to thank Rogger Correa, Shane White, and Christian Sanders for your help with lab work and Lara Townsend, Alison King, and Georgia Foley for helping orchestrate my stay and successful fieldwork from the admin side. And of course, I want to thank the numerous friends I made while there, in particular Caroline, Anna, and Rogger. This project would also not have been possible without guidance from Adina Paytan and Adrienne Sponberg.

Thank you to my fellow graduate students and friends in Hawai‘i – this would not have been possible without all of you. In particular, I want to thank my office mates (719D Snack Buddies!) - Diamond and Brytne, for all the fun, advice, and comradery over the years. I also want to give a special shout-out to the old crew – Kate, Julie, Genesis, Daniel, Michael, Liz, and Warren for making the first few years of grad school particularly fun. I am also thankful to the HIGP grad students (Caroline, Chiara, Abbey, Emily) for letting me be part of your circle. Thank you also to Lauren, Laura, Mikayla, Val, Wendy, Hannah, Leslie, and countless others (please don't be offended if I didn't list your name) for your friendship.

Throughout my education, several individuals in particular influenced by desire to pursue a PhD, including John Kershaw (University of New Brunswick), Colin Goldblatt (University of Victoria), and Dennis Hore (University of Victoria). I also want to thank Mahdi Belcaid, Neil Frazer, Barb Bruno, Deb Eason, and Kim Burnett for sharing their expertise, encouragement and advice throughout the course of my graduate school experience. I also want to thank Arlene, Susan, and Lily for all of their help with paperwork, reimbursements, and logistics.

This dissertation was supported by numerous funding sources, including: University of Hawai‘i Sea Grant, Hawai‘i Data Science Institute Fellowship, Hawai‘i EPSCoR ‘Ike Wai project, Honolulu Board of Water Supply, Australian Research Council, Association for the Sciences of Limnology and Oceanography Limnology (ASLO) and Oceanography Research Exchange (LOREX) fellowship, ARCS Foundation Toby Lee Award in Earth Sciences, two Fred M. Bullard fellowships, William T. Coulbourn Marine Geology Research Grant, Geological Society of America (GSA) graduate student research grant, GSA On to the Future grant, University of Hawai‘i Graduate Student Organization (GSO) Merit Award for Research, GSO travel grant, and a L&O Letters Early Career Publication Honor. I also want to thank the Hawai‘i Department of Health, Hawai‘i Department of Transportation, City and County of Honolulu, and the Honolulu Board of Water Supply for providing access to field sites.

Finally, I want to thank my family for their love and support. Thank you to my parents, sisters, and Warren's parents for everything over the years. Of course, I also need to thank Warren for his patience and support throughout this PhD. He has been by #1 fan and I could not have done it without him! I also want to thank my dog, Breadfruit, for being a good boy and for all of the love he gives.

ABSTRACT

Submarine groundwater discharge (SGD), or groundwater that flows to the coastal ocean, is a significant source to both water and dissolved chemical budgets. While SGD fluxes frequently rival or exceed those associated with river discharge, it remains poorly characterized along most coastlines. SGD is also a frequently overlooked contaminant flux pathway, despite being a well-documented vector for excess nutrients or other contaminants derived from urban, agricultural, or industrial land-use to reach the coastal ocean. Commonly, local-scale SGD studies consider the coastal ocean in isolation from stream inputs, particularly stream baseflow, despite the direct connection between one another.

Wastewater discharge is a common source of poor water quality. Aging wastewater infrastructure (WIS) that often uses antiquated technology leads to leakage to the groundwater that is difficult to detect. Onsite sewage disposal systems (OSDS; e.g., cesspools, septic tanks) are a common alternative to municipal wastewater treatment, while also a frequent source of groundwater pollution. This is particularly the case in areas with a high density of OSDS constructed along the coast, such as in Hawai‘i. In addition to OSDS, fractured sewer lines are another potential source of wastewater leakage to groundwater. Wastewater discharge to natural waters remains a major issue globally, in part because it can be difficult to isolate the source and cause of the pollution. Contaminants of emerging concern (CECs; e.g., pharmaceuticals, industrial chemicals, pesticides) are pervasive in the environment, but can be used as tracers due to their uniquely anthropogenic source.

Sea level rise (SLR) can also indirectly threaten water quality in coastal areas. In addition to surficial flooding, SLR will lead to groundwater inundation (GWI) of WIS and underground tanks or lead to increased salinization of water resources. To date, most SLR impact studies either focus on surface water impacts or are modeling-based studies, meaning few direct observations of GWI and its linkage to water quality decline exist.

Chapter 2 of this dissertation links poor coastal water quality and nutrient pollution to total groundwater (stream baseflow + SGD) discharge along the steam-coastal continuum in a watershed with a high density of OSDS (Kāne‘ohe, Hawai‘i) using radon as a groundwater tracer. Additionally, SGD was also compared between perigean spring (king) and spring tides. Increased SGD and nutrient fluxes were observed during the king tide, implying worsening water quality with SLR.

Chapter 3 demonstrates that SGD is a source of wastewater contamination to the coastal ocean in a highly urbanized embayment (Sydney Harbour, Australia) using radium isotopes as groundwater tracers and CECs are the primary tracer for for wastewater. Major findings include: (1) SGD is a pathway for CECs to reach the coastal ocean; (2) increasing CEC inventories are related to increasing water residence time; and (3) two of the measured CECs – dioxins and ibuprofen – were in concentrations that pose a risk to the ecosystem.

Chapter 4 provides field-based observations of tidally driven GWI of WIS using radon and CECs as tracers during spring tides in Honolulu, Hawai‘i. Two pathways were studied: (1) direct GWI of coastal WIS that flows to the coastal ocean as SGD, and (2) indirect inundation of WIS through flooded storm drains. For the direct pathway, CEC fluxes increased at high tide, reflecting additional inundation of WIS with rising water levels. In comparison, CEC concentrations decreased at high tide via the indirect pathway, signifying dilution of constantly leaking sewer lines by the rising water table. This chapter demonstrates a tidal connection between groundwater discharge and water quality and has implications for worsening water quality with SLR.

This dissertation examined groundwater as a contaminant vector to streams and the coastal ocean using a combination of groundwater (radon and radium) and contaminant (CECs, nutrients, dissolved organic carbon) tracers. Radon was used in two innovative ways in this dissertation: (1) separation of groundwater and surface water along the stream-coastal continuum – leading to a better understanding of contaminant pathways in a polluted watershed; and (2) during spring tides linking GWI of coastal WIS to groundwater discharge to the coastal ocean and storm drains. The results also demonstrate promising use of CECs as wastewater tracers in novel environments and under transient conditions. Future work can build upon this dissertation by conducting further studies that consider groundwater discharge ridge to reef, increasing the number of CECs analyzed as tracers (particularly in groundwater and non-freshwater environments), and running additional studies in coastal areas that add direct evidence for tidally-driven GWI.

TABLE OF CONTENTS

LIST OF TABLES

LIST OF FIGURES

CHAPTER 1: INTRODUCTION

Submarine groundwater discharge (SGD) refers to groundwater that discharges to the coastal ocean and is an important contributor to water and solute budgets. Total SGD includes both fresh (terrestrially sourced) and saline (re-circulated) groundwater (Fig. 1.1; Burnett et al., 2006). Globally, an estimated 12 x 10^{13} m^3/year of water is discharged to the coastal ocean as total SGD (Kwon et al. 2014), or 300 to 400% the flux (3.0 to 3.5 x 10^{13} m^3/year) from rivers to the ocean (Milliman, 2001; Dai & Trenberth, 2002). SGD is primarily driven by the hydraulic gradient between the aquifer and the ocean but is also affected by secondary factors such as tidal pumping, wave setup, and pressure gradients generated by currents (Taniguchi, 2002; Burnett et al., 2006; Santos et al., 2009). Tidal pumping, a process that supplies water to the aquifer during the flood tide and partially drains during the ebb tide, is frequently the most significant component (comprising 39 to 95%) of saline SGD (Michael et al., 2005; Kim & Hwang, 2002; Santos et al., 2009). The remaining percentage of saline SGD is typically driven by a combination of wave setup (a change mean water levels caused by breaking waves) and localized pressure gradients (Michael et al., 2005; Santos et al., 2009). There are still unknowns about the exact mechanisms and contributions of each process to total SGD. For instance, coastal hydrology may be very specific on a local scale, a gap this dissertation aims to address.

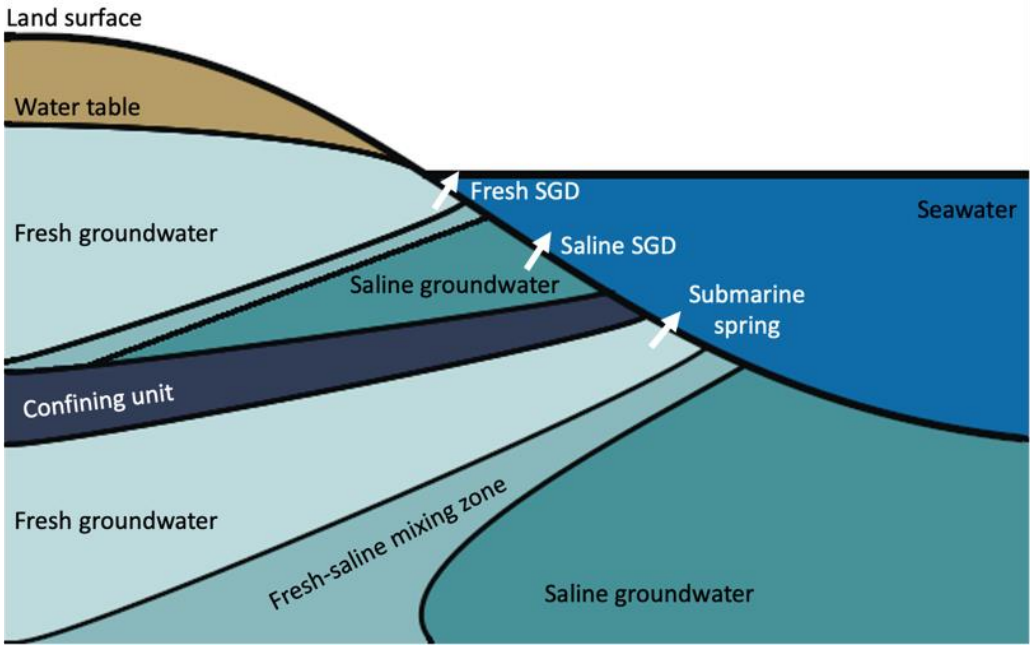

Figure 1.1 Components of SGD (after Swarzenski & Kindiger, 2004). Total SGD is the sum of fresh and saline SGD.

While groundwater plays an important role in biogeochemical cycling and processes such as primary productivity, it can also be a vector for contaminants to reach streams and the coastal ocean. SGD is nutrient-rich and subject to reducing conditions prior to discharge in comparison to coastal surface waters, leading to its association with coastal eutrophication, harmful algal blooms, and water quality deterioration (Moore, 1999; Valiela et al., 1990). SGD also has the capacity to carry anthropogenic pollutants that seep into the aquifer that are derived from industrial, agricultural, or urban land uses. With increasing development and population migration to coastlines worldwide (UN, 2017), SGD can represent a disproportionately important pathway for contaminants to reach coastal waters.

Wastewater is an example of a common source of pollution to natural waters globally and can be transported via both groundwater and surface water. Annually, 1,900 trillion liters of wastewater are generated worldwide, and improper disposal poses a threat to not only water resources, but also environmental and human health (WWAP, 2017). Proper wastewater disposal is a universal problem and not just limited to developing and third world countries. Globally, 80% of the estimated 1,900 trillion liters of wastewater produced per year is released to the environment without treatment (WWAP, 2017). Aging wastewater infrastructure (WIS), such as fractured sewer lines, also offer a pathway for wastewater to reach natural waters. In the United States alone, it is estimated that 23% of sewer lines are currently leaking (USEPA, 2002a). Onsite sewage disposal systems (OSDS; e.g., cesspools, septic tanks), are a common alternative to municipal wastewater treatment, but frequently are a major source of groundwater pollution especially in low lying coastal areas (Whittier and El-Kadi, 2009). This dissertation aims to improve wastewater tracing, by focusing on understudied pathways (e.g., SGD) and conditions using an innovative suite of tracers.

Aging or inadequate WIS and disproportionate development along the coast globally combined with sea level rise (SLR) will likely lead to declines in coastal water quality. Currently, nearly 40% of the world's population lives within 100 km of the coast (UN, 2017), with both the percentage of the world's population and population density increasing in coastal cities (UN Atlas of the Oceans). Conservatively, SLR is projected to increase by 0.3 to 1 m by 2100, with less conservative estimates ranging up to 2 m or greater (Wong et al., 2014). Negative impacts, such as nuisance flooding, beach erosion, flooding of coastal infrastructure, and water quality degradation have already been observed during perigean spring tides (or king tides), and by proxy

will occur with greater frequency because of SLR (Thompson et al., 2019; Sweet et al., 2020). For coastal cities, the efficacy of wastewater treatment will likely decrease with SLR, as wastewater treatment plants (WWTP) are typically constructed in low lying areas to take advantage of gravity-driven flow (National Research Council, 1993). Additionally, other factors, such as aging WIS coupled with population growth will further stress these systems, resulting in decreased treatment efficacy. As cities adapt and mitigate climate change effects, factoring in potential environmental hazards and pathways for hazardous substances released by processes related to SLR to reach water resources should be prioritized (Hawai‘i Climate Change Mitigation and Adaptation Commission, 2017). Modeling based studies have shown increased coastal GWI with SLR (Habel et al., 2017; Habel et al., 2020; Befus et al., 2020), but there are few direct observations documenting this to date.

1.1 Tracers

One way to study subsurface hydrological processes, including SGD, which are the underlying transport mechanism for WIS leakage, and to provide evidence of the leakage itself is through the use of tracers. Characteristics of an ideal tracer (for example groundwater) include: (1) universally present in groundwater; (2) unique to groundwater; and (3) easy and cost effective to measure accurately. Tracers are particularly useful in highly complex environments (such as in the subsurface) because they can constrain or provide evidence for a specific process occurring (e.g., groundwater discharge).

Groundwater is traced in this dissertation using well-established methods taking advantage of naturally-occurring radionuclides that groundwater is enriched in – ^{222}Rn (radon) and three different radium (^{223}Ra, ^{224}Ra, ^{226}Ra) isotopes (Table 1.1). Radon, a noble gas, is generally used in environments with recent, localized groundwater inputs in low energy coastal environments due to its relatively short half-life and tendency to volatilize (Charette et al., 2008). In comparison, radium isotopes represent a wider range of half-lives, allowing for characterization of groundwater age, water residence times, and seawater circulation (Charette et al., 2008). The dissociation constant (K_D) of radium decreases with increasing salinity, leading to desorption from suspended particles and higher radium activities in saline groundwater (Charette et al., 2008).

Isotope	Half-life	Primordial Parent Isotope
^{222}Rn	3.8 days	^{238}U
^{223}Ra	11 days	^{235}U
^{224}Ra	3.66 days	^{232}Th
^{226}Ra	1,600 years	^{238}U

Table 1.1 Naturally occurring radioisotopes used as groundwater tracers in this dissertation. For each isotope, its half-life and primordial parent isotope is indicated.

Contaminants of emerging concern (CECs), which include pharmaceuticals, industrial chemicals, pesticides, and other organic anthropogenically-sourced compounds, can be used as tracers for wastewater leakage, industrial or agricultural runoff (Kolpin et al., 2002; Lapworth et al., 2012). In the environment, CECs are found in most water bodies due to their refractory nature, generally in trace concentrations (ng/L – μg/L). These compounds are good tracers because of their unique source (e.g., pharmaceuticals for human-sourced wastewater) and widespread anthropogenic application, while also offering challenges in their use as their sources are variable and they can degrade once in the environment. In this dissertation, CECs with varying degradation properties were used to trace wastewater and industrial sources through groundwater and surface water (Table 1.2). Nutrients have numerous sources, including wastewater. While nutrients are not unique tracers, their measurements frequently accompany wastewater discharge studies because nutrients are the most often documented and regulated contaminant affecting coastal ecosystems (e.g., Manuel, 2014).

Table 1.2 Properties of CECs studied in this dissertation compiled from the Pubchem Database – carbamazepine (CBZ), caffeine (CFN), ciprofloxacin (CPX), sulfamethoxazole (SMX), ibuprofen (IBU), and dioxins (TCDD). None of these CECs are anticipated to volatilize as predicted by the Henry's Law constant, except for TCDD, which may volatilize from dry sediments. Sorption tendency to suspended sediments is determined by the log Kow (octanol/water partition coefficient). Koc (organic carbon/water partition coefficient) is a metric that established mobility in soils. Biodegradation tendency is determined in lab settings. Photolysis is determined in both lab and environmental settings and describes a compound's tendency to degrade upon exposure to sunlight. *caffeine Koc values are highly substrate-dependent and range from 71 in sand (highly mobile) to 7762 (immobile) in sandy loam soils with higher organic carbon and clay content.

CEC	Use	Sorption (log Kow)	Mobility (Koc)	Biodegradation	Photolysis
CBZ	Anti-convulsant	Yes (2.45)	Moderate (510)	No	Yes (1-38 days)
CFN	Lifestyle compound	Yes (-0.07)	Variable* (71-7762)	Yes	Yes (1.5 days)
CPX	Fluoroquinolone Antibiotic	Yes (0.28)	Immobile (61,000)	No	Yes (2-8 hrs)
SMX	Sulfoamide Antibiotic	No (0.89)	High (72)	No	Yes (0.2 - 5 days)
IBU	NSAID	Yes (3.97)	Slightly (3,400)	Yes	No
TCDD	Combustion product	Yes (7.39)	Immobile ($2.45x10^7$)	No	Yes (4-6 hours)

1.2 Dissertation Organization and Significance

This dissertation addresses gaps in our understanding about how groundwater transport pathways can operate as conduits for contamination derived from wastewater and industrial runoff to reach surface waters. The science produced in this dissertation is relevant to those interested in managing water quality such as land managers and government agencies. While Chapters 2-4 have co-authors associated with the publication demonstrating collaboration, I am the first author on each manuscript, signifying that I was the primary contributor to each work.

Chapter 2 focuses on terrestrial SGD and addresses the linkage between stream and coastal water quality through the stream baseflow-SGD continuum, which takes a novel approach by linking water quality in both streams and the coastal ocean through groundwater discharge. This chapter uses radon as a groundwater tracer and follows nutrient concentrations in a watershed with a high density of OSDS. The hypotheses for this chapter are (1) groundwater fluxes (stream baseflow + SGD) are equal to or greater than stream discharge, (2) groundwater-derived nutrient

fluxes are greater than those associated with stream surface water, and (3) SGD fluxes and associated nutrient fluxes will be greater during a perigean spring tide compared to a spring tide. The objectives for this chapter are to highlight the importance of SGD as a hydrologic pathway and as a significant nutrient source to coastal waters.

Chapter 3 presents new evidence of CECs and wastewater discharge via SGD (both terrestrial and saline) in a highly urbanized area, while developing CECs as tracers for wastewater and industrial pollution. This chapter uses radium isotopes (^{223}Ra, ^{224}Ra, ^{226}Ra) as tracers for groundwater and CECs, nutrients, and dissolved organic carbon (DOC) as tracers for contamination. The hypotheses for this chapter are (1) SGD is a source of wastewater and industrial runoff to the coastal ocean, and (2) spatial variation of CECs are related to the land-use gradient and radium-derived water residence times. Similar to Chapter 2, this chapter illustrates the importance of SGD as a hydrologic pathway. This chapter expands upon Chapter 2 by demonstrating the existing connection between land-use and the coastal ocean.

Chapter 4 investigates tidally driven groundwater inundation of coastal WIS during spring tides using radon as a groundwater tracer and CECs and nutrients as tracers for contamination, with a focus on SGD where the terrestrial fraction is overwhelmed by tidal perturbations. The hypotheses for this chapter are (1) future SLR conditions can be approximated under spring tide conditions, and (2) a combination of SGD and wastewater tracers provide evidence for GWI of coastal WIS and subsequent flow to storm drains and the coastal ocean.

Chapter 5 will summarize the major findings from Chapters 2-4 of the dissertation and discuss future research directions.

CHAPTER 2: PARALLELS BETWEEN STREAM AND COASTAL WATER QUALITY ASSOCIATED WITH GROUNDWATER DISCHARGE

Published as: McKenzie, T., Dulai, H., Chang, J. (2019). Parallels between stream and coastal water quality associated with groundwater discharge. *PLoS ONE, 14*(10), e0224513. doi: 10.1371/journal.pone.0224513

Abstract

Groundwater-surface water interactions drive water quality in both streams and the coastal ocean, where groundwater discharge occurs in streams as baseflow and along the coastline as submarine groundwater discharge (SGD). Groundwater contributions to streams and to the coastal ocean were quantified in three urban streams in Kāneʻohe Watershed, Hawaiʻi. We used radon as a groundwater tracer to show that baseflow contributions to streams ranged from 22 to 68% along their reaches leading to the coast of Kāneʻohe Bay. Total SGD was 4,500, 18,000, and 23,000 m^3/day for the northwest, central, and southern sectors of the bay, respectively. Total groundwater (stream baseflow + SGD) dissolved nutrient fluxes were significantly greater than those sourced from stream surface runoff. The studied streams exhibited increasing nutrient levels downstream from groundwater inputs with high nutrient concentrations, negatively impacting coastal water quality. SGD dynamics were also assessed during the anomalously high perigean spring tides in 2017, where SGD was four times greater during the perigean spring tide compared to a spring tide and resulted in strong shifts in N:P ratios, suggesting that rising sea level stands may disrupt primary productivity with greater frequency. This study demonstrates the importance of considering baseflow inputs to streams to coastal groundwater budgets and suggests that coastal water quality may be improved through management and reduction of groundwater contaminants.

2.1 Introduction

Groundwater-surface water interactions impact nutrient and pollutant transport and directly affect water quality in streams and coastal ecosystems. Gaining reaches of streams receive groundwater, which affects stream discharge as well as its water quality (Winter et al., 1998). Groundwater can also flow directly to the ocean as submarine groundwater discharge (SGD), and can be volumetrically comparable to stream discharge (Moore, 2010). Polluted groundwater discharge to streams and coastline is a common problem for island watersheds with densely

populated coastal plains, which in addition are often upstream of coral reefs and other sensitive coastal ecosystems that coastal communities depend on. Groundwater tends to be enriched in nutrients and other dissolved constituents sourced from land-use. For instance, non-channelized streams typically have nitrogen: phosphorus (N:P) ratios around 14, whereas N:P ratios in SGD commonly exceed the Redfield ratio of 16 (Seitzinger et al., 2005; Moore, 1999; Valiela et al., 1990; Slomp & Van Cappellen, 2004). Groundwater discharge can particularly impact streams in urban settings that may be fully or partially channelized, leading to a lack of hyporheic flow and riparian vegetation in addition to an increase in the velocity of stream water flow to the coastal ocean (Walsh et al., 2005). This study explores the evolution of groundwater and stream water quality in mostly channelized, gaining streams and the coastal ocean across a watershed and evaluates the role of groundwater on both stream and coastal water quality. Groundwater collects solutes from overlying land-use (Moore, 1999; Valiela et al., 1990; Slomp & Van Cappellen, 2004), meaning groundwater discharge directly affects surface water quality and should be of concern in stream and coastal water quality studies.

High volcanic pacific islands (HVPI), such as the Hawaiian Islands, are described by small watersheds that extend from the mountain ridge to the reef, steep topography, and permeable hydrogeology (Lau & Mink, 2006). Fresh groundwater resources on HVPI are replenished from rainfall and are stored in high-level aquifers confined by dike complexes, in basal lens aquifers, and less frequently in perched aquifers (Lau & Mink, 2006). Groundwater from these aquifers can discharge either to streams that subsequently flow to the ocean or directly to the coastal ocean as SGD.

Streams are one vector of groundwater and groundwater-derived solute transport to the coastal ocean in Hawai‘i. Perennial streams on the windward side of O‘ahu, Hawai‘i, are groundwater fed, with as much as 70% groundwater contribution to the total stream discharge in the form of baseflow during the dry season on average (Izuka et al., 1993). Streams tend to be prone to flash flooding and are fed by surface runoff particularly during the wet season (Takasaki et al., 1969). Due to the steep topography and high-level dike impounded groundwater that is generally characteristic of windward Hawaiian watersheds, these streams are commonly gaining from dike complexes upstream (high-level aquifer baseflow), losing in mid-stream reaches, and gaining in the coastal plain from the basal aquifer (basal aquifer baseflow) (Takasaki et al., 1969). These processes are collectively termed surface water-groundwater interactions and are known to

drive stream water and chemical budgets (Winter et al., 1998). While stream fluxes are volumetrically large, draining 48-69% of water output from the watershed (Izuka et al., 1993), they still comprise by large part groundwater from baseflow.

Groundwater from coastal plain aquifer discharges to streams and estuaries and continuously along the coastline in the form of SGD. Although freshwater SGD is estimated to represent less than 10% of river discharge to the ocean globally (Zekster, 2000; Moosdorf et al., 2015; Taniguchi et al., 2002), total SGD can be a major term in the water budget on a local scale (Taniguchi et al., 2002; Kroeger et al., 2007; Swarzenski et al., 2001; Dulai et al., 2016). On a local scale, SGD fluxes can comprise of up to two to four times greater water volumes compared to surface runoff, in addition to also transporting higher nutrient loads than surface pathways (Kroeger et al., 2007). Globally, an estimated 2,400 km^3/year of terrestrially derived fresh SGD is discharged, where major Pacific Islands, despite making up a comparatively small landmass, contribute to about 25% of global SGD (Zekster, 2000). Although both SGD and streams have been widely studied, few studies have looked at both comprehensively as a continuous system connected by subsurface hydrological pathways and the water quality trends along this continuum. This study shows that surface water quality is affected by groundwater discharge, which links streams and the coastal ocean. In other words, management actions eliminating contaminants from groundwater will be more effective than treating streams and coastlines as separate units.

The effect of groundwater on coastal water quality depends on the physical, biological and chemical processes (Moore, 1999; Gonneea et al., 2013; Burnett et al., 2006) that it undergoes once it discharges in the stream and its estuary or the subterranean estuary (STE) in the case of SGD. Analogous to a surface estuary, the STE connects terrestrially-derived groundwater and re-circulated seawater (both considered SGD) with the coastal ocean (Moore, 1999). The STE is a subsurface zone that is highly biogeochemically active. Groundwater-derived dissolved nutrients undergo chemical transformations in the STE before entering the coastal ocean via SGD (Moore, 1999). Most importantly, while there are changes in the hydraulic gradient between groundwater and the coastal ocean due to seasonality in precipitation as well as both semi-diurnal and semi-monthly tidal fluctuations (Gonneea et al., 2013; Burnett et al., 2006), baseflow and SGD are usually persistent year-round, whereas surface runoff tends to be associated with periods of high rainfall.

While groundwater affects multiple parameters of coastal water quality that are important from the perspective of coastal ecosystems (e.g., temperature, nutrient and heavy metal loads, salinity, alkalinity), nutrient loading has gained most attention for its linkage to eutrophication. Groundwater is comparatively nutrient-rich and generally exceeds the N:P Redfield ratio of 16:1 compared to the coastal ocean (Moore, 1999; Valiela et al., 1990; Slomp & Van Cappellen, 2004; Redfield, 1963) and SGD has been linked to coastal eutrophication, and harmful algal blooms from increased primary productivity (Kim et al., 2011; Dailer et al., 2010) as well as decreased net community calcification (Richardson et al., 2017; Lubarsky et al., 2018).

Contaminants carried by groundwater are typically sourced from anthropogenic modifications to land-use (e.g., agricultural and industrial runoff; domestic and industrial wastewater), and can include substantial quantities of nutrients, heavy metals, and other regulated and unregulated chemicals. These may discharge to the coastal ocean either directly or indirectly via stream baseflow. Contaminants discharged to streams by baseflow may undergo biogeochemical transformations in the stream, during hyporheic exchange processes, or in the estuary (White, 1993). Stream baseflow derived from the coastal basal aquifer, however, has a very short distance and stream travel time to the coast, meaning its composition, especially with respect to refractory chemicals, remains mostly unaltered. In addition, due to topography of coastal plains and estuarine hydrogeology, groundwater discharge is preferentially focused in estuaries compared to the coastal ocean (Dulaiova et al., 2006). Therefore, this study proposes that baseflow and SGD represent a continuum, i.e., there is no set boundary to where SGD and related contaminant flow ends, and rather than trying to define a boundary, it is just as important to look farther upstream in the watershed and evaluate high-level aquifer baseflow, basal aquifer baseflow, and SGD as different but dependent vectors of contamination to the coastal ocean. This allows for a better identification of the type and spatial extent of contaminant sources across the watershed. From a management perspective, characterizing groundwater quality and discharge locations may explain the sources of many stream and coastal water quality problems.

In that context, this study examines surface and groundwater interactions, with a main focus on groundwater discharge, along a continuum from the upstream reaches of streams to the coastal ocean, i.e., a ridge to reef extent. The study area is in Kāneʻohe Bay, Oʻahu, Hawaiʻi where groundwater flow as well as surface runoff have been identified as sources of persistent stream and coastal water contamination (Dulai et al., 2016; Hoover, 2002; De Carlo et al., 2007). Surface

and groundwater contributions to water discharge across the stream-coastline continuum are significant for (1) water budgets of streams and the coastline, and (2) fractions of dissolved load contributions to overall water quality in both streams and the coastal ocean. While the former is important to know for water budgets and resources management, it is also the basis for our understanding and management of the latter. An additional dimension to this complex problem is sea level rise, coastal flooding and extreme tides that affect the fresh and saline components of baseflow and SGD.

In the summer of 2017, Hawai‘i experienced anomalously high perigean spring tides (or “king tides”) with a tidal range up to 1.03 m (June 23, 2017) compared to the average range of 0.45 m (Hawai‘i and Pacific Islands King Tides Project, 2017). These anomalously high tides caused localized flooding, both surface flooding sourced directly from the high tidal height as well as indirectly via groundwater inundation (Hawai‘i and Pacific Islands King Tides Project, 2017). This study captured SGD during the perigean spring tides and compares SGD and its composition to regular tidal events. This natural experiment gives us a peek into the future on how SGD and solute fluxes will be different at a future higher sea level stand.

2.2 Materials and methods

2.2.1 Study Site

The study was conducted in three sub-watersheds of Kāne‘ohe Watershed (Kahalu‘u, ‘Āhuimanu, and Kāne‘ohe) feeding into Kāne‘ohe Bay, O‘ahu, Hawai‘i and the bay’s nearshore waters (Fig 2.1). Kāne‘ohe Bay is subdivided into three sectors (northwest, central and south), which differ in terms of residence time, bathymetry, and influence from land-use. The larger Kāne‘ohe Watershed has seven perennial streams that feed into Kāne‘ohe Bay and is partitioned into fourteen steep amphitheater-shaped sub-watersheds (Fig 2.1; Laws & Redalje, 1979; Smith et al., 1981). An estimated 96 million m^3/year of freshwater enters Kāne‘ohe Bay (Takasaki & Mink, 1985).

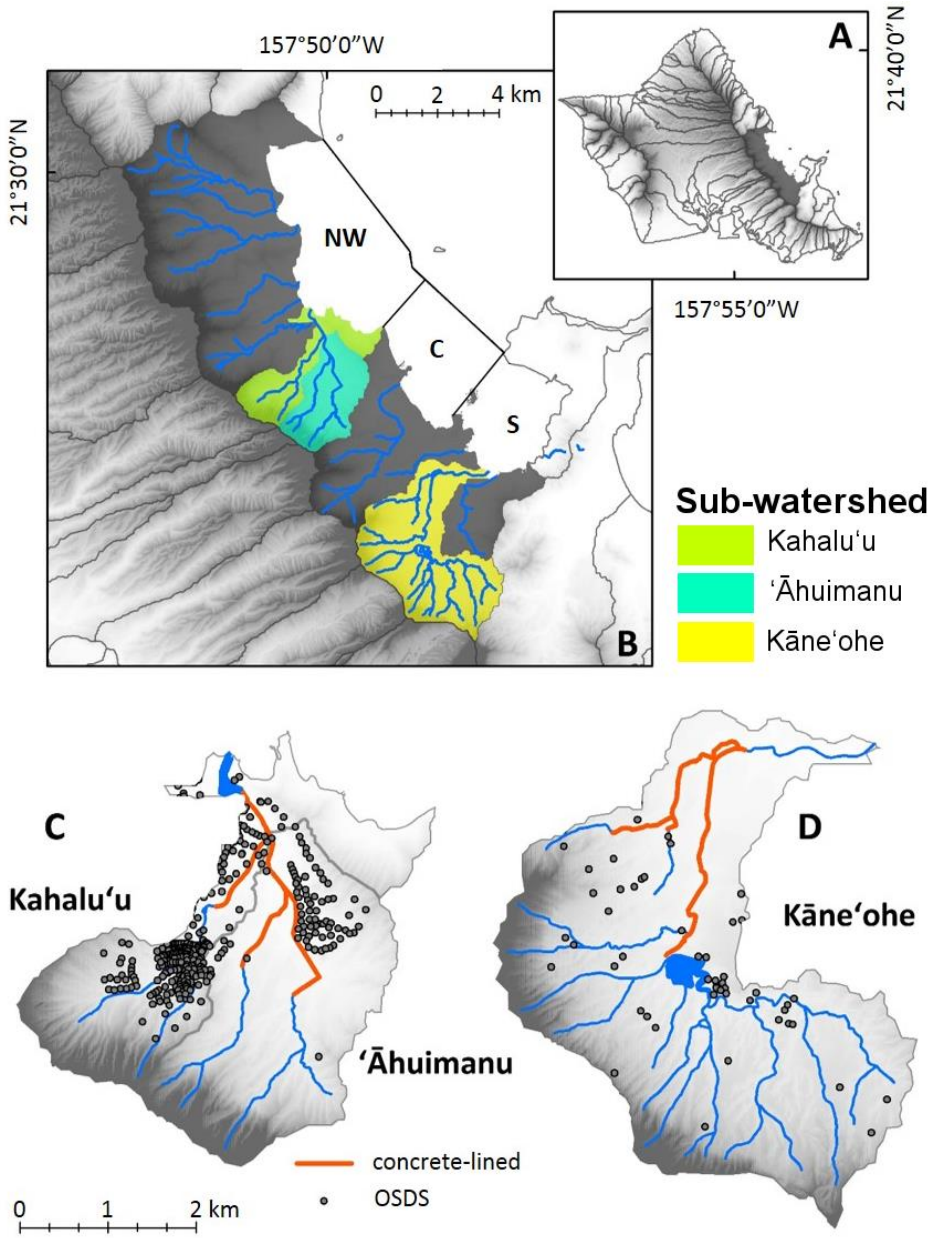

Fig 2.1. Map of study area. (A) Location of study area on the island of Oʻahu, (B) Sectors of Kāneʻohe Bay (NW, C, and S), Kāneʻohe watershed and streams, and sub-watersheds (Kahaluʻu, ʻĀhuimanu, and Kāneʻohe) studied. Detailed view of (C) Kahaluʻu and ʻĀhuimanu and (D) Kāneʻohe sub-watersheds. Portions of the stream that are lined with concrete are in orange. Each dot represents an individual onsite sewage disposal system (OSDS), which are predominantly cesspools in the region (Whittier & El-Kadi, 2009).

Geology

Kāneʻohe Watershed is mostly comprised of basalt with overlying alluvium. Koʻolau basalt (theoleiitic in composition) is the prevailing basalt type in Kāneʻohe watershed, and its thickness ranges from 0.6 to 24 m (3 m on average) (Fig 2.2; Lau & Mink, 2006; Stearns & Vaksvik, 1935; Wentworth, 1951). The younger Honolulu volcanic series are interspersed throughout the watershed and are generally of an alkalic composition. Alluvium (sand, silt, clay, and gravel) covers about 60% of the coastal plains in the watershed (Hunt, 1996). Soils in the study area are predominantly utisols (kaolinite-rich, high capacity for phosphorus fixation), oxisols (rich in oxide-clay minerals, high capacity for phosphorus fixation), and inceptisols (Fig 2.2; Hawaiʻi Soil Atlas, 2014).

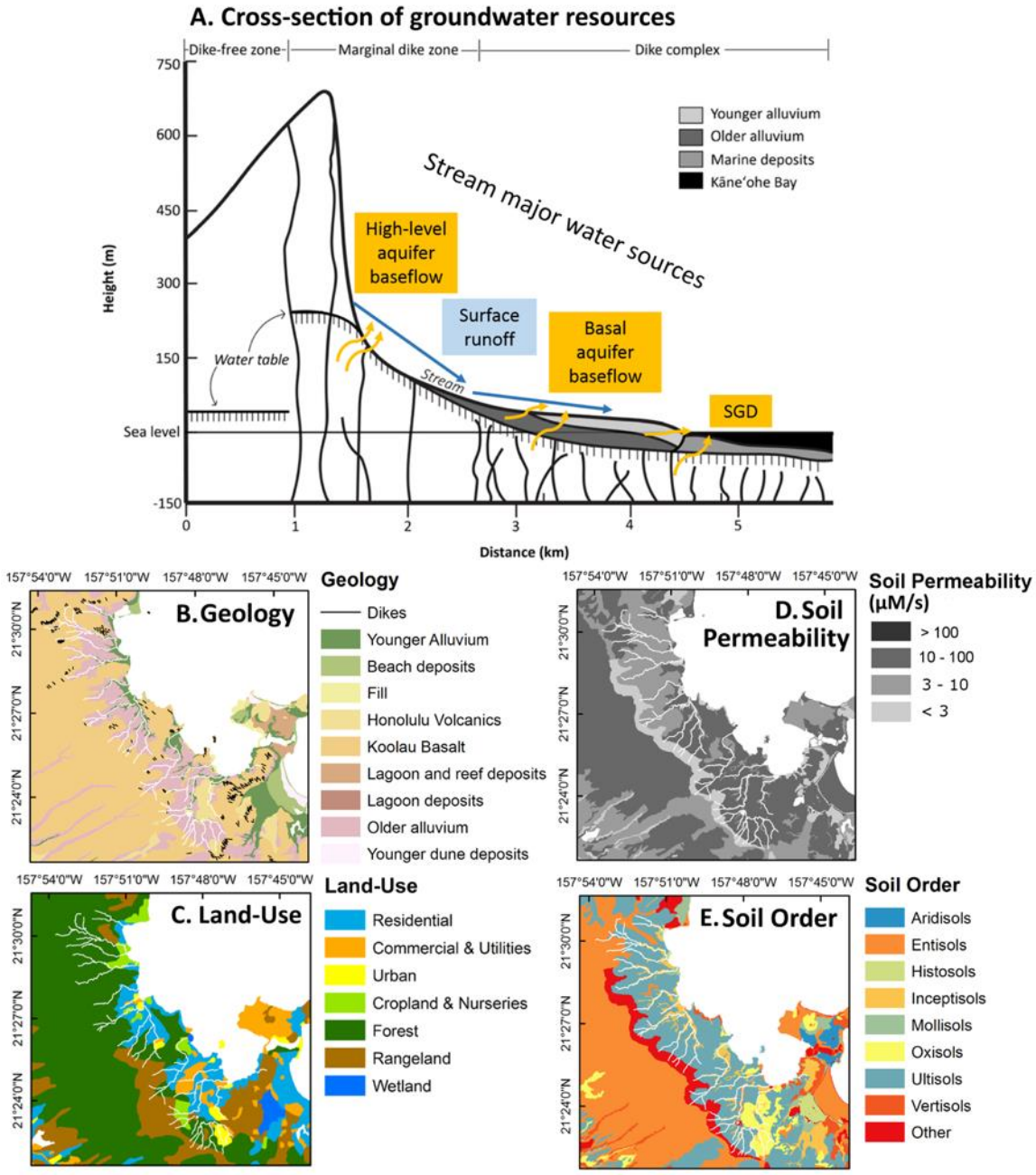

Fig 2.2. Geology of Kāne'ohe Watershed and Bay. (A) Idealized cross-section of groundwater resources and flow in Kāne'ohe Watershed and Bay (after Takasaki & Mink, 1985); (B) geology; (C) land-use; (D) soil permeability, and (E) soil order of the study area (Hawai'i Soil Atlas, 2014; Sherrod et al., 2007; Hawaii Statewide GIS Program).

Kāneʻohe Bay and watershed

Kāneʻohe Bay is a reef-dominated embayment located on the windward side of Oʻahu and has been historically, as well as currently, susceptible to contamination (De Carlo et al., 2007; Smith et al., 1981; Jokiel, 1991; De Carlo et al., 2004). From 1963 until 1979, municipal sewage effluent was directly discharged to the southern portion of Kāneʻohe Bay, resulting in low oxygen conditions, high primary productivity in the water column, and coral reef areal decline (Laws & Redalje, 1979; Smith et al., 1981; Jokiel, 1991). After the elimination of the sewage effluent outfall, surface runoff has been thought to be the major pathway responsible for delivering contaminants to Kāneʻohe Bay (De Carlo et al., 2007; Hoover & MacKenzie, 2009), recent research has indicated that SGD-derived nutrient inputs (Dulai et al., 2016) are comparable to those coming from surface runoff (Smith et al., 1981).

The windward slopes of the Hawaiian Islands receive high quantities of rainfall due to orographic lifting and prevailing trade-wind patterns (Giambelluca et al., 2013). Precipitation tends to be relatively consistent in the upper slopes however, rainfall on Oʻahu's coastal plains occurs mostly (about 70% of annual rainfall) from October through April (Hunt, 1996). Seasonality between surface runoff and groundwater discharge dominance into Kāneʻohe Bay are anticipated due to high rainfall during the wet season (Table 2.1). During the wet season, surface runoff is the dominant input of freshwater into the bay (Leta et al., 2016). Groundwater storage, however, is not instantaneously discharged and thus dominates freshwater flow during the dry season, peaks about 4 to 5 months later (Leta et al., 2016). The annual average water budget of the watershed can be broken down to 2400 mm precipitation, 1350 mm evapotranspiration, 800 mm recharge, and 350 mm surface runoff, or about 56%, 33%, and 11% of total precipitation, respectively (Giambelluca et al., 2013; Safeeq et al., 2013).

Table 2.1. Comparison of Kāneʻohe Bay's watersheds by sector: northwest (NW), central (C), and southern (S). Watershed area is from (Koʻolaupoku Watershed Management Plan, 2012). Rainfall for the 2016 dry season (May – October 2016) and wet season (November 2016 – April 2017) (National Weather Service Hydronet), missing values were interpolated using 30-year average monthly values (Giambelluca et al, 2013). Total stream length and percentage of discharge of total stream input into Kāneʻohe Bay are from (Hoover, 2002; Koʻolaupoku Watershed Management Plan, 2012; Shade & Nichols, 1996). Stream baseflow is estimated to be 70% of daily mean stream flow (Hoover, 2002; Koʻolaupoku Watershed Management Plan, 2012; USGS, 2018). Recharge from OSDS are based on estimates from (Whittier & El-Kadi, 2009). * Northwest and central sectors were considered as one.

Sector	**Area** (km^2)	**Total Annual Precip** (mm)	**Dry Season Precip** (mm)	**Wet Season Precip** (mm)	**Avg. Annual Precip** (mm)	**Stream Length** (km)	**Stream Q %**	**Base flow** (10^4 m^3/d)	**Recharge from OSDS*** (10^4 m^3/d)
NW	31.4	3140	2010	1130	2380	46.1	50	3.93	0.325
C	27.0	2410	1404	1002	1900	27.2	25	1.62	
S	32.5	2660	1720	938	2130	38.9	25	3.04	0.0988

The three sub-watersheds and streams studied represent a large variability in human development and population density and were selected to highlight land-use differences. The Kahaluʻu and ʻĀhuimanu sub-watersheds drain into north-central Kāneʻohe Bay. Kahaluʻu Stream flows into ʻĀhuimanu Stream about 250 m before discharging into Kahaluʻu Estuary (Fig 2.1). Additionally, downstream portions of both streams are channelized in concrete-lined culverts for about 1.6 km prior to feeding into Kahaluʻu Estuary. Kahaluʻu has comparatively lower population and area than ʻĀhuimanu but has a significantly higher OSDS density and number of cesspools (Table 2.2) because the sewer connection only serves ʻĀhuimanu. Other potential sources of contaminants are sourced from agriculture (Koʻolaupoku Watershed Management Plan, 2012). The Kāneʻohe sub-watershed drains into southern Kāneʻohe Bay. Upstream reaches of Kāneʻohe Stream are predominantly undeveloped compared to downstream reaches and the stream has two main tributaries, Kamoʻoaliʻi and Kapunahala. Kāneʻohe Stream is intermittently channelized for 4 km in concrete culverts. Kāneʻohe sub-watershed has substantially fewer OSDS, however it is comparatively more urban compared to the other studied areas. Agriculture is another potential contaminant source in Kāneʻohe (Koʻolaupoku Watershed Management Plan, 2012).

Table 2.2. Comparison of the studied sub-watersheds and streams. (A) Sub-watersheds. Area and maximum elevation are from (Koʻolaupoku Watershed Management Plan, 2012). Population is based off the 2010 United States Census. Percent impervious surface represents the area of the sub-watershed, which has been developed in a way that prevents water infiltration (Koʻolaupoku Watershed Management Plan, 2012). OSDS density includes the number of cesspools, septic tanks, aerobic, and soil treatment units divided by the area of the sub-watershed (Whittier & El-Kadi, 2009). Percent cesspool represents the number of cesspools compared to the total OSDS in each sub-watershed, and the number of cesspool units (Whittier & El-Kadi, 2009). Groundwater withdrawal by pumping rates are from Koʻolaupoku Watershed Management Plan, 2012. (B) Streams. Total stream length is calculated from a GIS layer (State of Hawaiʻi Office of Planning and Permitting). Percentage concrete refers to the percentage of the total stream length that has been altered and lined with concrete (as opposed to natural substrate). Wet and dry season discharge from USGS Stream Gages (USGS, 2018). * indicate there is no active USGS stream gage present and stream discharge was estimated based off of relative discharge between Kahaluʻu and ʻĀhuimanu Streams established in previous literature (Hoover, 2002; Koʻolaupoku Watershed Management Plan, 2012). Kāneʻohe Stream includes Kamoʻoaliʻi and Kapunahala tributaries and upper Kāneʻohe stream.

A. Sub-watersheds							
Sub-watershed	**Area** (km^2)	**Max Elev.** (m)	**Population**	**Impervious surface (%)**	**OSDS density** (units/ km^2)	**% Cesspool (# of units)**	**GW withdrawal by pumping** (10^4 m^3/d)
Kahaluʻu	3.38	768	4,738	13.1	33.1	76 (234)	4.5
ʻĀhuimanu	6.24	859	8,810	1.21	11.2	74 (82)	
Kāneʻohe	14.7	851	34,597	22.8	3.73	91 (50)	2.2

B. Streams				
Stream	**Stream Length** (km)	**Stream lined with concrete (%)**	**Wet Season Q** (10^4 m^3/d)	**Dry Season Q** (10^4 m^3/d)
Kahaluʻu	3.53	35	1.13	0.821
ʻĀhuimanu	5.34	56	2.78*	2.03*
Kāneʻohe	10.9	37	4.00	2.81

2.2.2 Sample collection and analysis

Our goals were to quantify (1) ground and surface water fluxes within the watershed along streams and the coastal ocean and (2) to characterize water quality in ground and surface water fractions through basic water quality parameters (temperature, conductivity and dissolved oxygen) as well as dissolved nutrient concentrations. Surface water was sampled from the coastal zone and streams, and groundwater was collected from the beach face (at depths ranging from 20 to 60 cm), stream bank weepholes, and upland wells through a series of snapshot studies aiming to capture both dry and wet seasons between September 2016 through July 2017 for Kahaluʻu and ʻĀhuimanu sub-watersheds and July through November 2017 for Kāneʻohe sub-watershed. Groundwater samples were taken from locations with visible groundwater discharge. Coastal water surveys for Kāneʻohe Bay were conducted only during the dry season. In addition, high spatial resolution studies were carried out along the coastline and in the streams feeding the northwestern (Kahaluʻu and ʻĀhuimanu Streams) and southern (Kāneʻohe Stream) sectors of Kāneʻohe Bay in order to gain a better understanding of the role of groundwater along the stream-coastal ocean continuum. Groundwater in stream banks and along the shoreline were collected with a peristaltic pump though push-point samplers (MHE Products). Total stream discharge rates were higher during the dry season compared to the wet season during our study period due to dry season fieldwork concurring with La Niña conditions (Ocean Niño Index (ONI): -0.7 ± 0.5 °C) known to cause wetter dry seasons, which was subsequently followed up by an atypically dry wet season (NWS: Climate Prediction Center, 2018). Because of the co-occurrence of fieldwork with La Niña, we will subsequently refer to the dry (May through October) and wet (November through April) seasons as "July" and "February" sampling periods, respectively.

Water fluxes

Stream discharge was measured in regular intervals along the streams to determine both total flow and gaining portions via seepage runs (Rosenberry & Labaugh, 2008) using a stream flow meter (SonTek Flowtracker). Since this method may not capture simultaneous in and outflow, groundwater discharge was also estimated using a ^{222}Rn (radon) mass balance (see section 3.3 below) for which radon measurements were performed in the stream and along the coastline. Ground (n = 76) and surface water (n = 97) radon grab samples were collected into 250 mL glass bottles and analyzed the same day with a RAD-H_2O radon-in-air analyzer equipped with water

analysis accessory (Durridge Inc.). Measured radon activities were decay-corrected to the time of sample collection. The maximum radon groundwater radon concentration from each sector or stream (n = 6) was used as an endmember for the radon mass balance models described below. We used maximum concentrations because they provide the most conservative SGD estimates because other processes such as tidal pumping may factor into our estimates.

In addition to grab sampling, surface water surveys along the coastline and in streams were conducted using a RAD-AQUA (Durridge Inc.) placed into a wheel barrel or kayak. For tidally influenced locations, radon surveys were conducted at low tide, when SGD is predicted to be highest (Dulaiova et al., 2010). This was achieved by continuously pumping water with a bilge pump through an air-water exchanger and then into the radon-in-air analyzer with a measurement interval of five minutes. Measurements of conductivity, temperature, and depth were taken simultaneously with a CTD probe (both a Schlumberger Inc. CTD diver and YSI Multiparameter Sonde (V2-2 6960) were used) to allow for correction of radon inventories and to calculate a radon mass balance (Dulaiova et al., 2010; Burnett & Dulaiova, 2003).

Three radon time series were conducted in Kahaluʻu Estuary and Beach between May and June 2017. Two were conducted during the 2017 perigean spring tide at Kahaluʻu Estuary (21.4570, -157.8385) and Kahaluʻu Beach Park (21.4602, -157.8398) during the May 2017 perigean spring tide (tidal range = 0.90 m), and June 2017 perigean spring tide (tidal range = 0.99 m), respectively. The third time series was done at the same location at Kahaluʻu Beach Park, during a spring tide (tidal range = 0.66 m).

Water quality

Ground and surface water were sampled for dissolved nutrients. Water quality parameters such as temperature and salinity were measured with an YSI Multiparameter Sonde (V2-2 6960). Dissolved nutrient samples were filtered upon collection through a 0.45 µm filter into acid-cleaned 60 mL HDPE bottles and stored in dark and at 4^{O} C until analysis. Samples were analyzed for Total Dissolved Nitrogen (TN), Total Dissolved Phosphorus (TP), NO_3^- + NO_2^- (because of negligible NO_2^-, from here on only listed as NO_3^-), PO_4^{3-} (DIP), NH_4^+, and SiO_4^{4-} (DSi) with a SEAL AutoAnalyzer 3 HR in the S-Lab at the University of Hawaiʻi, Mānoa. One in every ten samples were analyzed in duplicate for quality control and to estimate measurement uncertainties for each batch of measurement. Sample precisions within one standard deviation based on

duplicates were 0.10 µM for NO_3^-, 0.19 µM for NH_4^+, 0.015 µM for PO_4^{3-}, and 2.5 µM for DSi. Dissolved inorganic nitrogen (DIN) concentrations were calculated as the sum of NO_3^- and NH_4^+, and DON concentrations were determined by difference between TN and DIN.

Nutrient concentrations were corrected for salinity using previously established coastal endmembers from Kāneʻohe Bay (Table 2.3).

Table 2.3. Dissolved nutrient coastal and ridge endmembers. Coastal nutrient (DIN and DIP) endmembers are from (Laws & Redlaje, 1979), DSi bay endmember from McGowan, 2004, and DON endmember from Smith et al., 1981. Groundwater endmembers (n = 10) are the mean values from upland wells sampled in this study, which span the three studied sectors of the watershed.

		Nutrient concentrations (µM)			
	Salinity	**DIN**	**DIP**	**DSi**	**DON**
Coastal	35	1.9	0.29	36	4.7
Groundwater	0.076 ± 0.021	12 ± 2.7	1.5 ± 0.41	530 ± 88	2.8 ± 2.7

The coastal end-members were used to correct dissolved nutrient concentrations for salinity with Equation 1 where C* represents the salinity corrected concentration, C_{mix} is the uncorrected sample concentration, C_b is the bay end-member concentration, S_{mix} is the salinity of the sample, S_{gr} is the salinity of the groundwater end-member, and S_b is the salinity of the bay end-member.

$$C* = Cmix + (Cmix - Cb) \times \frac{(Smix - Sgr)}{(Sb - Smix)} \quad (1)$$

Nutrients were corrected for salinity with the assumption that nutrient concentrations in excess of the coastal endmember are terrestrially sourced and thus to allow for estimation of land-derived nutrient fluxes, where brackish and saline samples are diluted by salty bay water.

Groundwater and nutrient flux calculation

Radon mass balances derived from (Dulaiova et al., 2010; Burnett & Dulaiova, 2003; Cartwright & Hofmann, 2015) were calculated for both riverine and coastal settings resulting in groundwater fluxes. Total SGD fluxes in m^3d^{-1} (includes both fresh and re-circulated saline SGD) along the coastline were calculated using Equation 2, where A_{Rn_sw} and A_{Rn_gw} are the coastal ^{222}Rn activities, corrected for in-situ ^{222}Rn produced by ^{226}Ra and by diffusion from sediments as well as losses due to atmospheric evasion (Macintyre et al., 1995) (both in (Bq m^2 day^{-1}), and

groundwater ^{222}Rn end-member stream and sector of the bay, V is the volume of water represented by the length of shoreline per measurement, water depth and distance from shore (m^3), and τ is the coastal residence time of the water (we conservatively used 12.42 hours, reflecting flushing by semi-diurnal tides, acknowledging that certain areas may have faster circulation).

$$QSGD_{tot} = \frac{A_{Rn\_sw} \times V}{\tau \times A_{Rn\_gw}} \quad (2)$$

Sources of uncertainty in SGD estimation arise from the choice of ^{222}Rn endmember, water residence time, and assumptions of static conditions (i.e., no spatiotemporal variation) per volume of water used in the mass balance. Uncertainties associated with these parameters are propagated throughout the calculation of SGD. Gas transfer velocities calculated using wind speed (Macintyre et al., 1995) were in agreement with those found using ^{3}He/SF_6 in Kāneʻohe Bay (Ho et al., 2018). Fresh and saline SGD fluxes were estimated using Equation 3, after (Dulaiova et al., 2010).

$$QSGD_{fresh} = \frac{(S_b - S_{sample}) \times V}{\tau \times S_b} \quad (3)$$

Groundwater fluxes in streams were calculated using a radon mass balance (Fig 2.3) in regular intervals (here called boxes) along the stream using Equation 4 (after Cartwright & Hofmann, 2015), where $\frac{dQ}{dx}$ is the change in stream discharge per box, Q is the flux in/out measured during the seepage runs (m^3 day^{-1}), Rn is the radon concentration in/out (Bq m^{-3}), w and L are width and length of the box (in m), and E accounts for evasion (Bq m^2 day^{-1}) and was calculated accounting for wind speed, current speed, and stream depth (Dulaiova et al., 2010).

$$\frac{dQ}{dx} = \frac{Q_{in}Rn_{in} - Q_{out}Rn_{out}}{W_{box}L_{box}} + E \quad (4)$$

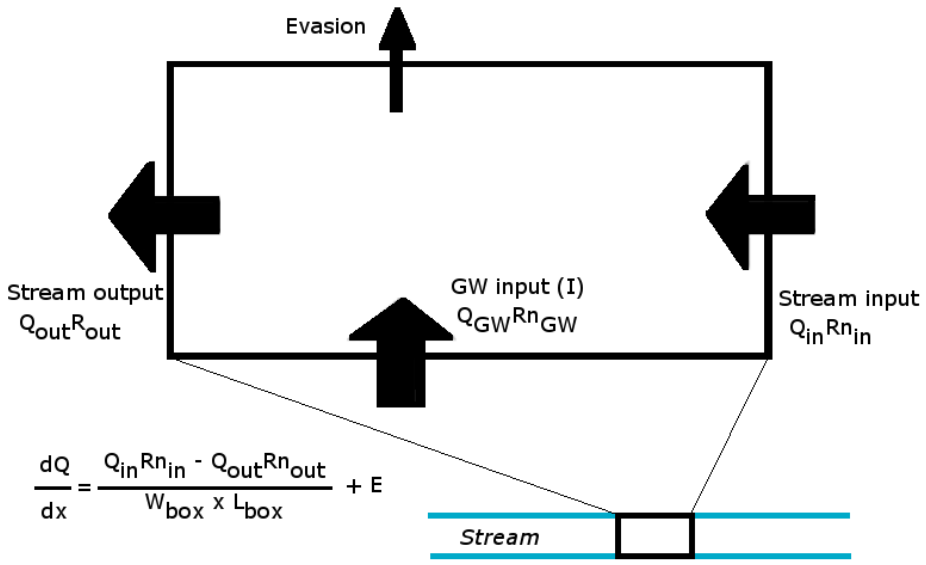

Fig 2.3. Radon box model used to calculate groundwater fluxes in streams. Groundwater discharge was calculated for each measured segment from upstream to downstream.

Radon survey data were corrected to account for the delay in radon air-water equilibration in the RAD-AQUA apparatus and ingrowth of its decay products (hereafter referred to as "modeled" radon). This was done by establishing the kinetic delay between radon in water and radon in air concentrations in laboratory experiments and applying those to correct for the kinetic and decay delay in field data (Petermann & Schubert, 2015). For comparison and sensitivity analysis modeled results as well as "non-modeled" results, which did not apply the additional corrections for the kinetic and decay delay, were used to derive groundwater fluxes.

Groundwater discharge for radon time-series data were determined using a transient mass-balance model (Burnett & Dulaiova, 2003). To calculate radon inventories, excess radon (in excess of ^{226}Ra produced) activities were calculated. These inventories were then corrected for flood and ebb tides, mixing losses, and atmospheric evasion for each time step. Radon fluxes (Bq m^2 day^{-1}) were converted to groundwater fluxes (m^3/day) by dividing the radon flux by the local maximum groundwater end-member radon concentration. Groundwater radon concentrations were measured for each segment of the coastline. Nutrient fluxes were calculated by multiplying discharge by nutrient concentrations measured in groundwater from beach porewater samples.

2.3 Results

2.3.1 Radon Surveys and groundwater sampling

Coastal radon concentrations and SGD rates were spatially variable. Radon concentrations for all of Kāneʻohe Bay shoreline water ranged from 20 to 330 Bq/m^3 (median = 88 Bq/m^3) and 150 to 3,050 Bq/m^3 (median = 980 Bq/m^3) in coastal surface and beach face groundwater samples (Fig 2.4), respectively, and also varied by sector (Appendix A: S1 Table; S2 Table).

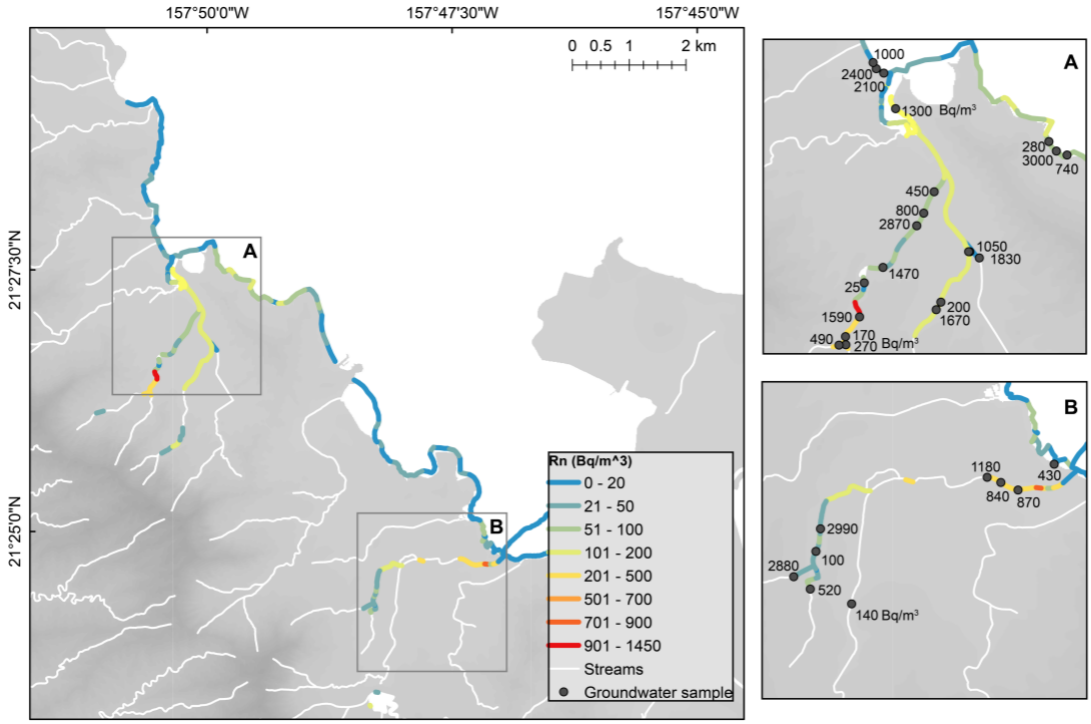

Fig 2.4. Non-modeled coastal and stream surface radon (Bq/m^3) concentrations for Kāneʻohe Bay and studied streams (July sampling period). Stream surface radon concentrations (lines) and discrete (dots) groundwater radon concentrations are shown for (A) Kahaluʻu and ʻĀhuimanu and (B) Kāneʻohe areas.

SGD fluxes using non-modeled radon concentrations ranged from 4,500 to 23,000 m^3/day per sector (Table 2.4A) and were greatest in the southern sector of the bay. In comparison, SGD fluxes estimated using modeled radon concentrations were only about three to four percent greater than non-modeled estimates so only the non-modeled will be considered in further discussion (Appendix A: S4 Table). Factoring in the shoreline length (in km) for each sector, SGD fluxes were lowest in the northwestern sector and greatest in the southern sector (Table 2.4A).

Table 2.4. SGD and Stream Fluxes. (A) SGD and stream fluxes for the July sampling period, and associated DIN, DIP, DSi, and DON fluxes by sector. SGD (m^3/km/day) per km of shoreline and median (Me) nutrient concentrations used for nutrient flux calculations are shown in italics. Modeled SGD fluxes (not shown; Appendix A: S4 Table) were within 4% of the non-modeled fluxes. Stream discharge data averaged by sampling period and location from USGS stream gage data (USGS, 2018). The northwestern sector includes Waikāne, Waiāhole, Waiheʻe, and Kahaluʻu Streams, the central sector includes Heʻeia Stream, and the southern sector includes Kāneʻohe and Kawa Streams. (B) Groundwater (GW), surface water (SW), total stream fluxes and respective nutrient fluxes by sampling period and sub-watershed. Percentages in italics indicate the proportion that groundwater and surface water contribute to total stream discharge. Median nutrient concentrations used for flux calculations are indicated in italics underneath the respective nutrient flux.

A. SGD (10^4 m^3/day)				**GW** (mol/day)			
Sector	**Samping Period**	**Q_{SGD}** ***SGD/km shoreline***	**Q_{Stream}**	**Q_{DIN}** ***Me***	**Q_{DIP}** ***Me***	**Q_{DSi}** ***Me***	**Q_{DON}** ***Me***
Northwest	July	0.45 ± 0.20 *1,400*	11	780 ± 1,300 *49*	47 ± 52 *1.8*	4,400 ± 2,100 *640*	360 ± 360 *96*
Central	July	1.8 ± 1.1 *3,900*	0.63	690 ± 260 *240*	0.40 ± 0.30 *0.27*	1,700 ± 710 *500*	100 ± 35 *310*
South	July	2.3 ± 1.9 *4,000*	2.3	670 ± 340 130	8.4 ± 9.5 *1.6*	5,500 ± 920 *780*	670 ± 1,500 *92*

B. Streams (10^4 m^3/day)					**GW** (mol/day)				**SW** (mol/day)			
Stream	**Sampling Period**	**Q_{GW}** ***%Q_{Stream}***	**Q_{SW}** ***%Q_{Stream}***	**Q_{Stream}**	**Q_{DIN}** ***Me***	**Q_{DIP}** ***Me***	**Q_{DSi}** ***Me***	**Q_{DON}** ***Me***	**Q_{DIN}** ***Me***	**Q_{DIP}** ***Me***	**Q_{DSi}** ***Me***	**Q_{DON}** ***Me***
Kahaluʻu	July	0.57 ± 0.28 *49%*	0.66 ± 0.29 *51%*	1.2	92 ± 79 *16*	4.4 ± 4.5 0.77	3,800 ± 1,600 *660*	260 ± 230 *46*	73 ± 51 *11*	5.5 ± 4.9 *0.83*	3,600 ± 320 *550*	36 ± 73 *5.5*
	February	0.66 ± 0.19 *68%*	0.32 ± 0.45 *32%*	1.0	330 ± 380 *50*	3.8 ± 2.9 *0.57*	3,500 ± 1,900 *520*	290 ± 86 *43*	38 ± 4.8 *12*	2.7 ± 1.1 *0.85*	1,500 ± 240 *470*	17 ± 7.7 *5.2*
ʻĀhuimanu	July	0.67 ± 0.47 *22%*	2.3 ± 0.47 *78%*	2.9	110 ± 300 *16*	2.5 ± 3.9 *0.37*	4,500 ± 1,600 *670*	210 ± 150 *31*	160 ± 74 *6.9*	7.7 ± 6.4 *0.34*	11,000 ± 1,100 *490*	230 ± 110 *10*
	February	0.95 ± 0.89 *40%*	1.5 ± 0.88 *61%*	2.4	110 ± 320 *12*	3.7 ± 3.1 *0.39*	5,700 ± 1,700 *600*	190 ± 93 *20*	110 ± 71 7.5	9.2 ± 7.7 *0.61*	6,900 ± 1,800 *460*	99 ± 56 *6.6*
Kāneʻohe	July	1.6 ± 0.53 *42 %*	2.3 ± 0.84 *58 %*	3.9	420 ± 510 *26*	18 ± 21 *1.1*	8,200 ± 4,500 *510*	450 ± 1,100 *28*	390 ± 690 17	12 ± 8.1 *0.54*	12,000 ± 2,800 *520*	230 ± 370 *10*
	February	1.7 ± 0.33 *56%*	1.3 ± 0.80 *44%*	3.1	540 ± 220 *31*	15 ± 7.1 *0.83*	7,800 ± 1,900 *450*	660 ± 880 *38*	160 ± 170 *12*	7.9 ± 3.3 *0.61*	6,200 ± 1,100 *480*	140 ± 79 *11*

In streams, radon concentrations and groundwater discharge rates differed on both spatial and seasonal scales. For all studied sub-watersheds, radon concentrations in streams ranged from 21 to 3,400 (median = 270 Bq/m^3) in surface, and from 23 to 3,500 (median = 940 Bq/m^3) in groundwater samples. Median radon concentrations varied between sampling periods by sub-watershed (Appendix A: S3 Table). For Kahaluʻu and ʻĀhuimanu sub-watersheds, radon concentrations in both surface and groundwater were lower during the February sampling period compared to the July sampling period. The opposite was true for Kāneʻohe sub-watershed. Groundwater fluxes in streams were calculated using both non-modeled and modeled results and a local radon endmember (Appendix A: S4 Table). Non-modeled groundwater fluxes ranged from 5,700 to 16,000 m^3/day in the July sampling period and 6,600 to 17,000 m^3/day in the February sampling period. Taking a conservative approach, we chose to use the non-modeled discharge rates for all subsequent calculations.

Baseflow (both in terms of volume and percentage of total stream flow) was greater during the February sampling period compared to the July sampling period for all three streams. Baseflow represented 49%, 22%, and 42% of total stream flow during the July sampling period and 68%, 40%, and 56% during the February sampling period for the studied sections of Kahaluʻu, ʻĀhuimanu, and Kāneʻohe Streams, respectively. Baseflow during the July sampling period was well under the USGS estimate for baseflow (70% of total stream discharge). Of the streams studied, only baseflow during the February sampling period for Kahaluʻu Stream was consistent with the USGS baseflow estimate.

2.3.2 Nutrients in coastal and stream samples

Dissolved nutrient concentrations and fluxes varied by sector of Kāneʻohe Bay (Table 2.4; Appendix A: S1 Table; salinity corrected concentrations in S5 Table). For coastal samples, dissolved nutrient concentrations in groundwater were statistically higher than corresponding concentrations in surface water for DIN, DON, DIP, and DSi according to the Kruskal-Wallis H-test. Coastal SGD nutrient fluxes were calculated as total SGD times the median nutrient concentrations in coastal groundwater, and were the greatest in the northwestern, and the least in the southern sectors of Kāneʻohe Bay for DIN and DIP, while DSi and DON fluxes were the greatest in the southern sector (Table 2.4).

In streams, dissolved nutrient concentrations were statistically higher in groundwater samples compared to surface samples for DIN, DON, and DSi, but were not statistically differentiable for DIP according to the Kruskal-Wallis H-test (Table 2.4; Appendix A: S1 Table; S6 Table). Application of the same statistical test revealed that dissolved nutrient concentrations in stream and streambed-groundwater samples were not statistically differentiable between sampling periods. In-stream groundwater- and surface runoff-derived nutrient fluxes by season for the three studied sub-watersheds were highly spatially variable, particularly between groundwater and surface water fractions (Table 2.4).

2.3.3 Radon time series

Three radon time series were conducted in Kahaluʻu estuary over a half tidal cycle during May and June of 2017 (Fig 2.5). Salinities ranged from 6.0 to 30 (average = 25), 13 to 26 (average = 18), and 17 to 30 (average = 23) for the May 26, June 14, and June 23 sampling dates, respectively.

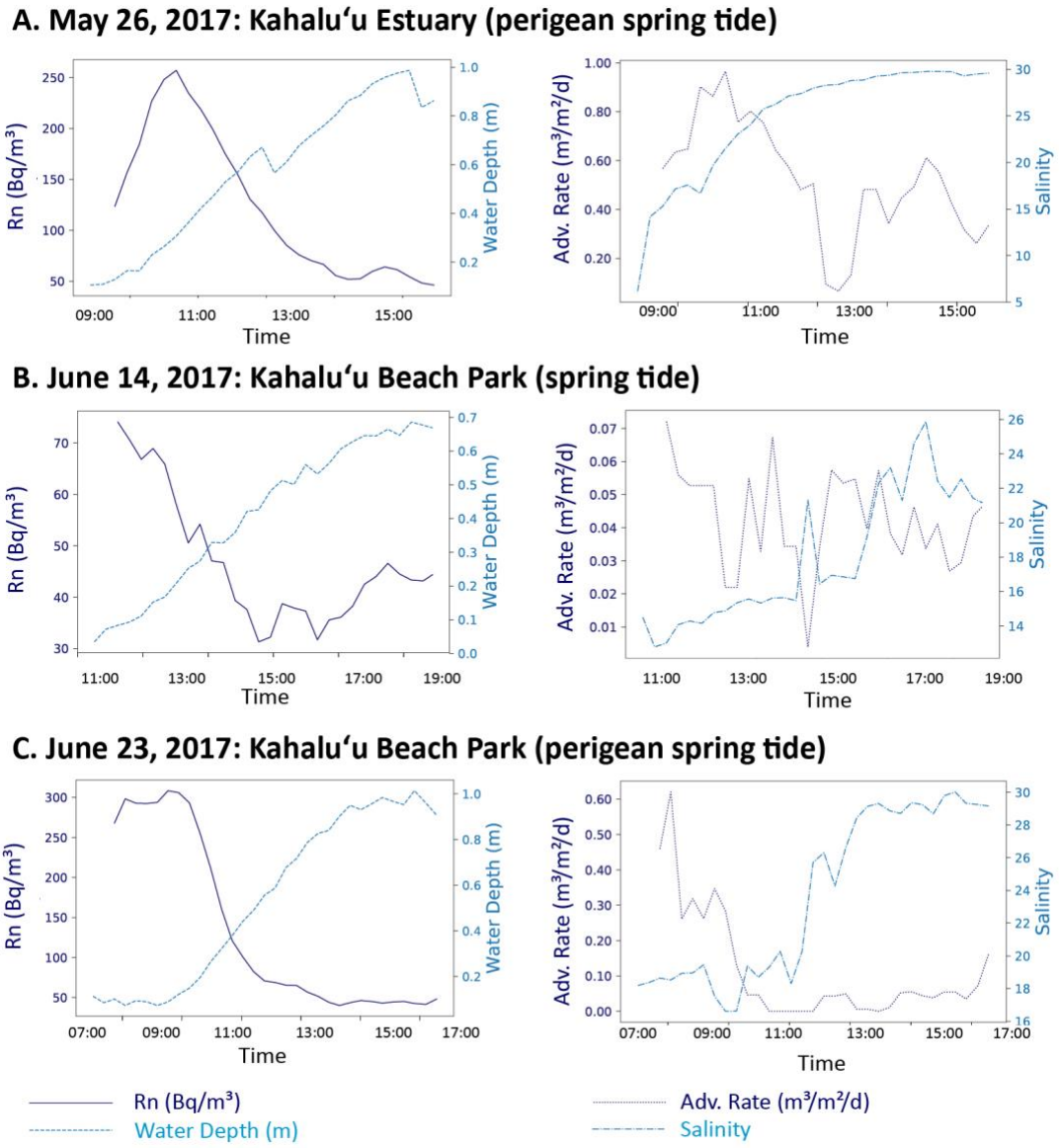

Fig 2.5. Radon time series. Radon (dark blue, in Bq/m^3) and water depth (light blue, in m), and three-point running average advection rates (m^3/m^2/d) and salinity time series from low to high tide. Results from (A) May 26, 2017 (perigean spring tide, tidal range = 0.09 to 0.99 m) from Kahaluʻu estuary, (B) June 14, 2017 (spring tide, tidal range = 0.03 to 0.69 m) from Kahaluʻu Beach Park, (C) June 23, 2017 (perigean spring tide, tidal range = 0.02 to 1.01 m) from the same location at Kahaluʻu Beach Park.

For the two time series conducted at Kahaluʻu Beach Park, DIN, DSi, and DON concentrations and fluxes were greatest during low tide during the perigean spring tide (Table 2.5). Perigean spring tide nutrient fluxes averaged over the half tidal cycle were 3.6, 1.0, 1.7, and 6.9 times that of spring tide nutrient fluxes for DIN, DIP, DSi, and DON, respectively.

Table 2.5. Time series nutrient concentrations and fluxes sorted by tide. Comparison of median dissolved nutrient (DIN, DIP, DSi, and DON) concentrations in groundwater, SGD, and nutrient fluxes between spring tide (ST) and perigean spring tide (KT) for samples collected at low (LT) and high (HT) tides at Kahaluʻu Beach Park. Perigean spring tide to spring tide (KT:ST) concentrations and fluxes were greater during LT compared to HT. Nutrient concentrations were greater during the KT compared to the ST for DIN and DON. Nutrient fluxes were greater during the KT compared to the ST for DIN, DSi, DIP, and DON at both LT and HT.

		Concentration (µM)				(m^3/d)	**Flux (mol/d)**			
		DIN	**DIP**	**DSi**	**DON**	**SGD**	**DIN**	**DIP**	**DSi**	**DON**
ST	LT	5.5	2.2	580	15	110	0.61	0.24	65	1.7
	HT	5.3	6.6	630	12	26	0.14	0.17	16	0.31
KT	LT	5.1	1.1	220	16	330	1.7	0.36	72	5.2
	HT	3.9	1.0	240	27	270	1.1	0.27	65	7.3
KT: ST	LT	0.92	0.48	0.39	1.1	3.0	2.7	1.5	1.1	3.1
	HT	0.73	0.16	0.38	2.4	10	7.7	1.6	4.0	23

For the two locations in Kahaluʻu where radon time series were conducted, SGD rates were greatest at low tide. Anomalously high perigean tides resulted in greater total SGD fluxes at Kahaluʻu Beach at both low and high tides compared to a typical summer spring tide at the same location (Table 2.6). June 14 (spring tide) coastal advection rates averaged at 0.04 ± 0.5 m^3/m^2/day with an average coastal salinity of 18 ± 3.8. June 23 (perigean spring tide) coastal advection rates averaged at 0.13 ± 0.24 m^3/m^2/day with an average coastal salinity of 23 ± 5.2. Advection rates were greater in Kahaluʻu Estuary compared to the coastal ocean and average advection for the May 26 perigean spring tide was 0.54 ± 0.25 m^3/m^2/day with an average salinity of 24 ± 6.2. A substantially greater percentage of saline SGD was discharged during the perigean spring tide in comparison to the spring tide.

Table 2.6 Groundwater advection rates from radon time series. Average advection rates for low and high tides, percentage of fresh SGD, tidal range, and salinity for radon time series conducted at Kahaluʻu Estuary and Beach. * denotes a perigean spring tide.

Date	**Tidal Range** (m)	**Low Tide Avg. Adv. Rate** ($m^3/m^2/d$)	**% Fresh GW**	**High Tide Avg. Adv. Rate** ($m^3/m^2/d$)	**% Fresh GW**	**Low Tide Avg. Salinity**	**High Tide Avg. Salinity**
May 26, 2017	0.90 – 0.99*	0.54 ± 0.25	--	0.44 ± 0.18	--	15 ± 4.4	30 ± 0.2
June 14, 2017	0.03 – 0.69	0.06 ± 0.08	69%	0.04 ± 0.03	51%	14 ± 0.72	23 ± 1.8
June 23, 2017	0.02 – 1.01*	0.30 ± 0.36	47%	0.12 ± 0.12	14%	18 ± 1.0	29 ± 0.4

2.4 Discussion

2.4.1 Review of the types and volumes of ground and surface water fluxes into Kāneʻohe Bay

Stream flow and the contribution of baseflow to total discharge

Streams are a significant source to Kāneʻohe Bay's freshwater and nutrient budgets (De Carlo et al., 2007; Hoover & MacKenzie, 2009). For example, streams in the southern sector have been shown to supply 50% of the reactive nitrogen and almost all of the phosphate budget, albeit in form of particulate-bound organic compounds delivered during storm events (Hoover, 2002; Hoover & MacKenzie, 2009). These authors also acknowledge that more studies should be focusing on groundwater as an additional nutrient pathway (Hoover & MacKenzie, 2009). This study looked at streamflow in order to define what fraction of total stream discharge originates as baseflow from groundwater as well as determine the locations of these groundwater inflows within the watershed.

Total stream discharge was partitioned into baseflow and surface runoff. Because the aquifer structure in this watershed includes marginal dikes extending all the way to the shoreline (Fig 2.2), baseflow can be expected not only from the high-level and basal aquifers, but also between these zones through the dike structures. The marginal dike zone, although covered by alluvium, extends beneath the full length of the streambed. The baseflow reported here includes only that captured within the study region and mostly represents discharge from the basal lens through the alluvium. Discrepancies between baseflow estimates provided by the USGS and this study are likely the result of field work occurring during atypical climate conditions and by not capturing baseflow in the upper part of the watershed. Surface runoff or upstream baseflow not captured in this study comprised of about half of total stream flow for Kahaluʻu and Kāneʻohe Streams and represented nearly 80% of total stream flow for ʻĀhuimanu Stream during the dry season. During the February sampling period, the percentage of total stream flow represented by surface runoff decreased for all three streams.

The spatial distribution of groundwater inflows is heavily impacted by both geologic and anthropogenic factors. Substantial portions of the studied streams are lined with concrete, which alters surface water and groundwater flow paths and stream chemistry by disrupting hyporheic flow and decreasing water residence time resulting in faster flushing and less time for bioremediation (Walsh et al., 2005). Stream discharge, and particularly storm runoff, are accelerated in the concrete-lined portions due to the smooth, impervious surface. Geologically, for

the streams studied, the highly conductive marginal dike zone intersects the streams upslope of most residential development and is the major contribution of baseflow to the streams. Downstream of the marginal dike zone, older (low conductivity) and younger (low to moderate conductivity) alluvium prevails. The basal lens is the primary source of groundwater in these areas, however because a large portion of the streams are lined with concrete, groundwater inflows are inconsistent and limited to isolated locations (Fig 2.6). Groundwater contributions in these sections occur through drainage pipes, weepholes, and springs through cracks in the concrete-lining. Groundwater contribution in these outlets was confirmed based on their radon levels. In Kahaluʻu Stream, residential areas with OSDS are concentrated within a 200 m radius of the stream, which also coincides with gaining portions of the stream (Fig 2.6). Losing reaches of Kahaluʻu Stream are most significant in portions of the stream with a concrete substrate. Interestingly, this is not the case for ʻĀhuimanu Stream, where relatively high volumes of groundwater inflows and outflows occur within the concrete-lined section of the stream (Fig 2.6). This is likely the result of the numerous cracks observed within the concrete-lining, which were more pronounced within ʻĀhuimanu Stream compared to the others studied. Kāneʻohe Stream has mostly gaining reaches, particularly downstream of the portions lined with concrete (Fig 2.6).

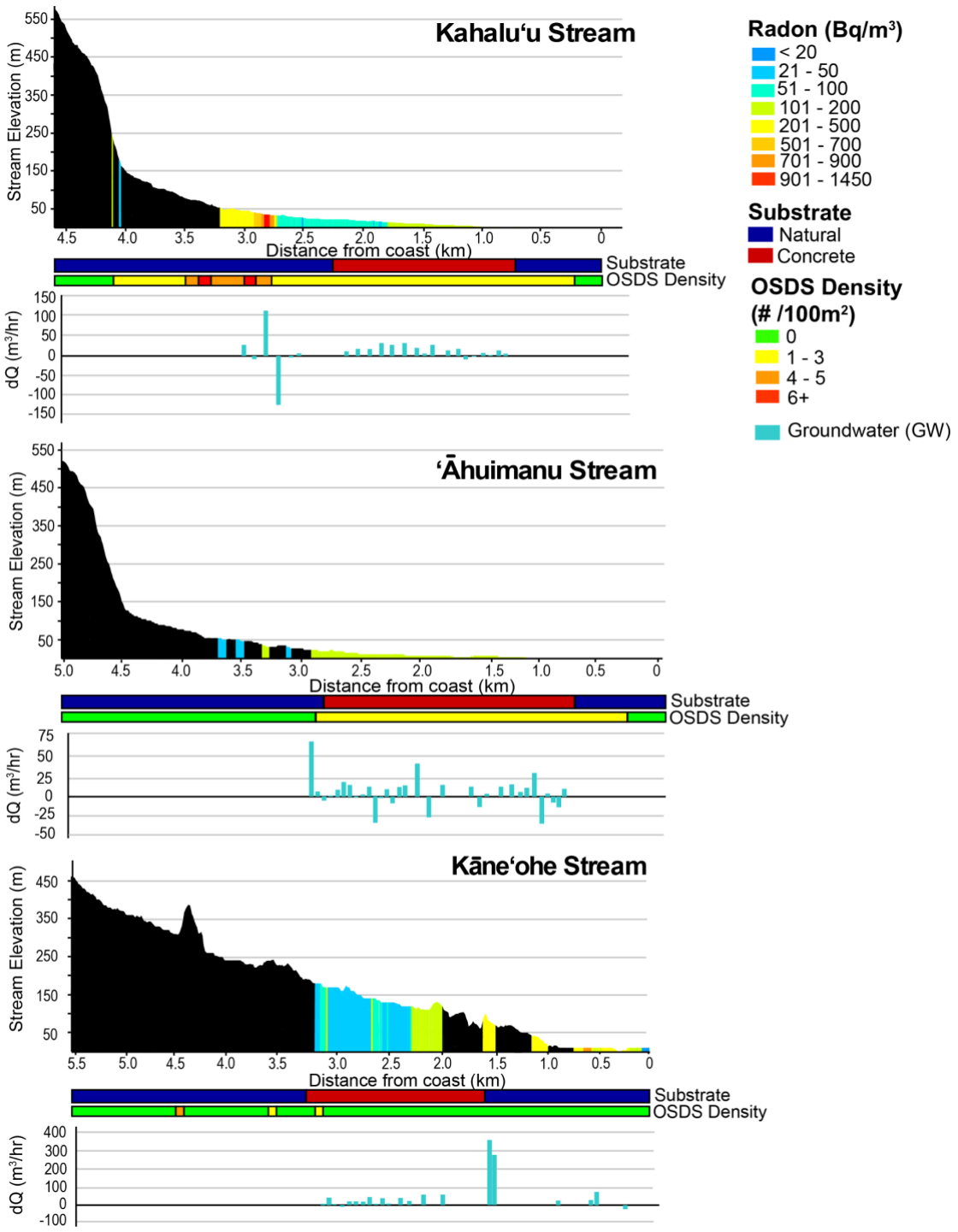

Fig 2.6. Groundwater fluxes in Kahalu'u, 'Āhuimanu, and Kāne'ohe Streams (using non-modeled results) for the July sampling period. Stream elevation (Hawai'i Coastal Geology Group, 2013) is shown in m with surface water radon concentrations overlain in Bq/m^3. Stream substrate (natural – blue, concrete – red) and the number of OSDS units within 100 m of the stream (Whittier & El-Kadi, 2009) are indicated below the graph showing stream elevation and radon concentrations. Corresponding changes in groundwater discharge are based on radon and stream discharge measurements.

Conclusions about groundwater fluxes in streams were inconsistent between using the modeled and non-modeled radon (Appendix A: S4 Table). Non-modeled and modeled groundwater discharge rates during the July and February sampling periods were within error of one another for Kahaluʻu Stream. Similarly, non-modeled and modeled July results were comparable for Kāneʻohe Stream. July sampling period modeled (2.1×10^4 m^3/day) results for ʻĀhuimanu Stream however, were significantly greater than non-modeled (0.67×10^4 m^3/day) results. The discrepancy for ʻĀhuimanu Stream may be attributed to rapid fluctuations in radon concentrations, causing the modeled results (which are calculated in part using weighted averages and cubic splines) to overestimate the concentration.

SGD

Total nearshore SGD was 0.45 ± 0.20, 1.8 ± 1.1, and $2.3 \pm 1.9 \times 10^4$ m^3/day in the northwestern, central, and southern sectors, respectively; however, total bay-wide SGD was smaller volumetrically than stream inputs (Table 2.4). While total SGD was less than streamflow, it still represents a significant contribution to the overall water budget. Total SGD measured in this study was less than previous SGD estimates (1.1 to 9.4×10^5 m^3/day) for the northwestern and central sectors using radon and radium (Dulai et al., 2016) because this study only captured nearshore SGD within 50 to 100 m of the shoreline. Another study in the area that used a MODFLOW model to estimate SGD (3.1×10^4 m^3/day) matched our estimates for SGD much more closely (Mathioudakis, 2018). For the southern sector, SGD rates were 50% lower than total stream flow. The central sector had the greatest SGD rates across the bay, which were nearly three times greater than total stream flow. For the northwestern sector, SGD was 50% lower than total stream discharge.

Recirculated SGD was the primary component of total nearshore SGD bay-wide. The fresh component of total SGD bay-wide was 5.4×10^3 m^3/day, or 12% of total SGD. The volume of fresh SGD was highly variable by sector and represented 45%, 1.2%, and 20% of total SGD to the northwestern, central, and southern sectors, respectively.

For the sub-watersheds studied, SGD and baseflow were significant terrestrial water sources to the bay. For Kahaluʻu sub-watershed, 0.21×10^4 m^3/day of SGD (55% of which is fresh SGD), and 0.57×10^4 m^3/day of baseflow discharge into Kāneʻohe Bay, which together contribute nearly 1.2 times that of surface runoff fraction of stream flow. For Kāneʻohe sub-watershed, 0.45

x 10^4 m^3/day (75% fresh SGD), and 1.6 x 10^4 m^3/day of baseflow discharge into the bay, contributing nearly equal parts of groundwater and surface runoff fraction of stream flow. Overall, 2.9 x 10^4 m^3/day of groundwater discharges to the bay from the Kahaluʻu and Kāneʻohe sub-watersheds via baseflow and SGD, making groundwater an equal source of water to surface flow from streams to the bay in these areas.

Total SGD accounting for offshore SGD can be estimated if we assume that the same radon concentrations would be measured as far as 200 m offshore as was previously observed (Dulai et al., 2016). If we extend our radon mass balance volumes to 200 m offshore and water depth 1.4 m as previously observed (Dulai et al., 2016), offshore SGD is estimated as 22,000, 31,000, and 31,000 m^3/day for the northwestern, central, and southern sectors respectively. Our offshore SGD estimates for the northwestern and central sectors (the southern sector was not included in that study) are consistent with those in previous research (Dulai et al., 2016; Mathioudakis, 2018). Our offshore SGD estimates are 490%, 170%, and 130% of our nearshore SGD estimates for the northwestern, central, and southern sectors, respectively, suggesting that SGD plumes and discharge points may extend offshore and SGD is potentially a substantial portion of the water budget, with water fluxes greater than stream inputs for both the central and southern sectors.

Our SGD estimates are somewhat lower in comparison to other studies using radon conducted globally in highly conductive substrates. Mean total SGD for Kāneʻohe Bay in this study was 2.5 m^3/m/day (maximum = 29 m^3/m/day). This is comparable to some studies conducted in other locations in Hawaiʻi, such as in Maui, where mean total SGD rates of 1.1 to 6.9 m^3/m/day were found (Bishop et al., 2015), but significantly lower than discharge rates reported by other authors in Kona (96 m^3/m/day) (Knee et al., 2010). Further comparisons between previous SGD studies conducted in Hawaiʻi have been detailed extensively in the literature (Kelly et al., 2018). Mean SGD, for instance, in Mauritius ranged from 5.2 to 56 m^3/m/day (Burnett et al. 2006; Rapaglia et al., 2006). Similarly, mean SGD for Manila Bay, Philippines was 12 m^3/m/day (Taniguchi et al., 2008) and 15 m^3/m/day for Taiwan (Martin et al., 2013). Differences between our SGD estimates and other studies may be attributed to local and regional differences in hydrogeological substrates (such as hydraulic conductivity or structure) and the fact that a significant portion of groundwater is channeled into stream as baseflow.

2.4.2 Dissolved nutrient concentrations and fluxes

While major water quality problems associated with large point sources of pollution in Hawai‘i, such as the sewage effluent outfall to Kāne‘ohe Bay in the 1960’s to 1980’s (Smith et al., 1981), have been eradicated, non-point source pollution sourced from OSDS and agriculture are currently the largest contributors that still negatively impact coastal water quality (Dailer et al., 2010; Richardson et al., 2017; Laws & Redalje, 1979; Bishop et al., 2015). These pollutant sources can negatively impact coral reefs by shifting their accretion-erosion balance or contributing to the proliferation of invasive algae (Lubarsky et al., 2018; Smith et al., 1981; LaValle, 2018). In Kāne‘ohe Bay, the impact of OSDS has never been studied in detail and at a bay-wide scale across population and hydrogeological gradients. As described earlier, both, streams and SGD are a pathway of terrestrial groundwater and therefore of land-derived sources of nutrients.

The Hawai‘i Department of Health (HDOH) nutrient water quality standards for streams during the dry season were exceeded for 61% of TN and 33% of TP samples during the July sampling period (Hawai‘i Administrative Rules 11-54). For the February sampling period, 70% of TN and 5% exceeded the HDOH nutrient water quality standards for the wet season (Hawai‘i Administrative Rules 11-54). Nutrient concentrations within streams exceeded HDOH water quality standards for TN and TP (Hawai‘i Administrative Rules 11-54). Median concentrations during the July sampling period in surface waters of TN for all three streams studied were greater than the dry season HDOH limit of 13 µM, and less than the TP dry season HDOH limit of 0.97 µM (Hawai‘i Administrative Rules 11-54). Only Kāne‘ohe Stream exceeded the median wet season concentrations for TN (HDOH limit = 18 µM) and none of the median values for streams exceeded the wet season TP limit of 1.6 µM. Based on the locations of groundwater discharge and associated nutrient fluxes, it is obvious that water quality in both, streams and the coastal ocean can be impaired by groundwater contributions. Specific to Kahalu‘u Stream and downstream sections of ‘Āhuimanu Stream, the substantial number of cesspools within 100 m of the stream itself mean that groundwater contributions likely reflect a wastewater source (Fig 2.6). In particular, DIN and DIP concentrations and fluxes in surface water drastically increases where OSDS density exceeds 100 OSDS/km^2, a metric which indicates a high risk for groundwater contamination (USEPA, 2002b). According to the Mann-Whitney Rank Sum Test, concentrations of DIN ($p = 0.002$) and DIP ($p = > 0.001$) in surface water are significantly greater in the upstream portions with high OSDS density compared to downstream portions. In Kahalu‘u Stream, upstream

portions have an OSDS density that exceeds 100 OSDS/km^2, where surface water nutrient concentrations (median TN = 19 ± 19 µM and TP = 1.1 ± 0.25 µM) exceed the HDOH limits of 13 and 0.97 µM for TN and TP, respectively. Nutrient concentrations are also enriched in groundwater despite low population density but high OSDS density, further suggesting that groundwater flows to streams in this area are impacted by wastewater. Nutrient concentrations were comparatively lower in the downstream portions of Kahaluʻu and ʻĀhuimanu Streams (median TN = 18 ± 9.5 µM and TP = 0.30 ± 0.19 µM), while median TN concentrations still exceeded the HDOH limit. Similarly, in Kāneʻohe Stream, downstream portions (where the Kamoʻaliʻi and Kapunahala tributaries merge; also the area with the highest population density) had significantly higher nutrient concentrations (median TN = 58 ± 58 µM and TP = 1.1 ± 1.2 µM) compared to upstream portions (median TN = 12 ± 17 µM and TP = 0.53 ± 0.28 µM). In particular, median TN concentrations were significantly higher compared to those measured from Kahaluʻu and ʻĀhuimanu Streams, which is consistent with previous literature indicating correlations of excess nitrogen with increasing population (Valiela, 1990; USEPA, 2002b) although this area does not have high density of OSDS. These results demonstrate that elevated stream nutrient concentrations can be traced back to groundwater nutrient levels and thus wastewater inputs because (1) radon analyses demonstrate groundwater connectivity to the streams and (2) locations with elevated stream nutrient concentrations had correspondingly high groundwater nutrient concentrations.

Median salinity corrected nutrient concentrations in SGD were higher than those measured in stream groundwater samples, which suggest that groundwater accumulates nutrients as it flows downstream in the watershed. Groundwater along the shoreline was brackish (salinity ranged from 3.2 to 28), meaning another potential contributor of nutrients (both organic and inorganic) to groundwater is seawater intrusion (Kroeger & Charette, 2008). For example, previous research found elevated nutrient concentrations in salty porewater in Heʻeia, suggesting that remineralization associated with oxygenated saltwater cycling through sediments can be a source of inorganic nutrients (Briggs et al., 2013). The median concentration of DIN in coastal groundwater was nearly three times greater than that of stream groundwater. Similarly, DIP and DON in coastal groundwater were nearly twice and four times greater than median concentrations of groundwater from streams. Coastal surface waters had elevated nutrient concentrations and SGD is likely one of the important sources of these nutrients given the high median concentrations

in SGD relative to stream inputs. One of the potential sources for the high nutrient concentrations along the coastline is the prevalence of coastal OSDS systems in the area, which may be compromised due to shallow groundwater levels (Whittier & El-Kadi, 2009). Another potential explanation for the higher nutrient concentrations in SGD as opposed to stream groundwater inputs is that SGD is a result of converging groundwater flow paths at the coastline and many of these paths may be comparatively longer and thus are accumulating more nutrients.

While median DIN and DIP concentrations did not vary between sampling periods in surface water, DIN: DIP ratios did vary between sampling periods in groundwater. DIN: DIP ratios can intensify from either an increase in nitrogen (e.g., sources from wastewater or fertilizers) or a decrease in phosphorus concentration or its increased sorption on aquifer solids. For Kahaluʻu sub-watershed, the median DIN: DIP ratio in groundwater was over four times higher during the February sampling period (N:P = 83 ± 308), compared to the July sampling period (N:P = 21 ± 106; Fig 2.7), which given the potential sources of nitrogen in the sub-watershed, is likely a result of rainfall infiltrating the groundwater (and perhaps flooding the OSDS) and carrying excess nitrogen from the high density of OSDS in the sub-watershed (Whittier & El-Kadi, 2009). The opposite trend was observed for ʻĀhuimanu sub-watershed, where the median DIN: DIP ratio in groundwater during the July sampling period (N:P = 82 ± 49) was greater than the February sampling period (N:P = 20 ± 45; Fig 2.7) due to a decrease in nitrogen concentrations. In Kāneʻohe sub-watershed, DIN: DIP ratios were similar between July (N:P = 24 ± 48) and February (N:P = 39 ± 75) sampling periods.

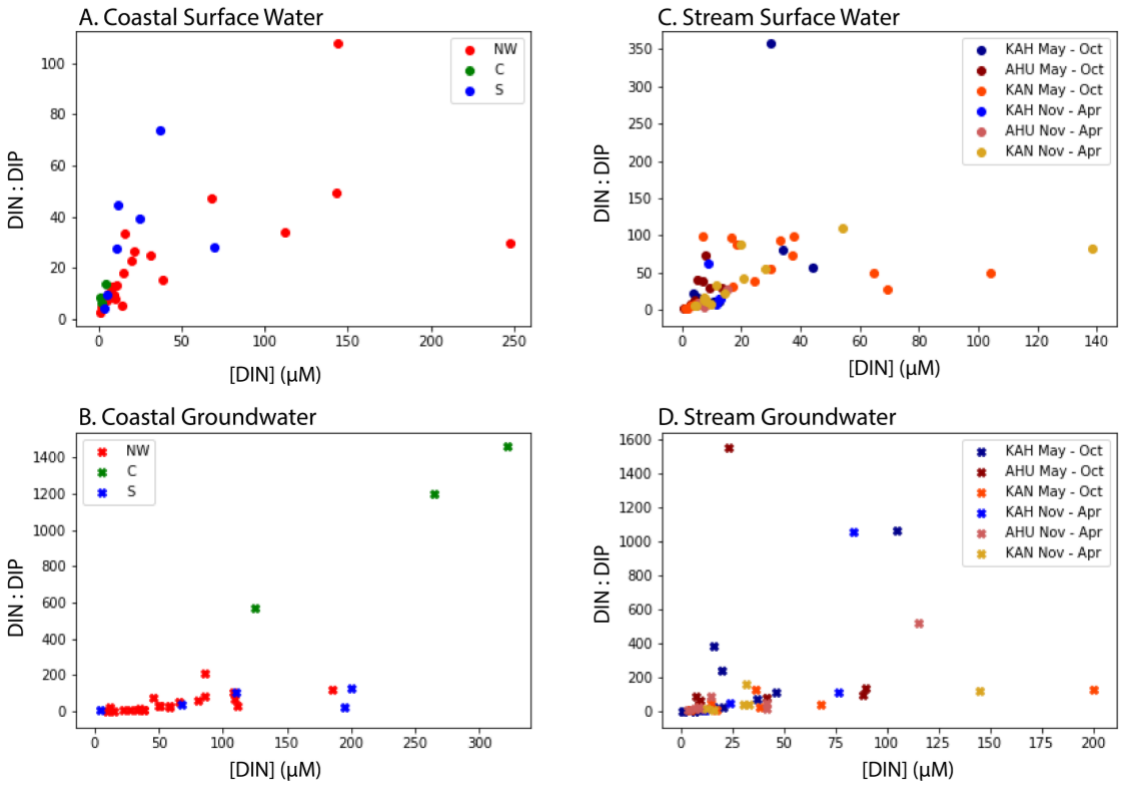

Fig 2.7. Salinity corrected DIN: DIP ratios vs. DIN concentrations by sector/sub-watershed, sampling period, and type of water. (A) Coastal surface water and (B) coastal groundwater, color-coded by NW, C, and S sectors. (C) Stream surface water and (D) stream groundwater, color-coded by sub-watershed: Kahaluʻu (KAH), ʻĀhuimanu (AHU), and Kāneʻohe (KAN) and sampling period.

In the nearshore environment, median salinity corrected DIN: DIP ratios were variable by sector in surface and groundwater across the bay (Fig 2.7). The central sector had a median DIN: DIP ratio in surface waters less than the anticipated Redfield ratio of 16 (Redfield, 1963) and thus N-limiting, consistent with previous research in the area (Smith et al., 1981; Ringuet & MacKenzie, 2005). Despite a large number of OSDS units upstream, Heʻeia Stream flows into a wetland prior to discharging to the coastal ocean in the central sector and may be a significant removal term of nitrogen through denitrification as observed in other wetlands in similar environments (Dulai et al., 2016). In contrast to the central sector, surface waters in the northwestern and southern sectors had DIN: DIP ratios greater than Redfield ratios. For all of nearshore Kāneʻohe Bay, DIN: DIP ratios in groundwater were consistent with ranges found for SGD in other locations around the world, with a DIN: DIP ratio several orders of magnitude greater than the Redfield ratio (Cho et al., 2018).

Dissolved silica is primarily delivered to streams and the nearshore area via groundwater and is an essential nutrient for silica-based organisms. Silicates are sourced in Hawai‘i almost exclusively from weathered basalt and soils (Vitousek et al., 2004). Surface waters in streams naturally had higher median salinity corrected concentrations of DSi (median concentrations were 530, 480, and 500 µM for Kahalu‘u, ‘Āhuimanu, and Kāne‘ohe Streams, respectively) compared to coastal waters (median DSi concentrations were 440, 230, and 370 µM for the northwestern, central, and southern sectors, respectively) due to the contribution of baseflow to streams. Groundwater concentrations of salinity corrected DSi were greater in coastal groundwater (median concentrations were 690 and 860 µM for the north-western and southern sectors) compared to groundwater samples from streams (median concentrations were 600, 620, and 450 µM for Kahalu‘u, ‘Āhuimanu, and Kāne‘ohe Streams, respectively). Overall, stream surface water DSi concentrations found in this study are consistent with previous research in the area that stated that streams under baseflow conditions had 400 to 500 µM DSi on average (Hoover, 2002).

Along the stream-coastal continuum, nutrient additions show relationships between groundwater flow paths and localized inputs. The Kahalu‘u Stream-coastal continuum shows that the streams are progressively gaining from the upstream reaches above the concrete-lined portion and then once again where Kahalu‘u Stream flows into Kahalu‘u Estuary to the coastal ocean, as evidenced with DSi concentrations (Fig 2.8). Coastal groundwater is enriched in DSi, which is consistent with the assumed deeper and longer groundwater flow path also surmised for increased nitrogen levels, DSi largely depends on groundwater residence time (Freeze & Cherry, 1972). The lowest concentrations of DSi in groundwater samples within the concrete-lined portions of the stream (particularly at 1500-2500 m downstream) likely reflect input from storm drains, which is low in DSi. Additions of TN also increase with distance downstream, likely due to increased anthropogenic influence, such as OSDS density, in addition to longer groundwater flow paths forced by alteration of the stream’s natural substrate and channel (Fig 2.8). Concentrations of DIP in general show a decreasing trend with respect to distance downstream in both surface water and groundwater for the northwest sector, likely reflecting local inputs from OSDS as trends between (Fig 2.8). For the southern sector, DIP concentrations actually increase in surface waters with respect to distance downstream, until reaching the estuary, which instead is likely sourced from the decay of plants growing within the concrete lining of the streambed (Fig 2.8). The Kāne‘ohe Stream-coastal continuum shows a similar trend (Fig 2.8), however it is complicated by several

factors including higher population density, fewer springs within the concrete-lined section, and vegetation within the concrete-lined portions of the streams. Moreover, the highest concentrations of both TN and DIP coincide with downstream areas with the highest population density. The salinity correction surmises the assumption that a large fraction of the nutrient concentrations observed at the coast is terrestrially derived but may over-estimate the concentration if the source of the input is at the shoreline itself to brackish waters (such as OSDS units located on the coastline).

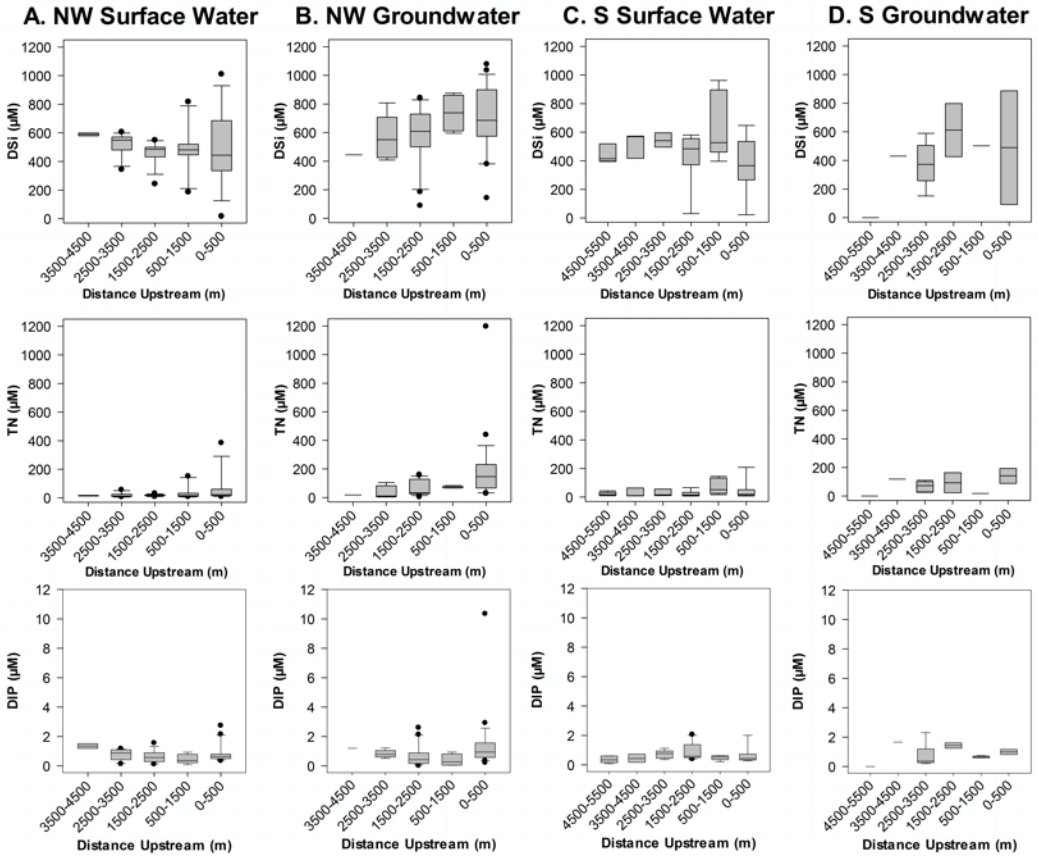

Fig 2.8. Salinity-corrected DSi, TN, and DIP (µM) boxplots by distance downstream (m) for the Kahaluʻu and Kāneʻohe Stream-Coastal continuums. (A) Surface water and (B) groundwater for Kahaluʻu Stream flowing into the NW sector. (C) Surface water and (D) groundwater for Kāneʻohe Stream flowing into the S Sector.

Salinity-corrected nutrient fluxes to the northwestern and southern sectors of Kāneʻohe Bay were primarily groundwater (SGD and stream baseflow) derived (Table 2.7). For both sectors studied, DIN and DON fluxes were primarily delivered to the bay via groundwater (SGD and baseflow combined). Previous research indicated that 3, 1, 0.1, and 26 kmol/day of DIN, DON,

DIP, and DSi, respectively are loaded to the southern sector of Kāneʻohe Bay (Smith et al., 1981). Our results for southern Kāneʻohe Bay closely match these fluxes (Table 2.7), with the exception of DSi, which is 46% (12 kmol/day) greater. This discrepancy may be due to the increased development and erosion or previous underestimation of SGD fluxes.

Table 2.7. Total (SGD and stream) dissolved nutrient loading to Northwestern (NW) and Southern (S) Kāneʻohe Bay during the dry season. % SGD and % Stream represent the percentage contribution to the total groundwater-derived nutrient flux for DIN, DON, DIP, and DSi for the high-resolution study areas. % Groundwater refers to the percentage that SGD and stream baseflow contribute to the total (groundwater + surface water) nutrient flux.

		Total (kmol/d)	**% SGD**	**% Stream**	**% Groundwater**
NW	DIN	0.38	58	42	81
	DON	0.73	59	41	95
	DIP	0.018	45	55	69
	DSi	10	28	72	65
S	DIN	3.8	79	21	90
	DON	2.8	76	24	92
	DIP	0.067	55	45	82
	DSi	38	47	53	69

2.4.3 Temporal variation of SGD during normal and extreme tidal cycles

The above reported bay-wide SGD rates represent only a snapshot of discharge rates. It is well documented that SGD variation is driven by tides. For the two locations in Kahaluʻu where radon time series were conducted, SGD rates were greatest at low tide, in accordance with previous SGD studies in Hawaiʻi (Dulai et al., 2016; Richardson et al., 2017; Bishop et al., 2015). A substantially greater percentage of saline SGD was discharged during the perigean spring tide in comparison to the spring tide, which is consistent with previous literature suggesting increased saline SGD at high sea level stands (Moore, 1999). These temporal variations also have implications for SGD flux estimates, where our results from Kahaluʻu suggest that bay-wide SGD would likely be significantly greater during a perigean spring tide compared to a spring tide and especially compared to a neap tide.

Anomalously high tides offer a snapshot into future coastal scenarios given projected sea levels in the next 30 to 100 years (Slangen et al., 2014; Sweet et al., 2017), where potential examples of impacts include coastal nuisance flooding and inundation of OSDS (Habel et al., 2017). The higher rates of groundwater discharge and nutrient fluxes observed during the perigean

spring tide suggest that these impacts are highly likely to be occurring today during high tide cycles, which has important implications for coastal biogeochemical systems. Non-point pollution sources, such as OSDS, in Kāneʻohe Bay and within the state of Hawaiʻi, are frequently located along coastlines, meaning coastal water quality will likely worsen with increasing sea-levels due to the inundation of these systems.

Increasing population and development along coastlines coupled with projections of increased global mean sea level (conservatively, 0.3 to 1 m within the next 100 years) may exacerbate future coastal water quality deterioration, not only in Hawaiʻi and on HVPI, but also globally (Cooper et al., 2016; Wong et al., 2014). This study is one of the first, to our knowledge, to directly study the impact of increasing sea levels on SGD discharge rates and associated nutrient fluxes. We observed an increase in total SGD, which has important implications for coastal ecosystems. Increases in total SGD allow for higher rates of groundwater discharge, and contaminants associated with land use that travel via groundwater, such as excess nutrients and sewage, to reach the coastal zone. While we observed a higher percentage of saline SGD during the perigean spring tide, low tide fresh SGD was still 3.4 times greater during the perigean spring tide compared to the spring tide (Table 2.6). Moreover, increased saline SGD may promote dissolution of metals and dissolved species, representing a potential additional source of contamination to the coastal ocean (Moore, 2010).

In this study, we have shown not only increased nutrient fluxes, but also higher nutrient concentrations during perigean spring tides, highlighting the importance of conducting more studies that investigate the relation of sea level to SGD composition. In particular, an excess in nitrogen sources were observed during the perigean spring tide compared to the spring tide, dramatically increasing the N:P ratio from 7.0 to 58 during low tide and from 1.4 to 26 during high tide (Table 2.5). Given these results, we suggest that rising sea levels may disrupt primary productivity with greater frequency due to increasing departure from the Redfield ratio.

2.4.4 Groundwater-surface water interactions along the stream-coastal continuum

This study takes a novel approach by looking at groundwater baseflow and SGD as a continuous vector for pollution via groundwater flow. Groundwater contributions to streams ranged from 22% to 68% along their studied reaches to the coast of Kāneʻohe Bay and Watershed, whereas nearshore SGD ranged from 1,400 to 4,000 m^3/km/day, or 9% to 58% of groundwater

discharged to the studied streams as baseflow. This is not surprising as streams intercept the aquifer and gain a significant amount of groundwater in the watershed, draining groundwater from the aquifers. In a ridge to reef concept, our results suggest that groundwater discharge is important for both the water and nutrient budgets of the studied reaches of the streams, estuaries, and coastal ocean.

Both streams and the coastal SGD are important vectors for nutrient delivery to Kāneʻohe Bay. Groundwater contributions of DIN, DIP, and DSi in streams discharging to Kāneʻohe Bay were 23%, 58%, and 46% of total stream inputs during the dry season, respectively. For the sub-watersheds in which stream inputs were measured, SGD contributes 810, 15, and 6,400 moles/day, or 83%, 38%, and 23% of DIN, DIP, and DSi, respectively compared to stream fluxes. This illustrates the importance of considering both baseflow and SGD as vectors of groundwater pollution to the coastal ocean. Groundwater-derived DON contributions were 85% of total stream flow, whereas SGD-derived DON added 840 moles/day, or 86% of stream inputs.

Salinity corrected coastal groundwater concentrations were mostly similar or greater compared to results from previous SGD studies conducted in Hawaiʻi. Our median bay-wide coastal groundwater DIN concentrations (62 µM) were greater than mean values measured in other SGD studies in Kona, Southern Molokaʻi, and Kāneʻohe Bay, similar to those measured in Wailupe but less than concentrations measured at Black Point and on Maui (Table 2.8), likely due to the suspected wastewater influence from OSDS, but comparatively less than sites such as Black Point and West Maui. Similarly, our coastal groundwater DIP concentrations (1.6 µM) were greater than those measured in Kona and Molokaʻi, Wailupe, and Kāneʻohe Bay, and less than those measured in Black Point, and on West Maui that have known OSDS pollution (Table 2.8). Median bay-wide DSi concentrations (640 µM) in coastal groundwater were greater than average concentrations found on Maui, Kona, Molokaʻi, but similar to those measured previously in Kāneʻohe Bay, and less than the average concentrations from Black Point and Wailupe (Table 2.8), which are likely associated with SGD rates (for Black Point and Wailupe) and island age and weathering (for sites on Maui, Molokaʻi, and Hawaiʻi).

Table 2.8. Comparison of coastal groundwater nutrient concentrations between this study and other studies in Hawai‘i.

	DIN (µM)	DIP (µM)	DSi (µM)	References
This Study	62	1.6	640	
Kāne‘ohe Bay, O‘ahu	12	1.6	540	Dulai et al., 2016
Wailupe, O‘ahu	71	1.7	810	Richardson et al., 2017
Black Point, O‘ahu	160	3.7	740	Richardson et al., 2017
Kona, Hawai‘i	14 - 39	0.83 – 1.8	110 – 210	Knee et al., 2012; Street et al., 2008
West Maui	120	3.0	510	Hawai‘i Coastal Geology Group, 2013
Kamiloloa, Moloka‘i	3.9	0.89	47	Street et al., 2008

Salinity corrected coastal groundwater nutrient concentrations in the nearshore waters were comparable to or greater than the global fresh SGD concentrations. The median DSi concentration in coastal waters was about five times greater compared to the global fresh SGD DSi end-member value of 130 ± 18 µM (Cho et al., 2018). Similarly, the median bay-wide DIP concentration was over twice the global end-member value for DIP (0.6 ± 0.2 µM) (Cho et al., 2018). This is not surprising as DSi and DIP are reported to be elevated in basalt aquifers (Chadwick et al., 1999; Nelson et al., 2013; Porder & Ramachandran, 2012). The median coastal DIN concentration found in this study, however, was consistent with the global DIN end-member concentration (56 ± 23 µM) (Cho et al., 2018).

The results from this study have important implications for our understanding of groundwater discharge to coastal environments, especially in areas subject to stream discharge. This is particularly the case for volcanic or karstic settings, which while dissimilar geologically, have similar hydrogeologic properties such as high permeability and porosity that lead to enhanced groundwater discharge (Burnett et al., 2006; Dimova et al., 2012). Channelization of streams coupled with a hydrologically conductive substrate resulted in increased groundwater discharge and nutrient fluxes, particularly to the coastal ocean. Parsing total groundwater and surface water

contributions leads to more informed land management decisions, which will become increasingly important in coming years under higher sea level stands.

2.5 Conclusion

Partitioning groundwater and surface water discharge along the stream-coastal continuum allowed for a greater spatial and temporal resolution of groundwater discharge dynamics, particularly in areas with substantial baseflow contribution to streams. Most studies have largely focused solely on either baseflow to streams or SGD to the coastal ocean as separate entities. While fresh SGD represents an estimated 10% of river discharge globally (Zekster, 2000), we suggest baseflow contributions to streams represent an important, yet understudied, addition to coastal groundwater budgets. The approach used in this study not only led to an improved understanding of nutrient delivery and contaminant flow paths to streams and the coastal ocean in Kāneʻohe Watershed and Bay, but also highlighted the importance of considering groundwater discharge via stream baseflow. Our major findings include:

1. Groundwater (stream baseflow + SGD) fluxes were equal to surface runoff for the studied streams, which demonstrates the importance of considering groundwater contributions to both, streams and the coastal ocean in water and geochemical budgets.
2. SGD-derived nutrient concentrations and fluxes were greater than stream-derived nutrient fluxes. In particular, nitrogen species were high in SGD, shifting nearshore N:P ratios substantially higher than conditions that promote balanced primary productivity.
3. SGD fluxes during a perigean spring tide were greater than those of a spring tide at the same location. Similarly, DIN, DON, DIP, and DSi fluxes were greater during the perigean spring tide. Sea level rise will stress coastal infrastructure globally - attempting to understand these impacts through field-based studies will help prepare individuals, land-managers, and governments, in addition to improving available data for modelers, for the future.

This research highlights the importance of considering groundwater discharge as a continuous water and solute source across the land-ocean interface, in addition to being one of the first field-based studies to look at groundwater discharge dynamics and contaminant transport under future sea level stands. We recommend future SGD studies in areas that are influenced by stream discharge use a similar approach to the one used in this study in order to account for total

groundwater discharge to the coastal ocean, particularly in volcanic and karstic substrates. As demonstrated by this study, water quality in streams and the coastal ocean are linked by groundwater discharge. While it is often difficult to detect coastal springs without specific SGD detection methods that are not available to all monitoring agencies, this work suggests that because of the similarities between groundwater discharge-driven coastal and estuarine water quality, estuarine monitoring often captures the groundwater signature and may inform about sources of coastal water quality problems as well.

Chapter 3: Submarine groundwater discharge: A previously undocumented source of contaminants of emerging concern to the coastal ocean (Sydney, Australia)

Published as: McKenzie, T., Holloway, C., Tucker, J., Sugimoto, R., Nakajima, T., Harada, K., Dulai, H., Santos, I.R. (2020). Submarine groundwater discharge and flushing times drive contaminants of emerging concern in the coastal ocean (Sydney, Australia). *Marine Pollution Bulletin*, 160: 111519. doi: 10.1016/j.marpolbul.2020.111519.

Abstract

Submarine groundwater discharge (SGD) is rarely considered as a pathway for contaminants of emerging concern (CECs). Here, we investigated SGD as a source of CECs in Sydney Harbour, Australia. CEC detection frequencies based on presence/absence of a specific compound were >90% for caffeine, carbamazepine, and dioxins, and overall ranged from 25-100% in five studied embayments. SGD rates estimated from radium isotopes explained >80% of observed CEC inventories for one or more compounds (caffeine, carbamazepine, dioxins, sulfamethoxazole, fluoroquinolones and ibuprofen) in four out of the five embayments. Radium-derived residence times imply mixing is also an important process for driving coastal inventories of these persistent chemicals. Two compounds (ibuprofen and dioxins) were in concentrations deemed a high risk to the ecosystem. Overall, we demonstrate that SGD can act as a vector for CECs negatively impacting coastal water quality.

3.1 Introduction

Contaminants of emerging concern (CECs) are ubiquitous in the environment due to their refractory nature and widespread human applications (Kolpin et al., 2002; Lapworth et al., 2012). CECs include pharmaceuticals, endocrine disrupting and industrial chemicals, pesticides, and other organic anthropogenically-sourced compounds. The presence of these compounds generally results from inefficient removal in wastewater treatment plants, and leakage of residential, industrial and agricultural waste (Kolpin et al., 2002; Yang et al., 2011). Concentrations of most CECs are unregulated (Lapworth et al., 2012) despite their pervasiveness and linkages to negative environmental impacts. For example, CECs contribute to the increased incidence of antibiotic resistant bacteria (Hernando et al., 2006) or intersex invertebrates and fish (Barber et al., 2007; Lange et al., 2008).

Attenuation of CECs in the environment (e.g., biodegradation, photolysis, dilution, sorption) are compound specific and highly variable (Lapworth et al., 2012). Numerous CECs can be suitable environmental tracers of wastewater pollution in both groundwater and surface water (e.g., Knee et al., 2010; Yoon et al., 2010; Birch et al., 2015). Compounds such as carbamazepine, acetaminophen, sulfamethoxazole, and acesulfame are sewage tracers given their high detection frequencies, ease of quantification, and definite wastewater source (e.g., Tran et al., 2014; James et al., 2016; McCance et al., 2018; White et al., 2019; Szymczycha et al., 2020). Other compounds, such as caffeine, have been linked to population density (Buerge et al., 2003).

Submarine groundwater discharge (SGD) can act as a vector for pollutants to reach coastal surface waters. Globally, SGD has been associated with coastal eutrophication, increased primary productivity, and deterioration of water quality because it is often nutrient-rich (Moore, 1999; Valiela et al., 1990). SGD also can carry anthropogenic pollutants derived from industrial, agricultural, or urban land uses that seep into aquifers. With increasing coastal development worldwide (Wong et al., 2014) leading to the release of legacy contaminants to aquifers (Rodríguez-Eugenio et al., 2018), SGD can represent an overlooked pathway for pollution to reach coastal waters (Welch et al., 2019).

Because groundwater discharges heterogeneously as point-source springs and diffuse seepage, SGD is often quantified indirectly using geochemical tracers such as radium isotopes (Taniguchi et al., 2019). Naturally occurring radium isotopes (^{223}Ra, $t_{1/2}$ = 11.4 days; ^{224}Ra, $t_{1/2}$ = 3.64 days; ^{226}Ra, $t_{1/2}$ = 1600 years; ^{228}Ra, $t_{1/2}$ = 5.75 years) originate from primordial ^{232}Th, ^{235}U, and ^{238}U that occur in nearly all soils and sediments (Burnett et al., 2006). Radium can be employed as a groundwater tracer in brackish to saline waters because it is desorbed from soils with increasing salinity. Once released from the aquifers to surface waters, radium acts conservatively (Webster et al., 1995). Radium measurements can be used to estimate total SGD (fresh + saline water), apparent radium ages (a proxy for residence times), beach tidal pumping, and porewater exchange (Moore, et al., 2006; Charette et al., 2013; Gonneea et al., 2008; Rodellas et al., 2017). SGD has been well established as a major pathway of nutrient, pathogen, and heavy metal pollution to the coastal ocean worldwide (e.g., Kwon et al., 2014; Valiela et al., 1990; Moore, 1999; Dulai et al., 2016; Taniguchi et al., 2019), yet it has only recently been suggested to be a source of CECs to the coastal ocean (Szymczycha et al., 2020).

In this study, we use pharmaceuticals as wastewater tracers in SGD in Sydney, Australia. Storm runoff causing flooded sewers has been long thought to be the major source of wastewater pollution to Sydney coastal waters (Birch et al., 2015). Recent research, however, has detected pharmaceuticals, artificial sweeteners and intermittent enterococci in surface waters apparently unrelated to storm runoff during dry conditions (NHMRC, 2008; Birch et al., 2015; Ahmed et al., 2020), suggesting wastewater sources other than surface runoff, perhaps SGD. We hypothesize that (1) SGD is a source of wastewater and industrial runoff to coastal surface waters, and (2) CEC distribution will be related to a land-use gradient and water residence times. We first quantify SGD using radium isotopes in coastal embayments downstream of a range of urban and industrialized catchments with known SGD (Sadat-Noori et al., 2018; Correa et al., 2020) and leakage from sewer pipes (Sydney Water, 2010). Then, we evaluate these data with respect to land use, population density, and water residence times.

3.2 Study Location

This study was conducted in two urbanized tidally dominated estuaries in New South Wales, Australia: Sydney Harbour and Botany Bay. The estuaries are surrounded by Greater Sydney, which has an estimated population of 5.029 million (407 people/km^2) (ABS, 2016). Over 99% of Greater Sydney's population lives within the urban core, with an average density of 1,237 people/km^2 (ABS, 2016). Sydney Basin is predominantly comprised of Hawkesbury Sandstone (Triassic) with shale superimposed in some areas (Roy, 1981). Within Sydney's urban core, heavy metal pollution, frequent water quality failures, enterococci counts intermittently exceeding the water quality guidelines, and sewage leaks threaten ecosystem health and recreational use of the surrounding waters (Montoya, 2015).

The Sydney Harbour Estuary is an oligotrophic drowned river valley with a history of wastewater and industrial pollution (Johnston et al. 2015). Sydney Harbour has an irregular bathymetry featuring deeps (average depth: 28 m) divided by shallower shoal water with an average depth less than 3.5 m (Das et al., 2000). The estuary has an average water depth of 13 m (range: 1 to 46 m), a surface area of 55 km^2, and is a length of 30 km (Birch & Rochford, 2009). The estuary has an average spring tidal range of 1.1 m, with a maximum tidal range of 2.1 m (Birch et al., 2015). Sydney Harbour is well mixed during dry conditions, which is primarily driven by the tidal cycle, with water levels oscillating in phase with flood and ebb tides (Das et al., 2000;

Birch & Rochford, 2009). Tidal currents can reach 1.5 m/s, but frequently don't exceed 1 m/s in the main channel with slower currents in the embayments (Middleton et al., 1996; Das et al., 2000). The general direction of the currents is along the main channel. Water residence times range from less than one day to 225 days (Das et al., 2000). Average embayment-scale Sydney Harbour residence times were about 100 days when estimated from a hydrodynamic model (Cardno and Baird, 2014), or <70 days when estimated from radium isotopes (Correa et al., 2020).

The embayment's pollution history stems from rapid urbanization and industrialization of the upstream land over a 100-year period (Montoya, 2015), in addition to activities within the harbor such as substantial dredging and filling with materials containing industrial waste (Suh et al., 2003). Dredging and filling of the embayment primarily occurred around 1900, and then again between the 1950's and 1970's, with about 22% of the embayment shoreline currently comprised of reclaimed land (Mayer-Pinto et al., 2015).

Botany Bay is an open oceanic embayment located to the south of Greater Sydney and holds Australia's second largest port. Botany Bay covers a surface area of 39.6 km^2 and has an average water depth of 11.4 m (NSW Environment and Heritage, 2018). The average spring tidal range is 1.3 m with a maximum tidal range of 2.1 m. Botany Bay has been subject to significant industrial pollution from adjacent industrial facilities. The North Botany Industrial Precinct is home to about 25% of hazardous facilities in the state of New South Wales (New South Wales EPA). Due to chemical (hydrocarbons, surfactants, solvents) leakage into the groundwater from the adjacent chemical plants, the Botany Bay aquifer is not potable (New South Wales EPA).

Shore-perpendicular transects were conducted at five locations: Foreshore Beach in Botany Bay, and Homebush, Rozelle, Hen and Chicken, and Watsons Bays in Sydney Harbour. These sites capture a wide range of land uses (Figure 3.1; Table 3.1). Foreshore Beach is an estuarine beach susceptible to wastewater pollution from sewage overflows into the upstream Mill Stream (NSW Office of Environment and Heritage, 2018). Foreshore Beach, while a swimming beach, has been rated as "very poor" with respect to water quality given the frequency of high enterococci counts (NSW Office of Environment and Heritage, 2018). Homebush Bay is surrounded by mangroves and has a substantial history of sediment pollution from heavy metals, polycyclic aromatic hydrocarbons, Dichlorodiphenyltrichloroethane (DDT), Agent Orange, and dioxins, which has resulted in the prohibition of fishing in the area (Birch & Taylor, 2000; Birch et al., 2007; Suh et al., 2004). Hen and Chicken Bay is currently surrounded by medium density

residential land use, but it was formerly the home of a base metal foundry and smelter prior to 1945 (Birch, 2007). Rozelle Bay has a history of sediment pollution from adjacent industrial plants and today is surrounded by high-density residential land use (Suh et al., 2003). Closest to the mouth of Sydney Estuary, Watsons Bay is surrounded by low and medium density residential land use (New South Wales Legislation, 2015).

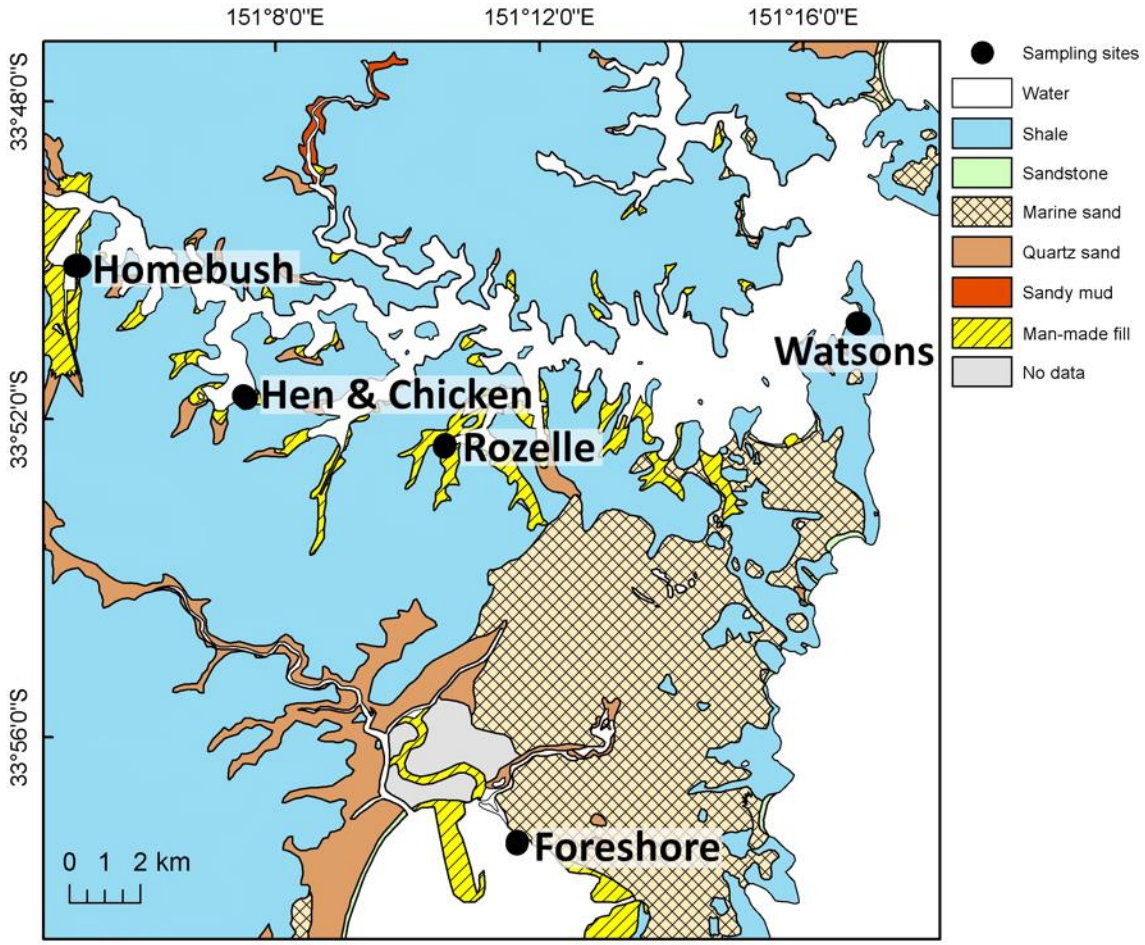

Fig 3.1. Map of study sites and regional geological classification (Australian Government Geoscience Australia).

Table 3.1. Study site location and characteristics. Population (ABS, 2016), geology (Suh et al., 2004; Birch et al., 2003) and land use (NSW Office of Environment and Heritage, 2018) in the 5 investigated embayments and population density (residents/km^2) indicate surrounding suburb population (ABS, 2016). Geology data are from Australian Government Geoscience Australia; Suh et al., 2004; Birch et al., 2003; 2004. Land-use data from NSW Office of Environment and Heritage, 2018, Birch & Taylor, 2000; Birch, 2007; Birch et al., 2007; Suh et al., 2003; Suh et al., 2004.

Estuary	Location	Population (density/km^2)	Geology	Land-Use
Botany Bay	Foreshore Beach	10,817 (1,067)	Sandstone and Fill	Industrial
Sydney Harbour Estuary	Homebush Bay (Parramatta River)	11,906 (11,906)	Anthropogenic Fill	Residential, Urban, former industrial
	Hen and Chicken Bay (Upper Estuary)	9,356 (3,819)	Sandstone and Anthropogenic fill	Residential, former industrial
	Rozelle Bay (Central Estuary)	9,451 (9,451)	Anthropogenic fill	Urban core, Residential, former industrial
	Watsons Bay (Lower Estuary)	850 (1,420)	Sandstone	Residential

3.3 Methods and Materials

Water samples (n = 44) were collected along shore-perpendicular transects at low tide between June 29 and July 3, 2019, coinciding with a perigean spring tide. Rainfall totaled 183 mm in the 30 days prior to sampling, with 70% of days receiving fewer than 5 mm and the other 30% receiving moderate (5 – 40 mm/day) rainfall (Australian Bureau of Meteorology, 2019). Baseflow conditions are expected in the region until heavy rainfall (greater than 50 mm/day) occurs.

Groundwater samples (n = 20) were collected from wells dug in the sand by pumping water with a peristaltic pump (additional information about sampling protocol can be found in Appendix S1). Wells were located along a transect as close as possible to the low tide, mid tide, high tide, and above high tide marks. Surface water samples (n = 24) were collected from the top 25 cm of each embayment at 2, 5, 10, 20, and 50 meters from shore using a bilge pump. Conductivity,

temperature, and pH were taken for each sample using a Hach HQ40D portable multi meter. Water samples were collected and analyzed for radium (^{223}Ra, ^{224}Ra, and ^{226}Ra), dissolved total nitrogen (TDN), phosphorus (TDP), inorganic nutrients (NO_3^-, NO_2^-, NH_4^+, PO_4^{3-}), CECs (carbamazepine, caffeine, fluoroquinolones, ibuprofen, sulfamethoxazole, and dioxins), and dissolved organic carbon (DOC).

Water samples (typically 60 L for surface water samples and 6 L for groundwater samples) for radium analysis were passed through 15 g of manganese oxide-coated acrylic fibers upon collection. Radium samples were analyzed using a Radium Delayed Coincidence Counter (RaDeCC). Analysis of ^{223}Ra and ^{224}Ra were completed within one week of sample collection following Moore & Arnold (1996). Samples were then sealed in airtight containers for one week to allow for ^{222}Rn ingrowth from ^{226}Ra then counted again on the RaDeCC as described in Peterson et al. (2009). Fibers were once again counted one month following sampling collection to allow for correction of ^{228}Th decay (Garcia-Solsona et al., 2008) and the estimation of excess ^{224}Ra.

Dissolved nutrient samples were filtered on site through a disposable 0.45 μM cellulose-acetate filter into 10 mL polycarbonate vials with polypropylene caps and kept at 0 °C until analysis. Nutrient samples were analyzed using a 5-channel Lachat Flow Injection Analyzer with precision and accuracy better than 5%.

All samples for CEC analysis were collected into pre-combusted and methanol rinsed amber glass bottles with Teflon-lined caps. Samples were filtered on site through a 0.45 μM filter (Nucleopore) and kept at 4 °C until analysis. CEC samples were analyzed for five different compounds (Table 3.2) at the University of Hawai‘i at Mānoa using an Enzyme Linked ImmunoSorbent Assay (ELISA) and compound-specific kits (Abraxis LLC). Samples were prepared following compound specific instructions provided with each kit and then analyzed at a wavelength of 450 nm on a spectrophotometric microplate reader (Abraxis ON 475010, microplate format, 96 well, Model 4303). Samples analyzed for fluoroquinolones were diluted with methanol by 10% prior to analyses. Detection limits ranged from 0.24 ng/L to 47 ng/L (Table 3.2).

Table 3.2. CECs analyzed and their mobility, solubility, and potential degradation pathways (Lapworth et al., 2012; Chemspider Database; Walters et al., 2010; Aris et al., 2014; Patel et al., 2019; Martínez-Hernández et al., 2014). Compounds that are less likely to degrade (e.g., via processes such as biodegradation, photolysis, volatilization) are considered persistent, such as carbamazepine and dioxins. Limit of detection (LOD) and limit of quantification (LOQ) are in ng/L.

CEC	Chemical Formula	Use	Mobility/ Solubility	Degradation Pathways	pKa	LOD (LOQ)
Carbamazepine	$C_{15}H_{12}N_2O$	Anti-convulsant	Immobile, insoluble	Resistant	14	10 (20)
Caffeine	$C_8H_{10}N_4O_2$	Lifestyle compound	Highly mobile, highly soluble	Biodegradable	6.1	47 (150)
Fluoroquinolones: Enrofloxacin Danofloxacin Ciprofloxacin	$C_{19}H_{22}FN_3O_3$ $C_{19}H_{20}FN_3O_3$ $C_{17}H_{18}FN_3O_3$	Antibiotic	Somewhat mobile, soluble	Highly photolytic	5.7-8.6	10 (16)
Ibuprofen	$C_{13}H_{18}O_2$	Anti-inflammatory, pain reliever	Highly mobile, highly soluble	Biodegradable	4.4	20 (132)
Sulfamethoxazole	$C_{10}H_{11}N_3O_3S$	Antibiotic	Mobile, insoluble	Highly photolytic	8.6	12 (29)
Dioxins: 2,3,7,8-TCDD 1,2,3,7,8-PnCDD	$C_{12}H_4Cl_4O_2$ $C_{12}H_3Cl_5O_2$	Combustion waste product	Immobile, insoluble	Resistant	6.8	0.24 (2.8)

Samples for DOC analysis were filtered through a Watman GF/F 0.7 μM filter into pre-combusted, acid washed borosilicate glass vials with Teflon caps and immediately spiked with 0.2 mL of 1 M H_3PO_4 and kept at 4 °C until analysis. DOC samples were analyzed at the National Marine Science Centre (Coffs Harbour) using an Aurora DOC analyzer.

3.3.1. Calculations

Apparent radium ages were calculated as proxies of water residence times. The apparent radium age (T_w), which refers to the average time since the sample left contact with sediments and the time of sampling, was estimated by calculating radium activity ratios (AR) (Moore, 2003; Charette et al., 2001):

$$T_w = \ln\left(\frac{AR_i}{AR_{obs}}\right) \times \left(\frac{1}{\lambda_S - \lambda_L}\right) \quad \text{Eq. 1}$$

where AR_i refers to the initial groundwater AR, AR_{obs} refers to the observed surface water sample AR, and λ_S and λ_L refer to the decay constants for the shorter- and longer-lived isotopes of radium, respectively. Radium AR were calculated for $^{224}Ra/^{223}Ra$ and $^{224}Ra/^{226}Ra$, with the assumption that radium is predominately supplied to the water column via SGD as previously demonstrated for Sydney Harbour (Correa et al., 2020). Radium is a well-established tracer for residence time (Moore, 2000; Moore et al., 2006; Knee et al., 2011) and previous studies have demonstrated reasonable agreement between hydrodynamic models and radium-derived ages (e.g., Rapaglia et al., 2010). Because the choice of groundwater endmember is considered the greatest source of uncertainty using this approach (Charette, et al., 2008), AR were calculated using the maximum groundwater endmember from each transect, resulting in the most conservative estimate for radium ages and SGD rates.

SGD fluxes (Q_{SGD}; m^3/d) were estimated using a steady-state box model (Appendix B: Figure S1), using an approach previously established by Moore (1996):

$$Q_{SGD} = \frac{\left(\left[\frac{(A - A_{ocn})}{T_w}\right] - \left[\phi D_S\left(\frac{\partial^2 A_{sed}}{\partial z^2_{sed}}\right)\right] - A\lambda\right) z_{wc}}{A_{gw}} \quad \text{Eq. 2}$$

where A is the measured radium activity (Bq/m^3), A_{ocn} represents ocean export (Bq/m^3), Tw is the apparent residence time (days), ϕ is the sediment porosity, Ds is the isotope diffusion coefficient (m^2/day), $\frac{\partial^2 A_{sed}}{\partial z^2 sed}$ represents radium diffusion from sediments (Correa et al., 2020), z_{wc} is the height of the water column (m), and A_{gw} is the radium activity of the groundwater end-member (Bq/m^3).

Pollution confidence levels were calculated to objectively assess whether anthropogenic pollution is present at a site and build comparisons across the different study sites (Abaya et al., 2018). This was done for each site by first taking the sum of normalized concentrations of carbamazepine, caffeine, sulfamethoxazole, ibuprofen, fluoroquinolones, dioxins, DOC, TDN, and TDP (after Abaya et al., 2018). Calculated pollution confidence levels were then normalized between 0 and 1. A confidence level of 0 indicates a low confidence and 1 high confidence of pollution by anthropogenic inputs. Additionally, risk quotients (RQ) were calculated using Equation 3:

$$RQ = \frac{Obs_{conc}}{PNEC} \quad \text{Eq. 3}$$

where Obs_{conc} refers to the observed CEC concentration in a sample and PNEC refers to the predicted no effect concentration. The RQ is a metric that is commonly used to assess the potential effect of a contaminant to the ecosystem (European Commission, 2003). The PNEC values are based off median lethal concentrations (LC50) or median effective concentrations (EC50). The LC50 value refers to point that the concentration of a substance leads to 50% of a community experiencing either mortality or suppression of functions (i.e., growth, reproduction; Ferrari et al., 2004). While PNEC values differ by species and environmental conditions, we opted for using the minimum PNEC in the literature following guidelines from the European Commission (Appendix B: Table S1; Mehrle et al., 1988; Ferrari et al., 2004; Han et al., 2006; Lin et al., 2008; Singer et al., 2019; European Commission, 2003).

In order to assess the role of SGD versus other sources, fluxes of CECs were calculated in two ways. First, the SGD-derived flux (Q_{SGD_CEC}) was obtained using Equation 4:

$$Q_{SGD\_CEC} = Q_{SGD} \times CEC_{gw} \quad \text{Eq. 4}$$

where CEC_{gw} refers to the maximum groundwater endmember concentration for each CEC at each site. Second, total CEC fluxes out of the embayment (Q_{Total_CEC}) were derived using Equation 5:

$$Q_{Total\_CEC} = \frac{CEC_{surf}}{T_w} \quad \text{Eq. 5}$$

where CEC_{surf} refers to surface water CEC concentrations in surface waters at each site. This approach provides confidence in the interpretation of sources and provides insight into the potential contribution of SGD to CEC exports from the marginal embayments to the main channel.

3.4 Results

Water quality parameters differed between surface and groundwater samples. Salinities ranged from 0.36 to 35.8 and 23.4 to 35.2 in groundwater and surface water, respectively (Appendix B: Table S2). Water temperature ranged from 13.9 to 20.6 °C, and pH from 6.59 to 8.29 in all samples (Appendix B: Table S2).

Radium concentrations varied between surface and groundwater samples and by location (Appendix B: Table S3; Figure 3.2). Radium was significantly higher in groundwater compared to surface water (Kruskal-Wallis Test; alpha = 0.05). Concentrations of ^{223}Ra ranged from 0.75 to 35 dpm/100 L and 0.56 to 8.6 dpm/100 L for groundwater and surface water, respectively, with the highest concentrations found in Hen and Chicken Bay. Similarly, ^{224}Ra concentrations ranged from 11 to 1,400 dpm/100 L in groundwater and 11 to 170 dpm/100 L in surface water samples. Rozelle Bay had the highest ^{224}Ra concentrations in groundwater samples (760 dpm/100 L), but the highest ^{224}Ra concentrations in surface water samples were found at Foreshore Beach and Watsons Bay (140 dpm/100 L). Concentrations of ^{226}Ra ranged from 10 to 130 dpm/100 L and 1.8 to 19 dpm/100 L in groundwater and surface water samples, respectively. The highest concentrations of ^{226}Ra were found in Rozelle Bay for groundwater samples and Watsons Bay for surface water samples.

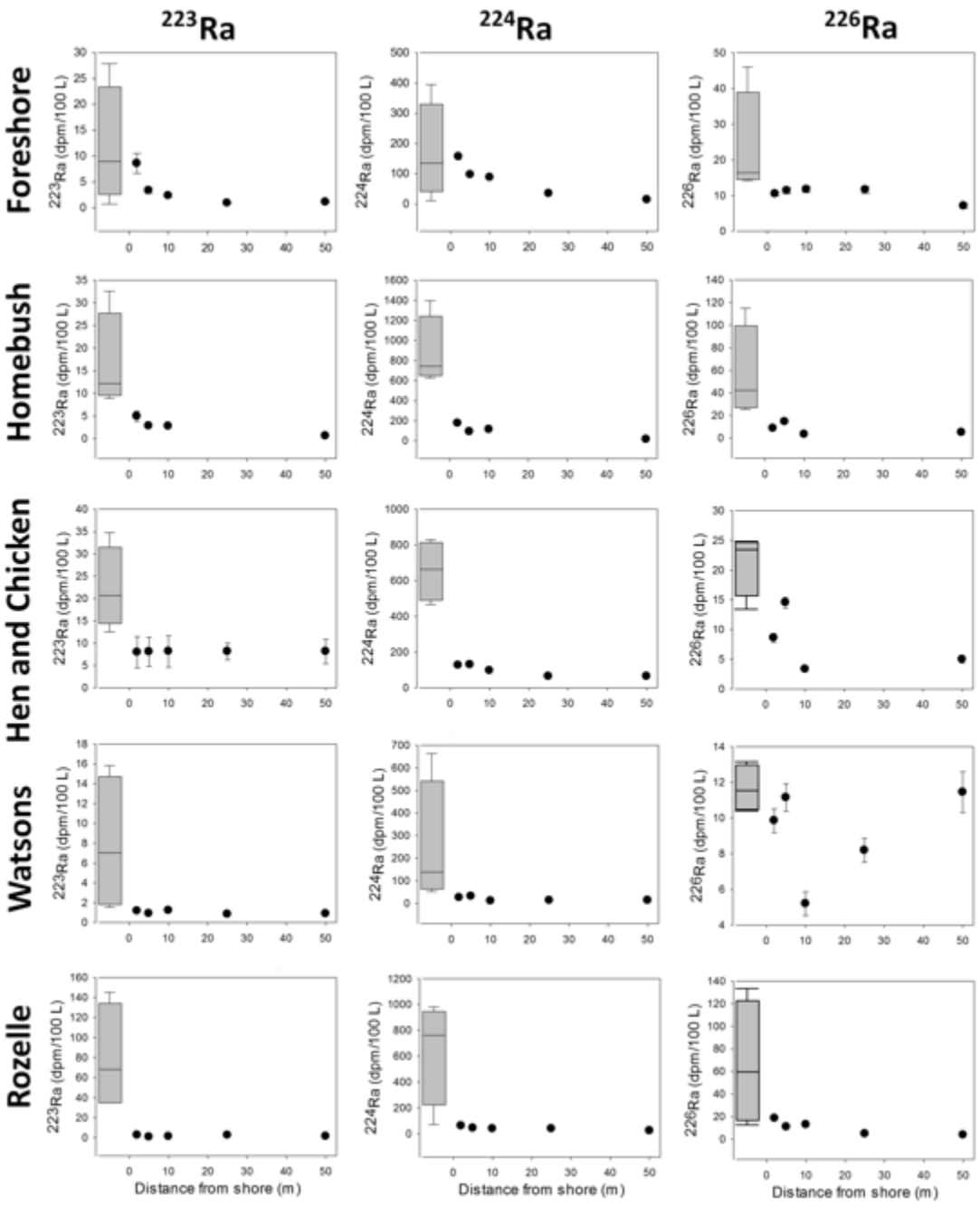

Fig 3.2. ^{223}Ra, ^{224}Ra, and ^{226}Ra transects by location showing radium (dpm/100 L) vs. distance from shore (m). The box plots show the distribution of radium in groundwater samples (n = 4 for each site).

Radium-derived apparent ages used as proxies for residence times (T_w) were estimated for each location. Median T_w based off of ^{224}Ra/^{223}Ra were the lowest at Foreshore Beach and Hen and Chicken Bay and the highest at Rozelle and Watsons Bays (Table 3.3). In comparison, median

T_w based off of $^{224}Ra/^{226}Ra$ were the lowest at Homebush Bay and the highest at Watsons Bay (Table 3.3).

Table 3.3. Median ± interquartile range (IQR) residence times (T_w; days) by location and activity ratio using the maximum endmember from each transect.

Location	T_w $^{224}Ra/^{223}Ra$ (days)	T_w $^{224}Ra/^{226}Ra$ (days)
Foreshore Beach (FS)	2.1 ± 0.44	6.6 ± 1.4
Homebush Bay (HB)	7.3 ± 1.4	1.5 ± 0.4
Hen and Chicken Bay (HC)	1.1 ± 0.30	14 ± 0.23
Rozelle Bay (ROZ)	11 ± 2.0	7.0 ± 4.0
Watsons Bay (WAT)	11 ± 1.4	17 ± 4.1

Using radium activities and residence times, SGD (m^3/day) and advection rates (cm/day) were estimated for each location (Table 3.4). Both SGD and advection rates were highest at Foreshore Beach and Hen and Chicken Bay, and lowest at Watsons Bay (Table 3.4). In addition, the $^{224}Ra/^{223}Ra$ – based residence time resulted in higher SGD compared to $^{224}Ra/^{226}Ra$ for all sites except Homebush Bay.

Table 3.4. Estimated SGD (10^{-2} m^3/day) and advection (cm/day) rates by location, residence time, and radium isotope. Uncertainties are propagated throughout the calculation of SGD.

Location	Tw	SGD (10^{-2} m^3/day)			Advection (cm/day)		
		^{223}Ra	^{224}Ra	^{226}Ra	^{223}Ra	^{224}Ra	^{226}Ra
FS	224/223	8.9 ± 0.67	32 ± 2.4	20 ± 10	1.0 ± 0.065	3.3 ± 0.13	1.7 ± 0.28
	224/226	14 ± 7.1	20 ± 9.3	3.9 ± 1.8	3.5 ± 1.8	4.8 ± 2.3	0.92 ± 0.44
HB	224/223	0.59 ± 0.11	0.88 ± 0.083	0.21 ± 0.019	0.11 ± 0.026	0.16 ± 0.018	0.038 ± 0.0040
	224/226	6.6 ± 2.6	6.5 ± 2.3	4.5 ± 2.4	0.96 ± 0.37	0.92 ± 0.30	0.76 ± 0.39
HC	224/223	2.6 ± 0.98	5.1 ± 1.7	9.5 ± 1.4	0.46 ± 0.17	0.90 ± 0.29	1.5 ± 0.29
	224/226	1.5 ± 0.87	2.7 ± 1.4	0.70 ± 0.067	0.24 ± 0.15	0.46 ± 0.24	0.098 ± 0.012
ROZ	224/223	0.35 ± 0.10	0.51 ± 0.28	0.32 ± 0.21	0.045 ± 0.017	0.075 ± 0.054	0.0057 ± 0.0042
	224/226	0.28 ± 0.16	1.0 ± 0.51	2.6 ± 1.3	0.033 ± 0.027	0.17 ± 0.085	0.44 ± 0.22
WAT	224/223	0.23 ± 0.031	0.36 ± 0.015	2.0 ± 0.27	0.032 ± 0.0050	0.056 ± 0.0027	0.29 ± 0.045
	224/226	0.021 ± 0.0040	0.027 ± 0.0024	0.87 ± 0.12	0.0043 ± 0.00073	0.0060 ± 0.00046	0.11 ± 0.019

Concentrations of TDN, TDP, and DOC (Appendix B: Table S4, Figure S2) were significantly higher in groundwater than surface water samples (Kruskal Wallis test; alpha = 0.05). Median concentrations of TDN were the highest in Foreshore Beach groundwater samples (290 μM) and the lowest in Watsons Bay surface water samples (14 μM). Watsons Bay groundwater samples had the highest median TDP concentrations (4.5 μM), with the lowest found in Rozelle Bay groundwater (0.34 μM). Median DOC concentrations were the highest in Watsons Bay groundwater samples (720 μM) but the lowest in Watsons Bay surface water samples (51 μM).

Concentrations and detection frequencies of CECs varied amongst compound and sampling site (Figure 3.3; Figure 3.4; Appendix B: Table S5). Only caffeine was significantly different between groundwater and surface water samples (Kruskal Wallis test, alpha = 0.05). Detection frequencies ranged from 18 to 100%, with caffeine, carbamazepine, and dioxins detection frequencies exceeding 90%. Median carbamazepine concentrations were highest in Homebush Bay groundwater (160 ng/L) and Hen and Chicken Bay surface water (81 ng/L). Both dioxins and fluoroquinolones median concentrations were the highest in groundwater (17 and 15 ng/L, respectively) and surface water (19 and 14 ng/L, respectively) at Rozelle Bay. Median caffeine concentrations were also the highest in Rozelle Bay groundwater (340 ng/L), but the highest in Hen and Chicken Bay surface water (910 ng/L). In groundwater samples, median sulfamethoxazole concentrations were highest in Homebush Bay (78 ng/L). In surface water samples median sulfamethoxazole concentrations were highest in Watsons Bay surface water (14 ng/L). Ibuprofen was primarily detected at Rozelle Bay, with median concentrations of 80 and 150 ng/L for groundwater and surface water, respectively.

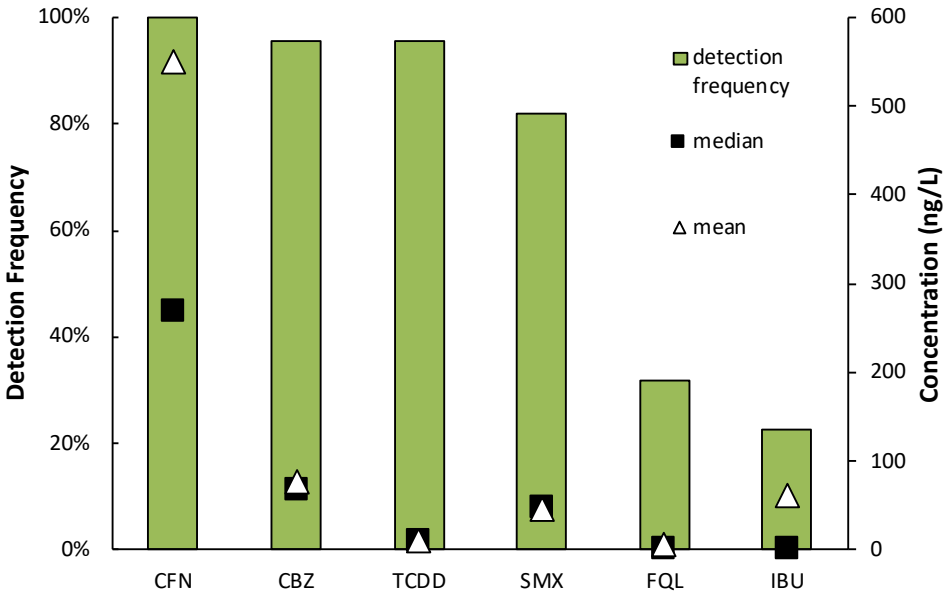

Fig 3.3. Detection frequency of CECs analyzed for both surface water and groundwater samples. The black squares and white triangles indicate the median and mean concentration, respectively. Caffeine (CFN), carbamazepine (CBZ), dioxins (TCDD), and sulfamethoxazole (SMX) had a detection frequency >82%. Fluoroquinolones (FQL) and ibuprofen (IBU) were the least frequently detected, with detection frequencies of 32% and 25%, respectively.

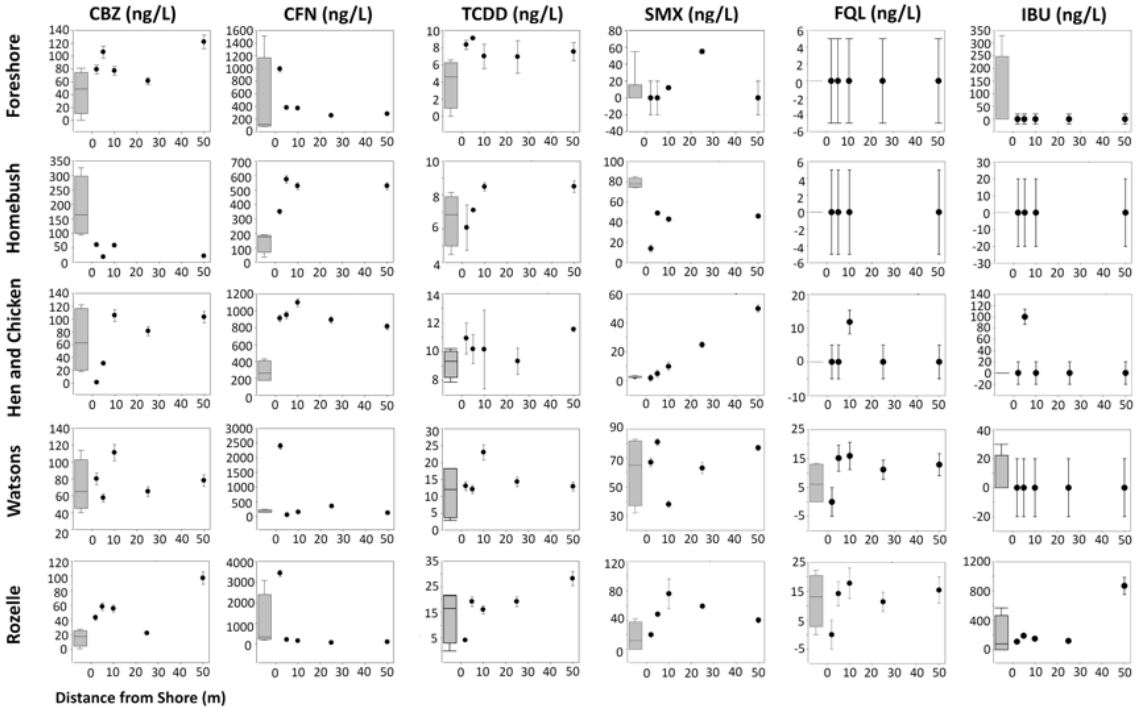

Fig 3.4. Transects of CECs (all in ng/L) by sampling site with respect to distance from the shore (m). Groundwater samples (n = 4 per site) are represented by the boxplots and surface water samples by the scatter plot.

3.5 Discussion

3.5.1 Groundwater discharge

Radium transects provide evidence for SGD into the five embayments. Foreshore Beach and Homebush Bay exhibited similar trends with steeper decrease in radium activities offshore. In contrast, Hen and Chicken, Watsons, and Rozelle Bays showed little spatial change in surface water radium concentrations, implying faster flushing. Radium-derived apparent ages were longest at Watsons and Rozelle Bays (Table 3.3). The method used to calculate apparent radium ages cannot accurately resolve residence times shorter than 3.5 days for $^{224}Ra/^{223}Ra$ (Knee et al., 2011), which seem to apply to Foreshore Beach and Hen and Chicken Bay. Median residence times calculated using $^{224}Ra/^{223}Ra$ were shorter for Foreshore Beach, Hen and Chicken and Watsons Bays than those calculated using $^{224}Ra/^{226}Ra$, suggesting that there may be multiple sources of groundwater to these sites. The groundwater endmember has inherent uncertainties. More specifically, the shorter half-lives of ^{224}Ra and ^{223}Ra compared to ^{226}Ra mean that additional ^{224}Ra and ^{223}Ra may be generated from thorium when considering the time scale (days to weeks). The short-lived radium isotopes can also be influenced by processes such as sediment desorption, diffusion, and bioturbation, which don't affect ^{226}Ra (Tamborski et al., 2020).

SGD is an important source of water to Sydney Estuary on the small scale (50 m shore-perpendicular transects) covered by this study. Foreshore Beach had the greatest SGD, with average discharge ranging from 13 to 20 x 10^{-2} m^3/day (2.0 to 3.1 cm/day). Watsons Bay had the lowest SGD, with averages ranging from 0.31 to 0.87 x 10^{-2} m^3/day, or 0.04 to 0.12 cm/day. Homebush Bay had average advection rates (0.10 to 0.88 cm/day) comparable to those previously found (0.4 cm/day) in the same location (Correa et al., 2020). Similarly, our average estimated nearshore advection rates for Hen and Chicken Bay (0.27 to 0.96 cm/day) were similar to the average (1.0 cm/day) estimated by Correa et al. (2020). Advection rates for Rozelle Bay (0.06 to 0.21 cm/day) were one to two orders of magnitude lower than previously estimates (2.2 cm/day) by Correa et al., 2020, which may reflect differences in sampling scales (nearshore versus bay scale), choice of radium ratios, and/or temporal variations.

3.5.2 CECs

The main drivers of CEC detection frequency appear to be degree of persistence and frequency of usage (Figure 3.3; Table 3.2). Caffeine was the most frequently detected (100% detection frequency) and also had the highest median concentration (270 ng/L), likely due to its widespread consumption (Buerge et al., 2003) and greater consumption coothan the other compounds (prescription and over the counter drugs, industrial chemicals). Average caffeine consumption per day in Australia is over 170 mg (Australian Bureau of Statistics, 2015) and it is considered the most widely consumed drug worldwide (Benowitz, 1990). The detection frequency and concentrations (37 to 3,020 ng/L) observed in Sydney are comparable other water bodies globally, such as Boston Harbor, USA (100% detection frequency, concentrations ranging from 140 to 1,600 ng/L; Siegener & Chen, 2002) and in the La Jalle (France) and Lopan (Ukraine) Rivers (100% detection frequency, concentrations ranging from 40 to 70 ng/L; Vystavna et al., 2012). In the Baltic Sea, caffeine concentrations in SGD reached 1528 ng/L with a 43% detection frequency (Szymczycha et al., 2020). We did not find a direct correlation between embayment population density and caffeine concentrations. Sydney has a high population density overall, so it is difficult to resolve on the embayment scale.

Carbamazepine and dioxins were the second most detected (both had a 95% detection frequency) with median concentrations of 67 and 9.1 ng/L, respectively. Both compounds do not easily degrade in the environment (Table 3.2). Carbamazepine concentrations measured in this study (<326 ng/L) are consistent with a range (5 to 680 ng/L) typical of marine waters (Nödler et al., 2014) and with those measured (5.6 to 200 ng/L; 95% detection frequency) in the River Thames, United Kingdom (White et al., 2019). Carbamazepine in Sydney was detected more frequently and in higher concentrations than in the Baltic Sea where the detection frequency was <10% and concentrations reached 41 ng/L (Szymczycha et al., 2020). Additionally, carbamazepine in was also significantly higher than previously documented in surface waters in Sydney Harbour (10% detection frequency; concentrations <2.7 ng/L; Birch et al., 2015). The substantial differences in both detection frequency and concentration may be attributed to differences in sampling locations and proximity to shore.

The remaining CECs had detection frequencies ranging from 25 to 82%. Both sulfamethoxazole (detection frequency = 82%; median concentration = 49 ng/L) and fluoroquinolones (detection frequency = 32%; median concentration = 0 ng/L) are highly

photolytic compounds, but the differences in detection frequency are likely because sulfamethoxazole is more mobile (Table 3.2). Our detection frequency for sulfamethoxazole was similar to that found for the River Thames (76%; White et al., 2019), but greater than found in SGD in the Baltic Sea (less than 10%; Szymczycha et al., 2020). Differences in shoreline morphology may also influence the higher CEC concentrations. The Bay of Puck in the Baltic Sea has an open shoreline compared to the Sydney embayments (Szymczycha et al., 2020). This likely leads to shorter water residence times and thus dilution of CEC concentrations. Ibuprofen, a highly biodegradable compound, had the lowest detection frequency (25%). Birch et al., (2015) also measured sulfamethoxazole, caffeine, ciprofloxacin (a fluoroquinolone), and ibuprofen in Sydney Harbour, but all were below detection for all sites. Concentrations of CECs can decrease through microbial processes, adsorption to sediment, photolysis, or dilution. Lower CEC concentrations in surface waters than groundwater, and sites with decreasing concentrations offshore (Foreshore Beach, Homebush Bay, and Rozelle Bay) imply attenuation or dilution.

Physiochemical parameters such as pH and salinity can also influence CEC distribution. A positive relationship was observed between CEC concentrations and salinity in both groundwater and surface water samples (Appendix B: Figure S3). Possible explanations include increased dissolution of CECs at higher salinities (Patel et al., 2019) or inputs from other water sources. Sorption to colloids (particles ranging from 1 to 1000 nm in size) or suspended sediments may also influence concentrations of dissolved CECs (Bagnis et al., 2018). Colloids can act as an intermediary phase for CECs between soils and solution (Xing et al., 2015). While the interaction between CECs and colloids is not well understood, higher soil adsorption coefficients (Koc) for CECs bound to colloids in seawater compared to freshwater have been observed (Bagnis et al., 2018). Therefore, a greater proportion of CECs may be colloid bound at higher salinities, potentially creating some false negatives in this study. A relationship between decreasing carbamazepine concentrations and increasing water pH (more basic) was also observed (Appendix B: Figure S4). This is likely not directly related to pH specifically, as the pKa of carbamazepine is 13.9 (Table 3.2). More likely, this relationship reflects differences in microbial activities or conditions that promote carbamazepine desorption. No correlation was observed between temperature and dissolved oxygen with any CECs in this study.

This comparison to other sites and to previous studies within Sydney Harbor highlights the importance of targeted sampling. Previous studies did not focus on nearshore environments where

SGD inputs are most obvious and may have overlooked SGD as a pathway. At the same time, SGD may be important only on nearshore scales and do not affect CEC inventories on a bay-wide scale. As demonstrated by our observations, SGD was a source of CECs to coastal waters in the Sydney area.

3.5.3 Pollution

Pollution confidence levels were calculated by factoring all measured potential sources of pollution to each site. Higher confidence levels were largely driven by high CEC concentrations rather than the total number of compounds present. Relative pollution increased with residence time - Watsons Bay had the highest median pollution confidence levels for surface waters (median = 0.67, ranging from 0.58 to 0.70) and the longest residence times, and Foreshore Beach had the lowest pollution confidence levels (median = 0.14, ranging from 0.12 to 0.32) and the shortest residence times (Figure 3.5; Table 3.3). Application of Mood's median test (alpha = 0.05) revealed longer residence times (Figure 3.5; Table 3.3) at Watsons and Rozelle Bays resulting in higher concentrations of CECs and nutrients in surface waters. Because Watsons Bay is a residential area with an adjacent boat harbor, it is not surprising that it had the highest pollution confidence levels in surface waters. Groundwater pollution confidence levels for Watsons Bay were not as high (median = 0.47, ranging from 0.44 to 0.53); supporting that groundwater is not the only local source of pollution.

In contrast, Rozelle Bay, which is subject to both urban and industrial sources, had high pollution confidence levels in both surface water (median = 0.63, ranging from 0.54 to 0.98) and groundwater (median = 0.47, ranging from 0.29 to 1.0). Hen and Chicken Bay had similar pollution confidence levels between surface water and groundwater and may be subject to wastewater input from leaking sewers due to surrounding residential land use. While Homebush Bay had lower surface water pollution confidence levels (median = 0.26, ranging from 0.13 to 0.29), it had the highest groundwater pollution confidence levels (median = 0.56, ranging from 0.47 to 0.74). Sediment pollution from previous industrial land use in Homebush Bay has been well documented (Suh et al., 2004) and may explain the discrepancy between ground and surface water quality.

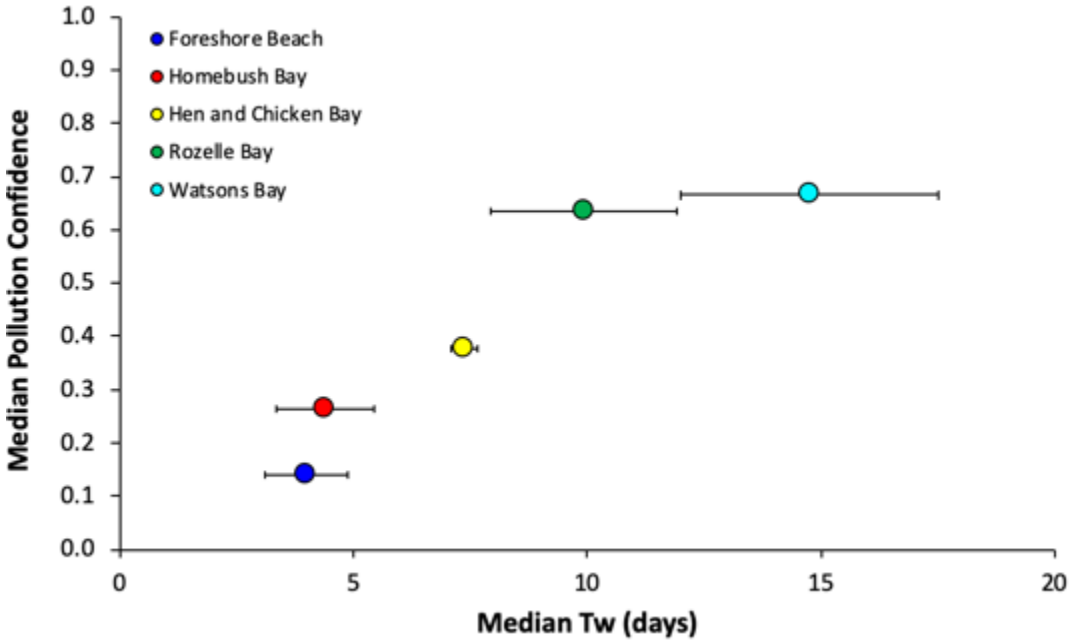

Fig 3.5. Pollution confidence levels by location, residence time, and distance from shore. Median surface water confidence levels by the median radium ($^{224}Ra/^{223}Ra$ and $^{224}Ra/^{226}Ra$) apparent residence time (days) ± IQR by location.

Despite receiving attention for frequent water quality issues related to sewage input from the adjacent Mill Stream and proximity to the Botany groundwater plume (NSW Office of Environment and Heritage, 2018), Foreshore Beach had the lowest pollution confidence levels for both surface water (median = 0.14, ranging from 0.12 to 0.32) and groundwater (median = 0.17, ranging from 0 to 0.71). This may result from faster flushing or dilution into a larger volume of water. The relationship between CEC concentrations and radium-derived residence times (application of Mood's median test with alpha = 0.05 confirmed statistically differentiable distributions) imply that any CECs will remain in the embayment for longer periods of time. A similar relationship between residence time and nutrients, metals, and organic compounds have been observed in other environments (e.g., Jickells, 1998; Davis, 1993; Freeze & Cherry, 1982).

We conducted an environmental risk assessment by calculating risk quotients based off observed detectable CEC concentrations in surface water and PNECs (Figure 3.6). Following Hernando et al. (2006), we ranked each RQ as low risk (0.01 – 0.1), medium risk (0.1 – 1.0), and high risk (> 1.0). Both dioxins and ibuprofen pose a high risk to the ecosystem with RQ values exceeding 1.0 for all samples even in the low concentrations found in this study, ranging from 2.3 to 16 and 1.0 to 8.7, respectively. While dioxins have been well documented health risks to both

human and animal health (Mehrle et al., 1988), previous studies have also highlighted the high risk that ibuprofen poses to ecosystems (e.g., Mendoza et al., 2015; Verlicchi et al., 2012), supporting our findings. Other CECs measured in this study posed no to medium risk. Fluoroquinolones (RQ ranging 0.17-0.28) and sulfamethoxazole (RQ ranging 0.02-0.14) indicate low to medium risk. Carbamazepine and caffeine pose negligible to low risk, with RQ values ranging from 0.01 to 0.05 and 3.7×10^{-6} - 3.4×10^{-4}, respectively.

Examples of the threats CECs may pose to marine life include disruption to reproductive cycles or feeding rate, inhibition of growth, or even premature mortality (Brodin et al., 2014; Backhaus, 2014). These impacts as a whole indirectly can for instance lead to changes in community structure, migration patterns, or trophic cascades (Brodin et al., 2014). The calculation of RQ only considers risk for a single compound and doesn't account for mixtures of CECs, which frequently present a significantly greater ecotoxicological risk (Backhaus, 2014). Importantly, while storm runoff and storm-related sewer overflows represent episodic inputs of CECs, tidally driven SGD is expected to be present year-round and can expose coastal ecosystems to pollution by pharmaceuticals and industrial compounds.

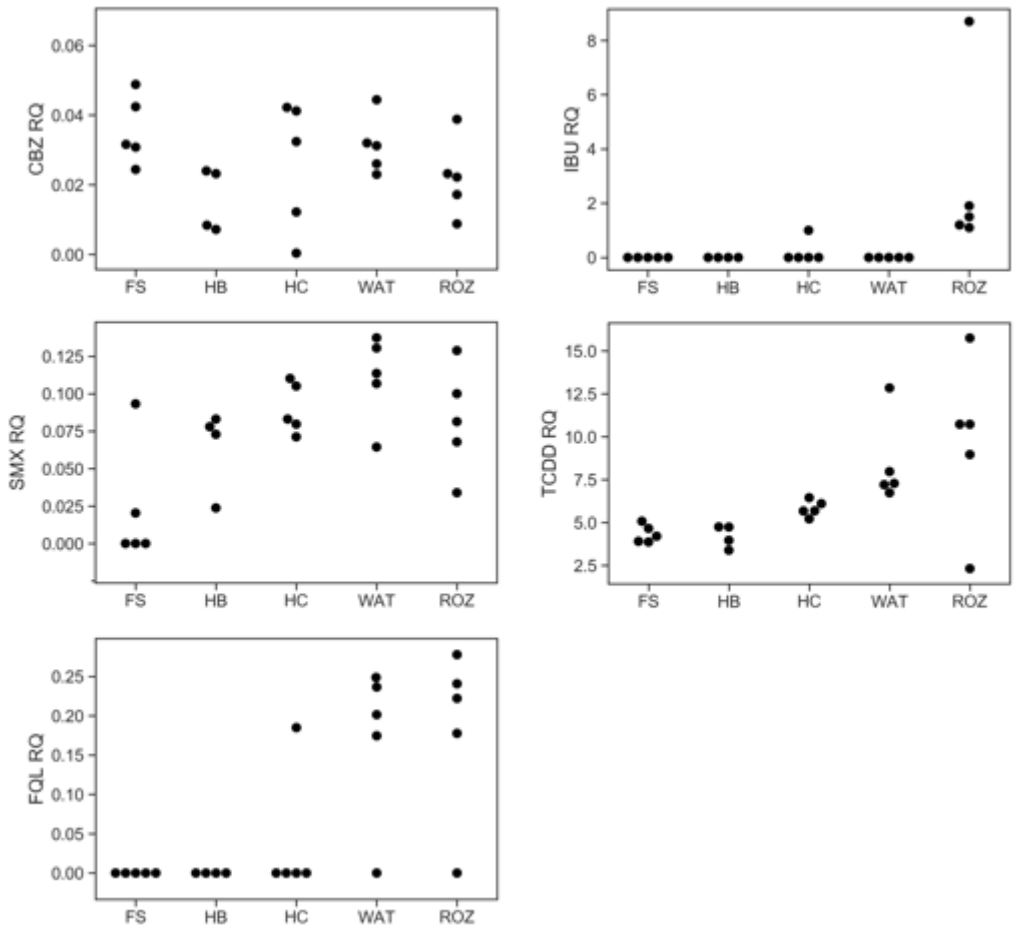

Fig 3.6. Risk quotients for all surface water samples by location and CEC compound.

3.5.4 SGD-derived CEC fluxes

In absence of major surface discharge, there are two primary pathways for CECs to enter the bays: SGD or mixing with the open harbor where sources may be outfalls or wastewater released from boats. In this study, SGD rates were estimated using radium isotopes, and harbor input is inferred from trends of CECs in surface water samples. Higher concentrations of CECs observed away from the shore would indicate inputs from the harbor. This was observed in all sampling sites for at least one compound, implying sources other than SGD, such as mixing with water from outside the embayment.

We calculated both total CEC fluxes within embayments and SGD-derived CEC fluxes to determine the proportion that SGD contributes CECs to each embayment (Equations 4 and 5). Total CEC fluxes using results from the $^{224}Ra/^{223}Ra$ residence time ranged from 0.057 to 290 μg/day (Table 3.5). In comparison, SGD-derived fluxes using the results from the $^{224}Ra/^{223}Ra$

residence time resulted in CEC fluxes ranging from 0.048 to 130 μg/day for ^{223}Ra (Table 3.5), 0.068 to 490 μg/day for ^{224}Ra, and 0.017 to 300 μg/day for ^{226}Ra. Foreshore Beach received the largest SGD-derived carbamazepine, caffeine, ibuprofen, and dioxins fluxes (Table 3.5). Foreshore Beach also had the largest percentage of caffeine (46 to >100%) and ibuprofen (100%) discharged via SGD. Despite having some of the highest CEC fluxes, pollution confidence levels were low for Foreshore Beach due to its short residence time (Figure 3.5). Hen and Chicken Bay had the highest sulfamethoxazole flux (2.2 to 7.9 μg/day) and the highest proportion of SGD-derived sulfamethoxazole (24 to 87%). While all CEC fluxes were relatively low for Homebush Bay, this location had a higher percentage of carbamazepine (64 to 95%) delivered via SGD (Table 3.5), which may be due to retention of carbamazepine in local mangroves (Bayen, 2012). Overall, Watsons Bay had the lowest proportion of SGD-derived CEC fluxes to the total flux, likely due to the long residence times.

Table 3.5. Total CEC fluxes and SGD-derived fluxes in μg/day. Total fluxes are based off the $^{224}Ra/^{223}Ra$ residence time and surface water CEC concentrations. SGD-derived fluxes are calculated using SGD results for ^{223}Ra and $^{224}Ra/^{223}Ra$ residence time by location and ranges in percentage that SGD contributes of each CEC to the total CEC flux. For SGD fluxes, the ^{223}Ra and $^{224}Ra/^{223}Ra$ residence time was used because it provided the most conservative estimates of the SGD-derived CEC flux. For the percentage SGD of total flux, the range represents results using ^{223}Ra, ^{224}Ra, and ^{226}Ra and $^{224}Ra/^{223}Ra$ residence time.

Location		CBZ	CFN	SMX	FQL	IBU	TCDD
FS	Total (μg/day)	68 ± 41	290 ± 170	35 ± 31	< LOD	< LOD	6.8 ± 4.4
	SGD (μg/day)	7.2 ± 4.5	130 ± 73	1.7 ± 0.92	< LOD	290 ± 20	6.8 ± 0.37
	% SGD	11 - 38%	46 - >100%	4.9 - 18%	< LOD	100%	8.6 - 31%
HB	Total (μg/day)	3.0 ± 0.55	64 ± 10	5.6 ± 0.88	< LOD	< LOD	1.0 ± 1.6
	SGD (μg/day)	1.9± 1.7	1.1 ± 0.93	0.50 ± 0.42	< LOD	< LOD	1.0 ± 0.039
	% SGD	64 - 95%	0.61 – 2.6	3.2 - 13%	< LOD	< LOD	1.6 – 6.9%
HC	Total (μg/day)	14 ± 4.4	150 ± 58	9.0 ± 3.2	0.057 ± 0.023	2.6 ± 2.6	1.8 ± 0.68
	SGD (μg/day)	3.2 ± 1.1	110 ± 3.8	2.2 ± 0.72	< LOD	< LOD	1.8 ± 0.097
	% SGD	22 - 82%	7.3 - 26%	24-87%	< LOD	< LOD	15 - 53%
ROZ	Total (μg/day)	19 ± 3.2	24 ± 3.9	9.4 ± 1.7	3.2 ± 1.1	160 ± 32	5.7 ± 1.0
	SGD (μg/day)	0.34 ± 0.26	7.2 ±5.1	0.099 ± 0.26	0.052 ± 1.9	1.3 ± 0.26	5.7 ± 0.039
	% SGD	1.8 - 16%	30 - >100%	1.1-9.1%	1.6 - 14%	0.83-7.2%	0.89 - 7.7%
WAT	Total (μg/day)	8.1 ± 1.3	21 ± 2.9	7.8 ± 1.1	1.4 ± 0.44	< LOD	1.5 ± 0.24
	SGD (μg/day)	0.40 ± 0.37	0.84 ± 0.74	0.29 ± 0.25	0.046 ± 0.052	0.10 ± 0.10	1.5 ± 0.060
	% SGD	4.9 – 7.1%	3.7 - 5.9%	3.4 – 5.4%	3.2 – 5.0%	0%	4.1 – 6.4%

For most CECs in the studied embayments, the SGD-derived CEC flux was lower than the total observed flux potentially due to unquantified surface water sources, uncertainties in the groundwater endmembers, and CEC complex chemistry. Many CECs have higher adsorption-desorption distribution coefficients (Kd) in fresh or brackish water. This would cause an additional release of CECs in the subterranean estuary resulting in higher surface water concentrations compared to groundwater. While the estimated contribution of CECs via SGD to each embayment may be low, the results still show that SGD releases these compounds to the coastal ocean.

To date, few studies have been published on CECs in SGD (e.g., Szymczycha et al., 2020; Welch et al., 2019), despite the fact that SGD can be a major term in regional water, nutrient, and trace metal coastal budgets (e.g., Luijendijk et al., 2020; Valiela et al., 1990; Dulai et al., 2016). Urban estuaries such as Sydney Harbour are frequently polluted from a mixture of sewage, industrial, and agricultural sources and CECs offer a means to assess other pollutant origins (Birch & Taylor, 2000; Feng et al., 1998; Yang et al., 2011). This study demonstrates the importance of considering SGD as a pathway for CECs, in addition to nutrients and DOC, to coastal waters. The positive association between residence time and CEC inventories reveal that tidal flushing and mixing lead to effective reduction of coastal CEC inventories. Mixing may also mask significant CEC inputs at the coastline. Additionally, this research conveys the need for increased monitoring of CECs, particularly in urban areas.

3.6 Conclusion

We investigated SGD as a pathway for wastewater and industrial pollution and assessed drivers of CECs in coastal waters around Sydney. Overall, we found caffeine, carbamazepine, and dioxins with a detection frequency exceeding 90%. While we did not link CEC concentrations to population density, we did find a positive relationship between longer residence times and CECs. Two (ibuprofen and dioxins) out of six compounds were observed in concentrations that pose a high risk to the ecosystem. Despite many CECs' strong sorption and biodegradation characteristics, SGD can be an alternative, viable pathway for their release into coastal water bodies.

Chapter 4: Tidally-driven groundwater inundation of wastewater infrastructure observed during higher tides

In submission with co-authors: McKenzie, T.**,** Habel, S., Dulai, H.

Abstract: Sea-level rise (SLR) is expected to compromise coastal wastewater infrastructure (WIS) via groundwater inundation (GWI). We conducted a field-based study in urban Honolulu, Hawai‘i using spring tides as a proxy for future sea levels, to quantify the hydrologic connection of WIS. This study focused on two possible pathways: 1) direct GWI of WIS and subsequent discharge into the coastal ocean and 2) indirect inundation of WIS evidenced in storm drains. We used geochemical tracers and contaminants of emerging concern (CECs) to monitor groundwater discharge and wastewater fluxes. CEC fluxes increased at high tide for coastal sites. In comparison, CEC concentrations decreased at high tide in storm drains, reflecting dilution of leakage from sewer pipes by increasing groundwater levels. This study presents some of the first field-based evidence for GWI of coastal WIS and demonstrates that SLR is creating new wastewater pathways posing a direct risk to environmental and human health.

4.1 Introduction

Sea-level rise (SLR) is expected to increase 0.3 to 1 m by 2100, with less conservative estimates ranging up to 2 m or greater (Wong et al., 2014; Sweet et al., 2017). Perigean spring (or king) tides provide an early glimpse of negative SLR impacts, such as flooding, beach erosion, and water quality degradation (Thompson et al., 2019; Sweet et al., 2020). While most studies addressing SLR impacts have focused on surface flooding and seawater intrusion, a few recent studies have highlighted the effects of groundwater inundation (GWI) (e.g. Habel et al., 2017; Elmir, 2018; Befus et al., 2020). For example, as the water table rises with SLR (Rotzoll & Fletcher, 2012), it potentially leads to GWI of wastewater infrastructure (WIS), such as sewage pipes or onsite sewage disposal systems (OSDS) (Habel et al., 2017), decreasing treatment efficacy. WIS are already in critical decline in many areas – for instance, an estimated 23% of sewer lines in the U.S. are currently leaking (USEPA, 2002). A frequently used alternative to municipal wastewater treatment, OSDS (e.g. septic tanks, cesspools), are also a common groundwater contaminant source in Hawai‘i (Whittier and El-Kadi, 2009). It is expected that the frequency of wastewater-

related water quality problems will increase with SLR as infrastructure becomes progressively more inundated.

Groundwater fluctuates with sea level in coastal areas, where the water table is frequently at or above mean sea level (Rotzoll & Fletcher, 2012). This hydrologic connection serves a double role, causing water table uplift resulting in inundation of and leakage from WIS while also facilitating discharge of released wastewater contaminants as water drains back into the ocean. Submarine groundwater discharge (SGD) refers to groundwater that discharges to the coastal ocean and can be a major source of excess nutrients, metals, and contaminants of emerging concern (CECs; e.g. pharmaceuticals, pesticides) to coastal water bodies (e.g. Luijendijk et al., 2020; Moore, 2010; Szymczycha et al., 2020; McKenzie et al., 2020). Total SGD is comprised of both saline and fresh terrestrial/meteoric groundwater. Fresh SGD is primarily driven by the hydraulic gradient and is typically highest at low tide. Tidal pumping, a significant component of saline SGD, adds water to the aquifer during high tide and then partially drains to the ocean during low tide (Michael et al., 2005; Kim & Hwang, 2002; Santos et al., 2009). Tidal pumping under SLR will lead to decreased efficacy of deficient WIS in locations where the coastal vadose zone becomes inundated, due to the loss of filtration within the unsaturated zone.

While models can capture WIS inundation under future SLR (Rotzoll & Fletcher, 2012), this is the first field-based geochemical study documenting SLR-driven GWI impact on coastal WIS. The overarching hypotheses for this study are (1) spring tides act as a proxy for future SLR conditions, where WIS inundation leads to subsequent wastewater discharge to storm drains and the coastal ocean, and (2) GWI of WIS and subsequent discharge to storm drains and the coastal ocean can be evidenced by a combination of SGD and wastewater tracers. Two pathways for SLR to impact water quality via GWI were evaluated at two model sites in Honolulu, Hawai‘i: (1) direct inundation of coastal WIS affected by tidal pumping and resulting discharge as SGD and (2) storm drain backflow through inundation of coastal storm drains (Figure 4.1).

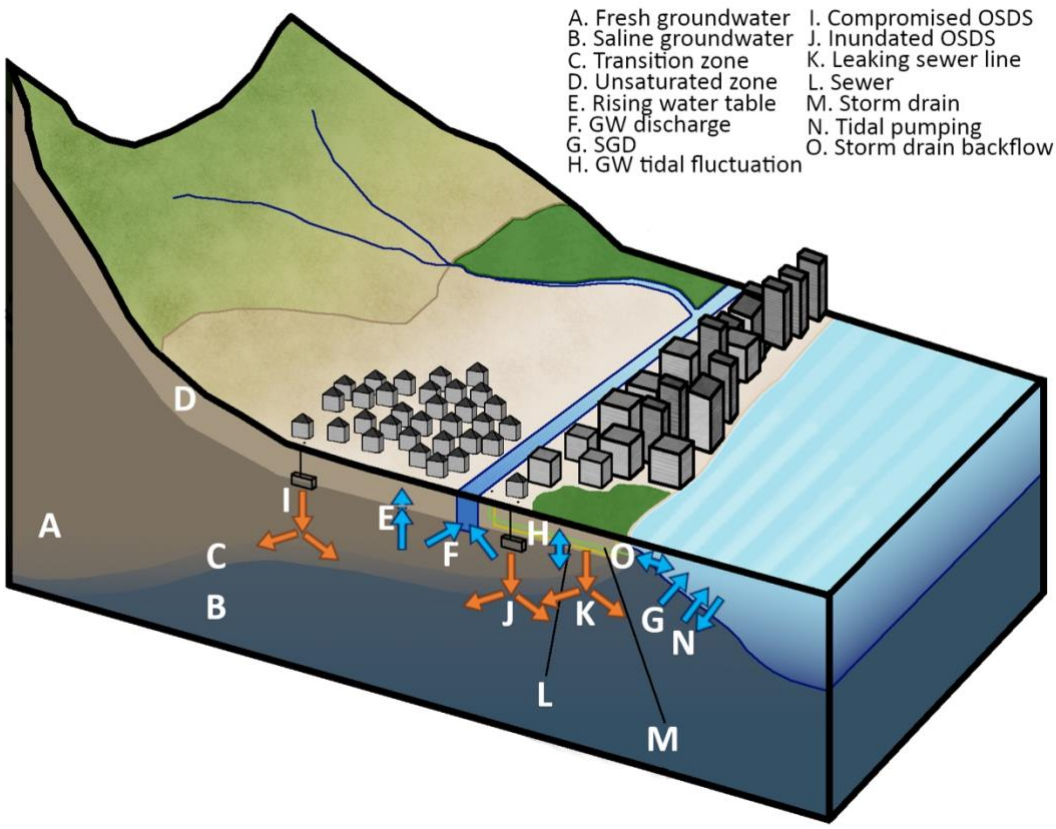

Figure 4.1. Connection between groundwater, surface water, storm drains, and WIS. Wastewater flow is indicated by orange arrows and groundwater flow by blue arrows. This study aims to investigate how groundwater and wastewater flow are linked to one another at higher water levels during spring tides.

4.2 Methods

4.2.1 Study Site

This study was conducted in two low-lying urban districts of Honolulu, Hawai‘i (Māpunapuna and Waikīkī) (Figure 4.2; Appendix C: Table S1; Appendix C-1). Waikīkī, a popular tourist destination, was marshland prior to construction of the Ala Wai Canal and addition of anthropogenic fill (Wiegel, 2008). The Ala Wai Canal is tidally influenced, receives stream input from Mānoa-Palolo and Makiki Streams, and is chronically polluted, in part because of poor circulation and retention of stream pollution (USEPA, https://mywaterway.epa.gov/waterbody-report/21HI/HIW00034/2018, last accessed July 15, 2020). Water residence times within the canal are poorly constrained but range from a few hours to >8 days (Gonzalez, 1971). Māpunapuna is an industrial district located within 0.5 km from the coast, bordered by the Daniel K. Inouye International Airport and Kahauiki Stream. The area is subject to frequent nuisance flooding

during high tides or heavy rainfall due to storm drain backflow of ocean water from Keʻehi Lagoon (Habel et al., 2020).

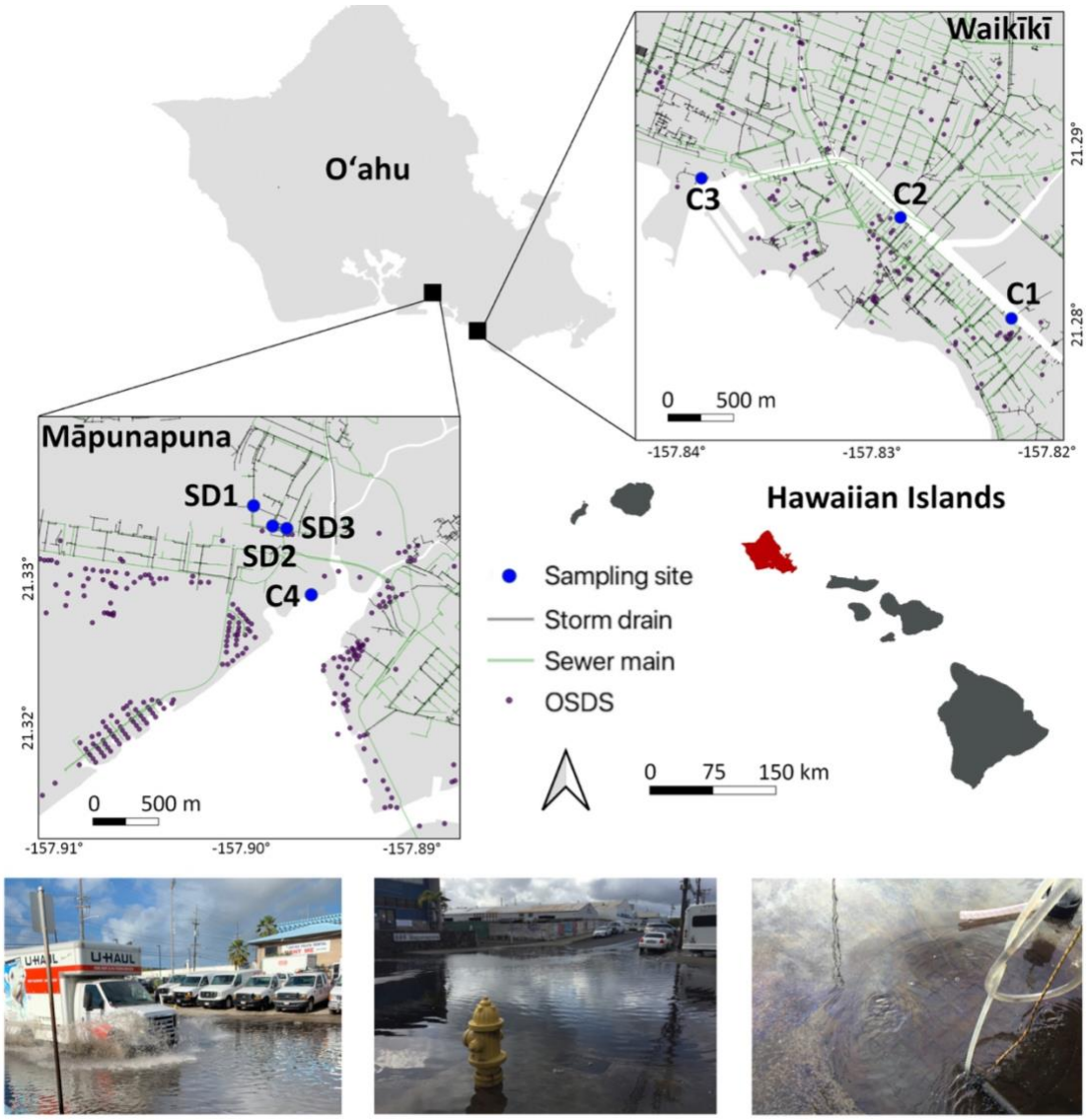

Figure 4.2. Locations of study sites on the island of Oʻahu. Waikīkī and Māpunapuna are districts within Honolulu. Sampling sites are indicated with a larger blue dot, OSDS with a smaller purple dot, and the storm drain and sewer mains are shown with black and green lines, respectively. Photos show high tide nuisance flooding in Māpunapuna at sites SD1 and SD2.

SLR is anticipated to result in both rising coastal waters and GWI in Waikīkī and Māpunapuna due to narrow unsaturated spaces and proximity to the coastline (Habel et al., 2017; Habel et al., 2020). The Honolulu tide gage record (NOAA; station ID: 1612340) has a semi-diurnal range of 0.58 m with a 1.51 ± 0.21 mm/year (30-year average) rate of SLR. Models show that nuisance flooding can occur when tides exceed 0.20 – 0.35 m above the mean higher high water (MHHW) datum (Sweet et al., 2014; Habel et al., 2020).

In addition to the narrow unsaturated space, proximity to the coast, and low elevation, Waikīkī and Māpunapuna are prime candidates for groundwater wastewater contamination. There are 96 OSDS in Waikīkī and Māpunapuna, all of which are cesspools, offering no wastewater treatment (Whittier & El-Kadi, 2009). OSDS require at least 4.4 m of unsaturated space to function properly, however models show that 86% of OSDS between the Downtown and Waikīkī neighborhoods are at least partially inundated by groundwater during mean spring tide conditions today (Habel et al., 2017). Significant portions of storm drains and sewer lines are also predicted to flood (Spirandelli et al., 2018).

4.2.2 Sampling Strategy and Analysis

Water samples were collected from seven locations (four coastal and three storm drain sites) between July and October 2018 during king and spring tides (Figure 4.2; Appendix C: Table S1). Radon is a well-established, naturally occurring groundwater tracer (e.g. Burnett & Dulaiova, 2003), and was used as the primary groundwater tracer in this study. Continuous radon time series of surface/storm drain water and discreet sampling (coastal groundwater) were conducted for each site. At low, mid, and high tide, water was also sampled and filtered onsite through a 0.45 μM filter for CECs and nutrients and kept at 4 °C until analysis. For coastal sites, both surface water and groundwater were sampled through push-point samplers (MHE products). Low and high tide water table heights for all dates sampled were modeled as described in Habel et al. (2020). Total SGD fluxes were calculated using both a transient mass balance model and residence-time based approach (Burnett & Dulaiova, 2003; Dulaiova et al., 2010; Appendix C-2; Appendix C: Figure S1). Nutrient and CEC fluxes were estimated by multiplying the SGD flux by the median groundwater nutrient and CEC concentration for each study site and date of sampling.

Three CEC compounds were analyzed (carbamazepine, caffeine, and fluoroquinolones), which differ in terms of environmental persistence and mobility (Appendix C: Table S2). Samples

were collected (n = 49) into pre-combusted amber glass bottles with Teflon-lined caps. CECs were analyzed at the University of Hawai‘i at Mānoa using an Enzyme Linked ImmunoSorbent Assay (ELISA) compound-specific kits (Abraxis LLC). Compound-specific instructions were followed for sample preparation and then analyzed at a 450 nm wavelength on a spectrophotometric microplate reader (Abraxis ON 475010, microplate format, 96 well, Model 4303). Detection limits were 24, 150, and 10 ng/L for carbamazepine, caffeine, and fluoroquinolones, respectively. To assess environmental risk, risk quotients (RQ) were also calculated following European Union guidelines for environmental risk assessment (European Commission, 2003, Appendix 3).

Dissolved nutrients were collected into acid-cleaned HDPE bottles. Samples were analyzed for Total Dissolved Nitrogen (TDN), Total Dissolved Phosphorus (TDP), $NO_3^- + NO_2^-$, PO_4^{3-}, and NH_4^+ with a SEAL AutoAnalyzer 3 HR in the S-Lab at the University of Hawai‘i at Mānoa. Dissolved inorganic nitrogen (DIN) concentrations were calculated as the sum of $NO_3^- + NO_2^-$ and NH_4^+. Dissolved organic nitrogen (DON) concentrations reflect the difference between TDN and DIN.

CEC and nutrient scores were calculated using Equations 1 and 2 (after Abaya et al., 2018), where CBZ_{norm}, CFN_{norm}, FQL_{norm}, TDN_{norm}, and TDP_{norm} refer to the normalized concentrations of carbamazepine, caffeine, fluoroquinolones, TDN, and TDP. CEC and nutrient scores were calculated to allow for comparison between sampling sites and tidal stages. Storm drain and coastal sites were normalized separately from one another because they represent different environments.

$$CEC_{score} = CBZ_{norm} + CFN_{norm} + FQL_{norm} \quad \text{Eq. 1}$$

$$Nut_{score} = TDN_{norm} + TDP_{norm} \quad \text{Eq. 2}$$

Relationships, correlations, and conclusions were confirmed using several statistical methods, including principal components analysis (PCA) and Mood’s median test.

4.3 Results

4.3.1 Groundwater discharge

Radon concentrations and SGD were higher during king tides compared to spring tides for the Waikīkī sites (Figure 4.3; Appendix C: Table S3). Groundwater advection rates based on the radon time-series analysis, were 3.4, 1.3, and 3.3 times greater during king tides at C1, C2, and C3, respectively. SGD rates were 6.9×10^5, 2.6×10^5, and 0.54×10^5 m^3/d for C1, C2, and C3 during the

king tide and $2.0x10^5$, $2.0x10^5$, and $0.17x10^5$ m^3/d for the spring tide (Appendix C: Table S3). Increases in advection rates at high tide were also observed for all king tide samplings (Appendix C: Table S3; Appendix C: Figure S2), with advection rates 1.3, 1.6, and 5.4 times greater for C1, C2, and C3, respectively.

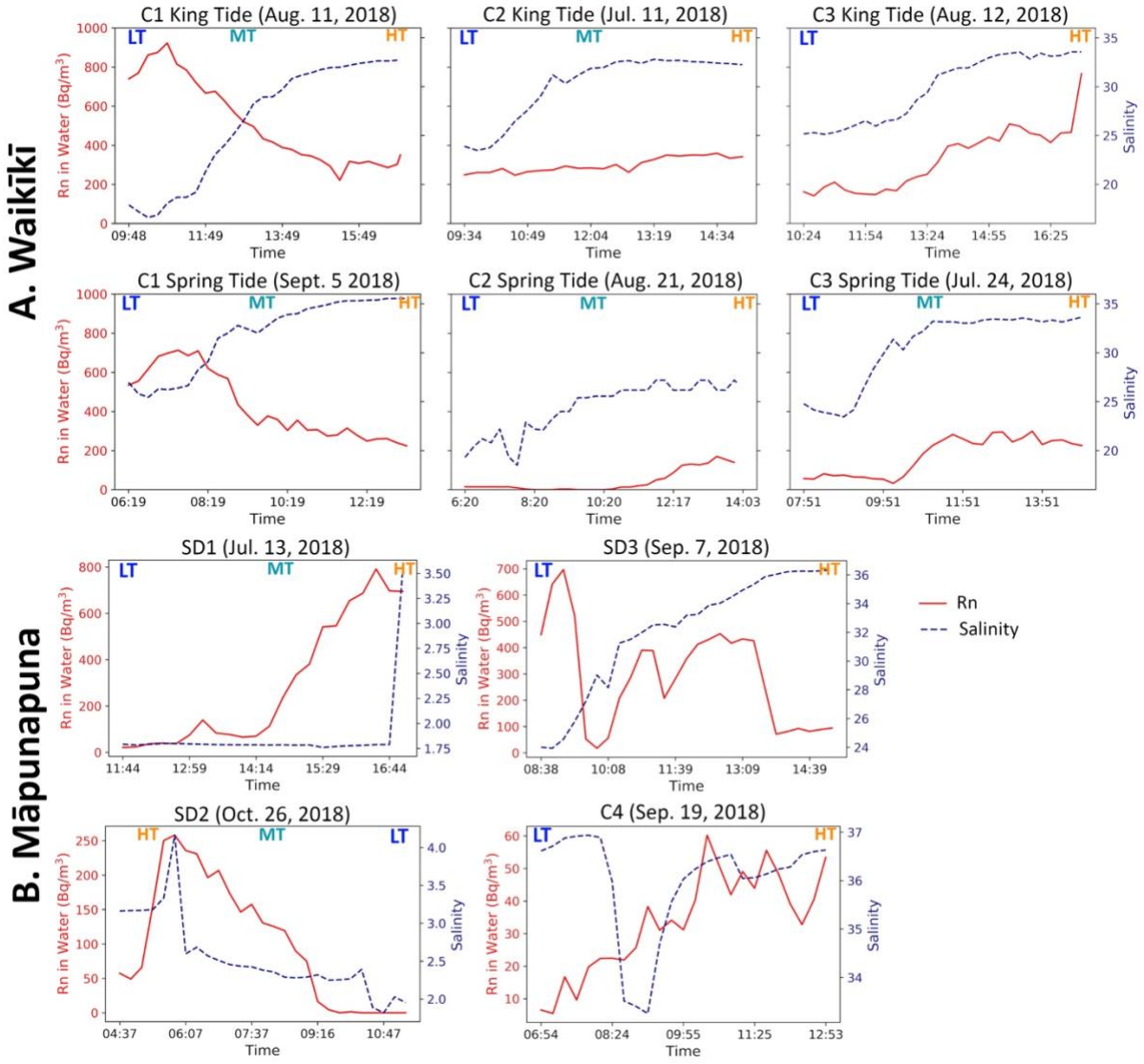

Figure 4.3. Radon (groundwater tracer; solid red line; Bq/m^3; average uncertainty ± 21%) and salinity (dashed blue line) over a half-tidal cycle. Timing of low tide (LT), mid tide (MT), and high tide (HT) grab samplings are indicated for each survey. Time is indicated in Hawai‘i standard time. A. Waikīkī time series by location and tide (king tide vs. spring tide). C1, C2, and C3 are all coastal sites. B. Māpunapuna time series by location, where SD1, SD2, and SD3 are all storm drain sites and C4 is a coastal site where the storm drains discharge. The time series for SD1 was conducted during a king tide and the remaining Māpunapuna time series (SD2, SD3, and C4) were conducted during spring tides.

For Māpunapuna, SD1 and SD2 showed significant increases in both radon and salinity at high tide, preceding flooding of the street via storm drains by several minutes (Figure 4.3). Radon concentrations increase from background concentrations to nearly 800 and 250 Bq/m^3 for SD1 and SD2, respectively. The other storm drain site, SD3, which is not directly connected to SD1 and SD2, had decreasing radon concentrations from low to high tide coincident with increasing salinity. The one Māpunapuna coastal site (C4) had advection rates that were one to two orders of magnitude lower than those measured in Waikīkī.

4.3.2 Nutrients and CECs

Nutrient concentrations were greatest at C1 and CECs at C2 and C3 in Waikīkī (Figure 4.4, Appendix C: Table S4). Nutrients at C1 were dominated by nitrate in surface water (range = 36 to 100 μM) and ammonium in groundwater (range = 51 to 81 μM). From low to high tide, TDN increased at C1 in surface water and decreased in groundwater. The other Waikīkī sites, C2 and C3 had comparable nitrogen compositions in both surface water and groundwater, with TDN decreasing from low to high tide. Nutrient concentrations remained mostly consistent between king and spring tide samplings.

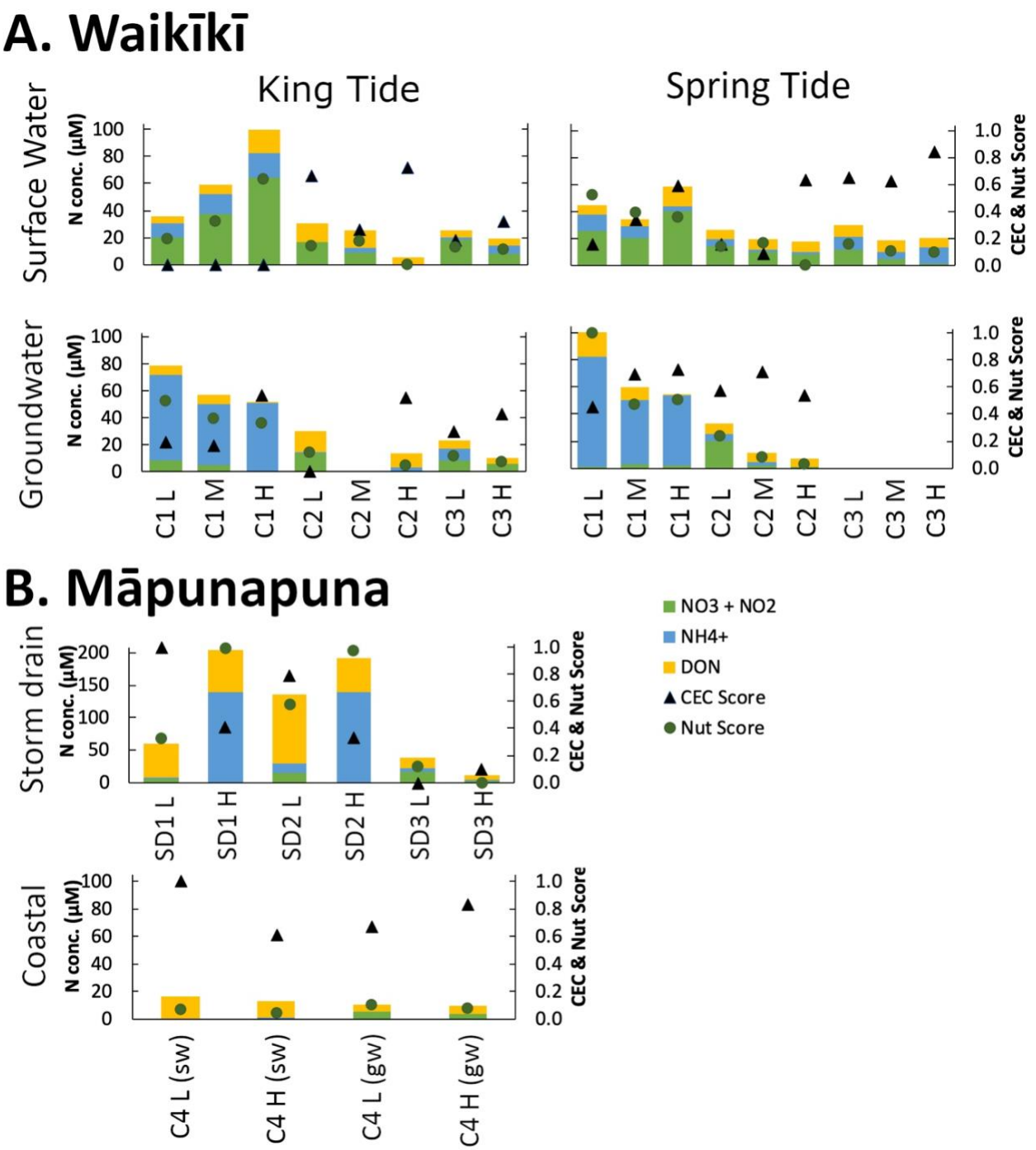

Figure 4.4. Distribution of nitrogen species (NO_3^- + NO_2^-, NH_4^+, and DON) concentrations (µM), nutrient and CEC scores. (A) Waikīkī coastal sites separated by king vs. spring tide and surface water vs. groundwater. (B) Māpunapuna storm drain and coastal sites. Nutrient and CEC scores were normalized separately for coastal and storm drain sites.

CECs had greater variability from low to high tide. Carbamazepine and caffeine concentrations ranged from < MDL to 330 ng/L and < MDL to 3000 ng/L, respectively (Figure 4.4; Appendix C: Table S4). Fluoroquinolones were only detectable at SD1 and SD2 with concentrations ranging from 19 to 61 ng/L. Detection frequencies of carbamazepine, caffeine, and fluoroquinolones were 54%, 89%, and 0% and 93%, 57%, and 16% for coastal and storm drain sites, respectively. In coastal Waikīkī surface waters, carbamazepine concentrations increased or stayed consistent from low to high tide. The same trend was observed for Waikīkī groundwater, with the exception of C2 ST. Carbamazepine and caffeine concentrations decreased from low to high tide at SD1, SD2, and C4 surface water. In contrast to SD3, SD1 and SD2 had increasing nutrient concentrations with decreasing CEC concentrations at high tide.

While nutrient concentrations did not change significantly, nutrient and CEC fluxes were greater during the king tide for most coastal sites (Appendix C: Figure S3). TDN fluxes were about three times greater during the king tide for all coastal sites. Carbamazepine, caffeine, and TDP fluxes were greater during the king tide compared to the spring tide for sites C1 and C3 (ranging up to three times greater), yet the opposite was true for C2. Overall, fluxes ranged from $1.3x10^5$ to $2.5x10^6$ μg/d, $1.1x10^6$ to $4.7x10^7$ μg/d, $2.9x10^4$ to $3.4x10^6$ μM/d, and $1.2x10^3$ to $1.0x10^5$ μM/d for carbamazepine, caffeine, TDN, and TDP, respectively (Appendix C: Figure S3).

4.4 Discussion

4.4.1 Groundwater discharge

One component of SGD is tidally-driven seawater intrusion and its subsequent discharge after mixing with groundwater (Robinson et al., 2007). Infiltrating seawater causes the fresher groundwater lens to float, inundate the otherwise unsaturated zone, and in some instances rise above the ground surface. GWI contributes significantly to nuisance flooding (Rotzoll & Fletcher, 2012). Here we used geochemical tracers to document tidally-driven GWI and its subsequent discharge to the ocean in two urban areas.

Radon activity in coastal and storm drain water above that supported by diffusion and in-situ production provides direct evidence for groundwater discharge to both coastal waters and inland urban areas and was observed at all studied locations. Highest groundwater discharge is commonly observed at low tide (Dulaiova et al., 2006); however, high tide radon concentrations and advection rates were equal to or greater than those found at low tide for most coastal sites,

except for C1. Increases in radon and advection rates at high tide may be explained by marine SGD drivers. Tidal fluctuations cause vertical and horizontal displacement of the freshwater lens (Appendix C: Table S5; Rotzoll & Fletcher, 2012) along with local pressure gradients occurring as water is pushed onshore through permeable sediments. This is similar to processes described across barrier islands (Chanton et al., 2006), resulting in increased groundwater discharge on the canal side of Waikīkī during high tide. Increased groundwater infiltration occurs at storm drains when the water table intersects the fractured storm drain network. While we were unable to quantify groundwater fluxes into storm drains due to their unknown geometry, sharp increases in radon at high tide provide clear evidence for GWI into the pipes at SD1 and SD2.

Assuming tidal inundation affects the Waikīkī area uniformly (Habel et al., 2020), a volume of 2.9×10^6 and 2.2×10^6 m^3 is added to the aquifer at high tide for king and spring tides, respectively. About half, or 1.5×10^6 and 1.1×10^6 m^3 per tidal cycle is expected to drain during the falling tide to the Ala Wai Canal. Overall, the total SGD for C1, C2 and C3 was $8.55 \pm 2.12 \times 10^4$ m^3/day and $3.27 \pm 1.26 \times 10^4$ m^3/day during king and spring tides, respectively. While a significant volume, this estimated SGD is entirely feasible, capturing 5-10% of the theoretical tidal inundation volume. The average advection rate for Waikīkī was 0.89 ± 0.51 m/d, which is within range of other Hawai‘i studies (e.g. Richardson et al., 2017; Kelly et al., 2019).

4.4.2 Pollution pathways

There are multiple pathways for effluent from WIS to impact adjacent waterways (Figure 4.1). Wastewater leakage may create saturated conditions in the unsaturated zone, reducing the bioremediation capacity (Elmir, 2018). In a more extreme scenario, WIS can be directly flooded by either chronic (SLR) or episodic (tidal) inundation. All of these pathways lead to treatment failure when wastewater moves unimpeded in a saturated environment.

Over 94% of coastal samples had at least one detectable CEC compound, establishing a hydrologic connection between WIS and our study sites (Appendix C: Table S1). CEC concentrations were consistent with other coastal studies conducted in areas subject to wastewater pollution (e.g. Sczymycha et al., 2020; McKenzie et al., 2020). From low to high tide, CECs increased but nutrient concentrations (Appendix C: Figure S4; Appendix C-4) decreased for most coastal samples. Averaging CEC concentrations by site and tide, carbamazepine consistently increased from low to high tide in both surface and groundwater for all Waikīkī sites. Caffeine

also increased from low to high tide for all Waikīkī sites except for C1 (Figure 4.5). While we did not observe dramatic differences in nutrient concentrations between king and spring tides, nutrient fluxes were up to three times greater during king compared to spring tides, demonstrating that higher tide levels occurring today have the potential to lead to negative consequences to coastal waters.

CEC scores were calculated to compare relative wastewater presence between the study sites, Coastal Waikīkī CEC scores increased during high tide (0.53) compared to low tide (0.29) (Figure 4.5). This implies increased flux from WIS to the Ala Wai Canal due to the tidally influenced water table.

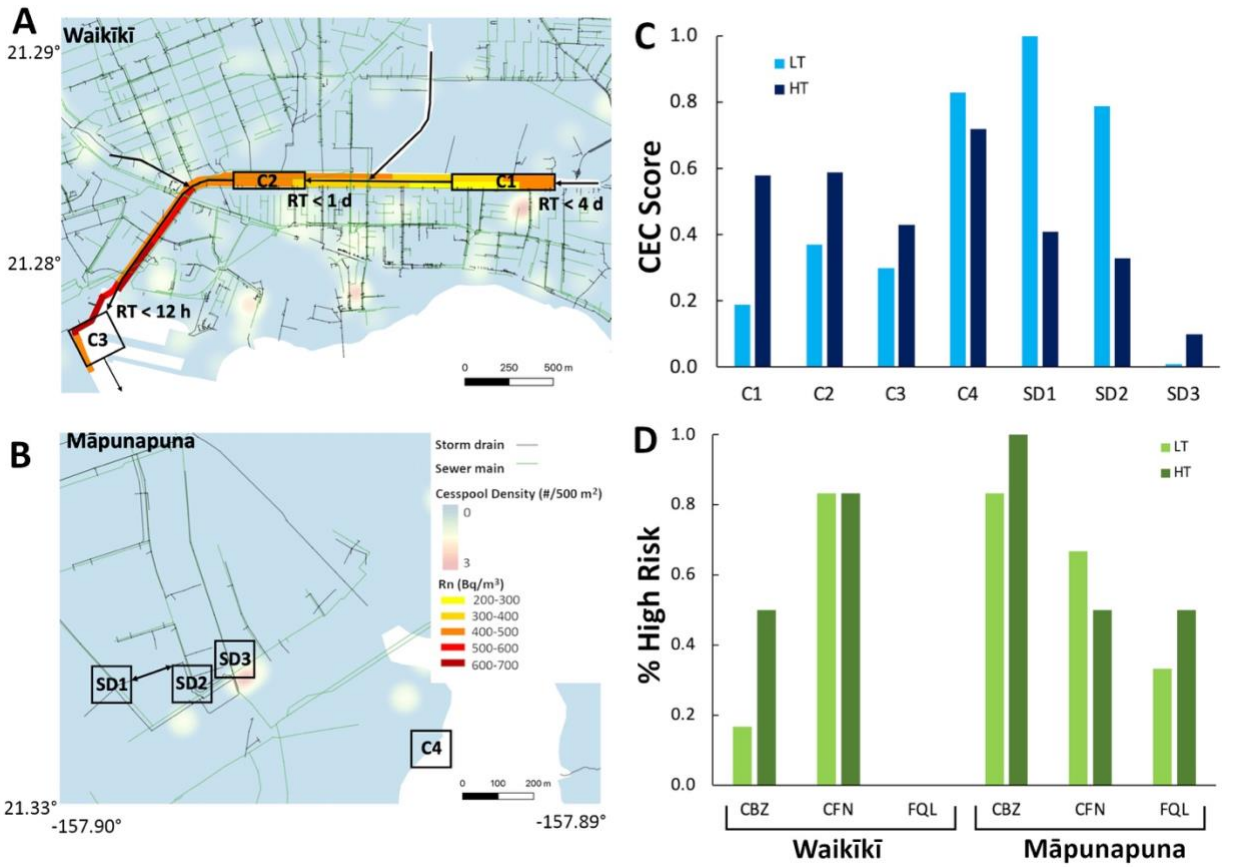

Figure 4.5. CEC scores and percentage of samples with a RQ > 1 (high ecological risk) at low and high tide. (A) Waikīkī and (B) Māpunapuna sampling sites. Storm drains and sewer mains are indicated on the map using blue and green lines, respectively. Cesspool density is indicated by the color gradient as the number of individual units per 500 m^2. In (A), the Ala Wai Canal is colored according to radon concentrations in water (Bq/m^3) from a radon survey (Appendix C: Figure S1) and maximum estimated residence times (RT) are indicated by location. (C) low (LT) vs. high (HT) tide CEC scores by sampling site. Coastal CEC scores include the median surface and groundwater results together. Waikīkī sites have median CEC scores from king and spring tides combined and CEC scores increased from low (light blue) to high (dark blue) tide for all Waikīkī sites and SD3. (D) The percentage of samples that pose a high risk to the ecosystem increase from low (light green) to high (dark green) tide for carbamazepine and fluoroquinolones where above the detection limit. For caffeine (a highly mobile and soluble compound), the percentage of samples that pose a high risk decrease or remains the same at high tide.

Storm drains SD1 and SD2 exhibited the opposite trend from low to high tide compared to coastal sites, where CEC scores decreased (Figure 4.5). SD1 and SD2 are directly connected to one another and are not exposed to sunlight compared to SD3. Sunlight exposure at SD3 leads to differences between CEC scores. Differences between coastal and storm drain sites likely reflect divergence in the inundation pathway and WIS source. Due to the comparitively lower density of

OSDS in Māpunapuna, storm drains are more likely impacted by leaking sewer lines instead of OSDS.

While CECs are applied here as wastewater tracers, they also pose an environmental risk (Figure 4.5). Average RQs for surface water and storm drain samples were above 1, demonstrating that even under current conditions, CECs render a high risk to the ecosystem. Overall, RQs were high risk in 62% of samples for carbamazepine and caffeine and 24% for fluoroquinolones (Appendix C: Table S6) and may threaten growth or result in premature mortality of aquatic organisms (European Commission, 2003).

4.5 Conclusion

The frequency, duration, and severity of wastewater contamination to Waikīkī and Māpunapuna water bodies are projected to increase with SLR. Here, we focused on two different site types to study multiple mechanisms of GWI. Higher nutrient and CEC fluxes were observed for most coastal sites during king tides compared to spring tides. Additionally, higher CEC scores were observed at high tide compared to low tide for coastal Waikīkī sites. Tidally driven CEC concentrations observed in Waikīkī and Māpunapuna demonstrate the connection between groundwater and WIS and serves as a warning for the future.

Of significance is that storm drains in low lying inland areas can overflow every spring tide (with greater frequency in the future), becoming channels for untreated wastewater onto streets and sidewalks. From an anthropogenic perspective, this flooding of contaminated water also poses a health risk to pedestrians navigating the area during high tide. This connection demonstrates that SLR has generated new wastewater pathways posing direct environmental and human health risks.

While this study was based in Honolulu, it has applications to coastal communities elsewhere. For instance, the number of days per year that U.S. coastal cities experience nuisance flooding has doubled between 2000 and 2019 and is estimated to increase to 270 days/year in some coastal communities by 2050, particularly in areas vulnerable to storm surge (Sweet et al., 2020). SLR will expedite WIS leakage to coastal water bodies, reducing opportunities for natural remediation and potentially lead to ecological decline and increases in water-borne illness.

Chapter 5: Conclusions and Future Work

5.1 Summary

This dissertation investigated groundwater as a conduit for contaminants to reach streams and the coastal ocean using a combination of groundwater and contaminant tracers:

Chapter 2 connected groundwater discharge from headwaters to the coastal ocean by linking stream baseflow and SGD using radon as a groundwater tracer. Frequently, studies focus on either streams or the coastline, but not both as a continuous system. This chapter contributed new findings to the body of science by linking water quality with the stream-coastal continuum as well as being the first to demonstrate decreased water quality during perigean spring tides. Major findings from this chapter include (1) groundwater fluxes (stream baseflow + SGD) was equal to surface runoff in streams in Kāneʻohe Watershed; (2) nutrient fluxes and concentrations in SGD were greater than stream-derived fluxes; and (3) SGD and associated nutrient fluxes were greater during a perigean spring tide compared to a spring tide at Kahaluʻu Beach Park. This chapter highlighted the importance of considering stream flow and SGD in concert with one another. Additionally, this chapter demonstrated the consequence of temporal variation of SGD, particularly under SLR.

Chapter 3 demonstrated that SGD is a source of wastewater and industrial runoff to the coastal surface waters to Sydney Harbour, which is surrounded by a highly urbanized area. SGD is frequently overlooked as a vector for contaminants, and this was one of the first studies to demonstrate that SGD is a transport source of CECs to the coastal ocean. This chapter had three major findings: (1) SGD was a vector for CECs to the coastal ocean; (2) CEC inventories increased with increasing water residence time; and (3) ibuprofen and dioxins were in concentrations that pose a high ecological risk. While SGD is frequently neglected in CEC and water quality studies, this chapter demonstrated that it is a viable route for contaminants to reach the coastal ocean and have a negative impact on coastal ecosystems and aquatic organisms.

Chapter 4 provided field-based evidence for GWI of WIS during spring tides in Honolulu, Hawaiʻi. This chapter contributed the first field-based confirmation of tidally driven GWI of WIS, confirming conclusions from previous modeling studies. In this chapter, two pathways for GWI of WIS to occur were studied – direct inundation of WIS and subsequent discharge as SGD and indirect inundation through storm drain backflow. Major findings from this chapter include: (1)

spring tides increased the water table height, approximating future sea levels; (2) GWI of WIS and subsequent discharge to storm drains or the coastal ocean was confirmed using radon and CEC tracers; and (3) 24-62% of CEC observations posed a high ecological risk. The results from this chapter demonstrated the tidal connection between coastal WIS and groundwater even under current conditions. This situation will worsen as sea levels continue to rise, leading to further water quality declines.

5.2 Future Work

Future studies can build upon this dissertation by further investigating spatiotemporal variation of groundwater discharge and increasing the number of locations that consider the whole system – ridge to reef (i.e., stream-coastal continuum). This is a particularly important consideration for Pacific Islands, which frequently have small watersheds with vulnerable water resources. Additionally, further constraining temporal variations along this continuum (e.g., tidal, seasonal) will provide greater insight into groundwater discharge dynamics and potentially help isolate contaminant sources, leading to contaminant remediation and improved water quality.

CECs have only really become viable to quantify in environmental matrices in the last decade or so. Future studies would benefit from increasing the number of CEC compounds studied, increasing the number of study locations that look at SGD as a vector, further evaluation of CEC attenuation in the subsurface, and an expansion of CEC ecotoxicity studies (e.g., expanding CEC ecotoxicity research for organisms from a wider variety of climates and ecosystems).

On top of current water quality issues, sea levels are increasing and will lead to further water quality decline (amongst numerous other problems) in the future. Right now, we have an opportunity to prepare for major increases in sea level and studies that aim to address these threats should be a priority. Future research that further assesses spatiotemporal variation of GWI of coastal WIS, ideally pinpointing specific sources of leaks, or that links pathogens to tidal cycles would greatly benefit our understanding and ability to mitigate potential hazards.

APPENDIX A: Chapter 2 Supplementary Materials

Supporting information

S1 Table. Unprocessed data for all grab samples and radon survey samples in this study. (A) Grab sample data are categorized by type (groundwater – gw, surface water – surf, and well) and location. Date collected and lat long indicate the sampling date and location of sampling. Rn concentrations (Bq/m^3), temperature (°C), and salinity are given for each grab sample. Additionally, nutrient data (TN, TP, DIP, DSi, NOx, NH_4^+, DIN, and DON) are provided in µM. (B) Radon survey data show location (lat long), date and time of measurement, water depth (m), salinity, and temperature (°C), and the radon concentration (Bq/m^3).

A. Grab Sample Data

ID	Type	Location	Date Coll	Lat	Long	Rn Bq/m^3	Temp	Sal	TN µM	TP µM	DIP µM	DSi µM	Nox µM	NH3 µM	DIN µM	DON µM
1	gw	Kahaluu Stream	11/18/16	21.4447	-157.8403	1468	24.03	0.24	94.43	0.81	0.42	437.14	13.73	32.32	46.05	48.38
2	gw	Kahaluu Stream	11/18/16	21.4447	-157.8403	508	22.50	0.24	1.33	1.62	1.25	696.01	0.19	1.03	1.23	0.11
3	gw	Kahaluu Stream	11/18/16	21.4480	-157.8374	2322	23.21	0.30	6.20	2.34	2.12	717.27	0.08	6.30	6.39	0.00
4	gw	Kahaluu Stream	11/18/16	21.4480	-157.8374	2865	23.08	0.30	6.72	2.27	2.04	723.70	0.08	6.52	6.61	0.11
5	gw	Kahaluu Stream	6/19/17	21.4446	-157.8407	930	24.77	0.28	112.83	0.11	0.10	263.03	83.53	20.54	104.07	0.00
6	gw	Kahaluu Stream	6/19/17	21.4490	-157.8368	928	23.00	0.41	46.35	1.02	0.94	652.75	2.13	18.04	20.16	0.00
7	gw	Kahaluu Stream	7/10/17	21.4434	-157.8419	24	22.50	0.08	28.06	0.94	1.10	549.80	10.49	0.14	10.64	17.42
8	gw	Kahaluu Stream	7/10/17	21.4419	-157.8431	1585	22.36	0.08	35.13	0.61	0.52	407.59	1.93	34.98	36.91	0.00
9	gw	Kahaluu Stream	7/10/17	21.4394	-157.8436	171	22.17	0.08	3.28	0.32	0.77	806.60	0.29	0.57	0.86	2.43
10	gw	Kahaluu Stream	7/10/17	21.4385	-157.8437	269	24.36	0.09	52.12	0.55	0.68	443.37	12.49	3.57	16.06	36.05
11	gw	Kahaluu Stream	7/10/17	21.4385	-157.8443	486	22.48	0.08		0.97	1.23	550.30	10.85	0.57	11.42	
12	gw	Kahaluu Stream	10/24/16	21.4490	-157.8368	798	22.86	0.25	30.59	1.48	0.08	814.32	0.14	19.37	19.51	19.17
13	gw	Kahaluu Stream	10/24/16	21.4507	-157.8359	449	22.31	0.30	35.34	0.97	0.04	870.51	0.03	15.64	15.67	23.91
14	surf	Kahaluu Stream	9/30/16	21.4439	-157.8408	45	22.34	0.11	10.02	0.71	0.17	542.96	3.66	0.25	3.91	6.10
15	surf	Kahaluu Stream	9/30/16	21.4503	-157.8367	304	23.49	0.14	9.66	0.67	0.30	546.59	4.98	0.00	4.98	4.68

16	surf	Kahaluu Stream	9/30/16	21.4500	-157.8364	331	23.55	0.14	30.59	1.48	0.08	814.32	10.41	19.37	29.78	0.81
17	surf	Kahaluu Stream	9/30/16	21.4528	-157.8353	318	26.01	0.15	10.26	0.62	0.37	511.31	4.79	0.00	4.79	5.47
18	surf	Kahaluu Stream	10/14/16	21.4371	-157.8436	508	23.10	0.11	34.41	0.36	0.42	342.85	33.63	0.36	33.98	0.43
19	surf	Kahaluu Stream	10/14/16	21.4386	-157.8444	2322	20.87	0.11	12.57	1.00	1.16	500.96	11.42	0.21	11.64	0.93
20	surf	Kahaluu Stream	10/14/16	21.4435	-157.8418	1468	22.96	0.12	12.42	0.90	1.07	499.30	12.21	0.21	12.42	0.00
21	surf	Kahaluu Stream	7/10/17	21.4434	-157.8419	70	21.74	0.08	29.70	1.00	1.10	548.05	11.71	0.21	11.92	17.78
22	surf	Kahaluu Stream	7/10/17	21.4419	-157.8431	74	22.17	0.08	24.92	0.84	1.13	550.80	10.07	0.29	10.35	14.56
23	surf	Kahaluu Stream	7/10/17	21.4394	-157.8437	1412	24.18	0.32								
24	surf	Kahaluu Stream	7/10/17	21.4392	-157.8437	314	22.65	0.13	12.48	0.93	0.88	570.01	10.48	0.15	10.63	1.85
25	surf	Kahaluu Stream	7/10/17	21.4385	-157.8437	262	24.87	0.09	50.12	0.94	0.77	457.27	41.62	2.43	44.05	6.07
26	surf	Kahaluu Stream	7/10/17	21.4385	-157.8443	262	21.80	0.08		0.90	1.10	549.05	9.92	0.64	10.57	
27	gw	Kahaluu Stream	3/15/17	21.4514	-157.8353	1086	22.12	0.46	24.03	0.73	0.46	589.71	0.49	22.97	23.46	0.57
28	gw	Kahaluu Stream	4/19/17	21.4446	-157.8407	1367	23.61	0.25	99.97	0.46	0.08	87.60	69.02	14.12	83.14	16.83
29	gw	Kahaluu Stream	4/19/17	21.4473	-157.8382	100	24.34	0.26	113.82	0.72	0.66	738.57	74.00	1.99	76.00	37.83
30	surf	Kahaluu Stream	1/23/17	21.4353	-157.8521	25	20.342	0.09	17.56	1.42	1.52	579.19	11.64	0.14	11.78	5.78
31	surf	Kahaluu Stream	2/15/17	21.4447	-157.8410	144	24.19	0.26	16.03	1.06	0.84	498.09	12.61	0.24	12.85	3.18
32	surf	Kahaluu Stream	2/15/17	21.4526	-157.8352	818	23.39	0.38	20.34	0.91	0.84	435.66	12.33	0.13	12.46	7.88
33	surf	Kahaluu Stream	3/15/17	21.4526	-157.8353	26	22.49	0.17	12.66	0.50	0.15	447.79	8.67	0.38	9.05	3.61
34	gw	Ahuimanu Stream	9/30/16	21.4419	-157.8354	1618	23.89	0.14	56.81	0.65	0.54	542.81	30.11	11.37	41.48	15.33
35	gw	Ahuimanu Stream	9/30/16	21.4430	-157.8349	651	24.28	0.14	10.68	1.69	0.14	727.25	0.23	8.90	9.13	1.55
36	gw	Ahuimanu Stream	9/30/16	21.4459	-157.8329		26.26	0.15	11.58	1.89	0.20	813.87	0.21	8.12	8.33	3.25
37	gw	Ahuimanu Stream	11/18/16	21.4419	-157.8354	196	24.40	0.22	101.78	0.92	0.65	549.91	75.09	13.85	88.95	12.84
38	gw	Ahuimanu Stream	11/18/16	21.4413	-157.8358	1672	23.95	0.23	100.16	1.23	0.89	559.05	71.10	16.86	87.97	12.19
39	gw	Ahuimanu Stream	7/28/17	21.4317	-157.8384	106	21.2	0.25	5.22	0.98	0.87	603.50	4.03	0.38	4.41	0.81

40	gw	Ahuimanu Stream	10/24/16	21.4459	-157.8330	1049	24.02	0.29	16.82	1.31	0.09	788.31	0.02	7.28	7.30	9.52
41	gw	Ahuimanu Stream	10/24/16	21.4454	-157.8321	1825	23.59	0.34	35.92	1.17	0.02	836.05	0.12	23.06	23.18	12.74
42	surf	Ahuimanu Stream	9/30/16	21.4469	-157.8335	722	26.18	0.08	19.63	0.46	0.10	485.32	7.50	0.27	7.76	11.87
43	surf	Ahuimanu Stream	9/30/16	21.4527	-157.8351	751	28.36	0.10	16.15	0.41	0.13	500.29	4.81	0.51	5.32	10.82
44	surf	Ahuimanu Stream	9/30/16	21.4393	-157.8376	595	22.59	0.14	10.91	0.67	0.34	521.19	2.77	0.00	2.77	8.15
45	surf	Ahuimanu Stream	9/30/16	21.4430	-157.8349	1091	24.28	0.14	18.33	0.36	0.18	490.75	6.64	0.27	6.91	11.43
46	surf	Ahuimanu Stream	9/30/16	21.4459	-157.8329	1057	26.26	0.15	24.38	0.41	0.32	486.31	9.40	0.00	9.40	14.98
47	surf	Ahuimanu Stream	9/30/16	21.4535	-157.8356	593	27.72	0.15	13.27	0.47	0.33	510.83	3.67	0.74	4.41	8.86
48	surf	Ahuimanu Stream	10/14/16	21.4396	-157.8375	25	25.04	0.13	16.49	0.48	0.68	479.33	7.35	0.14	7.50	9.00
49	surf	Ahuimanu Stream	10/14/16	21.4462	-157.8331	75	26.05	0.15	17.85	0.39	0.45	434.39	13.07	0.21	13.28	4.57
50	surf	Ahuimanu Stream	10/14/16	21.4453	-157.8323	0	27.50	0.17	7.07	0.32	0.36	427.73	0.36	0.29	0.64	6.43
51	surf	Ahuimanu Stream	7/28/17	21.4317	-157.8384	23	20.73	0.24	5.91	1.10	0.91	602.81	4.67	0.12	4.79	1.11
52	surf	Ahuimanu Stream	10/7/16	21.4481	-157.8345	128	29.87	0.16	18.28	0.45	0.61	412.42	6.78	1.00	7.78	10.49
53	gw	Ahuimanu Stream	3/15/17	21.4471	-157.8336	149	24.19	0.26	10.59	0.61	0.35	498.29	2.69	0.91	3.60	6.99
54	gw	Ahuimanu Stream	3/15/17	21.4446	-157.8332	855	23.86	0.29	16.66	0.35	0.16	605.11	9.07	5.39	14.46	2.19
55	gw	Ahuimanu Stream	3/15/17	21.4455	-157.8323	376	24.57	0.30	116.16	3.55	2.59	832.74	41.31	0.22	41.52	74.63
56	gw	Ahuimanu Stream	3/15/17	21.4455	-157.8322	491	24.68	0.36	63.53	1.41	0.80	596.07	39.71	1.24	40.95	22.57
57	gw	Ahuimanu Stream	3/15/17	21.4468	-157.8335	462	23.39	0.38	11.30	1.13	0.42	603.16	0.03	6.47	6.51	4.80
58	gw	Ahuimanu Stream	3/15/17	21.4455	-157.8323	358	24.08	0.38	13.76	1.16	0.59	632.69	0.25	9.15	9.40	4.36
59	gw	Ahuimanu Stream	4/19/17	21.4431	-157.8349	1608	24.34	0.18	11.38	0.45	0.36	230.90	1.02	7.62	8.63	2.74
60	gw	Ahuimanu Stream	4/19/17	21.4418	-157.8355	669	24.23	0.20	127.72	0.32	0.22	183.21	105.37	9.47	114.84	12.88
61	surf	Ahuimanu Stream	2/15/17	21.4466	-157.8333	130	22.49	0.17	21.30	0.69	0.54	458.32	14.91	0.19	15.10	6.19
62	surf	Ahuimanu Stream	2/15/17	21.4480	-157.8345	793	23.86	0.29	21.27	1.56	1.55	240.19	7.34	0.12	7.47	13.80
63	surf	Ahuimanu Stream	2/15/17	21.4392	-157.8377	126	22.12	0.46	11.49	0.70	0.60	476.12	5.27	0.44	5.71	5.78

64	gw	Kahaluu Lagoon	5/26/17	21.4571	-157.8386	274	25.4	24.07	17.62	0.99	0.91	151.56	2.40	2.40	4.80	12.82
65	gw	Kahaluu Lagoon	5/26/17	21.4571	-157.8386	890	25.06	26.93	22.12	0.54	0.45	219.41	1.05	20.20	21.24	0.88
66	gw	Kahaluu Lagoon	5/26/17	21.4571	-157.8386	1308	25.84	19.41	9.33	0.72	0.37	428.56	0.70	5.54	6.23	3.10
67	surf	Kahaluu lagoon	10/7/16	21.4562	-157.8393	27	24.77	1.33	15.78	0.81	0.55	432.89	4.71	0.14	4.85	10.92
68	surf	Kahaluu lagoon	10/7/16	21.4553	-157.8380	0	24.98	2.01	15.71	0.77	0.94	451.62	6.57	2.14	8.71	7.00
69	surf	Kahaluu lagoon	10/7/16	21.4570	-157.8385	0	23.93	2.10	12.85	0.77	0.77	429.40	11.71	2.21	13.92	0.00
70	surf	Kahaluu lagoon	10/7/16	21.4545	-157.8365	51	29.32	2.22	16.85	1.29	0.74	426.90	5.43	0.71	6.14	10.71
71	surf	Kahaluu lagoon	10/7/16	21.4577	-157.8404	27	25.47	2.62	15.78	0.74	0.65	412.09	5.64	2.36	8.00	7.78
72	surf	Kahaluu lagoon	10/7/16	21.4590	-157.8401	24	24.25	3.93	18.28	0.77	0.81	402.77	15.42	2.57	17.99	0.29
73	surf	Kahaluu lagoon	10/7/16	21.4601	-157.8396	27	24.26	4.93	14.99	0.84	0.74	375.22	7.14	2.28	9.42	5.57
74	surf	Kahaluu Beach	2/3/17	21.4552	-157.8374	113	22.77	15.00	10.23	0.56	0.39	28.80	0.20	4.95	5.15	5.08
75	surf	Kahaluu Beach	2/3/17	21.4601	-157.8396	72	23.32	17.78	9.74	0.66	0.51	251.35	4.20	0.76	4.96	4.78
76	surf	Kahaluu Beach	2/3/17	21.4570	-157.8385	314	22.52	26.34	8.29	0.66	0.53	70.57	1.63	0.93	2.56	5.73
77	surf	Kahaluu Beach	2/3/17	21.4590	-157.8401	179	23.52	28.28	10.67	0.60	0.48	72.61	2.25	2.23	4.48	6.19
78	surf	N Kaneohe	10/28/16	21.4838	-157.8418	20	21.83	9.20	10.79	0.55	0.41	117.71	1.40	0.67	2.07	8.72
79	surf	N Kaneohe	10/28/16	21.4770	-157.8418	39	23.41	23.60	32.35	1.28	0.66	331.51	22.34	1.16	23.50	8.85
80	surf	N Kaneohe	10/28/16	21.4701	-157.8441	96	23.53	28.00	15.84	0.85	0.72	217.58	7.48	1.71	9.19	6.65
81	surf	N Kaneohe	10/28/16	21.4673	-157.8423	171	23.45	23.80	17.50	0.93	0.60	325.35	10.40	0.13	10.53	6.97
82	surf	N Kaneohe	10/28/16	21.4651	-157.8428	209	23.99	10.00	8.59	0.83	0.48	320.05	3.14	1.43	4.58	4.02
83	surf	N Kaneohe	10/28/16	21.4615	-157.8413	95	24.55	11.00	7.05	0.40	0.35	108.68	0.47	0.79	1.26	5.80
84	surf	Kahaluu Beach	3/27/17	21.4606	-157.8407	701	23.87	1.58	29.40	1.11	0.79	384.34	7.25	13.57	20.82	8.58
85	surf	Kahaluu Beach	3/28/17	21.4535	-157.8255	90	25.35	32.05	29.33	1.37	0.96	76.66	6.31	16.30	22.61	6.72
86	surf	Kahaluu Beach	3/28/17	21.4592	-157.8320	23	23.53	32.64	6.84	0.76	0.43	22.62	1.33	0.63	1.97	4.88
87	surf	Kahaluu Beach	3/28/17	21.4540	-157.8259	676	23.28	2.38	181.73	3.20	2.73	945.06	129.85	4.17	134.02	47.71
88	surf	Kahaluu Beach	3/28/17	21.4531	-157.8251	156	25.52	20.30	57.47	2.12	1.55	284.63	0.47	47.66	48.13	9.34

89	surf	Heeia Beach	3/29/17	21.4401	-157.8086	43	24.65	16.24	6.43	0.39	0.31	211.32	0.08	1.82	1.90	4.52
90	surf	Heeia Beach	3/29/17	21.4400	-157.8090	0	23.05	21.20	9.01	0.58	0.30	111.85	0.13	2.74	2.87	6.14
91	surf	Heeia Beach	3/29/17	21.4405	-157.8087	65	28.75	22.72	6.10	0.43	0.24	72.95	0.17	1.40	1.58	4.52
92	surf	Heeia Beach	3/29/17	21.4404	-157.8087	44	26.53	27.42	31.04	0.35	0.21	87.70	0.03	24.17	24.20	6.84
93	surf	Kahaluu Beach	3/28/17	21.4534	-157.8254	248	25.02	1.68	81.69	2.62	2.15	1076.64	46.61	0.34	46.94	34.75
94	surf	Kaneohe Bay	7/14/17	21.4130	-157.7857	46		18.59	11.46	0.47	0.34	189.27	3.75	2.44	6.19	5.27
95	surf	Kaneohe Bay	7/14/17	21.4128	-157.7850	23		15.46	10.68	0.35	0.27	225.01	4.35	2.97	7.31	3.37
96	gw	Kahaluu Beach	3/27/17	21.4601	-157.8402	2090	25.45	8.35	39.40	2.38	1.49	443.54	0.08	26.94	27.02	12.38
97	gw	Kahaluu Beach	3/27/17	21.4610	-157.8412	966	24.61	9.20	50.30	0.91	0.53	401.12	0.08	34.13	34.21	16.09
98	gw	Kahaluu Beach	3/27/17	21.4610	-157.8412	1150	24.71	15.96	55.33	1.20	0.35	308.61	0.10	47.48	47.58	7.75
99	gw	Kahaluu Beach	3/27/17	21.4610	-157.8412	2705	25.07	16.49	61.11	1.27	0.97	430.37	0.18	58.66	58.84	2.27
100	gw	Kahaluu Beach	3/27/17	21.4606	-157.8407	2349	24.72	23.61	66.91	0.99	0.68	336.01	0.11	61.42	61.53	5.38
101	gw	Kahaluu Beach	3/27/17	21.4606	-157.8407	2487	25.08	24.69	166.80	0.42	0.22	231.10	0.14	152.85	152.99	13.81
102	gw	Kahaluu Beach	3/28/17	21.4532	-157.8250	737	24.77	32.15	9.72	0.86	0.59	53.66	0.99	3.84	4.83	4.90
103	gw	Kahaluu Beach	3/28/17	21.4534	-157.8254	3053	24.52	0.46	9.74	4.34	3.35	721.80	0.44	4.33	4.77	4.97
104	gw	Kahaluu Beach	3/28/17	21.4540	-157.8259	274	24.72	26.69	12.30	1.91	1.59	125.21	1.77	6.10	7.87	4.42
105	gw	Heeia Beach	3/29/17	21.4400	-157.8090	700	24.99	26.73	64.56	3.74	0.19	160.84	0.03	63.72	63.75	0.81
106	gw	Heeia Beach	3/29/17	21.4401	-157.8086	153	25.68	27.16	29.50	0.37	0.21	71.62	0.02	29.20	29.22	0.29
107	gw	Heeia Beach	3/29/17	21.4400	-157.8090	394	24.90	27.43	77.05	5.67	0.18	169.02	0.02	70.86	70.88	6.16
108	surf	Kaneohe Bay	7/14/17	21.4126	-157.7841	114		15.08	14.33	0.49	0.43	281.06	8.48	2.13	10.61	3.72
109	surf	Hoomaluhia Reservoir	7/14/17	21.3884	-157.8064	273		0.25	13.52	0.10	0.07	412.21	4.52	2.30	6.82	6.70
110	surf	Hoomaluhia Reservoir	7/14/17	21.3906	-157.8052	45		0.52	43.13	0.27	0.17	412.58	6.29	10.23	16.52	26.60
111	surf	Kapunahala Stream	7/18/17	21.4105	-157.8032	113	29.70	0.28	6.51	0.66	0.64	576.52	1.02	0.78	1.81	4.70
112	surf	Kapunahala Stream	7/18/17	21.4040	-157.8075	133	26.80	0.25	9.72	0.49	0.44	566.30	2.55	0.36	2.91	6.80
113	surf	Kapunahala Stream	7/18/17	21.4045	-157.8058	0	26.68	0.24	10.25	0.97	0.87	570.29	7.45	0.11	7.56	2.70
114	surf	Kamooalii Stream	7/18/17	21.3993	-157.8027	69	29.75	0.25	54.91	0.37	0.36	492.88	32.28	0.90	33.19	21.72

115	surf	Kamooalii Stream	7/18/17	21.4074	-157.8018	45	30.10	0.24	58.61	0.40	0.38	499.15	33.85	3.68	37.53	21.08
116	surf	Kaneohe Stream	7/19/17	21.4118	-157.7910	370	23.40	0.27	27.93	0.45	0.21	524.10	18.37	0.11	18.48	9.45
117	surf	Kaneohe Stream	7/19/17	21.4112	-157.7896	307	23.22	0.95	30.28	0.64	0.54	446.54	18.30	10.76	29.06	1.21
118	surf	Kaneohe Stream	7/19/17	21.4108	-157.7888	309	23.48	1.07	29.03	0.70	0.61	517.85	22.73	1.05	23.77	5.26
119	surf	Kaneohe Stream	7/19/17	21.4112	-157.7864	315	24.28	7.20	70.35	2.84	2.01	221.21	0.45	55.18	55.63	14.72
120	surf	Kaneohe Stream	7/19/17	21.4110	-157.7854	223	25.48	15.09	25.82	0.42	0.41	324.86	14.18	7.91	22.09	3.73
121	surf	Kapunahala Stream	8/2/17	21.4030	-157.8061	25	20.63	0.23	10.70	1.21	0.89	538.62	6.01	0.12	6.13	4.57
122	surf	Kapunahala Stream	8/2/17	21.4109	-157.8009	137	23.35	0.2	11.00	0.55	0.51	395.69	2.08	3.11	5.19	5.81
123	surf	Kapunahala Stream	8/2/17	21.4100	-157.8047	166	23.42	0.19	11.59	1.10	0.54	350.26	3.78	0.36	4.14	7.45
124	surf	Piho Stream	8/25/17	21.3840	-157.8068	21		0.08	9.74	0.55	0.58	518.07	1.05	0.09	1.14	8.60
125	surf	Kaneohe Stream	8/25/17	21.4119	-157.7986	2450		0.15	129.41	2.36	2.05	961.43	102.60	1.53	104.13	25.28
126	surf	Kaneohe Stream	8/25/17	21.4119	-157.7986	497		0.13	85.99	1.30	1.28	873.76	64.59	0.00	64.59	21.41
127	gw	Kaneohe Stream	7/19/17	21.4118	-157.7910	1183	23.46	0.62	11.21	0.71	0.65	575.20	4.26	0.11	4.37	6.84
128	gw	Kaneohe Stream	7/19/17	21.4112	-157.7896	872	25.70	28.07	16.95	0.61	0.60	189.88	9.09	5.95	15.04	1.91
129	gw	Kaneohe Stream	7/19/17	21.4108	-157.7888	840	26.18	26.49	63.38	1.09	0.59	278.55	2.46	47.77	50.23	13.15
130	gw	Kapunahala Stream	7/28/17	21.4040	-157.8075	2885	26.78	0.36	43.21	1.93	1.66	427.53	0.38	37.48	37.85	5.35
131	gw	Kapunahala Stream	8/2/17	21.4030	-157.8061	515	21.26	0.28	19.86	2.78	2.32	586.71	0.84	16.00	16.83	3.03
132	gw	Kapunahala Stream	8/2/17	21.4060	-157.8056	98	25.04	0.19	28.98	0.61	0.40	151.58	7.94	0.53	8.47	20.51
133	gw	Kapunahala Stream	8/2/17	21.4078	-157.8052	2991	23.61	0.27	39.84	0.37	0.28	369.96	0.69	35.17	35.86	3.99
134	gw	Kamooalii Stream	8/2/17	21.4018	-157.8026	141	25.86	0.19	24.83	0.64	0.33	292.74	14.11	0.66	14.76	10.06
135	surf	Kaneohe Stream	11/13/17	21.4117	-157.7982	200	22.78	0.22	33.20	0.62	0.49	443.31	20.52	0.11	20.63	12.57
136	surf	Kaneohe Stream	11/13/17	21.4118	-157.7985	3417	24.50	0.23	142.96	1.82	1.66	914.26	136.91	1.11	138.02	4.94
137	surf	Kapunahala Stream	11/13/17	21.4039	-157.8058	32	22.27	0.16	15.89	1.46	1.12	594.60	9.42	0.13	9.56	6.33
138	surf	Kapunahala Stream	11/13/17	21.4054	-157.8059	252	22.79	0.01	8.18	0.77	0.66	31.21	0.66	3.58	4.25	3.93

139	surf	Kaneohe Stream	11/13/17	21.4077	-157.8052	1321	23.68	0.16	13.33	1.42	0.48	482.74	7.20	0.47	7.67	5.66
140	surf	Kaneohe Stream	11/13/17	21.4108	-157.8028	279	26.08	0.16	15.92	1.08	0.74	482.22	6.63	1.81	8.44	7.48
141	surf	Kaneohe Stream	11/17/17	21.4117	-157.7910	379	22.31	0.16	23.14	0.90	0.64	494.12	14.31	0.08	14.38	8.76
142	surf	Kaneohe Stream	11/17/17	21.4115	-157.7902	365	22.58	0.29	54.43	0.66	0.49	463.28	12.41	41.40	53.81	0.62
143	surf	Kaneohe Stream	11/17/17	21.4110	-157.7879	255	23.53	6.25	8.27	0.96	0.74	540.19	2.91	0.18	3.08	5.18
144	surf	Kaneohe Stream	11/17/17	21.4110	-157.7856	114	23.58	9.44	8.29	0.67	0.50	28.46	1.73	2.75	4.47	3.81
145	surf	Kamooalii Stream	11/17/17	21.4074	-157.8018	86	23.55	0.71	37.40	0.56	0.50	426.96	26.82	0.84	27.66	9.74
146	surf	Kuou Stream (Hoomaluhia)	11/17/17	21.3897	-157.8068	139	24.17	0.26	13.48	0.87	0.61	515.30	7.40	0.22	7.62	5.86
147	surf	Hoomaluhia Reservoir	11/17/17	21.3897	-157.8063	114	24.38	0.21	28.15	0.43	0.23	398.97	12.23	7.63	19.85	8.30
148	surf	Piho Stream (Hoomaluhia)	11/17/17	21.3873	-157.8044	320	25.07	0.20	18.13	0.53	0.34	393.81	8.10	3.44	11.54	6.59
149	surf	Kapunahala Stream	11/17/17	21.4041	-157.8075	97	23.23	0.21	8.41	0.81	0.74	569.95	4.59	0.27	4.86	3.55
150	gw	Kaneohe Stream	11/13/17	21.4117	-157.7982	702	23.43	0.40	23.21	1.92	1.62	422.82	15.63	0.13	15.76	7.45
151	gw	Kaneohe Stream	11/13/17	21.4118	-157.7985	1869	24.20	0.23	146.44	1.45	1.24	795.12	135.97	8.33	144.30	2.15
152	gw	Kapunahala Stream	11/13/17	21.4054	-157.8059	1537	25.02	0.22	34.41	1.53	0.82	474.39	1.04	31.80	32.84	1.58
153	gw	Kaneohe Stream	11/13/17	21.4077	-157.8052	3469	25.28	0.16	32.91	0.26	0.20	372.82	1.54	30.10	31.65	1.26
154	gw	Kaneohe Stream	11/17/17	21.4117	-157.7910	1883	23.00	0.41	17.13	0.92	0.70	498.36	11.93	0.38	12.31	4.82
155	gw	Kaneohe Stream	11/17/17	21.4115	-157.7902	2704	24.58	13.66	75.90	0.94	0.74	534.76	0.18	68.01	68.19	7.71
156	gw	Kaneohe Stream	11/17/17	21.4110	-157.7879	399	23.27	0.10	28.32	1.08	0.81	91.86	0.12	30.33	30.45	0.00
157	gw	Kaneohe Beach	11/17/17	21.4128	-157.7854	426	25.23	31.48	23.04	1.30	1.17	130.65	19.97	0.48	20.45	2.59
158	surf	Ahuimanu Stream	2/28/18	21.4291	-157.8418	23		0.24	12.87	1.43	1.19	599.57	11.28	0.07	11.35	1.52
159	surf	Ahuimanu Stream	2/28/18	21.4298	-157.8407	23		0.24	9.86	1.12	1.02	570.85	8.67	0.06	8.73	1.13
160	surf	Ahuimanu Stream	2/28/18	21.4307	-157.8390	92		0.24	6.73	0.98	0.78	568.52	5.09	0.05	5.14	1.59
161	gw	Kahaluu Beach	6/14/17	21.4601	-157.8399	1516	27.09	12.68	20.59	7.33	2.23	578.39	0.11	14.98	15.09	5.50

162	gw	Kahaluu Beach	6/14/17	21.4601	-157.8399	2006	27.09	7.02	15.72	3.04	2.91	658.09	0.05	8.06	8.11	7.61
163	gw	Kahaluu Beach	6/14/17	21.4601	-157.8399	1824	27.6	3.24	17.02	12.75	10.33	610.50	0.01	14.05	14.06	2.96
164	gw	Kahaluu Beach	6/23/17	21.4601	-157.8399	706	28.33	24.75	37.77	1.82	1.21	221.80	0.27	33.69	33.96	3.81
165	gw	Kahaluu Beach	6/23/17	21.4601	-157.8399	156	27.77	22.31	23.31	0.92	0.86	265.32	0.10	19.26	19.36	3.95
166	gw	Kahaluu Beach	6/14/17	21.4609	-157.8398	1427	26.36	13.52	53.03	1.13	1.03	591.43	0.05	30.97	31.02	22.01
167	gw	Kahaluu Beach	6/14/17	21.4609	-157.8398	1429	26.21	14.31	59.22	1.21	1.14	631.69	0.04	35.02	35.06	24.16
168	gw	Kahaluu Beach	6/14/17	21.4609	-157.8398	1786	26.68	14.209	71.25	0.80	0.71	602.35	0.02	65.02	65.04	6.21
169	gw	Kahaluu Beach	6/14/17	21.4609	-157.8398	2620	26.36	12.55	46.63	2.21	1.86	587.52	0.01	37.71	37.72	8.91
170	gw	Kahaluu Beach	6/23/17	21.4603	-157.8404	2034	24.16	15.29	71.30	1.00	0.89	627.61	0.04	46.14	46.18	25.12
171	gw	Kahaluu Beach	6/23/17	21.4603	-157.8404	943	26.64	23.29	19.38	1.81	1.68	230.93	0.44	11.91	12.35	7.03
172	gw	Kahaluu Beach	6/23/17	21.4611	-157.8395	859	26.82	25.33	22.44	0.77	0.57	218.22	0.06	19.26	19.32	3.12
173	gw	Kahaluu Beach	6/23/17	21.4611	-157.8395	582	27.07	27.89	11.59	1.42	1.23	178.62	0.21	8.96	9.17	2.42
174	well	Haiku tunnel	2/6/13	21.4064	-157.8312	571.2	18.52	0.06	12.35	1.081	1.326	381.30	12.71	0	12.71	-0.36
175	well	Haiku Well	2/6/13	21.4065	-157.8312	1057.5	19.32	0.07	12.07	1.193	1.538	536.00	11.62	0	11.62	0.45
176	well	Kapuna 1 springs	2/6/13	21.4113	-157.8223	9229.5	21.0	0.1	13.22	1.235	1.432	549.37	12.58	0	12.58	0.64
177	well	Kapuna 2 springs	2/6/13	21.4113	-157.8223	5896.6	21.71	0.11	10.82	1.173	1.365	680.91	10.11	0	10.11	0.71
178	well	Ioleka'a	2/6/13	21.4153	-157.8252	2551.9	21.79	0.09	9.095	2.409	2.662	626.95	7.723	0	7.72	1.37
179	well	Kahalu'u Tunnel	2/6/13	21.4355	-157.8528	831.0	19.02	0.07	16.95	1.111	1.466	486.79	12.93	0	12.93	4.01
180	well	Luluku Well	2/6/13	21.3918	-157.8166	4671.3	20.12	0.09	22.69	1.385	1.527	554.42	17.34	0	17.34	5.35
181	well	Waihee Tunnel	1/25/17	21.4464	-157.8583	1451.08	19.82	0.07	17.277	1.324	1.453	543.00	14.065	0.143	14.21	3.21
182	well	Waihee Inclined Well	1/25/17	21.4419	-157.8675	903	19.33	0.04	16.064	1.291	1.388	458.00	8.567	0.143	8.71	7.50
183	well	Kahaluu	1/23/17	21.4347	-157.8561	363	19.34	0.06	17.42	1.13	1.19	444.38	11.71	0.21	11.92	5.50

B. Radon survey data

Lat	Long	Datetime	Depth (m)	Salinity	Temp (deg C)	Rn (Bq/m^3)
21.4849	157.8470	10/28/16 9:44	0.42	15.87	22.42	0.00
21.4846	157.8463	10/28/16 9:49	0.43	15.18	22.44	19.70
21.4844	157.8456	10/28/16 9:54	0.43	14.22	22.44	0.00
21.4845	-157.8443	10/28/16 9:59	0.45	11.04	21.24	79.00
21.4854	-157.8427	10/28/16 10:04	0.45	7.88	21.55	19.70
21.4840	-157.8419	10/28/16 10:09	0.44	9.51	22.47	39.20
21.4838	-157.8418	10/28/16 10:14	0.45	21.18	23.15	98.30
21.4821	-157.8412	10/28/16 10:19	0.46	17.80	23.39	59.00
21.4803	-157.8414	10/28/16 10:24	0.46	20.63	23.36	19.30
21.4785	-157.8416	10/28/16 10:29	0.45	22.88	23.41	38.60
21.4775	-157.8417	10/28/16 10:34	0.45	23.12	23.48	38.50
21.4767	-157.8418	10/28/16 10:39	0.45	22.60	23.50	38.40
21.4758	-157.8422	10/28/16 10:44	0.45	23.76	23.31	115.00
21.4747	-157.8427	10/28/16 10:49	0.44	22.42	23.58	115.00
21.4734	-157.8432	10/28/16 10:54	0.46	23.49	23.40	173.00
21.4724	-157.8434	10/28/16 10:59	0.46	19.81	23.17	115.00
21.4716	-157.8444	10/28/16 11:04	0.45	18.24	23.44	96.00
21.4706	-157.8443	10/28/16 11:09	0.45	17.67	23.56	96.20
21.4700	-157.8441	10/28/16 11:14	0.45	17.79	23.83	76.70
21.4686	-157.8434	10/28/16 11:19	0.45	20.99	23.31	171.00
21.4683	-157.8422	10/28/16 11:24	0.44	24.10	23.38	133.00
21.4673	-157.8423	10/28/16 11:29	0.44	20.88	23.82	171.00
21.4666	-157.8422	10/28/16 11:34	0.44	11.88	23.97	75.70
21.4651	-157.8428	10/28/16 11:39	0.46	8.01	24.01	209.00
21.4645	-157.8427	10/28/16 11:44	0.45	10.80	23.84	190.00
21.4632	-157.8420	10/28/16 11:49	0.46	8.95	24.40	114.00
21.4619	-157.8415	10/28/16 11:54	0.45	12.02	24.81	94.90
21.4610	-157.8410	10/28/16 11:59	0.44	15.14	23.91	114.00

21.4134	-157.7852	8/7/17 9:12	0.50	20.65	25.88	18.51
21.4142	-157.7857	8/7/17 9:17	1.07	20.43	25.61	18.51
21.4140	-157.7860	8/7/17 9:22	0.33	20.89	25.70	148.10
21.4138	-157.7862	8/7/17 9:27	0.50	18.03	27.04	166.61
21.4137	-157.7863	8/7/17 9:32	0.50	17.35	27.05	222.15
21.4143	-157.7858	8/7/17 9:37	0.50	22.61	25.75	296.20
21.4145	-157.7866	8/7/17 9:42	0.57	22.50	25.91	222.15
21.4148	-157.7868	8/7/17 9:47	0.87	22.17	25.96	314.71
21.4149	-157.7870	8/7/17 9:52	0.72	22.03	26.06	333.22
21.4146	-157.7872	8/7/17 9:57	0.30	19.70	26.49	314.71
21.4145	-157.7873	8/7/17 10:02	0.50	19.72	26.97	314.71
21.4145	-157.7873	8/7/17 10:07	0.50	19.81	27.11	314.71
21.4145	-157.7873	8/7/17 10:12	0.50	20.16	26.92	277.68
21.4145	-157.7873	8/7/17 10:18	0.50	20.30	27.08	92.56
21.4153	-157.7867	8/7/17 10:23	1.77	25.29	26.32	111.07
21.4157	-157.7869	8/7/17 10:28	1.65	24.81	26.34	203.63
21.4160	-157.7869	8/7/17 10:33	5.55	25.03	26.45	203.63
21.4169	-157.7870	8/7/17 10:38	4.45	26.63	26.46	185.12
21.4179	-157.7876	8/7/17 10:43	0.50	26.65	26.43	74.05
21.4184	-157.7889	8/7/17 10:48	2.76	24.51	26.24	111.07
21.4193	-157.7891	8/7/17 10:53	7.13	24.75	26.34	92.56
21.4204	-157.7888	8/7/17 10:58	3.66	26.79	26.55	129.59
21.4214	-157.7882	8/7/17 11:03	1.13	27.47	27.15	92.56
21.4224	-157.7877	8/7/17 11:08	0.50	33.90	27.94	129.59
21.4235	-157.7879	8/7/17 11:13	4.02	33.90	27.86	74.05
21.4244	-157.7883	8/7/17 11:18	1.04	33.90	28.15	111.07
21.4252	-157.7893	8/7/17 11:23	1.12	33.90	28.25	185.12
21.4254	-157.7903	8/7/17 11:28	3.96	33.56	27.30	185.12
21.4260	-157.7909	8/7/17 11:33	1.18	33.81	27.68	129.59
21.4269	-157.7909	8/7/17 11:38	1.38	33.65	27.58	111.07

21.4282	-157.7911	8/7/17 11:43	1.40	33.61	27.47	37.02
21.4293	-157.7927	8/7/17 11:48	1.02	33.90	27.72	37.02
21.4295	-157.7942	8/7/17 11:53	1.37	33.90	27.81	111.07
21.4296	-157.7954	8/7/17 11:58	1.67	33.90	27.90	111.07
21.4285	-157.7960	8/7/17 12:03	1.34	33.90	28.07	92.56
21.4275	-157.7955	8/7/17 12:08	2.33	33.90	27.77	74.05
21.4268	-157.7953	8/7/17 12:13	2.18	33.90	28.36	74.05
21.4260	-157.7953	8/7/17 12:18	1.96	33.90	28.68	37.02
21.4257	-157.7963	8/7/17 12:23	1.15	33.90	28.44	74.05
21.4258	-157.7974	8/7/17 12:28	1.52	33.90	28.38	148.10
21.4255	-157.7981	8/7/17 12:33	1.85	33.90	28.68	111.07
21.4252	-157.7993	8/7/17 12:38	1.95	33.90	28.90	148.10
21.4255	-157.8004	8/7/17 12:43	1.43	33.90	28.44	111.07
21.4266	-157.8013	8/7/17 12:48	1.12	33.90	28.64	240.66
21.4274	-157.8028	8/7/17 12:53	0.92	33.90	28.50	129.59
21.4286	-157.8039	8/7/17 12:58	1.64	33.90	28.80	92.56
21.4299	-157.8042	8/7/17 13:03	1.25	33.90	28.50	203.63
21.4305	-157.8050	8/7/17 13:08	0.82	33.90	27.87	92.56
21.4317	-157.8054	8/7/17 13:13	1.10	33.90	27.80	92.56
21.4329	-157.8051	8/7/17 13:18	1.78	33.90	27.54	259.17
21.4341	-157.8047	8/7/17 13:23	1.47	33.90	27.45	74.05
21.4356	-157.8050	8/7/17 13:28	1.44	33.90	27.88	55.54
21.4367	-157.8053	8/7/17 13:33	1.71	33.90	28.09	129.59
21.4379	-157.8060	8/7/17 13:38	2.29	33.90	27.57	129.59
21.4390	-157.8069	8/7/17 13:43	2.24	33.90	27.82	92.56
21.4400	-157.8080	8/7/17 13:48	1.30	33.90	28.59	55.54
21.4404	-157.8088	8/7/17 13:53	0.89	33.90	29.22	74.05
21.4434	-157.8120	8/18/17 9:04	0.10	33.40	27.75	0.00
21.4439	-157.8123	8/18/17 9:09	0.10	33.04	27.30	0.00
21.4446	-157.8127	8/18/17 9:14	1.07	32.91	27.10	18.64

21.4455	-157.8131	8/18/17 9:19	1.43	32.87	27.11	18.64
21.4463	-157.8134	8/18/17 9:24	1.52	32.76	26.94	18.64
21.4474	-157.8139	8/18/17 9:29	1.04	32.75	27.12	37.29
21.4484	-157.8142	8/18/17 9:34	1.22	32.78	27.49	18.64
21.4494	-157.8143	8/18/17 9:39	1.40	32.74	27.29	0.00
21.4507	-157.8142	8/18/17 9:44	1.95	32.76	27.38	18.64
21.4519	-157.8146	8/18/17 9:49	2.32	32.75	27.26	93.22
21.4532	-157.8150	8/18/17 9:54	1.65	32.75	27.75	37.29
21.4546	-157.8158	8/18/17 9:59	1.92	32.73	27.75	37.29
21.4548	-157.8171	8/18/17 10:04	1.80	32.73	27.81	74.58
21.4542	-157.8184	8/18/17 10:09	1.10	32.67	27.53	74.58
21.4536	-157.8192	8/18/17 10:14	1.16	32.68	27.63	37.29
21.4528	-157.8203	8/18/17 10:19	1.13	32.63	27.52	130.51
21.4527	-157.8216	8/18/17 10:24	1.68	32.62	27.60	0.00
21.4531	-157.8228	8/18/17 10:29	1.19	32.63	27.55	55.93
21.4538	-157.8240	8/18/17 10:34	4.88	32.68	27.86	55.93
21.4534	-157.8249	8/18/17 10:39	0.73	32.50	28.05	93.22
21.4542	-157.8259	8/18/17 10:44	0.70	32.18	28.24	93.22
21.4552	-157.8264	8/18/17 10:49	1.19	31.63	28.33	111.87
21.4564	-157.8265	8/18/17 10:54	1.83	31.40	27.77	55.93
21.4565	-157.8276	8/18/17 10:59	1.16	31.97	28.04	55.93
21.4571	-157.8288	8/18/17 11:04	1.19	32.06	28.20	111.87
21.4581	-157.8300	8/18/17 11:09	1.25	31.44	27.93	74.58
21.4581	-157.8310	8/18/17 11:14	0.98	30.01	27.70	37.29
21.4588	-157.8316	8/18/17 11:19	0.91	28.85	27.67	55.93
21.4590	-157.8319	8/18/17 11:24	0.10	28.67	28.37	55.93
21.4128	-157.7853	9/8/17 9:19	1.07	17.31	28.03	127.00
21.4131	-157.7849	9/8/17 9:24	0.33	21.46	28.05	174.00
21.4132	-157.7844	9/8/17 9:29	0.50	27.78	27.83	133.00
21.4136	-157.7832	9/8/17 9:34	0.50	30.17	27.74	203.00

21.4144	-157.7825	9/8/17 9:40	0.50	32.05	28.15	252.00
21.4151	-157.7816	9/8/17 9:45	0.57	32.11	28.41	209.00
21.4156	-157.7810	9/8/17 9:50	0.87	32.15	28.34	211.00
21.4163	-157.7802	9/8/17 9:55	0.72	32.19	28.31	166.00
21.4166	-157.7796	9/8/17 10:00	0.30	32.30	28.30	192.00
21.4169	-157.7788	9/8/17 10:05	0.50	32.37	28.28	72.70
21.4172	-157.7781	9/8/17 10:10	0.50	32.42	28.30	122.00
21.4178	-157.7773	9/8/17 10:15	0.50	32.50	28.34	74.20
21.4184	-157.7765	9/8/17 10:20	0.50	32.54	28.36	99.30
21.4187	-157.7763	9/8/17 10:25	1.77	32.58	28.36	124.00
21.4191	-157.7754	9/8/17 10:30	1.65	32.64	28.39	0.00
21.4182	-157.7751	9/8/17 10:35	5.55	32.68	28.41	50.30
21.4180	-157.7742	9/8/17 10:40	4.45	32.74	28.42	25.40
21.4179	-157.7734	9/8/17 10:45	0.50	32.81	28.44	50.80
21.4179	-157.7723	9/8/17 10:50	2.76	32.89	28.49	25.40
21.4175	-157.7721	9/8/17 10:55	7.13	32.99	28.71	51.10
21.4170	-157.7718	9/8/17 11:00	3.66	33.05	28.74	103.00
21.4169	-157.7721	9/8/17 11:05	1.13	33.12	28.77	51.30
21.4153	-157.7723	9/8/17 11:10	0.50	33.18	28.78	0.00
21.4141	-157.7720	9/8/17 11:15	4.02	33.34	28.96	0.00
21.4137	-157.7719	9/8/17 11:20	1.04	33.59	29.71	26.10
21.4130	-157.7727	9/8/17 11:25	1.12	33.62	29.75	105.00
21.4133	-157.7742	9/8/17 11:30	3.96	33.47	29.03	79.60
21.4131	-157.7754	9/8/17 11:35	1.18	33.56	28.81	79.60
21.4125	-157.7767	9/8/17 11:40	1.38	33.64	28.78	53.10
21.4122	-157.7779	9/8/17 11:45	1.40	33.58	28.67	79.50
21.4122	-157.7791	9/8/17 11:50	1.02	33.69	28.92	53.10
21.4121	-157.7804	9/8/17 11:55	1.37	33.78	29.26	161.00
21.4116	-157.7812	9/8/17 12:00	1.67	33.92	29.96	26.90
21.4121	-157.7827	9/8/17 12:05	1.34	32.66	29.79	53.80

21.4123	-157.7840	9/8/17 12:10	2.33	33.65	29.73	27.00
21.4114	-157.7848	9/8/17 12:15	2.18	17.88	28.80	53.50
21.4110	-157.7854	9/8/17 12:20	1.96	8.13	28.33	241.00
21.4110	-157.7859	9/8/17 12:25	1.15	1.14	27.83	375.00
21.4110	-157.7862	9/8/17 12:30	1.52	0.50	26.65	1050.00
21.4110	-157.7868	9/8/17 12:35	1.85	0.20	26.21	1630.00
21.4111	-157.7873	9/8/17 12:40	1.95	0.20	26.58	1040.00
21.4108	-157.7887	9/8/17 12:45	1.43	4.60	28.33	1420.00
21.4542	-157.8259	6/28/17 10:47	1.40	32.78	29.56	0.00
21.4542	-157.8259	6/28/17 10:52	1.40	33.11	28.61	182.29
21.4542	-157.8258	6/28/17 10:57	1.40	33.13	28.59	547.03
21.4543	-157.8252	6/28/17 11:02	1.40	33.10	28.84	181.27
21.4543	-157.8250	6/28/17 11:07	1.40	33.14	28.92	0.00
21.4552	-157.8261	6/28/17 11:12	1.40	33.13	28.76	181.60
21.4566	-157.8268	6/28/17 11:17	1.40	33.06	28.67	0.00
21.4568	-157.8284	6/28/17 11:22	1.40	33.02	28.71	181.94
21.4577	-157.8295	6/28/17 11:27	1.40	32.98	29.64	177.96
21.4583	-157.8310	6/28/17 11:32	1.40	33.08	29.01	0.00
21.4591	-157.8315	6/28/17 11:37	1.40	33.10	29.58	178.07
21.4603	-157.8319	6/28/17 11:42	1.40	33.12	29.11	540.21
21.4608	-157.8322	6/28/17 11:47	1.40	33.10	29.05	0.00
21.4619	-157.8323	6/28/17 11:52	1.40	33.07	29.19	0.00
21.4624	-157.8336	6/28/17 11:57	1.40	30.38	28.40	0.00
21.4616	-157.8343	6/28/17 12:02	1.40	30.05	28.56	559.19
21.4613	-157.8354	6/28/17 12:07	1.00	29.65	29.82	181.27
21.4612	-157.8366	6/28/17 12:12	0.50	21.30	30.32	189.55
21.4609	-157.8377	6/28/17 12:17	0.50	20.01	28.24	603.66
21.4608	-157.8380	6/28/17 12:22	0.50	13.52	29.85	404.40
21.4452	-157.8323	4/19/17 8:44	0.01	0.05	28.07	20.90
21.4457	-157.8325	4/19/17 8:49	0.01	0.08	27.05	20.80

21.4458	-157.8325	4/19/17 8:54	0.01	0.16	24.00	21.20
21.4459	-157.8325	4/19/17 8:59	0.01	0.09	23.75	63.00
21.4459	-157.8325	4/19/17 9:04	0.01	0.13	23.23	62.40
21.4461	-157.8328	4/19/17 9:09	0.01	0.16	22.91	0.00
21.4464	-157.8331	4/19/17 9:14	0.01	0.16	22.77	40.40
21.4471	-157.8337	4/19/17 9:19	0.01	0.17	22.46	40.20
21.4477	-157.8342	4/19/17 9:24	0.16	0.18	22.35	225.00
21.4482	-157.8346	4/19/17 9:29	0.16	0.18	22.54	368.00
21.4489	-157.8349	4/19/17 9:34	0.16	0.19	22.59	368.00
21.4492	-157.8349	4/19/17 9:39	0.16	0.19	22.64	715.00
21.4501	-157.8346	4/19/17 9:44	0.16	0.19	22.72	490.00
21.4512	-157.8344	4/19/17 9:49	0.16	0.19	22.81	797.00
21.4521	-157.8347	4/19/17 9:54	0.16	0.20	22.87	818.00
21.4529	-157.8353	4/19/17 9:59	0.15	0.20	22.94	818.00
21.4529	-157.8354	4/19/17 10:04	0.15	0.19	22.52	838.00
21.4517	-157.8351	4/19/17 10:09	0.15	0.18	22.01	897.00
21.4506	-157.8361	4/19/17 10:14	0.19	0.17	21.76	669.00
21.4473	-157.8381	4/19/17 10:49	0.03	0.16	21.07	211.00
21.4467	-157.8387	4/19/17 10:44	0.03	0.16	21.29	222.00
21.4460	-157.8391	4/19/17 10:39	0.05	0.15	20.91	323.00
21.4453	-157.8394	4/19/17 10:34	0.03	0.15	20.69	808.00
21.4446	-157.8405	4/19/17 10:29	0.03	0.15	20.93	534.00
21.4492	-157.8368	4/19/17 10:24	0.03	0.17	21.12	646.00
21.4498	-157.8364	4/19/17 10:19	0.02	0.17	21.42	669.00
21.4481	-157.8374	4/19/17 10:54	0.04	0.16	21.04	251.00
21.4446	-157.8407	4/19/17 10:59	0.04	0.15	21.13	242.00
21.4446	-157.8407	4/19/17 11:04	0.05	0.16	21.42	384.00
21.4447	-157.8407	4/19/17 11:09	0.05	0.22	23.02	211.00
21.4446	-157.8407	4/19/17 11:14	0.05	0.25	23.64	263.00
21.4451	-157.8395	4/19/17 11:19	0.02	0.26	23.67	202.00

21.4468	-157.8386	4/19/17 11:24	0.02	0.26	23.77	182.00
21.4472	-157.8381	4/19/17 11:29	0.03	0.26	23.92	142.00
21.4473	-157.8382	4/19/17 11:34	0.03	0.26	24.16	81.10
21.4473	-157.8381	4/19/17 11:39	0.03	0.26	24.46	102.00
21.4473	-157.8381	4/19/17 11:44	0.03	0.26	24.75	102.00
21.4473	-157.8381	4/19/17 11:49	0.03	0.26	25.03	123.00
21.4487	-157.8369	4/19/17 11:54	0.03	0.26	25.28	61.20
21.4493	-157.8366	4/19/17 11:59	0.03	0.26	25.44	164.00
21.4492	-157.8367	4/19/17 12:04	0.03	0.23	25.68	103.00
21.4497	-157.8365	4/19/17 12:09	0.03	0.16	25.90	82.10
21.4509	-157.8357	4/19/17 12:14	0.26	0.14	25.95	123.00
21.4523	-157.8350	4/19/17 12:19	0.03	0.12	26.07	164.00
21.4519	-157.8346	4/19/17 12:24	0.03	0.12	26.29	0.00
21.4499	-157.8346	4/19/17 12:29	0.03	0.10	26.59	20.50
21.4487	-157.8348	4/19/17 12:34	0.03	0.04	26.88	0.00
21.4467	-157.8334	4/19/17 14:03	0.02	0.16	26.45	143.00
21.4455	-157.8329	4/19/17 14:00	0.01	0.16	25.27	204.00
21.4447	-157.8330	4/19/17 13:55	0.02	0.16	24.66	245.00
21.4441	-157.8336	4/19/17 13:50	0.03	0.16	24.62	213.00
21.4441	-157.8336	4/19/17 13:45	0.03	0.16	24.60	102.00
21.4438	-157.8342	4/19/17 13:40	0.03	0.16	24.61	254.00
21.4438	-157.8342	4/19/17 13:35	0.03	0.16	24.55	164.00
21.4431	-157.8349	4/19/17 13:29	0.03	0.16	24.64	246.00
21.4431	-157.8349	4/19/17 13:24	0.03	0.16	24.72	246.00
21.4431	-157.8349	4/19/17 13:19	0.03	0.18	24.52	143.00
21.4422	-157.8353	4/19/17 13:14	0.03	0.19	24.52	226.00
21.4419	-157.8354	4/19/17 13:09	0.03	0.19	24.42	82.30
21.4419	-157.8354	4/19/17 13:04	0.05	0.13	24.25	41.10
21.4410	-157.8360	4/19/17 12:59	0.05	0.11	24.18	29.70
21.4410	-157.8360	4/19/17 12:54	0.05	0.12	24.23	0.00

21.4400	-157.8371	4/19/17 12:49	0.05	0.13	24.28	0.00
21.4394	-157.8375	4/19/17 12:44	0.05	0.15	24.17	20.50
21.4475	-157.8340	4/19/17 12:39	0.05	0.03	27.10	0.00
21.4453	-157.8322	9/30/16 9:08	0.16	0.29	26.02	19.10
21.4456	-157.8322	9/30/16 9:13	0.16	0.28	25.36	39.10
21.4461	-157.8328	9/30/16 9:19	0.16	0.28	25.39	39.10
21.4466	-157.8332	9/30/16 9:24	0.16	0.30	25.64	58.70
21.4463	-157.8331	9/30/16 10:49		0.30	25.10	583.00
21.4459	-157.8329	9/30/16 10:44	0.19	0.29	24.00	641.00
21.4450	-157.8330	9/30/16 10:39	0.16	0.29	24.08	660.00
21.4443	-157.8334	9/30/16 10:34	0.16	0.29	23.92	543.00
21.4438	-157.8339	9/30/16 10:29	0.16	0.28	23.81	527.00
21.4437	-157.8343	9/30/16 10:24	0.16	0.28	23.84	607.00
21.4434	-157.8348	9/30/16 10:19	0.16	0.28	23.81	451.00
21.4429	-157.8350	9/30/16 10:14	0.16	0.28	23.71	392.00
21.4422	-157.8354	9/30/16 10:09	0.16	0.28	23.53	411.00
21.4417	-157.8355	9/30/16 10:04	0.16	0.28	23.46	392.00
21.4409	-157.8361	9/30/16 9:59	0.16	0.28	23.25	529.00
21.4407	-157.8362	9/30/16 9:54	0.16	0.28	23.19	411.00
21.4398	-157.8373	9/30/16 9:49	0.16	0.28	23.24	294.00
21.4392	-157.8377	9/30/16 9:44	0.16	0.28	23.31	176.00
21.4393	-157.8377	9/30/16 9:39	0.16	0.28	22.83	196.00
21.4393	-157.8377	9/30/16 9:34	0.16	0.28	22.56	137.00
21.4465	-157.8332	9/30/16 9:29	0.16	0.18	22.71	117.00
21.4464	-157.8332	9/30/16 10:54	0.16	0.04	23.17	718.00
21.4393	-157.8377	9/30/16 10:59	0.19	0.11	23.32	746.00
21.4393	-157.8377	9/30/16 11:04	0.19	0.29	22.55	699.00
21.4393	-157.8377	9/30/16 11:09	0.19	0.29	22.66	698.00
21.4392	157.8377	9/30/16 11:14	0.19	0.29	22.74	796.00
21.4393	-157.8377	9/30/16 11:19	0.19	0.29	22.99	699.00

21.4400	-157.8371	9/30/16 11:24	0.19	0.29	23.57	641.00
21.4412	-157.8358	9/30/16 11:29	0.19	0.29	23.87	680.00
21.4419	-157.8354	9/30/16 11:34	0.19	0.29	23.97	796.00
21.4419	-157.8354	9/30/16 11:39	0.19	0.29	23.88	785.00
21.4419	-157.8355	9/30/16 11:44	0.19	0.29	23.86	815.00
21.4425	-157.8353	9/30/16 11:49	0.19	0.28	24.24	874.00
21.4430	-157.8349	9/30/16 11:54	0.19	0.28	24.34	427.00
21.4430	-157.8349	9/30/16 11:59	0.19	0.28	24.53	427.00
21.4430	-157.8349	9/30/16 12:04	0.19	0.28	24.61	629.00
21.4430	-157.8349	9/30/16 12:09	0.19	0.28	24.79	525.00
21.4432	-157.8349	9/30/16 12:14	0.19	0.29	25.56	582.00
21.4442	-157.8335	9/30/16 12:19	0.19	0.29	26.05	621.00
21.4453	-157.8330	9/30/16 12:24	0.19	0.30	26.33	785.00
21.4459	-157.8329	9/30/16 12:29	0.19	0.29	26.64	408.00
21.4459	-157.8329	9/30/16 12:34	0.19	0.29	26.02	642.00
21.4459	-157.8329	9/30/16 12:39	0.19	0.29	25.74	718.00
21.4459	-157.8329	9/30/16 12:44	0.19	0.29	25.58	602.00
21.4459	-157.8329	9/30/16 12:49	0.19	0.30	25.49	776.00
21.4464	-157.8332	9/30/16 12:54	0.19	0.27	25.75	718.00
21.4469	-157.8335	9/30/16 12:59	0.19	0.05	26.50	514.00
21.4469	-157.8335	9/30/16 13:04	0.16	0.27	25.71	679.00
21.4469	-157.8335	9/30/16 13:09	0.16	0.30	25.43	513.00
21.4469	-157.8335	9/30/16 13:14	0.16	0.30	25.99	563.00
21.4470	-157.8336	9/30/16 13:19	0.16	0.31	27.10	688.00
21.4485	-157.8348	9/30/16 13:24	0.16	0.32	27.39	718.00
21.4499	-157.8347	9/30/16 13:29	0.16	0.33	27.79	669.00
21.4511	-157.8344	9/30/16 13:34	0.16	0.33	27.96	718.00
21.4526	-157.8351	9/30/16 13:39	0.16	0.24	28.27	972.00
21.4527	-157.8351	9/30/16 13:44	0.16	0.05	29.57	524.00
21.4527	-157.8351	9/30/16 13:49	0.16	0.05	30.98	602.00

21.4527	-157.8351	9/30/16 13:54	0.16	0.05	32.15	485.00
21.4527	-157.8351	9/30/16 13:59	0.16	0.15	31.37	330.00
21.4527	-157.8351	9/30/16 14:04	0.16	0.33	28.30	455.00
21.4439	-157.8408	9/30/16 15:35	0.26	0.31	27.55	95.00
21.4447	-157.8401	9/30/16 15:30	0.02	0.31	27.47	133.00
21.4452	-157.8394	9/30/16 15:25	0.02	0.31	27.13	247.00
21.4461	-157.8391	9/30/16 15:20	0.02	0.32	27.26	171.00
21.4469	-157.8385	9/30/16 15:15	0.02	0.30	26.31	266.00
21.4475	-157.8379	9/30/16 15:10	0.02	0.28	24.76	311.00
21.4482	-157.8372	9/30/16 15:05	0.02	0.28	24.29	389.00
21.4490	-157.8468	9/30/16 15:00	0.02	0.28	23.85	272.00
21.4497	-157.8336	9/30/16 14:55	0.02	0.28	23.46	331.00
21.4503	-157.8367	9/30/16 14:50	0.02	0.28	23.56	272.00
21.4510	-157.8356	9/30/16 14:45	0.02	0.28	23.55	369.00
21.4518	-157.8350	9/30/16 14:40	0.16	0.28	23.46	629.00
21.4529	-157.8352	9/30/16 14:35	0.16	0.27	23.35	486.00
21.4529	-157.8352	9/30/16 14:30	0.16	0.27	23.11	389.00
21.4529	-157.8352	9/30/16 14:24	0.02	0.27	22.94	414.00
21.4529	-157.8352	9/30/16 14:19	0.02	0.27	22.50	428.00
21.4529	-157.8352	9/30/16 14:14	0.26	0.27	22.25	777.00
21.4535	-157.8356	9/30/16 14:09	0.26	0.19	22.30	658.00
21.4100	-157.8047	8/25/17 9:02	0.07	0.57	26.79	186.45
21.4087	-157.8051	8/25/17 9:07	0.07	0.29	23.84	149.16
21.4071	-157.8052	8/25/17 9:12	0.06	0.23	23.10	167.80
21.4053	-157.8059	8/25/17 9:17	0.05	0.22	22.86	24.52
21.4045	-157.8060	8/25/17 9:22	0.07	0.21	22.83	279.67
21.4045	-157.8060	8/25/17 9:27	0.07	0.23	23.07	223.73
21.4045	-157.8057	8/25/17 9:32	0.07	0.23	23.29	130.51
21.4038	-157.8058	8/25/17 9:37	0.07	0.22	23.14	167.80
21.4039	-157.8057	8/25/17 9:42	0.07	0.21	22.70	205.09

21.4041	-157.8057	8/25/17 9:47	0.06	0.21	22.42	186.45
21.4046	-157.8057	8/25/17 9:52	0.06	0.21	22.53	354.25
21.4048	-157.8059	8/25/17 9:57	0.06	0.21	22.76	205.09
21.4053	-157.8059	8/25/17 10:02	0.06	0.22	23.56	298.31
21.4059	-157.8057	8/25/17 10:07	0.06	0.22	24.12	130.51
21.4062	-157.8055	8/25/17 10:12	0.07	0.21	23.55	223.73
21.4067	-157.8053	8/25/17 10:17	0.07	0.21	23.41	167.80
21.4074	-157.8052	8/25/17 10:22	0.05	0.21	23.67	24.52
21.4081	-157.8052	8/25/17 10:27	0.07	0.21	24.14	279.67
21.4089	-157.8051	8/25/17 10:32	0.07	0.21	24.74	223.73
21.4045	-157.8057	8/25/17 9:37	0.07	0.23	23.29	130.51
21.4038	-157.8058	8/25/17 9:42	0.07	0.22	23.14	167.80
21.4039	-157.8057	8/25/17 9:47	0.07	0.21	22.70	205.09
21.4041	-157.8057	8/25/17 9:52	0.06	0.21	22.42	186.45
21.4046	-157.8057	8/25/17 9:57	0.06	0.21	22.53	354.25
21.4048	-157.8059	8/25/17 10:02	0.06	0.21	22.76	205.09
21.4053	-157.8059	8/25/17 10:07	0.06	0.22	23.56	298.31
21.4059	-157.8057	8/25/17 10:12	0.06	0.22	24.12	130.51
21.4062	-157.8055	8/25/17 10:17	0.07	0.21	23.55	223.73
21.4067	-157.8053	8/25/17 10:22	0.07	0.21	23.41	167.80
21.4074	-157.8052	8/25/17 10:27	0.07	0.21	23.67	166.32

S2 Table. Median radon concentrations in coastal grab samples. Radon concentrations are in Bq/m^3 ± the interquartile range (IQR) by sector of Kāneʻohe Bay.

Location		Median Rn
Northwest	Ground (n = 25)	1,400 ± 1,200
	Surface (n = 23)	95 ± 150
Central	Ground (n = 3)	390 ± 270
	Surface (n = 4)	43 ± 17
South	Ground (n = 5)	860 ± 590
	Surface (n = 7)	170 ± 220

S3 Table. Median radon concentrations in stream grab samples. Radon concentrations are in Bq/m^3 ± IQR for the July and February sampling periods, by sub-watershed.

Location		July Sampling Period Rn	February Sampling Period Rn
Kahaluʻu	ground	800 ± 1,020 (n = 13)	730 ± 860 (n = 4)
	surface	310 ± 160 (n = 12)	85 ± 290 (n = 4)
ʻĀhuimanu	ground	1,050 ± 1,200 (n = 8)	480 ± 340 (n = 8)
	surface	590 ± 690 (n = 11)	130 ± 330 (n = 3)
Kāneʻohe	ground	900 ± 1,200 (n = 8)	1,900 ± 1,200 (n = 6)
	surface	140 ± 250 (n = 19)	250 ± 230 (n = 13)

S4 Table. Modeled vs. non-modeled groundwater fluxes. (A) Modeled SGD fluxes in 10^4 m^3/day for the July sampling period, percentage difference between SGD fluxes using non-modeled and modeled radon by sector of Kāneʻohe Bay. **(B)** Modeled groundwater (GW) fluxes in 10^4 m^3/day, by sampling period and sub-watershed. Percentages indicate the proportion that groundwater and surface water contribute to total stream discharge.

A.

Sector	Sampling Period	SGD (modeled)	Non-modeled vs. modeled Rn (%)
Northwest	July	0.46	97 %
Central	July	1.9	97 %
South	July	2.3	96 %

B.

Stream	Sampling Period	GW (modeled)	Non-modeled vs. modeled Rn (%)
Kahaluʻu	July	0.54	106 %
	February	0.52	127 %
ʻĀhuimanu	July	2.1	31.9 %
	February	0.65	146 %
Kāneʻohe	July	1.6	100 %
	February	N/A	N/A

S5 Table. Salinity-corrected nutrient concentrations for coastal samples. Median concentrations (µM) ± IQR of salinity-corrected nutrients for coastal samples by Kāneʻohe Bay sector and water type.

Location		DIN	DIP	DSi	DON
Northwest	ground (n = 24)	50 ± 54	1.8 ± 2.2	690 ± 300	93 ± 100
	Surface (n = 23)	14 ± 6.9	0.84 ± 0.72	440 ± 230	8.1 ± 9.7
Central	ground (n = 3)	260 ± 98	0.27 ± 0.20	530 ± 230	330 ± 120
	surface (n = 4)	3.4 ± 28	0.24 ± 0.22	230 ± 77	11 ± 37
South	ground (n = 5)	110 ± 130	1.6 ± 0.85	850 ± 120	7.0 ± 190
	surface (n = 5)	12 ± 23	0.59 ± 0.27	370 ± 220	7.5 ± 4.6

S6 Table. Salinity-corrected nutrient concentrations for stream samples. Median concentrations (µM) ± IQR of salinity-corrected nutrients by sub-watershed and water type for samples collected during dry and wet seasons.

Location		DIN	DIP	DSi	DON
July Sampling Period					
Kahaluʻu	ground (n = 13)	16 ± 14	0.77 ± 0.80	660 ± 280	46 ± 41
	surface (n = 12)	11 ± 7.8	0.83 ± 0.74	550 ± 48	5.5 ± 11
ʻĀhuimanu	ground (n = 8)	16 ± 45	0.37 ± 0.58	670 ± 240	31 ± 22
	surface (n = 11)	6.9 ± 3.2	0.34 ± 0.28	490 ± 49	10 ± 4.6
Kāneʻohe	ground (n = 8)	26 ± 32	1.1 ± 1.3	510 ± 280	28 ± 66
	surface (n = 19)	17 ± 30.0	0.54 ± 0.35	520 ± 120	10.0 ± 16
February Sampling Period					
Kahaluʻu	ground (n = 4)	50 ± 57	0.57 ± 0.43	520 ± 280	43 ± 13
	surface (n = 4)	12 ± 1.5	0.85 ± 0.34	470 ± 74	5.2 ± 2.4

ʻĀhuimanu	ground (n = 8)	12 ± 33	0.39 ± 0.33	600.0 ± 180	20.0 ± 9.8
	surface (n = 3)	7.5 ± 4.7	0.61 ± 0.51	460 ± 120	6.6 ± 3.7
Kāneʻohe	ground (n = 6)	31 ± 13	0.83 ± 0.41	450 ± 110	38 ± 51
	surface (n = 13)	12 ± 13	0.61 ± 0.25	480 ± 84	11 ± 6.1

APPENDIX B: Chapter 3 Supplementary Materials

Supplementary Material

Appendix S1. Additional description of the field sampling protocol.

Both groundwater and surface water samples were collected along a shore-perpendicular transect at each study site (Fig.S1.1)

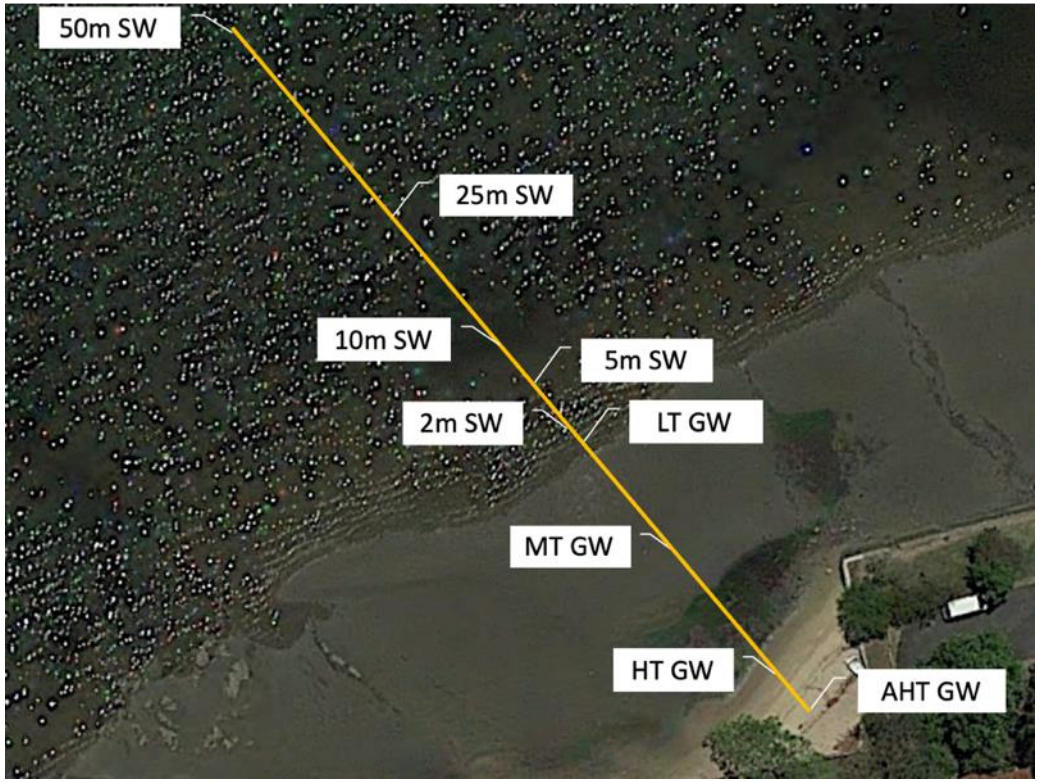

Fig. S1.1. Illustration of field sampling strategy. Groundwater (GW) was sampled at the above high tide (AHT), high tide (HT), mid tide (MT), and low tide (LT) marks and surface water (SW) was sampled along the same transect at 2, 5, 10, 25, and 50 m from the shoreline.

Groundwater wells were created at each site by digging a hole in the sand at the estimated low (LT), mid (MT), high (HT), and above high tide (AHT) marks along a perpendicular transect to the shoreline (Fig. S1.2).

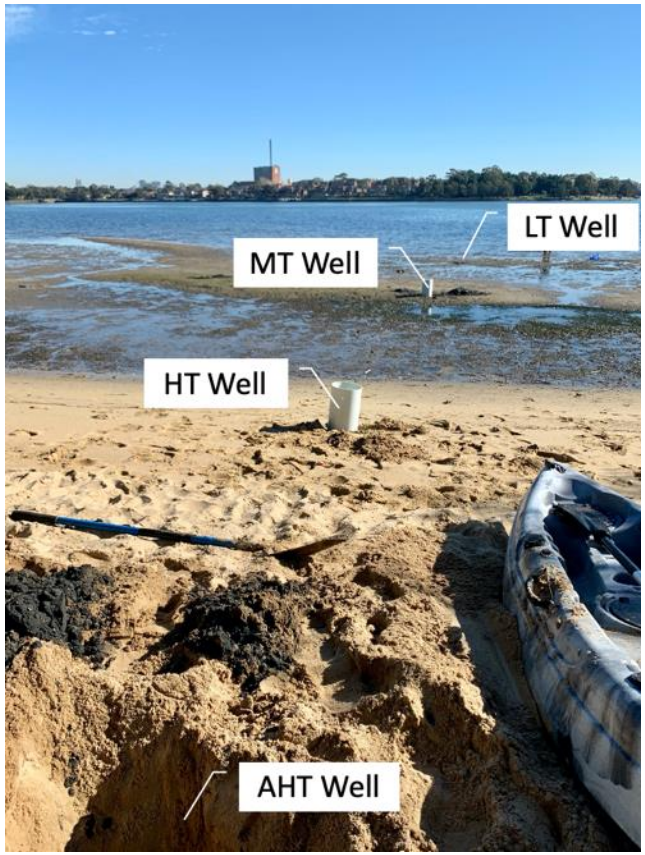

Fig S1.2. Field photo illustrating the transect of groundwater wells

Each well was dug until there was recharging water, thus the depth of each well varied (Fig S1.3).

Fig S1.3. Example of a well dug during this study.

PVC pipes were used as needed to reinforce unstable well walls. Water was pumped from each well using a peristaltic pump and tubing that was fed into the water (Fig S1.4).

Fig. S1.4. Photo of sampling from a groundwater well using a peristaltic pump.

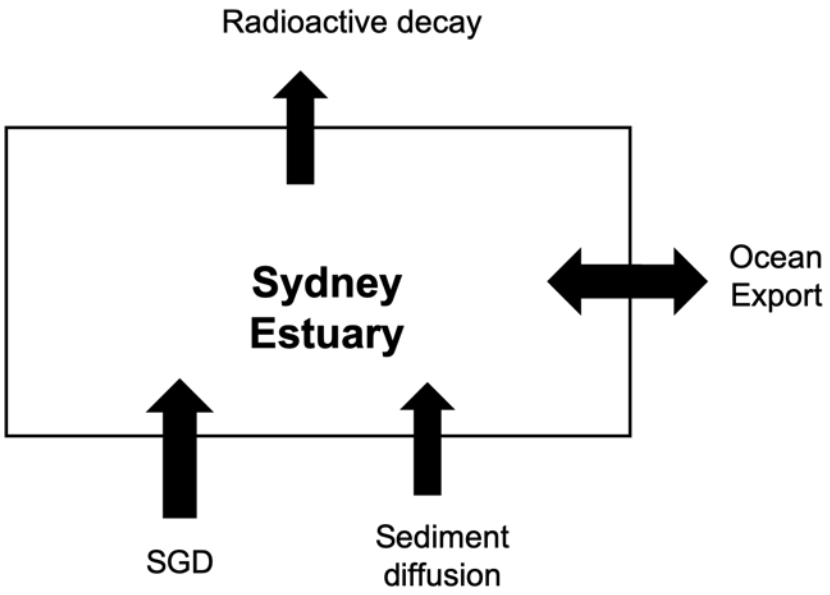

Fig. S1. Radium box model (Charette et al., 2008) describing the sources and sinks of radium to the coastal ocean.

Table S1. Predicted no effect concentrations (PNEC) for the studied CECs.

CEC	PNEC (ng/L)	Reference
CBZ	2500	Ferrari et al., 2004
CFN	10^7	Lin et al., 2008
SMX	590	Ferrari et al., 2004
FQL	64	Singer et al., 2019
IBU	100	Han et al., 2006
TCDD	1.79	Mehrle et al., 1988

Table S2. Tidal range (m) on date of sampling by location, and median salinity, temperature (° C) and pH values ± interquartile range (IQR).

Location	Tidal Range (m)	Type	Salinity	Temp	pH
FS	1.13 (0.55 – 1.68)	SW (n = 5)	32.9 ± 1.90	19.1 ± 1.2	7.99 ± 0.05
		GW (n = 4)	15.2 ± 11.0	15.6 ± 0.6	7.95 ± 1.85
HB	1.26 (0.52 – 1.78)	SW (n = 4)	23.7 ± 0.33	17.1 ± 0.5	7.74 ± 0.05
		GW (n = 4)	31.3 ± 7.38	14.4 ± 0.3	6.94 ± 0.20
HC	1.39 (0.49 – 1.88)	SW (n = 5)	28.6 ± 0.10	16.6 ± 1.4	8.11 ± 0.05
		GW (n = 4)	26.3 ± 5.20	16.3 ± 0.6	7.51 ± 0.26
ROZ	1.56 (0.46 – 2.02)	SW (n = 5)	33.9 ± 0.10	17.8 ± 0.4	7.83 ± 0.03
		GW (n = 4)	33.3 ± 4.48	17.6 ± 0.9	7.08 ± 0.37
WAT	1.50 (0.47 – 1.97)	SW (n = 5)	34.9 ± 0.30	17.7 ± 0.7	8.09 ± 0.02
		GW (n = 4)	16.8 ± 27.8	16.8 ± 1.7	8.12 ± 0.28

Table S3. Median radium concentrations ± interquartile range (IQR) for samples by location and type: surface water (SW) and groundwater (GW).

Location	Type	^{223}Ra (dpm/100 L)	^{224}Ra (dpm/100 L)	^{226}Ra (dpm/100 L)
FS	SW (n = 5)	2.4 ± 2.2	88 ± 62	11 ± 1.2
	GW (n = 4)	9.0 ± 8.2	140 ± 97	16 ±9.9
HB	SW (n = 4)	2.8 ± 1.1	100 ± 56	6.8 ± 5.5
	GW (n = 4)	12 ± 7.2	740 ± 250	42 ± 38
HC	SW (n = 5)	3.3 ± 0.79	96 ± 62	10 ± 8.3
	GW (n = 4)	21 ± 6.9	660 ± 250	23 ± 4.2
ROZ	SW (n = 5)	1.5 ± 1.2	39 ± 6.3	11 ± 8.1
	GW (n = 4)	1.5 ± 1.3	760 ± 350	59 ± 77
WAT	SW (n = 5)	0.91 ± 0.27	13 ± 13	9.9 ± 8.1
	GW (n = 4)	7.0 ± 10	140 ± 210	12 ± 2.0

Table S4. Median nutrient and DOC concentrations ± interquartile range (IQR) for samples by location and type: surface water (SW) and groundwater (GW).

Location	Type	TDN (μM)	TDP (μM)	NO_x (μM)	NH_4^+ (μM)	PO_4^{3-} (μM)	DOC (μM)
FS	SW (n = 5)	18 ± 8.1	0.59 ± 0.72	0 ± 0	0.99 ± 0.54	0.52 ± 0.081	97 ± 34
	GW (n = 4)	290 ± 220	0.98 ± 4.5	270 ± 200	3.0 ± 0.29	1.1 ± 0.075	140 ± 86
HB	SW (n = 4)	33 ± 2.4	0.97 ± 0.28	5.0 ± 6.1	1.5 ± 2.7	0.59 ± 0.46	140 ± 9.1
	GW (n = 4)	35 ± 14	12 ± 15	0 ± 0.092	1.8 ± 1.8	27 ± 33	470 ± 240
HC	SW (n = 5)	16 ± 3.4	0.95 ± 0.23	1.7 ± 1.2	3.5 ± 1.1	1.2 ± 0.62	120 ± 6.1
	GW (n = 4)	74 ± 19	3.1 ± 1.1	27 ± 53	13 ± 15	3.0 ± 1.1	170 ± 82
ROZ	SW (n = 5)	16 ± 0.50	0.38 ± 0.039	5.2 ± 0.65	1.3 ± 0.29	0.62 ± 0.41	80 ± 13
	GW (n = 4)	79 ± 92	0.34 ± 1.1	2.9 ± 19	50 ± 120	0.87 ± 1.1	130 ± 27
WAT	SW (n = 5)	14 ± 2.8	0.55 ± 0.83	4.9 ± 4.1	2.3 ± 0.60	0.96 ± 0.32	51 ± 26
	GW (n = 4)	100 ± 170	4.5 ± 5.6	58 ± 99	3.5 ± 2.8	4.3 ± 3.6	720 ± 1500

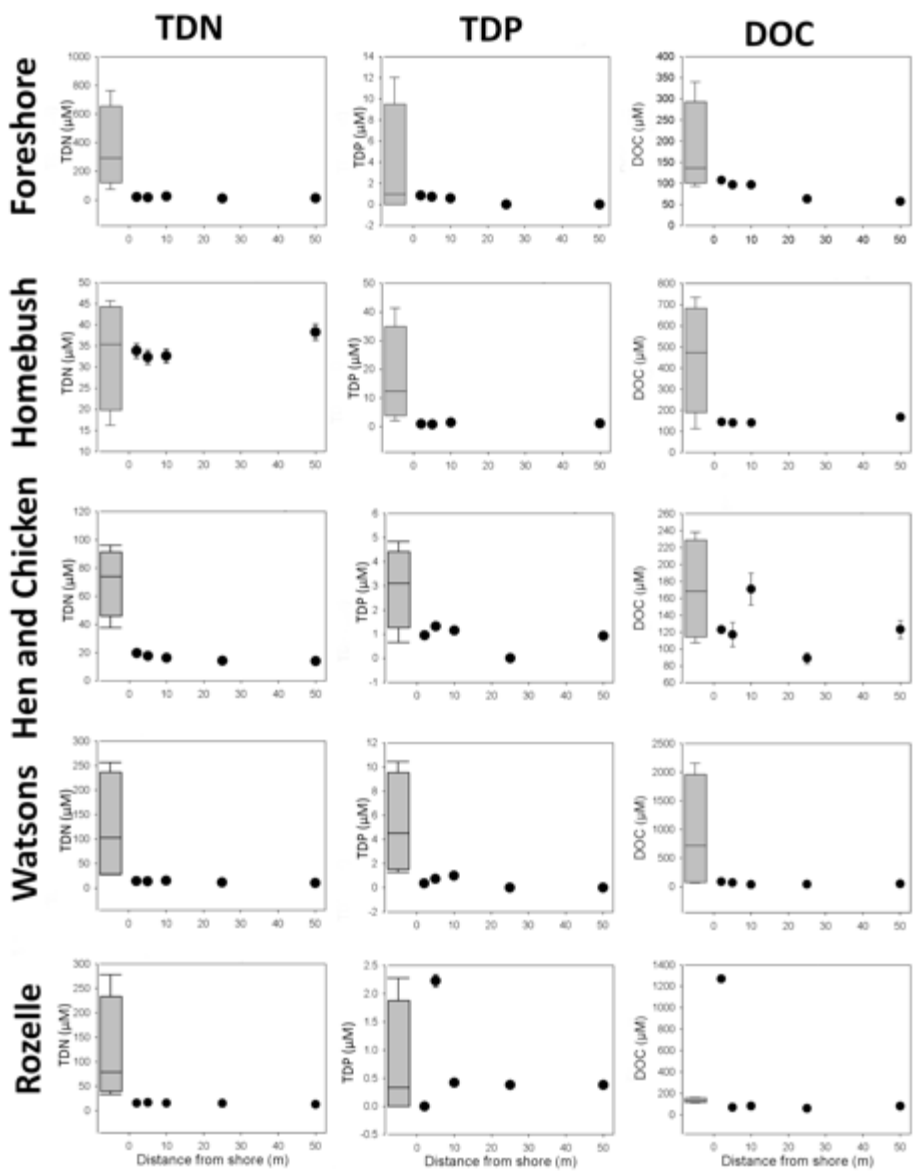

Figure S2. TDN, TDP, and DOC transects by location with respect to distance from the shore (m). All concentrations are in µM, groundwater samples (n = 4 per site) are represented by the boxplots and surface water samples by the scatter plot.

Table S5. Median CEC concentrations ± interquartile range (IQR) for samples by location and type: surface water (SW) and groundwater (GW).

Location	Type	CBZ (ng/L)	CFN (ng/L)	TCDD (ng/L)	SMX (ng/L)	FQL (ng/L)	IBU (ng/L)
FS	SW (n = 5)	79 ± 29	370 ± 98	7.5 ± 1.3	< LOD	< LOD	< LOD
	GW (n = 4)	49 ± 30	120 ± 390	4.6 ± 2.7	< LOD	< LOD	< LOD
HB	SW (n = 4)	40 ± 38	530 ± 56	7.8 ± 1.7	45 ± 11	< LOD	< LOD
	GW (n = 4)	160 ± 130	180 ± 46	6.8 ± 1.5	78 ± 5.8	< LOD	< LOD
HC	SW (n = 5)	81 ± 73	910 ± 58	10 ± 0.77	49 ± 20	< LOD	< LOD
	GW (n = 4)	63 ± 81	260 ± 190	9.3 ± 0.79	56 ± 7.0	< LOD	< LOD
ROZ	SW (n = 5)	56 ± 15	160 ± 110	19 ± 3.2	48 ± 19	14 ± 3.1	150 ± 70
	GW (n = 4)	68 ± 77	340 ± 770	17 ± 12	12 ± 29	13 ± 8.6	80 ± 170
WAT	SW (n = 5)	75 ± 15	250 ± 390	14 ± 7.9	65 ± 12	12 ± 3.2	< LOD
	GW (n = 4)	65 ± 25	170 ± 68	12 ± 13	65 ± 18	6.1 ± 13	< LOD

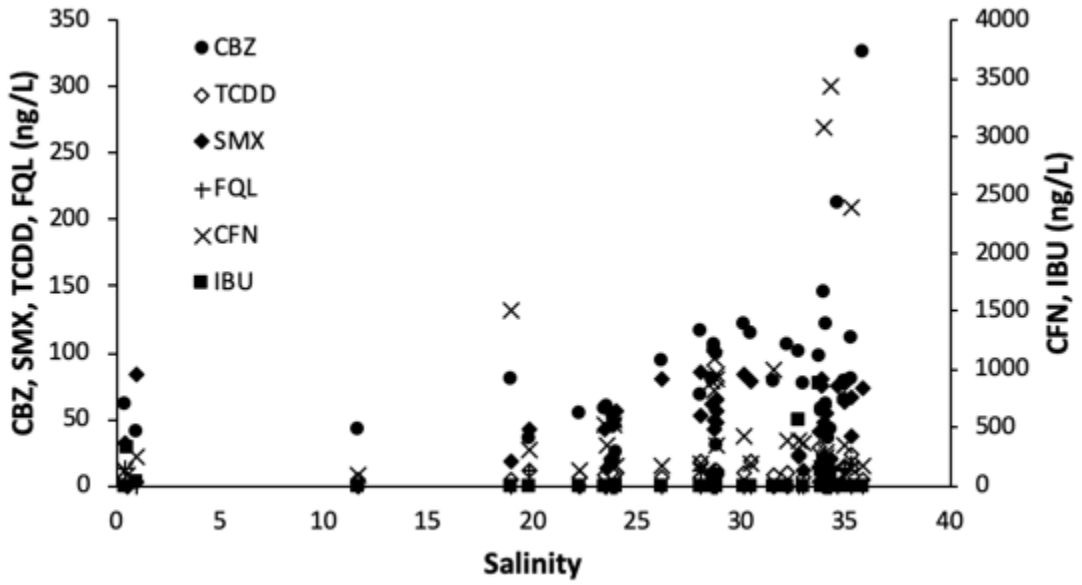

Figure S3. CEC concentrations (ng/L) versus salinity. Carbamazepine (black circles), sulfamethaoxazole (black diamonds), dioxins (white diamonds), and fluoroquinolones (crosses) are plotted on the primary y-axis, and caffeine (x's), and ibuprofen (black squares) are plotted on the seconday y-axis.

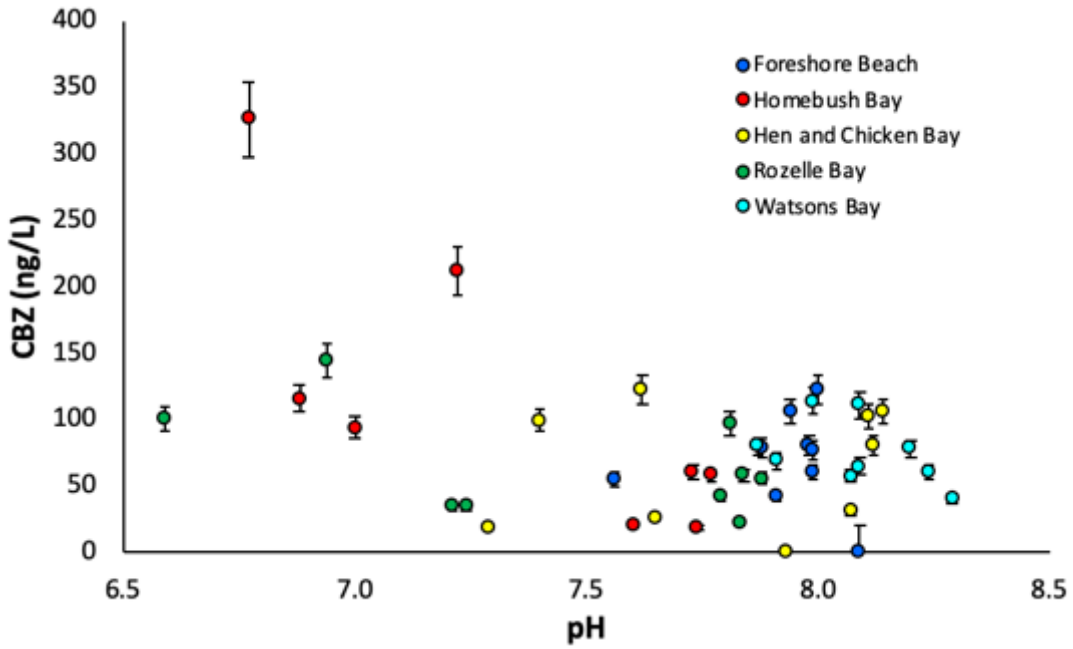

Figure S4. Carbamazepine concentrations (ng/L) vs. pH, color-coded by sampling site.

Unprocessed Data

Table 1. Sample sites

ID	Location	Date	Lat	Long	Type	GW/SW	Depth (cm)	Dist (m)	Sp. Cond (mS/cm)	Salinity	Temp	ODO (mg/L)	ODO %	pH
1	Foreshore	6/29/19	-33.9551	151.1944	AHT	GW		-5	0.867	0.50	15.7	5.67	56.2	8.09
2	Foreshore	6/29/19	-33.9551	151.1944	HT	GW		-5	15.52	11.52	14.8	7.55	73.3	7.91
3	Foreshore	6/29/19	-33.9552	151.1944	MT	GW		-5	24.8	18.93	15.4	7.08	69.4	7.98
4	Foreshore	6/29/19	-33.9552	151.1944	LT	GW		-5	29.4	22.20	16.3	4.35	44.0	7.56
5	Foreshore	6/29/19	-33.9552	151.1944	2m	SW	14	2	42.1	31.50	18.3	9.61	99.3	7.88
6	Foreshore	6/29/19	-33.9552	151.1944	5m	SW	21	5	43.0	32.10	18.6	9.55	99.7	7.94
7	Foreshore	6/29/19	-33.9553	151.1944	10m	SW	28	10	45.9	32.90	20.6	9.63	105.6	7.99
8	Foreshore	6/29/19	-33.9554	151.1944	25m	SW	39	25	46.4	34.00	19.8	9.39	102.3	7.99
9	Foreshore	6/29/19	-33.9557	151.1943	50m	SW	95	50	45.8	34.00	19.1	8.65		8.00
10	Homebush	6/30/19	-33.8346	151.0838	AHT	GW		-5	53.8	35.80	14.45	3.39	32.2	6.77
11	Homebush	6/30/19	-33.8346	151.0837	HT	GW		-5	34.3	28.00	13.9	4.42	42.5	6.88
12	Homebush	6/30/19	-33.8346	151.0835	MT	GW		-5	42.1	34.60	14.7	3.91	38.4	7.22
13	Homebush	6/30/19	-33.8345	151.0831	LT	GW		-5	32.4	26.10	14.3	7.09	68.5	7.00
14	Homebush	6/30/19	-33.8344	151.0830	2m	SW	10	2	30.8	23.50	16.2	10.92	106.5	7.73
15	Homebush	6/30/19	-33.8344	151.0829	5m	SW	10	5	31.8	23.80	17.0	11.03	111.0	7.74
16	Homebush	6/30/19	-33.8344	151.0829	10m	SW	70	10	31.6	23.40	17.5	11.06	112.8	7.77
17	Homebush	6/30/19	-33.8345	151.0825	50m	SW	130	50	31.9	23.80	17.2	10.33	104.1	7.60
18	Hen and Chicken	7/1/19	-33.8620	151.1256	LT	GW		-5	38.6	28.70	16.0	3.97	39.5	7.40
19	Hen and Chicken	7/1/19	-33.8617	151.1252	50m	SW	58	50	35.6	28.60	14.8	12.38	120.5	8.11
20	Hen and Chicken	7/1/19	-33.8622	151.1258	MT	GW		-5	38.8	30.10	16.4	1.46	14.7	7.62
21	Hen and Chicken	7/1/19	-33.8618	151.1254	25m	SW	35	25	36.3	28.50	15.7	11.97	117.2	8.12
22	Hen and Chicken	7/1/19	-33.8623	151.1259	HT	GW		-5	31.2	23.90	16.2	8.96	88.5	7.65
23	Hen and Chicken	7/1/19	-33.8619	151.1255	10m	SW	14	10	37.1	28.60	16.6	11.67	116.1	8.14
24	Hen and Chicken	7/1/19	-33.8620	151.1256	5m	SW	12	5	37.6	28.70	17.1	10.93	110.1	8.07

25	Hen and Chicken	7/1/19	-33.8620	151.1256	2m	SW	11	2	38.4	28.70	17.9	10.67	108.5	7.93
26	Hen and Chicken	7/1/19	-33.8623	151.1259	AHT	GW		-5	32.0	23.70	17.6	4.16	42.5	7.29
27	Watsons	7/2/19	-33.8466	151.2807	2m	SW	40	2	48.7	35.20	20.5	9.17		7.87
28	Watsons	7/2/19	-33.8467	151.2808	LT	GW		-5	33.1	28.00		9.64	99.8	7.91
29	Watsons	7/2/19	-33.8467	151.2808	MT	GW		-5	38.9	30.40	16.3	9.99	100.8	7.99
30	Watsons	7/2/19	-33.8466	151.2807	5m	SW	60	5	43.6	33.80	17.2	10.29	105.2	8.07
31	Watsons	7/2/19	-33.8466	151.2806	10m	SW	78	10	45.0	35.20	16.9	10.78	109.8	8.09
32	Watsons	7/2/19	-33.8467	151.2809	HT	GW		-5	1.562	0.95	16.8	9.35	95.5	8.29
33	Watsons	7/2/19	-33.8466	151.2805	25m	SW	104	25	45.5	34.90	17.7	10.37	108.3	8.09
34	Watsons	7/2/19	-33.8465	151.2802	50m	SW	165	50	45.7	34.90	17.9	11.49	121.3	8.20
35	Watsons	7/2/19	-33.8467	151.2809	AHT	GW		-5	0.653	0.36	19.7			8.24
36	Rozelle	7/3/19	-33.8724	151.1760	BLT	GW		-5	43.8	34.10	17.0	5.54	57.7	7.21
37	Rozelle	7/3/19	-33.8724	151.1760	2m	SW	18	2	45.2	34.20	18.7	8.15	85.0	7.79
38	Rozelle	7/3/19	-33.8724	151.1760	5m	SW	25	5	44.1	33.90	17.5	9.06	92.6	7.84
39	Rozelle	7/3/19	-33.8723	151.1760	10m	SW	53	10	43.8	33.80	17.8	8.17	82.9	7.88
40	Rozelle	7/3/19	-33.8724	151.1760	LT	GW		-5	44.5	33.90	17.9	7.63	78.3	6.94
41	Rozelle	7/3/19	-33.8722	151.1761	25m	SW	183	25	43.7	33.90	17.9	7.92	80.5	7.83
42	Rozelle	7/3/19	-33.8725	151.1760	MT	GW		-5	43.6	32.70	18.5	8.25	85.3	6.59
43	Rozelle	7/3/19	-33.8720	151.1761	50m	SW	497	50	43.5	33.70	17.1	7.67	77.9	7.81
44	Rozelle	7/3/19	-33.8725	151.1760	HT	GW		-5	27.0	19.80	17.2	3.55	37.5	7.24

Table 2. Radium data

ID	^{223}Ra (dpm/100L)	^{223}Ra Unc	$^{224}Ra_{ex}$ (dpm/100L)	$^{224}Ra_{ex}$ Unc	^{226}Ra (dpm/100L)	^{226}Ra Unc	^{228}Th (dpm/100 L)	^{228}Th unc
1	0.75	0.01	10.91	0.05	46.01	3.27	0.04	0.003
2	8.02	0.39	134.41	1.99	17.70	3.14	0.05	0.006
3	9.96	0.52	135.98	2.03	14.24	2.82	0.04	0.004
4	27.85	2.45	394.66	7.88	15.10	2.88	0.08	0.013
5	8.58	1.92	156.88	9.57	10.47	0.60	0.67	0.458
6	3.34	0.51	97.11	4.77	11.40	0.83	0.39	0.174
7	2.35	0.31	88.24	4.20	11.73	0.84	0.40	0.185
8	0.92	0.08	34.99	0.96	11.61	0.91	0.23	0.060
9	1.12	0.08	14.42	0.28	7.11	0.62	0.24	0.061
10	13.04	1.62	626.82	31.01	25.40	5.08	0.66	0.426
11	8.89	1.07	777.19	44.83	52.97	7.69	0.52	0.293
12	32.58	6.68	1396.98	116.59	114.98	10.01	1.32	1.864
13	11.31	0.99	705.82	26.60	31.62	4.37	0.49	0.251
14	4.91	1.11	173.75	15.13	8.58	0.73	1.08	1.126
15	2.78	0.35	91.02	4.14	14.54	0.91	0.41	0.220
16	2.72	0.34	112.84	5.63	3.34	0.49	0.80	0.660
17	0.56	0.03	14.36	0.32	4.97	0.60	0.34	0.116
18	12.53	1.54	466.95	21.78	24.84	3.30	0.28	0.106
19	2.71	0.42	63.60	3.12	2.13	0.39	0.67	0.448
20	34.78	6.35	829.03	49.03	13.40	2.41	0.30	0.127
21	1.86	0.26	63.87	3.25	10.00	0.74	0.56	0.339
22	21.54	2.56	560.53	21.97	22.57	3.86	0.30	0.107
23	3.54	0.65	95.89	6.01	11.78	0.84	0.70	0.530
24	3.27	0.59	128.83	9.27	1.78	0.35	0.83	0.748
25	3.50	0.49	125.49	7.00	10.46	0.92	0.86	0.812

26	19.82	2.82	768.35	41.89	24.29	4.18	0.55	0.321
27	1.17	0.12	25.63	0.80	9.85	0.68	0.11	0.024
28	11.45	1.15	177.64	6.08	10.40	2.11	0.13	0.028
29	15.82	2.12	663.51	36.33	12.40	2.45	0.20	0.077
30	0.91	0.08	31.48	1.07	11.15	0.78	0.31	0.108
31	1.21	0.11	10.89	0.28	5.20	0.66	0.11	0.019
32	1.55	0.05	97.93	1.52	13.15	2.84	0.08	0.012
33	0.85	0.07	13.12	0.36	8.19	0.67	0.12	0.022
34	0.90	0.08	13.39	0.37	11.44	1.15	0.05	0.007
35	2.59	0.08	52.35	0.62	10.66	2.11	0.12	0.021
36	19.73	3.33	845.33	62.45	90.49	10.52	0.88	0.931
37	2.71	0.49	61.74	3.95	18.54	1.44	1.18	1.488
38	0.82	0.09	44.32	2.25	10.91	0.79	0.57	0.387
39	1.32	0.18	38.87	1.99	12.90	1.20	0.63	0.475
40	15.37	2.24	676.10	43.73	28.46	5.56	1.33	1.727
41	2.55	0.42	38.04	1.84	4.84	0.72	0.35	0.167
42	27.41	3.69	979.75	53.93	133.34	10.62	0.96	0.931
43	1.54	0.17	23.46	0.79	3.71	0.48	0.22	0.066
44	0.79	0.02	71.07	0.94	12.66	2.50	0.19	0.046

Table 3. DOC and CEC concentrations

ID	DOC (uM)	DOC UNC	CBZ (ng/L)	CBZ UNC	CFN (ng/L)	CFN UNC	TCDD (ng/L)	TCDD UNC	SMX (ng/L)	SMX UNC	IBU (ng/L)	IBU UNC	FQL (ng/L)	FQL UNC
1	339.78	2.00	0.00	20.00	99.00	4.33	0	2.5	0	20.00	330	44.32	0.00	5.00
2	152.11	5.42	42.00	3.66	85.00	3.71	3.861	0.214	0	20.00	0	20.00	0.00	5.00
3	119.68	9.60	81.00	7.06	1515.00	66.21	5.335	0.265	19	0.88	0	20.00	0.00	5.00
4	93.62	0.41	55.00	4.79	139.00	6.07	6.571	0.615	0	20.00	0	20.00	0.00	5.00
5	107.36	3.71	79.00	6.89	990.00	43.26	8.33	0.525	0	20.00	0	20.00	0.00	5.00
6	96.79	0.18	106.00	9.24	380.00	16.61	9.085	0.525	0	20.00	0	20.00	0.00	5.00
7	96.66	0.24	77.00	6.71	372.00	16.26	6.99	0.525	12	0.56	0	20.00	0.00	5.00
8	63.03	4.71	61.00	5.32	255.00	11.14	6.92	0.525	55	2.55	0	20.00	0.00	5.00
9	57.20	0.94	122.00	10.63	282.00	12.32	7.52	0.525	0	20.00	0	20.00	0.00	5.00
10	734.89	8.65	326.00	28.42	181.00	7.91	4.475	2	74	1.20	0	20.00	0.00	5.00
11	530.49	3.12	116.00	10.11	189.00	8.26	6.5	0.38	85	3.43	0	20.00	0.00	5.00
12	414.84	6.42	212.00	18.48	37.00	1.62	8.145	0.25	76	3.94	0	20.00	0.00	5.00
13	113.61	11.72	94.00	8.19	170.00	7.43	7.16	0.37	80	3.52	0	20.00	0.00	5.00
14	144.54	0.59	60.00	5.23	350.00	15.29	6.06	1.343	14	3.71	0	20.00	0.00	5.00
15	141.12	1.18	18.00	1.57	573.00	25.04	7.09	0.045	49	0.65	0	20.00	0.00	5.00
16	141.12	2.00	58.00	5.06	527.00	23.03	8.48	0.24	43	2.27	0	20.00	0.00	5.00
17	167.43	1.06	21.00	1.83	527.00	23.03	8.495	0.335	46	1.99	0	20.00	0.00	5.00
18	107.15	0.59	99.50	8.67	347.00	15.16	7.895	1.375	56	2.13	0	20.00	0.00	5.00
19	123.18	10.42	103.00	8.98	813.00	35.53	11.54	0.155	42	2.59	0	20.00	0.00	5.00
20	201.24	4.24	122.00	10.63	430.00	18.79	9.475	0.92855	83	2.59	0	20.00	0.00	5.00
21	89.05	6.42	81.00	7.06	892.00	38.98	9.33	0.91434	62	1.95	0	20.00	0.00	5.00
22	135.50	10.54	26.00	2.27	178.00	7.78	9.19	0.90062	56	3.85	0	20.00	0.00	5.00
23	171.01	18.96	105.50	9.20	1097.00	47.94	10.15	2.72	49	2.87	0	20.00	11.83	3.51
24	117.06	14.25	30.50	2.66	950.00	41.51	10.17	0.99666	47	2.59	0	20.00	0.00	5.00
25	122.89	0.24	1.00	0.09	910.00	39.77	10.92	1.07016	65	2.27	0	20.00	0.00	5.00

26	238.58	2.41	18.00	1.57	176.00	7.69	10.215	1.00107	55	2.18	100	13.43	0.00	5.00
27	87.84	5.30	80.00	6.97	2393.00	104.57	13.035	1.27743	67	3.01	0	20.00	0.00	5.00
28	87.76	0.35	69.00	6.01	140.00	6.12	17.975	1.76155	52	2.55	0	20.00	12.24	3.63
29	66.19	1.41	114.00	9.94	197.00	8.61	18.235	1.78703	78	3.10	0	20.00	0.00	5.00
30	69.48	0.41	57.50	5.01	51.00	2.23	12.05	1.1809	81	2.41	0	20.00	15.13	4.49
31	38.09	3.12	111.00	9.68	148.00	6.47	22.99	2.25302	38	2.41	0	20.00	15.91	4.72
32	1353.96	7.89	40.00	3.49	243.00	10.62	2.876	0.387	83	3.61	0	20.00	0.00	5.00
33	43.29	4.47	65.00	5.67	347.00	15.16	14.265	1.39797	63	3.75	0	20.00	11.17	3.31
34	51.29	1.06	78.00	6.80	118.00	5.16	12.9	1.2642	77	1.76	0	20.00	12.89	3.82
35	2160.24	2.47	61.00	5.32	141.00	6.16	6.105	0.59829	32	3.85	30	4.03	13.32	3.95
36	117.23	3.18	35.00	3.05	198.00	8.65	0	2.5	0	1.48	0	20.00	15.09	4.47
37	1270.24	15.25	43.00	3.75	3424.00	149.63	4.145	0.40621	20	2.87	0	20.00	0.00	5.00
38	67.86	4.95	58.00	5.06	213.00	9.31	19.2	1.8816	48	1.95	20	2.69	14.21	4.21
39	80.93	0.71	55.50	4.84	155.00	6.77	16.045	1.57241	76	20.00	0	20.00	17.77	5.27
40	162.06	0.53	145.00	12.64	3075.00	134.38	20.8	2.0384	0	20.00	0	20.00	22.28	6.60
41	58.11	0.59	22.00	1.92	65.00	2.84	19.2	1.8816	59	0.93	110	14.77	11.37	3.37
42	136.50	22.90	101.00	8.80	380.00	16.61	21.75	2.1315	24	2.22	190	25.52	0.00	5.00
43	79.72	0.29	97.00	8.46	101.00	4.41	28.2	2.7636	40	3.52	150	20.15	15.40	4.57
44	111.82	0.47	35.00	3.05	309.00	13.50	12.4	1.2152	42	20.00	160	21.49	11.06	3.28

Table 4. Nutrient concentrations

ID	TDP (uM)	TDP unc	TDN (uM)	TDN unc	NO_3^- (uM)	NO_3^- unc	NO_2^- (uM)	NO_2^- unc	PO_4^{3-} (uM)	PO_4^{3-} unc	NH_4^+ (uM)	NH_4^+ unc
1	12.01	0.60	763.96	38.20	660.30	33.01	2.28	0.11	1.71	0.09	1.06	0.05
2	0.00	0.01	259.17	12.96	237.30	11.86	0.46	0.02	0.43	0.02	3.99	0.20
3	0.00	0.01	327.72	16.39	285.23	14.26	17.49	0.87	0.29	0.01	17.92	0.90
4	1.96	0.10	74.25	3.71	48.26	2.41	6.65	0.33	2.40	0.12	1.97	0.10

5	0.85	0.04	21.21	1.06	0.00	0.01	0.00	0.01	0.22	0.01	0.71	0.04
6	0.72	0.04	17.78	0.89	0.00	0.01	0.00	0.01	0.46	0.02	0.00	0.01
7	0.59	0.03	25.42	1.27	0.00	0.01	0.00	0.01	0.52	0.03	1.25	0.06
8	0.00	0.01	11.28	0.56	0.00	0.01	0.00	0.01	0.54	0.03	0.99	0.05
9	0.00	0.01	13.14	0.66	2.12	0.11	0.49	0.02	1.77	0.09	3.27	0.16
10	15.66	0.78	45.69	2.28	0.00	0.01	0.37	0.02	15.98	0.80	1.30	0.06
11	8.91	0.45	39.98	2.00	0.00	0.01	0.00	0.01	8.20	0.41	1.71	0.09
12	41.32	2.07	30.70	1.54	0.00	0.01	0.00	0.01	38.74	1.94	1.81	0.09
13	2.16	0.11	16.21	0.81	0.00	0.01	0.00	0.01	2.90	0.15	8.07	0.40
14	0.89	0.04	33.84	1.69	7.31	0.37	0.55	0.03	1.27	0.06	11.71	0.59
15	0.74	0.04	32.34	1.62	7.26	0.36	0.67	0.03	0.76	0.04	1.31	0.07
16	1.39	0.07	32.63	1.63	0.86	0.04	0.00	0.01	0.42	0.02	1.50	0.07
17	1.05	0.05	38.27	1.91	1.54	0.08	0.61	0.03	0.41	0.02	1.41	0.07
18	0.66	0.03	37.63	1.88	1.08	0.05	0.57	0.03	1.01	0.05	15.28	0.76
19	0.92	0.05	13.92	0.70	2.50	0.12	0.00	0.01	0.52	0.03	2.11	0.11
20	4.84	0.24	71.18	3.56	0.46	0.02	0.00	0.01	4.71	0.24	50.19	2.51
21	0.00	0.01	14.14	0.71	1.83	0.09	0.40	0.02	0.87	0.04	2.51	0.13
22	3.07	0.15	77.11	3.86	52.20	2.61	0.42	0.02	2.86	0.14	2.62	0.13
23	1.15	0.06	16.21	0.81	1.68	0.08	0.00	0.01	1.75	0.09	3.46	0.17
24	1.32	0.07	17.56	0.88	0.71	0.04	0.00	0.01	1.49	0.07	3.60	0.18
25	0.95	0.05	19.56	0.98	1.02	0.05	0.45	0.02	1.42	0.07	6.48	0.32
26	3.14	0.16	96.39	4.82	55.15	2.76	3.25	0.16	3.10	0.16	11.07	0.55
27	0.36	0.02	14.14	0.71	5.94	0.30	0.00	0.01	0.86	0.04	2.32	0.12
28	2.32	0.12	29.92	1.50	17.11	0.86	0.52	0.03	3.62	0.18	1.61	0.08
29	1.27	0.06	27.70	1.39	20.91	1.05	0.00	0.01	1.49	0.07	2.22	0.11
30	0.73	0.04	13.78	0.69	7.58	0.38	0.00	0.01	1.21	0.06	1.60	0.08
31	0.99	0.05	15.21	0.76	2.80	0.14	0.00	0.01	0.64	0.03	2.41	0.12
32	10.46	0.52	256.32	12.82	193.64	9.68	0.56	0.03	11.49	0.57	5.51	0.28

33	0.00	0.01	11.57	0.58	3.95	0.20	0.00	0.01	0.85	0.04	2.30	0.11
34	0.00	0.01	10.21	0.51	2.62	0.13	0.00	0.01	1.06	0.05	1.61	0.08
35	6.72	0.34	176.35	8.82	94.20	4.71	1.48	0.07	5.07	0.25	4.68	0.23
36	2.28	0.11	33.41	1.67	5.16	0.26	0.00	0.01	0.42	0.02	16.06	0.80
37	0.00	0.01	15.56	0.78	0.00	0.01	0.00	0.01	0.39	0.02	1.28	0.06
38	2.23	0.11	16.85	0.84	4.80	0.24	0.00	0.01	0.62	0.03	1.06	0.05
39	0.42	0.02	15.56	0.78	5.45	0.27	0.00	0.01	0.53	0.03	1.52	0.08
40	0.67	0.03	99.96	5.00	0.00	0.01	0.60	0.03	0.63	0.03	84.25	4.21
41	0.38	0.02	15.06	0.75	5.52	0.28	0.00	0.01	0.94	0.05	1.23	0.06
42	0.00	0.01	277.74	13.89	0.00	0.01	5.75	0.29	3.39	0.17	264.89	13.24
43	0.38	0.02	12.99	0.65	5.22	0.26	0.00	0.01	0.99	0.05	4.38	0.22
44	0.00	0.01	58.19	2.91	52.36	2.62	0.00	0.01	1.11	0.06	3.01	0.15

APPENDIX C: Chapter 4 Supplementary Materials

Supplementary Materials

Table S1. Study site locations, low and high tide heights (m) relative to the mean sea level (MSL) datum, tidal ranges (m), and the number of OSDS within a 200 m radius of the study site (Whitter & El-Kadi, 2009). Elevation is with respect to MSL in m.

Location	Site	Type	Lat long	Elev (m)	OSDS within 200 m	Low tide (m)	High tide (m)	Tidal range (m)
Waikīkī	C1 KT	Coastal	21.2779, -157.8213	2	10	-0.19	0.64	0.83
	C1 ST	Coastal	21.2779, -157.8213	2	10	-0.085	0.54	0.63
	C2 KT	Coastal	21.2849, -157.8294	1	3	-0.27	0.61	0.88
	C2 ST	Coastal	21.2849, -157.8294	1	3	-0.057	0.51	0.57
	C3 KT	Coastal	21.2877, -157.8440	1	1	-0.17	0.59	0.76
	C3 ST	Coastal	21.2877, -157.8440	1	1	-0.20	0.47	0.67
Māpunapuna	SD1	Storm drain	21.3373, -157.9001	1	0	-0.24	0.65	0.90
	SD2	Storm drain	21.3358, -157.8986	2	3	-0.012	0.48	0.49
	SD3	Storm drain	21.3356, -157.8975	2	3	-0.15	0.62	0.77
	C4	Coastal	21.3307, -157.8956	1	2	-0.021	0.46	0.48

Table S2. CEC compounds analyzed and their physiochemical properties. pK_a refers to the dissociation constant of the compound, meaning 50% of the compound will be ionized if the pK_a of a compound is the same as the solution it is in. log K_{ow} refers to the octanol water partition coefficient, or the tendency for a compound to sorb to organic matter. A smaller log K_{ow} means the compound is more soluble in water, compared to a larger log K_{ow} means the compound is more likely to bioaccumulate and remain in the environment for longer periods of time. Water solubility refers to the quantity of compound that will dissolve in water at 25 °C. Physiochemical properties were sourced from Pubchem. Predicted no effect concentrations (PNEC) used in this study are also given and were derived from literature values (Almeida et al., 2014; Pires et al., 2016; Dafouz et al., 2018; Zhang & Li, 2018).

CEC	**Use**	**pK_a**	**log K_{ow}**	**Water solubility (mg/L)**	**PNEC (ng/L)**
Carbamazepine (CBZ)	Anti-convulsant	13.9	2.45	18	30
Caffeine (CFN)	Lifestyle compound	14	-0.07	21,600	500
Fluoroquinolones (FQL) – Ciprofloxacin	Antibiotic	6.09	0.28	30,000	1

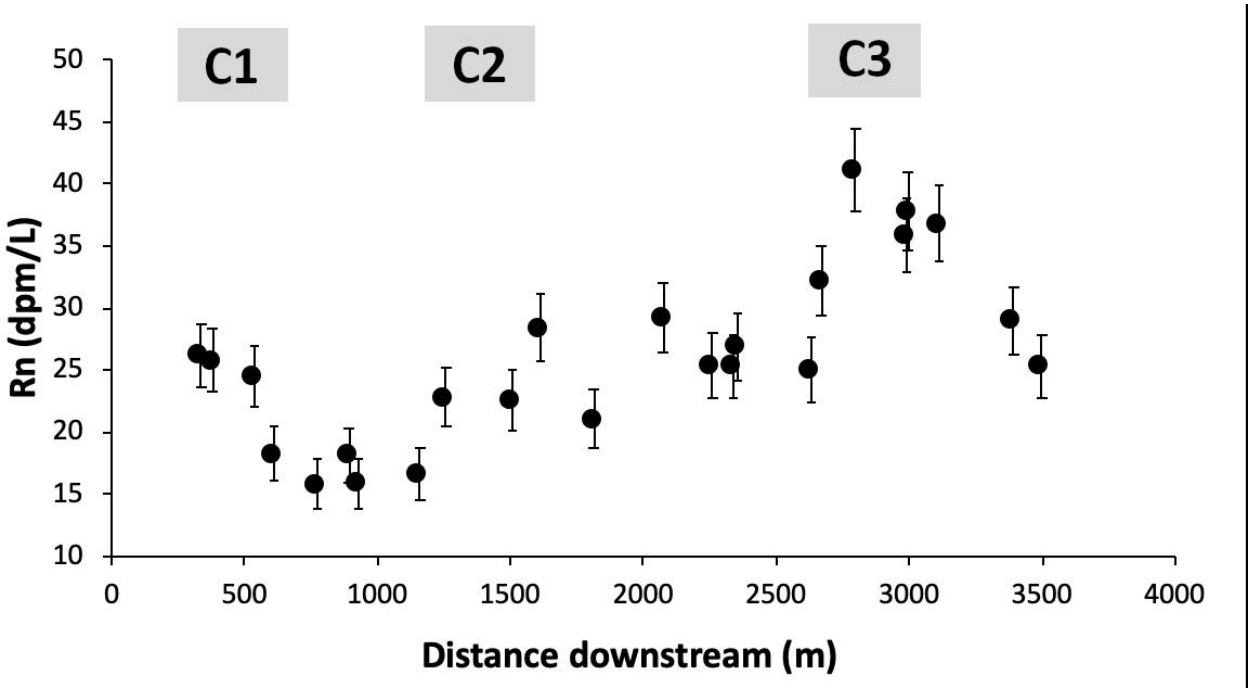

Figure S1. Results from a radon survey conducted July 23, 2010 along the Ala Wai Canal. These results were used to determine the area in Equation 3 (Appendix C-2), where C1, C2, and C3 correspond to locations in this study.

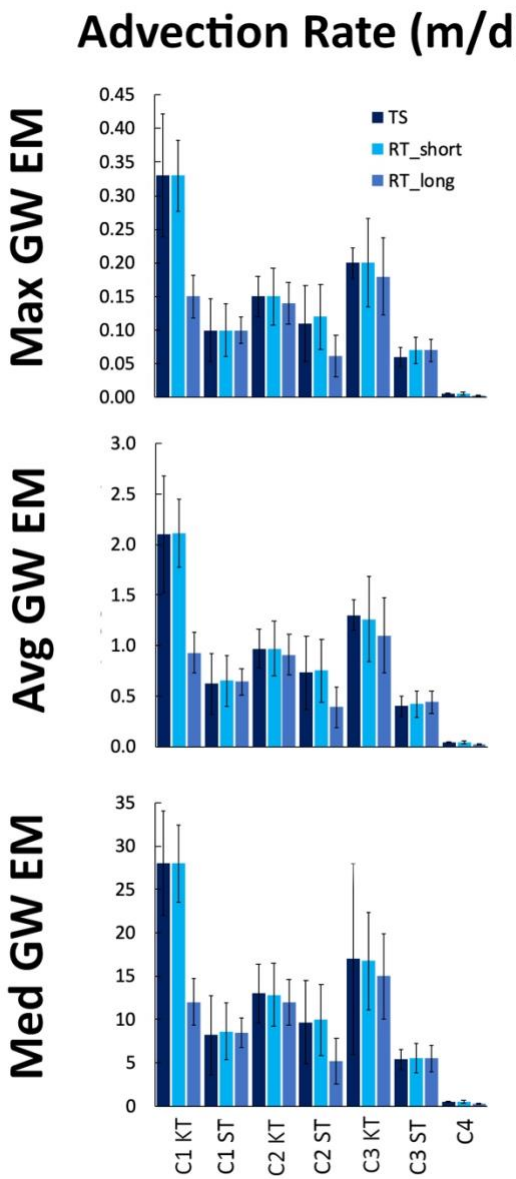

Figure S2. Advection rates (m/d) for coastal sites, separated by groundwater endmember (GW EM) used (maximum, average, and median) and calculation method (time series vs. short and long residence time).

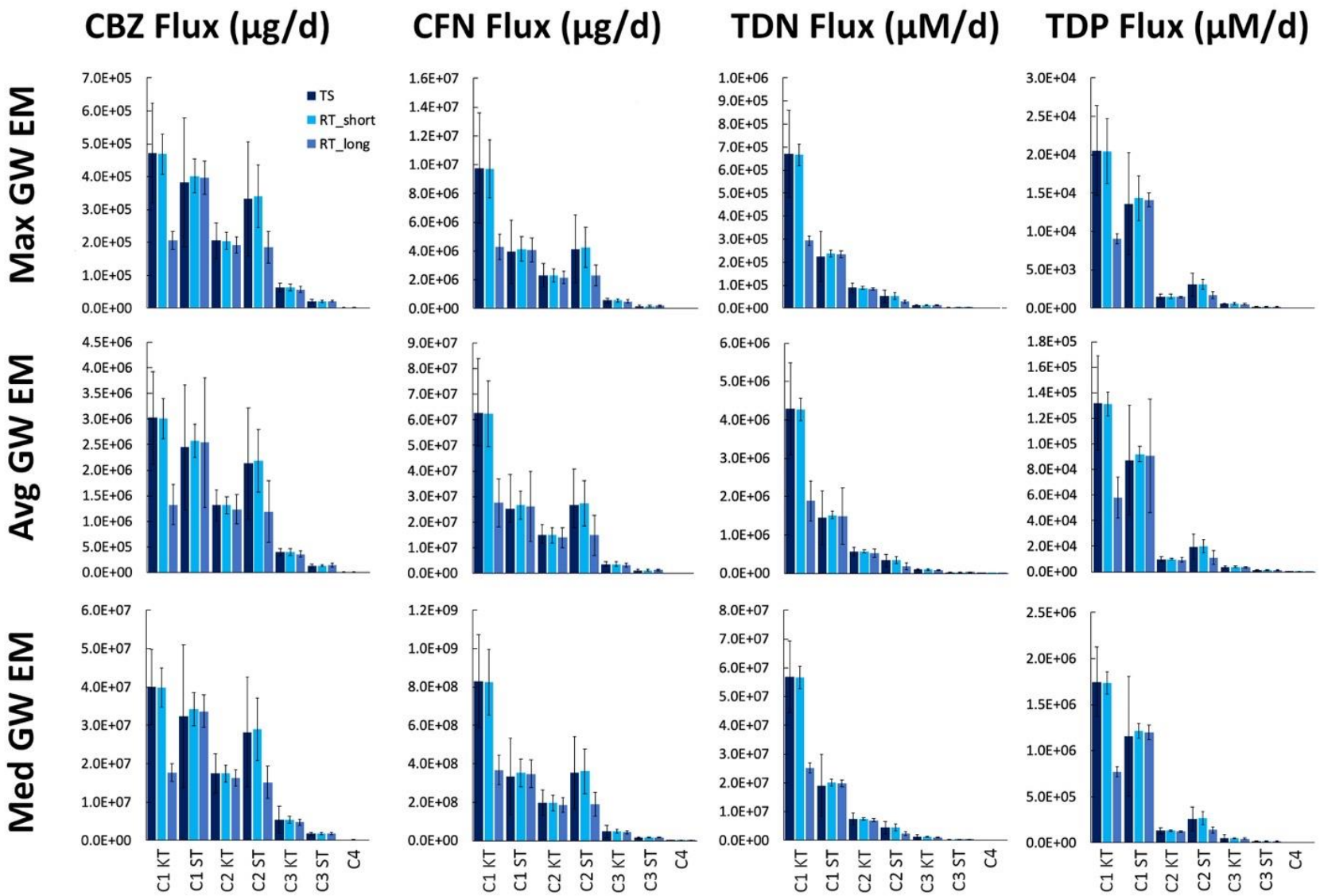

Figure S3. Coastal CEC (carbamazepine – CBZ and caffeine – CFN; µg/d) and nutrient (TDN and TDP; µM/d) fluxes separated by groundwater endmember (EM) used and flux calculation method (time series vs. short and long residence time).

Table S3. Groundwater results averaged over a half tidal cycle by site and date of sampling. Average radon in water concentrations (Bq/m^3) are given for all study sites (coastal and storm drains). Advection rates (m/d) and SGD fluxes (m3/d) are given for coastal sites based on the groundwater endmember (GW EM) and calculation method used (transient = ts; rt_short = shorter residence time estimate, rt_long = longer residence time estimate). We were unable to calculate advection rates and SGD for the storm drain sites as their geometry is unknown.

Site	Rn Bq/m^3	GW EM	Adv_{ts} m/d	Adv_{rt_short} m/d	Adv_{rt_long} m/d	SGD_{ts} m^3/d	SGD_{rt_short} m^3/d	SGD_{rt_long} m^3/d
C1 KT	520 ± 95	Max	0.33 ± 0.091	0.24 ± 0.053	0.15 ± 0.032	$1.1x10^4$ ± $3.0x10^3$	$7.8x10^3$ ± $3.8x10^2$	$4.7x10^3$ ± $2.3x10^2$
		Avg	2.1 ± 0.58	1.6 ± 0.34	0.93 ± 0.20	$6.9x10^4$ ± $1.9x10^4$	$5.0x10^4$ ± $2.4x10^3$	$3.0x10^4$ ± $1.4x10^3$
		Median	28 ± 6.0	21 ± 4.5	12 ± 2.7	$9.1x10^5$ ± $1.9x10^5$	$6.6x10^5$ ± $3.2x10^4$	$4.0x10^5$ ± $1.9x10^4$
C1 ST	430 ± 77	Max	0.10 ± 0.047	0.19 ± 0.039	0.10 ± 0.020	$3.1x10^3$ ± $1.5x10^3$	$6.1x10^3$ ± $2.6x10^2$	$2.1x10^4$ ± $1.4x10^2$
		Avg	0.62 ± 0.30	1.2 ± 0.25	0.64 ± 0.13	$2.0x10^4$ ± $9.7x10^3$	$3.9x10^4$ ± $1.7x10^3$	$3.2x10^3$ ± $8.7x10^2$
		Median	8.2 ± 4.6	16 ± 3.3	8.5 ± 1.7	$2.7x10^5$ ± $1.5x10^5$	$5.2x10^5$ ± $2.2x10^4$	$2.8x10^5$ ± $1.2x10^4$
C2 KT	300 ± 58	Max	0.15 ± 0.030	0.20 ± 0.042	0.14 ± 0.031	$4.0x10^3$ ± $8.0x10^2$	$5.2x10^3$ ± $2.4x10^2$	$3.8x10^3$ ± $1.8x10^2$
		Avg	0.97 ± 0.19	1.3 ± 0.27	0.91 ± 0.20	$2.6x10^4$ ± $5.1x10^3$	$3.4x10^4$ ± $1.6x10^3$	$2.4x10^4$ ± $1.1x10^3$
		Median	13 ± 3.4	17 ± 3.6	12 ± 2.6	$3.4x10^5$ ± $9.0x10^4$	$4.5x10^5$ ± $2.1x10^4$	$3.2x10^5$ ± $1.5x10^4$
C2 ST	150 ± 73	Max	0.11 ± 0.057	0.095 ± 0.048	0.061 ± 0.031	$3.1x10^3$ ± $1.5x10^3$	$2.5x10^3$ ± $6.4x10^2$	$1.7x10^3$ ± $4.0x10^2$

		Avg	0.73 ± 0.36	0.61 ± 0.31	0.39 ± 0.20	$2.0x10^4$ ± $9.6x10^3$	$1.6x10^4$ ± $4.1x10^3$	$1.1x10^4$ ± $2.6x10^3$
		Median	9.7 ± 4.8	8.1 ± 4.1	5.2 ± 2.6	$2.6x10^5$ ± $1.3x10^5$	$2.1x10^5$ ± $2.5x10^4$	$1.4x10^5$ ± $3.6x10^4$
C3 KT	330 ± 97	Max	0.20 ± 0.023	0.20 ± 0.066	0.18 ± 0.058	$8.4x10^2$ ± $9.8x10^1$	$8.4x10^2$ ± $9.5x10^1$	$7.5x10^2$ ± $8.2x10^1$
		Avg	1.3 ± 0.15	1.3 ± 0.42	1.1 ± 0.37	$5.4x10^3$ ± $6.3x10^2$	$5.4x10^3$ ± $6.1x10^2$	$4.8x10^3$ ± $5.3x10^2$
		Median	17 ± 11	17 ± 5.6	15 ± 4.9	$7.1x10^4$ ± $4.5x10^4$	$7.2x10^4$ ± $8.0x10^3$	$6.4x10^4$ ± $7.0x10^3$
C3 ST	130 ± 43	Max	0.06 ± 0.015	0.077 ± 0.020	0.070 ± 0.017	$2.7x10^2$ ± $6.6x10^1$	$3.3x10^2$ ± $2.3x10^1$	$2.9x10^2$ ± $1.9x10^1$
		Avg	0.40 ± 0.10	0.49 ± 0.13	0.44 ± 0.11	$1.7x10^3$ ± $4.2x10^2$	$2.1x10^3$ ± $1.5x10^2$	$1.9x10^3$ ± $1.2x10^2$
		Median	5.4 ± 1.2	6.5 ± 1.7	5.5 ± 1.5	$2.3x10^4$ ± $5.1x10^3$	$2.8x10^4$ ± $1.9x10^3$	$2.4x10^4$ ± $1.6x10^3$
C4	34 ± 15	Max	0.0060 ± 0.000078	0.0062 ± 0.0024	0.0031 ± 0.0010	9.0 ± 1.2	9.3 ± 1.4	4.6 ± 0.53
		Avg	0.039 ± 0.0050	0.040 ± 0.015	0.020 ± 0.0067	$5.8x10^1$ ± 7.5	$5.9x10^1$ ± 8.7	$3.0x10^1$ ± 3.4
		Median	0.51 ± 0.066	0.52 ± 0.20	0.26 ± 0.089	$7.7x10^2$ ± $1.0x10^2$	$7.9x10^2$ ± $1.2x10^2$	$3.9x10^2$ ± $4.5x10^1$
SD1	290 ± 58	--	--	--	--	--	--	--
SD2	100 ± 27	--	--	--	--	--	--	--
SD3	290 ± 58	--	--	--	--	--	--	--

Table S4. CEC (ng/L) and nutrient (μM) results averaged by location, date sampled, and low (LT) vs. high tide (HT).

	Site	Tide stage	CBZ (ng/L)	CFN (ng/L)	FQL (ng/L)	TDP (μM)	TDN (μM)	DON (μM)	NOx (μM)	NH_4^+ (μM)
Coastal surface water	C1 KT	LT	< MDL	< MDL	< MDL	0.71	36	5.1	20	11
		HT	< MDL	< MDL	< MDL	2.1	100	17	64	18
	C1 ST	LT	< MDL	690	< MDL	0.73	45	7.2	26	12
		HT	< MDL	2700	< MDL	0.40	58	14	40	4.1
	C2 KT	LT	130	1300	< MDL	0.31	31	14	17	0.12
		HT	150	1320	< MDL	0.26	5.7	5.1	0.55	< MDL
	C2 ST	LT	< MDL	720	< MDL	0.60	26	7.1	15	4.6
		HT	71	2000	< MDL	0.43	18	8.2	8.3	1.5
	C3 KT	LT	< MDL	810	< MDL	0.67	25	4.8	18	2.0
		HT	< MDL	1400	< MDL	0.76	20	5.0	8.5	6.0
	C3 ST	LT	< MDL	2900	< MDL	0.70	30	8.3	11	10
		HT	230	900	< MDL	0.57	20	7.1	1.7	11
	C4	LT	230	1600	< MDL	0.40	17	16	0.14	< MDL
		HT	110	1300	< MDL	0.26	13	12	0.49	0.19
Coastal GW	C1 KT	LT	< MDL	990	< MDL	2.1	79	6.6	8.9	63
		HT	130	880	< MDL	1.8	52	0.61	0.84	51
	C1 ST	LT	110	620	< MDL	6.8	100	19	1.1	81
		HT	130	1600	< MDL	3.6	55	0.74	1.6	53
	C2 KT	LT	< MDL	< MDL	< MDL	0.47	30	15	14	0.56
		HT	100	1200	< MDL	0.30	14	10	1.2	2.5
	C2 ST	LT	120	1100	< MDL	1.5	33	7.7	20	5.4
		HT	70	1500	< MDL	0.56	6.8	5.5	1.3	0.069
	C3 KT	LT	< MDL	1300	< MDL	0.60	24	6.2	8.8	8.6
		HT	150	< MDL	< MDL	0.84	11	5.0	5.6	0.20
	C4	LT	200	420	< MDL	1.2	10	5.1	4.9	0.081
		HT	230	830	< MDL	0.92	9.9	6.6	3.4	< MDL
Storm drain	SD1	LT	330	2000	61	3.0	60	53	6.0	1.1
		HT	160	1500	19	6.7	200	65	0.17	140
	SD2	LT	250	3000	23	3.7	140	110	14	15
		HT	130	850	28	6.9	190	53	0.40	140
	SD3	LT	< MDL	970	< MDL	1.0	38	16	16	5.5
		HT	150	420	< MDL	0.37	11	8.2	2.6	0.42

Table S5. Low vs. high tide comparison by study site and sampling date. Modeled water table heights (m) are with respect to mean sea level. Advection rates were calculated using the transient mass balance method and the average groundwater endmember.

Site	Tide Stage	Water table ht (m)	Adv_{ts} (m/d)
C1 KT	LT	-0.20	2 ± 0.8
	HT	0.65	3 ± 0.6
C1 ST	LT	-0.076	1 ± 0.7
	HT	0.55	0.4 ± 0.03
C2 KT	LT	-0.25	0.7 ± 0.1
	HT	0.60	1 ± 0.2
C2 ST	LT	-0.037	0.9 ± 0.1
	HT	0.53	1 ± 0.6
C3 KT	LT	-0.14	0.4 ± 0.04
	HT	0.59	2 ± 0.2
C3 ST	LT	-0.19	0.1 ± 0.01
	HT	0.46	0.4 ± 0.1
C4	LT	-0.011	0 .01± 0.002
	HT	0.26	0.06 ± 0.008
SD1	LT	-0.45	--
	HT	0.69	--
SD2	LT	0.28	--
	HT	0.43	--
SD3	LT	0.17	--
	HT	0.45	--

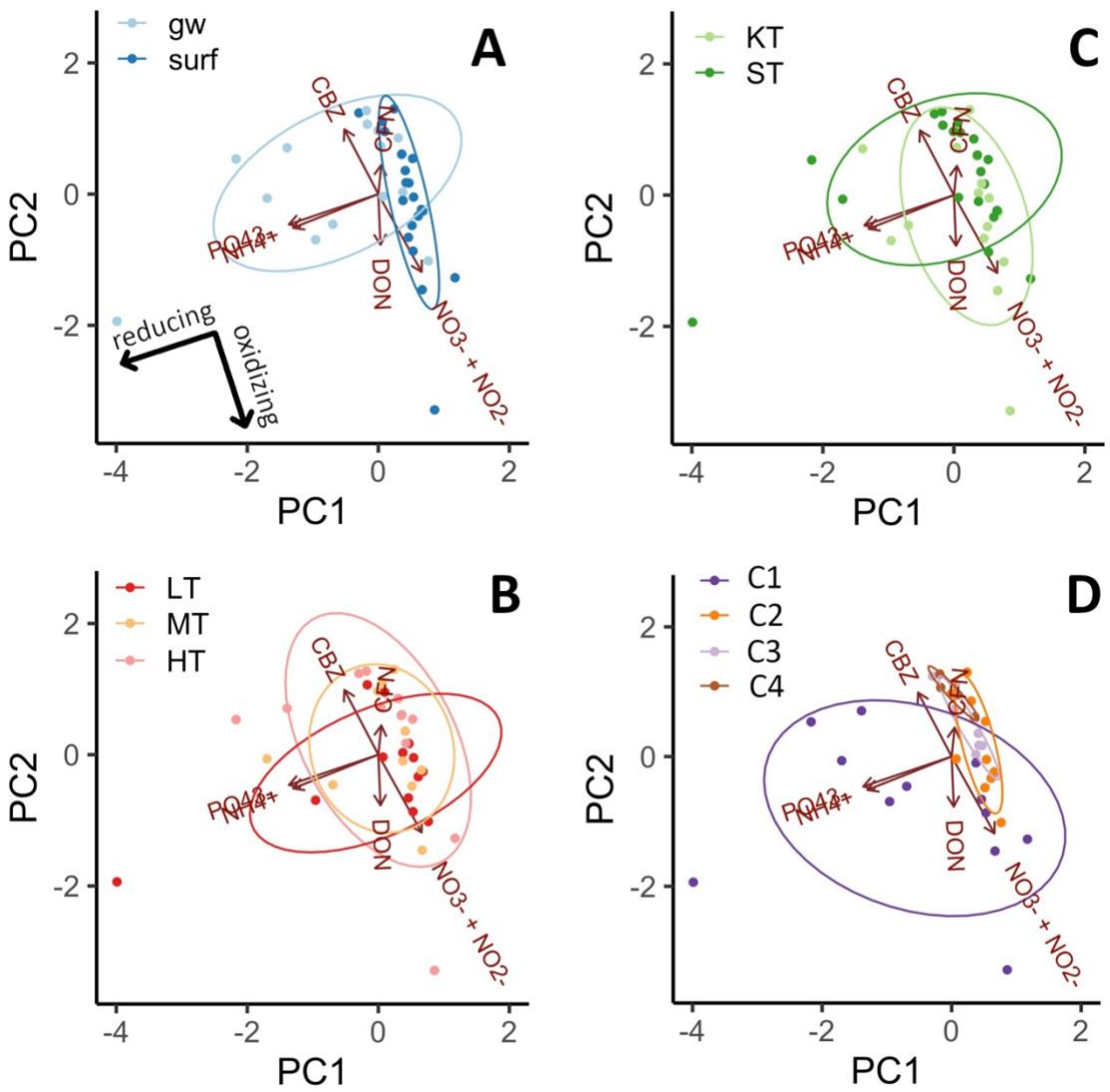

Figure S4. PCA for coastal samples with different groupings emphasized for A through D, demonstrating greater influence from reducing conditions at low tide and oxidizing conditions at high tide. The PC1 and PC2 axes are normalized, where PC1 explains 31%, PC2 explains 27% of the variation. PC3 and PC4 (not shown) explain 18% and 16% of the variation, respectively (cumulative proportion of variance explained by PC1-4 = 91%). (A) groundwater (gw) vs. surface water (surf). Groundwater aligns along the "reduced" axis (NH_4^+, PO_4^{3-}) whereas surface water follows the "oxidized" axis (NO_3^-). (B) Low (LT), mid (MT), and high (HT) tide. Similar to groundwater but with a less clear differentiation, LT samples are more aligned with the reduced axis and HT samples along the oxidized axis with MT samples falling in between the two. (C) King (KT) vs. spring (ST) tide. Because of higher SGD fluxes, KT samples tend to align with the reduced axis. (D) Samples by study site, most of C1 clearly separated from the other sites.

Table S6. Average RQs for carbamazepine (CBZ), caffeine (CFN), and fluoroquinolones (FQL) in surface and storm drain water.

Site	CBZ RQ	CFN RQ	FQL RQ
C1 (n = 6)	0.55	1.2	0
C2 (n = 6)	2.0	2.3	0
C3 (n = 5)	2.7	2.7	0
SD1 (n =6)	6.6	1.3	21
SD2 (n = 6)	5.5	1.5	26
SD3 (n = 2)	2.5	1.4	0
C4 (n = 2)	5.7	2.9	0

Appendix C-1. Additional Study Site Information

The geology of the area is described by Koʻolau Volcanics (primarily theoleiitic basalt) overlain by Honolulu Volcanics (Stearns & Vaksvik, 1935). A unit referred to as caprock lies on top of these basaltic layers. The caprock is considered impermeable and is comprised of post-erosional volcanics, lagoonal deposits, and coral debris (Stearns, 1935). Within the study area, anthropogenic fill (estuarine and coral sediments) has been placed over the aforementioned layers (Finstick, 1996; Stearns & Vaksvik, 1935).

Groundwater is stored within the basal lens approximated by the Ghyben-Herzberg principle mostly within the basalt aquifer with a small portion also within the caprock (MacDonald et al., 1983). While the caprock is considered a semi-confining layer, the upper layer of the caprock is unconfined and the groundwater is influenced by rainfall, marine forcings such as tides and seasonal sea-level changes, and can be easily polluted from urban land-use (Gingerich & Oki, 2000; Whitter & El-Kadi, 2009).

Both Waikīkī and Māpunapuna have been highlighted as highly vulnerable to SLR and inundated WWI (Spirandelli et al., 2018). Honolulu is projected to experience 2 to 100 days per year of high tide flooding by 2050 (Thompson et al., 2019; Sweet et al., 2020), leading to a greater frequency of flooding of OSDS and sewer lines. The Ala Wai canal is subject to chronic water quality problems, the U.S. EPA ranks the canal impaired due to high turbidity, nitrogen and fecal coliform levels (USEPA, https://mywaterway.epa.gov/waterbody-report/21HI/HIW00034/2018, last accessed July 15, 2020). While stream inputs have been considered a major source of contaminants, groundwater pathways especially those flushing WWI should be considered as well.

Appendix C-2. Measurement, Calculation, and Results of GW Fluxes

Radon time series spanning a half tidal cycle were conducted using a RAD7 radon-in-air detector equipped with a RAD-AQUA air-water exchanger (Durridge, Inc.) with a measurement interval of 15 minutes. Water was continuously pumped through Masterflex tubing using a peristaltic pump into the air-water exchanger. Concurrent logging of conductivity, temperature, and depth (Schlumberger Inc. CTD Diver) at the radon measurement intake were used to correct radon inventories and calculate radon mass balances. Radon grab samples were collected from groundwater using push-point sampler into 250 mL borosilicate glass bottles and analyzed on the day of

collection using a RAD-H_2O radon-in-air analyzer with water analysis accessory (Durridge, Inc.). Radon grab samples were decay corrected to the time of sample collection.

SGD was calculated using both transient and residence-time mass balance approaches. For the transient approach, first, radon in excess of ^{226}Ra production was accounted for to calculate radon inventories. Then radon inventories were corrected at each time step for flood and ebb tides, mixing losses, sediment diffusion, and atmospheric evasion. Advection rates (m/day) were then calculated by dividing the radon fluxes ($Bq/m^2/day$) by the median, average, and maximum groundwater radon endmember from all groundwater samples collected in this study. Advection rates were then converted to SGD fluxes (m^3/day) by multiplying the advection rate by the plume area, as based off of previous radon surveys in the same location (Appendix C: Figure S1). Uncertainties were propagated throughout the calculation.

Groundwater fluxes were also calculated using a residence-time based approach for comparison to the temporal mass balance model (Dulaiova et al., 2010). Total SGD fluxes were calculated using Equation 3, where A_{Rn_sw} is the radon activity measured at each time step, corrected for ^{226}Ra production, sediment diffusion and atmospheric evasion losses; V is the volume of water represented by the plume area (m^2) and water depth (m), A_{Rn_gw} is the radon activity of the groundwater endmember, and τ is the water residence time (days).

$$Q_{SGD} = \frac{A_{Rn\_sw} \times V}{\tau \times A_{Rn\_gw}} \qquad \text{Eq. 3}$$

Advection rates were again calculated using the same three groundwater endmembers as in the transient mass balance model. Two different residence times were used in this calculation as there is sparse literature available on the water residence time of the study locations. The short residence time (RT_short) refers to the residence time that would allow for the calculated advection rate to match the one calculated using the transient mass balance model. The long residence time (RT_long) refers to residence time that was estimated in a previous study 50 years ago (Gonzalez, 1971). Because the Ala Wai Canal has undergone substantial changes and dredging since

that study, we have opted to conservatively provide a range for residence time. For coastal areas, RT_long is 12 hours, reflecting semi-diurnal tidal flushing. Nutrient and CEC fluxes were estimated by multiplying the SGD flux by the median groundwater nutrient and CEC concentration for each study site and date of sampling.

Two main sources of uncertainty are associated with SGD estimation. The groundwater endmember is generally considered the greatest source of uncertainty (Charette et al., 2008). Groundwater was collected at each site at several stages in the tidal cycle, however we may not have completely captured site heterogeneity. The same radon concentration was used for all sites for the groundwater endmember as the Mood's median test ($\alpha = 0.05$) revealed that groundwater samples came from the same distribution, regardless of tidal stage or location. We also aimed to address uncertainties associated with the water residence time in Ala Wai Canal by estimating a lower and upper bound of previously published residence times and resulting SGD estimates.

Appendix C-3. Environmental Risk Assessment

Environmental impact was assessed by calculating risk quotients (RQ) for CECs in surface water and storm drain samples. These were calculated using Equation 4, where Obs_{conc} refers to the measured concentration in the sample and PNEC refers to the predicted no effect concentration.

$$RQ = \frac{Obs_{conc}}{PNEC} \qquad \text{Eq. 4}$$

PNECs differ by species, duration of exposure, and environment, and thus cover a substantial range. The PNECs used in this study (Appendix C: Table S2) are the minimum value found in the literature review in saline and chronic conditions and favored usage of the no observed effect concentration (NOEC), as suggested by the European Union guidelines for environmental risk assessment (European Commission, 2003).

Appendix C-4. Nutrient Concentrations

While we did not observe a change in nutrient concentration between king and spring tides in this study, increases in both concentration and flux have been observed in other areas, such as Kahaluʻu, Hawaiʻi (McKenzie et al., 2019). In this case, a difference in water mixing rates, circulation, inundation pathway, or pollutant source may explain differences between these two studies.

A strong correlation between TDN and TDP was observed for almost all groundwater ($r^2 = 0.72$, p-value = $7.0x10^{-5}$) and surface water ($r^2 = 0.55$, p-value = $1.7x10^{-4}$) samples, implying that dilution, not processes of nitrogen removal (e.g. denitrification), is the dominant process occurring. This further supports that inundation is actively preventing aerobic degradation as nitrifying bacteria require oxygen to produce the substrate for denitrification (Elmir, 2018). The correlation between TDN and TDP was even stronger for storm drains ($r^2 = 0.92$, p-value = 0.0092), again supporting inundation under saturated conditions leading to dilution, and limited biogeochemical cycling of contaminants. This stronger correlation between TDN and TDP is unsurprising, as storm drains tend to be low oxygen environments.

Unprocessed Data

Table 1. Study site and sampling information and radon (Bq/m^3), CEC (ng/L), and nutrient concentrations (μM).

ID	Date	Time	Lat	Long	Rn (Bq/m^3)	Sal	CBZ (ng/L)	CFN (ng/L)	FQL (ng/L)	Water Ht (m)	PO_4^{3-} (μM)	NOx (μM)	NH_4^+ (μM)	TDN (μM)	TDP (μM)
C2 KL surf	7/11/18	8:05	21.2849	-157.8294	166.29	14.65	132	1276	0	0.2093	0.27	16.82	0.12	30.91	0.31
C2 KL gw	7/11/18	8:20	21.2849	-157.8294	0.00	15.71	0	0	0	0.20149	0.25	14.12	0.56	29.81	0.47
C2 KM surf	7/11/18	11:45	21.2849	-157.8294	50.84	17.55	0	1143	0	0.62645	0.56	9.21	3.33	25.51	1.10
C2 KH surf	7/11/18	15:24	21.2849	-157.8294	505.66	23.78	148	1319	0	1.09297	0.17	0.55	0.00	5.66	0.26
C2 KH gw	7/11/18	15:26	21.2849	-157.8294	83.36	21.13	102	1150	0	1.09297	0.07	1.19	2.54	14.18	0.30
C3 SL surf	7/24/18	7:19	21.2877	-157.8440	57.59	24.66	0	2905	0	0.07376	0.47	11.38	9.89	29.56	0.70
C3 SM surf	7/24/18	10:05	21.2877	-157.8440	32.92	27.96	0	2800	0	0.24198	0.59	4.65	5.02	18.72	0.78
C3 SH surf	7/24/18	14:44	21.2877	-157.8440	233.15	33.47	226	902	0	0.67152	0.48	1.67	11.45	20.26	0.57
C1 KL gw	8/11/18	9:43	21.2779	-157.8213	8205.65	16.69	0	985	0	0.25342	0.90	8.86	63.12	78.60	2.11
C1 KL surf	8/11/18	9:52	21.2779	-157.8213	191.75	5.23	0	0	0	0.26308	0.65	20.22	10.69	36.02	0.71
C1 KM gw	8/11/18	12:26	21.2779	-157.8213	3745.40	18.80	0	874	0	0.63933	1.09	5.16	44.61	56.76	1.86
C1 KM surf	8/11/18	12:40	21.2779	-157.8213	86.33	7.71	0	0	0	0.68505	0.69	37.85	14.32	58.93	0.77
C1 KH gw	8/11/18	16:39	21.2779	-157.8213	2822.97	23.87	132	875	0	1.26781	1.53	0.84	50.57	52.03	1.78
C1 KH surf	8/11/18	16:50	21.2779	-157.8213	259.42	12.11	0	0	0	1.25808	1.19	64.12	18.43	99.70	2.05
C3 KL gw	8/12/18	10:10	21.2877	-157.8440	102.07	24.63	0	1340	0	0.0562	0.57	8.84	8.62	23.64	0.60
C3 KL surf	8/12/18	10:17	21.2877	-157.8440	98.00	23.45	0	810	0	0.04728	0.52	18.12	2.03	24.99	0.67
C3 KH gw	8/12/18	17:12	21.2877	-157.8440	74.67	24.85	151	0	0	0.82842	0.79	5.57	0.20	10.71	0.84
C3 KH surf	8/12/18	17:18	21.2877	-157.8440	76.16	26.02	0	1410	0	0.80089	0.58	8.54	5.97	19.46	0.76
C2 SL gw	8/21/18	6:15	21.2849	-157.8294	55.56	33.09	116	1118	0	0.33692	1.32	19.93	5.36	33.03	1.52
C2 SL surf	8/21/18	6:20	21.2849	-157.8294	83.41	24.20	0	719	0	0.3364	0.43	14.64	4.55	26.31	0.60
C2 SM gw	8/21/18	9:52	21.2849	-157.8294	27.49	36.11	140	1439	0	0.58675	0.75	1.58	2.79	11.70	0.93
C2 SM surf	8/21/18	10:10	21.2849	-157.8294	0.00	25.56	0	389	0	0.61697	0.19	9.59	2.48	19.97	0.41
C2 SH gw	8/21/18	13:34	21.2849	-157.8294	0.00	36.08	71	1528	0	0.94508	0.49	1.29	0.07	6.84	0.56
C2 SH surf	8/21/18	13:40	21.2849	-157.8294	53.54	25.45	71	1950	0	0.96185	0.20	8.26	1.53	17.97	0.43
C1 SL gw	9/5/18	5:50	21.2779	-157.8213	344.77	33.41	111	615	0	0.60009	6.60	1.08	80.95	100.97	6.77

C1 SL surf	9/5/18	6:00	21.2779	-157.8213	306.90	18.73	0	690	0	0.60696	0.71	25.77	11.72	44.74	0.73
C1 SM gw	9/5/18	9:18	21.2779	-157.8213	153.77	32.66	123	1560	0	0.79605	2.69	2.80	47.65	60.08	2.75
C1 SM surf	9/5/18	9:25	21.2779	-157.8213	175.45	11.03	99	259	0	0.81381	0.43	20.16	8.54	34.61	0.48
C1 SH gw	9/5/18	13:20	21.2779	-157.8213	96.54	32.76	133	1613	0	1.19119	3.43	1.57	52.64	54.95	3.56
C1 SH surf	9/5/18	13:30	21.2779	-157.8213	23.92	21.40	0	2655	0	1.2058	0.28	39.96	4.11	58.39	0.40
SD1 LT	7/13/18	12:17	21.3373	-157.9001	24.95	1.78	182	289	0	0.46825	3.48	40.71	26.08	135.50	4.46
SD1 MT	7/13/18	14:50	21.3373	-157.9001	118.92	1.79	260	0	0	0.44809	1.85	8.32	19.22	80.31	2.44
SD1 HT	7/13/18	16:53	21.3373	-157.9001	860.49	23.78	124	0	0	0.49909	3.56	0.74	15.31	59.52	4.84
SD3 LT	9/7/18	8:10	21.3356	-157.8975	107.71	25.16	0	967	0	0.40992	0.72	16.34	5.46	37.63	1.02
SD3 HT	9/7/18	14:45	21.3356	-157.8975	0.00	36.28	149	415	0	1.20771	0.15	2.60	0.42	11.26	0.37
C4 LT gw	9/19/19	6:12	21.3307	-157.8956	902.98	31.11	203	415	0	0.1363	1.02	4.93	0.08	10.13	1.22
C4 LT surf	9/19/19	6:19	21.3307	-157.8956	213.61	33.46	229	1570	0	0.13637	0.14	0.14	0.00	16.58	0.40
C4 HT gw	9/19/19	12:51	21.3307	-157.8956	28.75	33.89	229	830	0	0.60117	0.87	3.36	0.00	9.91	0.92
C4 HT surf	9/19/19	12:59	21.3307	-157.8956	53.39	35.72	112	1314	0	0.6035	0.11	0.49	0.19	12.76	0.26
SD2 LT	10/26/18	11:56	21.3358	-157.8986	0.00	1.53	246	2975	23.1	0.24875	2.89	13.85	14.80	135.74	3.65
SD2 HT	10/26/18	5:20	21.3358	-157.8986	825.00	3.01	128	849	27.5	0.36119	6.76	0.40	138.37	191.38	6.87
SD1 LT2	10/26/18	12:12	21.3373	-157.9001	0.00	0.35	326	2040	60.5		1.83	5.95	1.08	60.45	2.98
SD1 MT2	10/26/18	8:15	21.3373	-157.9001	24.40	0.17	138	0	45		2.12	10.62	17.18	64.36	3.12
SD1 HT2	10/26/18	6:00	21.3373	-157.9001	189.00	0.45	159	1480	18.7		6.64	0.17	138.80	204.03	6.73

Table 2. Radon time series results by study location and sampling date.

Site	Time	Temp (C)	Salinity	Water Ht (m)	Rn (Bq/m3)	Rn unc
C1 KT 8/11/18	10:03	26.88	17.89	0.26	739.54	122.32
	10:18	26.98	17.22	0.27	770.10	127.03
	10:33	27.03	16.62	0.30	861.64	140.14
	10:48	27.12	16.87	0.35	874.56	141.60
	11:03	27.35	18.06	0.41	923.03	148.86
	11:19	27.47	18.68	0.45	815.05	133.56
	11:34	27.65	18.69	0.49	784.97	128.85
	11:49	27.76	19.21	0.53	720.29	119.90
	12:04	27.97	21.31	0.58	666.58	110.98
	12:19	28.14	23.07	0.60	676.03	112.50
	12:34	28.28	24.03	0.63	625.68	105.27
	12:49	28.31	25.23	0.68	566.98	96.23
	13:04	28.44	26.56	0.74	518.95	89.32
	13:19	28.50	28.24	0.81	495.99	85.35
	13:34	28.57	28.93	0.86	433.24	76.08
	13:49	28.69	28.95	0.91	415.85	74.02
	14:04	28.63	29.71	0.97	388.73	69.91
	14:19	28.59	30.81	1.02	378.25	68.58
	14:34	28.57	31.16	1.06	352.12	64.66
	14:49	28.54	31.40	1.12	345.43	63.90
	15:04	28.48	31.73	1.18	324.64	60.62
	15:19	28.47	31.94	1.20	292.60	55.10
	15:34	28.46	31.98	1.23	221.41	45.64
	15:49	28.45	32.17	1.25	317.55	58.78
	16:04	28.42	32.37	1.26	307.88	57.72

	16:19	28.38	32.49	1.27	317.36	58.74
	16:34	28.35	32.63	1.28	301.56	57.05
	16:49	28.33	32.63	1.28	285.87	54.35
	17:04	28.32	32.70	1.26	303.22	57.23
	17:05	28.32	32.73	1.25	451.56	260.57
C1 ST 9/5/18	6:34	28.63	26.96	0.58	534.60	90.93
	6:49	28.38	25.79	0.58	555.54	94.72
	7:04	28.26	25.45	0.58	618.21	103.20
	7:19	28.33	26.30	0.58	681.32	113.19
	7:34	28.30	26.22	0.59	698.75	115.33
	7:49	28.30	26.40	0.60	712.62	117.82
	8:04	28.49	26.65	0.62	685.21	113.46
	8:19	28.70	28.27	0.65	709.66	116.76
	8:34	28.83	29.09	0.68	620.18	104.03
	8:49	29.19	31.48	0.72	587.73	98.58
	9:04	29.36	32.01	0.75	567.73	95.98
	9:19	29.50	32.79	0.78	435.50	76.87
	9:34	29.51	32.42	0.81	379.65	68.81
	9:49	29.55	32.02	0.85	329.51	61.44
	10:04	29.75	32.78	0.86	376.53	68.25
	10:19	29.84	33.53	0.89	358.62	66.09
	10:34	29.92	33.90	0.92	302.81	58.04
	10:49	29.97	34.00	0.96	354.89	65.51
	11:04	29.95	34.50	1.00	304.37	58.07
	11:19	29.98	34.70	1.02	306.77	58.27
	11:34	30.05	34.90	1.05	274.47	53.83
	11:49	29.96	35.19	1.09	279.00	54.30
	12:04	29.94	35.32	1.10	314.65	59.02

	12:19	30.03	35.31	1.13	278.30	54.16
	12:34	30.02	35.37	1.15	248.51	50.11
	12:49	29.96	35.39	1.19	259.23	51.21
	13:04	29.88	35.54	1.20	260.98	51.41
	13:19	29.88	35.55	1.20	240.11	48.27
	13:29	29.86	35.55	1.20	223.79	51.23
C2 KT 7/11/18	9:49	26.87	23.88	0.28	248.77	51.99
	10:04	27.03	23.48	0.31	260.59	53.09
	10:19	27.22	23.75	0.34	260.59	52.91
	10:34	27.46	24.89	0.37	280.81	55.76
	10:49	27.81	26.47	0.42	246.99	50.68
	11:04	27.79	27.60	0.47	265.08	52.29
	11:19	27.85	28.97	0.52	270.46	52.57
	11:34	27.93	31.20	0.57	273.83	53.59
	11:49	27.90	30.33	0.62	293.57	56.91
	12:04	27.87	31.19	0.66	282.34	54.51
	12:19	27.91	31.87	0.71	283.93	54.53
	12:34	28.02	31.96	0.76	279.82	54.02
	12:49	27.94	32.55	0.81	301.57	57.32
	13:04	27.88	32.67	0.85	261.83	52.15
	13:19	27.96	32.38	0.89	311.38	59.44
	13:34	27.64	32.80	0.93	327.36	61.26
	13:49	27.67	32.67	0.96	349.88	64.73
	14:04	27.62	32.69	1.00	345.46	64.28
	14:19	27.66	32.56	1.01	350.21	65.84
	14:34	27.60	32.52	1.05	349.24	65.78
	14:49	27.59	32.41	1.07	359.23	65.84
	15:04	27.55	32.36	1.08	333.93	62.10

	15:19	27.62	32.25	1.09	341.69	62.92
C2 ST 8/21/18	7:17	27.64	19.30	0.34	14.69	4.09
	7:32	27.68	20.40	0.35	14.56	4.05
	7:47	27.75	21.20	0.36	14.46	4.02
	8:02	27.76	20.80	0.37	14.49	4.03
	8:17	27.98	22.20	0.38	14.27	3.97
	8:32	27.46	19.40	0.38	14.74	4.10
	8:47	27.41	18.50	0.39	8.90	3.78
	9:02	28.60	22.90	0.42	3.35	3.39
	9:17	28.35	22.20	0.43	0.00	20.00
	9:32	28.35	22.10	0.45	0.00	20.00
	9:47	28.44	23.20	0.48	0.00	20.00
	10:02	28.53	24.00	0.49	3.33	3.37
	10:17	28.47	24.00	0.53	3.34	3.37
	10:32	28.34	25.41	0.55	0.00	20.00
	10:47	28.36	25.40	0.58	0.00	20.00
	11:02	28.35	25.56	0.62	0.00	20.00
	11:17	28.25	25.56	0.63	0.00	20.00
	11:32	28.26	25.56	0.68	3.32	3.35
	11:47	28.19	26.19	0.72	13.25	3.81
	11:02	28.15	26.19	0.74	13.26	3.81
	11:17	28.21	26.19	0.77	19.87	7.19
	11:32	28.10	26.19	0.81	24.90	9.02
	11:47	28.08	27.20	0.83	49.48	14.94
	12:02	28.11	27.20	0.85	57.69	18.39
	12:17	28.16	24.17	0.85	88.23	26.63
	12:32	28.15	24.19	0.87	126.57	33.72
	12:47	28.17	24.19	0.88	132.23	34.14

	13:02	28.17	24.20	0.91	129.53	33.93
	13:17	28.26	24.20	0.92	138.99	34.62
	13:32	28.31	24.19	0.92	172.48	40.09
	13:47	28.34	24.19	0.95	156.43	37.37
	14:02	28.30	24.20	0.96	141.84	34.83
	14:03	28.33	25.40	0.94	278.84	383.77
C3 KT 8/12/18	10:39	29.43	25.17	0.05	161.81	38.33
	10:54	29.68	25.29	0.07	140.94	33.82
	11:09	29.74	25.12	0.09	186.34	41.55
	11:24	29.95	25.31	0.08	210.73	44.86
	11:39	30.30	25.62	0.11	170.62	38.51
	11:54	30.41	26.05	0.12	153.94	35.69
	12:09	30.34	26.51	0.16	149.96	35.31
	12:24	30.29	25.96	0.18	147.85	35.25
	12:39	30.51	26.51	0.22	174.97	38.64
	12:54	30.51	26.61	0.27	167.06	37.92
	13:09	30.32	27.26	0.30	217.03	46.07
	13:24	29.94	28.65	0.35	238.79	49.28
	13:39	29.74	29.37	0.37	251.28	50.51
	13:54	29.32	31.18	0.42	311.48	59.83
	14:09	29.28	31.55	0.46	394.94	71.78
	14:24	29.26	31.91	0.50	408.07	73.18
	14:40	29.25	31.92	0.56	384.90	70.63
	14:55	29.21	32.47	0.59	411.68	73.51
	15:10	29.06	32.96	0.61	441.19	78.71
	15:25	28.80	33.28	0.67	421.24	75.65
	15:40	28.70	33.41	0.72	509.07	88.44
	15:55	28.60	33.54	0.74	497.37	87.15

	16:10	28.82	32.83	0.77	461.39	82.13
	16:25	28.69	33.43	0.78	451.54	80.05
	16:40	28.81	33.11	0.78	413.93	74.87
	16:55	28.74	33.19	0.80	462.70	81.33
	17:10	28.58	33.57	0.82	466.31	81.77
	17:25	28.53	33.56	0.81	766.86	1098.65
C3 ST 7/24/18	8:06	26.79	24.78	0.10	56.65	20.67
	8:21	26.74	24.15	0.12	53.66	20.61
	8:36	26.83	23.89	0.13	80.81	25.36
	8:51	26.92	23.72	0.14	70.97	23.16
	9:06	27.00	23.44	0.17	74.27	24.93
	9:21	27.39	24.16	0.19	64.78	24.09
	9:36	28.03	26.35	0.21	63.45	23.38
	9:51	28.46	28.35	0.26	55.45	22.49
	10:06	28.82	29.87	0.29	53.12	22.00
	10:21	28.93	31.38	0.34	31.87	17.85
	10:36	29.04	30.29	0.39	64.67	25.37
	10:51	29.11	31.67	0.44	121.35	35.61
	11:06	29.08	32.20	0.48	183.56	45.47
	11:21	28.91	33.22	0.52	226.45	52.72
	11:36	28.82	33.15	0.56	253.50	57.61
	11:51	28.99	33.17	0.58	281.87	61.22
	12:06	29.09	33.02	0.62	259.80	57.97
	12:21	29.16	33.03	0.65	236.15	54.62
	12:36	28.98	33.33	0.69	230.53	54.22
	12:51	28.82	33.45	0.65	291.80	63.39
	13:06	28.81	33.40	0.63	295.07	63.71
	13:21	28.79	33.37	0.66	243.99	55.53

	13:36	28.86	33.54	0.68	263.42	58.37
	13:51	28.96	33.39	0.66	298.65	63.91
	14:06	28.99	33.16	0.68	230.72	54.26
	14:21	29.04	33.34	0.69	250.28	57.10
	14:36	29.01	33.15	0.70	253.89	57.49
	14:51	28.97	33.40	0.68	235.15	54.61
	15:06	29.00	33.63	0.69	225.31	53.69
C4 9/19/18	7:09	26.74	36.61	0.13	6.55	8.05
	7:24	26.90	36.71	0.13	5.46	7.52
	7:39	27.22	36.88	0.16	16.71	11.29
	7:54	27.33	36.92	0.17	9.62	9.53
	8:09	27.42	36.94	0.17	19.76	12.85
	8:24	27.51	36.89	0.20	22.38	12.92
	8:39	27.09	35.98	0.23	22.44	13.12
	8:54	26.40	33.51	0.23	21.91	13.54
	9:09	26.75	33.40	0.27	25.65	13.57
	9:25	26.88	33.25	0.29	38.31	17.18
	9:40	27.65	34.70	0.30	31.04	14.91
	9:55	27.72	35.56	0.34	34.10	14.94
	10:10	27.73	36.03	0.33	31.17	14.77
	10:25	27.86	36.24	0.35	40.22	16.59
	10:40	27.90	36.39	0.38	60.20	20.52
	10:55	28.06	36.47	0.41	50.96	18.50
	11:10	28.37	36.54	0.42	41.94	16.47
	11:25	28.49	36.04	0.46	49.03	18.28
	11:40	28.66	36.06	0.49	43.93	17.95
	11:55	28.75	36.14	0.50	55.56	19.93
	12:10	29.30	36.23	0.54	48.47	17.92

	12:25	29.60	36.28	0.56	39.14	15.93
	12:40	29.09	36.53	0.55	32.76	14.36
	12:55	28.97	36.60	0.59	40.41	16.18
	13:08	29.10	36.63	0.60	53.39	21.01
SD1 7/13/18	11:59	27.03	1.79	0.47	14.43	0.47
	12:14	27.03	1.78	0.47	14.51	0.47
	12:29	27.03	1.79	0.47	18.89	0.47
	12:44	27.05	1.80	0.47	18.99	0.47
	12:59	27.05	1.80	0.47	18.88	0.47
	13:14	27.05	1.80	0.46	26.37	0.46
	13:29	27.05	1.79	0.46	36.07	0.46
	13:44	27.05	1.79	0.45	26.90	0.45
	13:59	27.05	1.79	0.45	26.50	0.45
	14:14	27.06	1.79	0.44	24.03	0.44
	14:29	27.07	1.79	0.45	26.11	0.45
	14:44	27.08	1.78	0.44	32.40	0.44
	14:59	27.08	1.79	0.45	52.31	0.45
	15:14	27.09	1.78	0.46	66.21	0.46
	15:29	27.09	1.79	0.46	73.73	0.46
	15:44	27.12	1.76	0.46	96.32	0.46
	15:59	27.12	1.77	0.47	96.76	0.47
	16:14	27.12	1.78	0.47	112.73	0.47
	16:29	27.12	1.78	0.48	117.64	0.48
	16:44	27.11	1.79	0.48	132.23	0.48
	16:59	27.11	1.79	0.50	118.82	0.50
	17:14	27.98	3.54	0.48	117.31	0.48
SD2 10/26/18	4:52	29.63	3.16	0.36	20.40	0.36
	5:07	29.58	3.17	0.36	19.98	0.36

	5:22	29.45	3.17	0.36	22.67	0.36
	5:37	29.39	3.18	0.37	37.27	0.37
	5:52	29.37	3.33	0.37	51.65	0.37
	6:07	30.25	4.16	0.47	53.01	0.47
	6:22	29.46	2.60	0.49	48.96	0.49
	6:37	28.63	2.68	0.49	49.03	0.49
	6:52	27.84	2.57	0.49	44.99	0.49
	7:07	27.42	2.51	0.49	46.20	0.49
	7:22	27.22	2.46	0.48	41.90	0.48
	7:37	27.19	2.43	0.48	36.46	0.48
	7:52	27.26	2.43	0.48	38.95	0.48
	8:07	27.20	2.38	0.47	35.24	0.47
	8:22	27.20	2.36	0.48	36.60	0.48
	8:38	27.26	2.29	0.47	37.93	0.47
	9:01	27.63	2.28	0.47	35.97	0.47
	9:16	28.09	2.29	0.47	33.06	0.47
	9:31	28.72	2.32	0.46	17.48	0.46
	9:46	29.18	2.25	0.44	8.97	0.44
	10:01	29.50	2.25	0.43	0.00	0.43
	10:17	30.11	2.27	0.39	7.07	0.39
	10:32	29.57	2.39	0.30	0.00	0.30
	10:47	29.03	1.89	0.26	0.00	0.26
	11:02	29.23	1.82	0.24	0.00	0.24
	11:17	29.90	2.03	0.25	0.00	0.25
	11:22	30.13	1.95	0.24	0.00	0.24
SD3 9/7/18	8:53	26.95	24.00	0.45	82.12	0.45
	9:08	26.99	23.93	0.48	109.14	0.48
	9:23	27.13	24.56	0.48	117.30	0.48

	9:38	27.33	25.79	0.50	101.33	0.50
	9:53	27.61	27.20	0.53	26.13	0.53
	10:08	27.75	29.02	0.56	14.98	0.56
	10:23	27.73	28.15	0.56	22.92	0.56
	10:38	27.84	31.25	0.63	46.12	0.63
	10:53	27.90	31.51	0.66	57.07	0.66
	11:09	27.84	31.98	0.69	71.18	0.69
	11:24	27.86	32.51	0.74	74.01	0.74
	11:39	27.89	32.55	0.81	45.81	0.81
	11:54	27.91	32.38	0.83	56.39	0.83
	12:09	27.93	33.18	0.89	67.36	0.89
	12:24	27.96	33.24	0.90	75.33	0.90
	12:39	27.96	33.88	0.95	77.28	0.95
	12:54	27.98	34.03	0.98	80.59	0.98
	13:09	27.97	34.46	1.02	75.55	1.02
	13:24	27.96	34.93	1.05	77.24	1.05
	13:39	28.04	35.33	1.09	76.35	1.09
	13:54	28.12	35.87	1.12	49.94	1.12
	14:09	28.31	36.04	1.16	22.44	1.16
	14:24	28.55	36.21	1.18	24.31	1.18
	14:39	28.89	36.26	1.20	26.28	1.20
	14:54	28.88	36.25	1.20	24.21	1.20
	15:09	28.98	36.28	1.21	25.97	1.21
	15:12	28.71	36.37	1.22	52.07	1.22

References

Abaya, L. M., Wiegner, T. N., Colbert, S. L., Beets, J. P., Carlson, K. M., Kramer, K. L., … Couch, C. S. (2018). A multi-indicator approach for identifying shoreline sewage pollution hotspots adjacent to coral reefs. *Marine Pollution Bulletin*, *129*(1), 70–80. doi: 10.1016/j.marpolbul.2018.02.005

Ahmed, W., Payyappat, S., Cassidy, M., Harrison, N., & Besley, C. (2020). Sewage-associated marker genes illustrate the impact of wet weather overflows and dry weather leakage in urban estuarine waters of Sydney, Australia. *Science of The Total Environment, 705*, 135390. doi: 10.1016/j.scitotenv.2019.135390

Almeida, Â., Calisto, V., Valdemar, I.E., Schneider, R.J., Soares, A.M.V.M., Figueira, E., Freitas, R. (2014). Presence of the pharmaceutical drug carbamazepine in coastal systems: Effects on bivalves. *Aquatic Toxicology, 156*, 74-87. doi: 10.1016/j.aquatox.2014.08.002

Australian Bureau of Statistics (ABS). (2015). Australian Health Survey: Nutrition First Results—Foods and Nutrients, 2011–12.

Austrailian Bureau of Statistics (ABS). (2016). *Census.* Australia: Canberra, ATC.

Australian Government Geoscience Australia. https://www.ga.gov.au/

Backhaus, T. (2014). Medicines, shaken and stirred: a critical review on the ecotoxicology of pharmaceutical mixtures. *Philosophical Transactions of the Royal Society B: Biological Sciences*, *369*(1656), 20130585. doi: 10.1098/rstb.2013.0585

Bagnis, S., Fitzsimons, M. F., Snape, J., Tappin, A., & Comber, S. (2018). Processes of distribution of pharmaceuticals in surface freshwaters: implications for risk assessment. *Environmental Chemistry Letters, 16*(4), 1193–1216. doi: 10.1007/s10311-018-0742-7

Barber, L., Lee, K., Swackhamer, D., & Schoenfuss, H. (2007). Reproductive responses of male fathead minnows exposed to wastewater treatment plant effluent, effluent treated with XAD8 resin, and an environmentally relevant mixture of alkylphenol compounds. *Aquatic Toxicology*, *82*(1), 36–46. doi: 10.1016/j.aquatox.2007.01.003

Bayen, S. (2012). Occurrence, bioavailability and toxic effects of trace metals and organic contaminants in mangrove ecosystems: A review. *Environment International*, 48, 84-101. doi: 10.1016/j.envint.2012.07.008

Befus, K. M., Barnard, P. L., Hoover, D. J., Hart, J. A. F., & Voss, C. I. (2020). Increasing threat of coastal groundwater hazards from sea-level rise in California. *Nature Climate Change*. doi: 10.1038/s41558-020-0874-1

Benowitz, N. L. (1990). Clinical Pharmacology of Caffeine. *Annual Review of Medicine*, *41*(1), 277–288. doi: 10.1146/annurev.me.41.020190.001425

Birch, G. F., & Taylor, S. E. (2000). Distribution and possible sources of organochlorine residues in sediments of a large urban estuary, Port Jackson, Sydney. *Australian Journal of Earth Sciences*, *47*(4), 749–756. doi: 10.1046/j.1440-0952.2000.00806.x
Birch, G. F., & Scollen, A. (2003). Heavy metals in road dust, gully pots and parkland soils in a highly urbanised sub-catchment of Port Jackson, Australia. *Soil Research*, *41*(7), 1329. doi: 10.1071/sr02147

Birch, G. F., and Taylor, S. E. (2004). 'Sydney Harbour and Catchment: Contaminant Status of Sydney Harbour Sediments: A Handbook for the Public and Professionals.' (Geological Society of Australia, Environ- mental, Engineering and Hydrogeology Specialist Group: Canberra, ACT.)

Birch, G. (2007). A short geological and environmental history of the Sydney estuary, Australia. In Gavin Birch (Eds.), *Water Wind Art and Debate - How environmental concerns impact on disciplinary research*, (pp. 214-242). Sydney: Sydney University Press.

Birch, G., Harrington, C., Symons, R., & Hunt, J. (2007). The source and distribution of polychlorinated dibenzo-p-dioxin and polychlorinated dibenzofurans in sediments of Port Jackson, Australia. *Marine Pollution Bulletin*, *54*(3), 295–308. doi: 10.1016/j.marpolbul.2006.10.009

Birch, G., Drage, D., Thompson, K., Eaglesham, G., & Mueller, J. (2015). Emerging contaminants (pharmaceuticals, personal care products, a food additive and pesticides) in waters of Sydney estuary, Australia. *Marine Pollution Bulletin*, *97*(1-2), 56–66. doi: 10.1016/j.marpolbul.2015.06.038

Birch, G. F., & Rochford, L. (2009). Stormwater metal loading to a well-mixed/stratified estuary (Sydney Estuary, Australia) and management implications. *Environmental Monitoring and Assessment*, *169*(1-4), 531–551. doi: 10.1007/s10661-009-1195-z

Bishop, J.M., Glenn, C.R., Amato, D.W., Dulai, H. (2015). Effect of land use and groundwater flow path on submarine groundwater discharge nutrient flux. *Journal of Hydrology: Regional Studies, 11*, 194–218. doi: 10.1016/j.ejrh.2015.10.008.

Briggs, R.A., Ruttenberg, K.C., Ricardo, A.E., Glazer, B.T. (2013). Constraining sources of organic matter to tropical coastal sediments: consideration of non-traditional end members. *Aquatic Geochemistry, 19*(5–6): 543–563.

Brodin, T., Piovano, S., Fick, J., Klaminder, J., Heynen, M., & Jonsson, M. (2014). Ecological effects of pharmaceuticals in aquatic systems—impacts through behavioural alterations. *Philosophical Transactions of the Royal Society B: Biological Sciences*, *369*(1656), 20130580. doi: 10.1098/rstb.2013.0580

Buerge, I. J., Poiger, T., Müller, M. D., & Buser, H.-R. (2003). Caffeine, an Anthropogenic Marker for Wastewater Contamination of Surface Waters. *Environmental Science & Technology, 37*(4), 691–700. doi: 10.1021/es020125z

Burnett, W. C., & Dulaiova, H. (2003). Estimating the dynamics of groundwater input into the coastal zone via continuous radon-222 measurements. *Journal of Environmental Radioactivity, 69*(1-2), 21–35. doi: 10.1016/s0265-931x(03)00084-5

Burnett, W., Aggarwal, P., Aureli, A., Bokuniewicz, H., Cable, J., Charette, M., … Turner, J. (2006). Quantifying submarine groundwater discharge in the coastal zone via multiple methods. *Science of The Total Environment, 367*(2-3), 498–543. doi: 10.1016/j.scitotenv.2006.05.009

Cardno and Baird (2014). Sydney Harbour Ecological Response Model.

Cartwright, I., Hofmann, H. (2015). Using geochemical tracers to distinguish groundwater and parafluvial inflows in rivers (the Avon Catchment, SE Australia). *Hydrology and Earth System Science, 12*, 9205-9246 p.

Chadwick, O.A., Derry, L.A., Vitousek, P.M., Huebert, B.J., Hedin, L.O. (1999). Changing sources of nutrients during four million years of ecosystem development. *Nature, 397*(6719), 491–497.

Chanton, J. P., Burnett, W. C., Dulaiova, H., Corbett, D. R., & Taniguchi, M. (2003). Seepage rate variability in Florida Bay driven by Atlantic tidal height. *Biogeochemistry, 66*(1/2), 187–202. doi: 10.1023/b:biog.0000006168.17717.91

Charette, M. A., Buesseler, K. O., & Andrews, J. E. (2001). Utility of radium isotopes for evaluating the input and transport of groundwater-derived nitrogen to a Cape Cod estuary. *Limnology and Oceanography, 46*(2), 465–470. doi: 10.4319/lo.2001.46.2.0465

Charette, M. A., Moore, W. S., and Burnett, W. C. (2008). "Uranium- and thorium-series nuclides as tracers of submarine groundwater discharge," in U-Th Series Nuclides in Aquatic Systems, eds S. Krishnaswami and J. Kirk Cochran (Amsterdam; Elsevier), 155–191. doi: 10.1016/S1569-4860(07)00005-8

Charette, M.A., Henderson, P.B., Breier, C.F., Liu, Q. (2013). Submarine groundwater discharge in a river-dominated Florida estuary. *Marine Chemistry*, 156, 3–17. doi: 10.1016/j.marchem.2013.04.001

Chemspider Database. Royal Society of Chemistry.

Cho, H.M., Kim, G., Kwon, E.Y., Moosdorf, N., Garcia-Orellana, J., Santos, I.R. (2018). Radium tracing nutrient inputs through submarine groundwater discharge in the global ocean. *Scientific Reports, 8*(1), 4–10.

Cooper, J.A., Loomis, G.W., Amador, J.A. (2016). Hell and high water: Diminished septic system performance in coastal regions due to climate change. *PLoS One*, *11*(9), 1–18.

Correa, R. E., Tait, D. R., Sanders, C. J., Conrad, S. R., Harrison, D., Tucker, J. P., … Santos, I. R. (2020). Submarine groundwater discharge and associated nutrient and carbon inputs into Sydney Harbour (Australia). *Journal of Hydrology*, *580*, 124262. doi: 10.1016/j.jhydrol.2019.124262

Dailer, M.L., Knox, R.S., Smith, J.E., Napier, M., Smith, C.M. (2010). Using δ15N values in algal tissue to map locations and potential sources of anthropogenic nutrient inputs on the island of Maui, Hawai'i, USA. *Marine Pollution Bulletin*, *60*(5), 655–671. doi: 10.1016/j.marpolbul.2009.12.021

Dafouz, R., Cáceres, N., Rodríguez-Gil, J. L., Mastroianni, N., López de Alda, M., Barceló, D., de Miguel, Á. G., & Valcárcel, Y. (2018). Does the presence of caffeine in the marine environment represent an environmental risk? A regional and global study. *Science of the Total Environment*, *615*, 632–642. doi: 10.1016/j.scitotenv.2017.09.155

Dai, A., & Trenberth, K. E. (2002). Estimates of Freshwater Discharge from Continents: Latitudinal and Seasonal Variations. *Journal of Hydrometeorology*, *3*(6), 660–687. doi: 10.1175/1525-7541(2002)003<0660:eofdfc>2.0.co;2

Das, P., Marchesiello, P., & Middleton, J. H. (2000). Numerical modelling of tide-induced residual circulation in Sydney Harbour. *Marine and Freshwater Research*, *51*(2), 97. doi: 10.1071/mf97177

Davis, W. (1993). Contamination of coastal versus open ocean surface waters. *Marine Pollution Bulletin*, *26*(3), 128–134. doi: 10.1016/0025-326x(93)90121-y

De Carlo, E.H., Beltran, V.L., Tomlinson, M.S. (2004). Composition of water and suspended sediment in streams of urbanized subtropical watersheds in Hawaii. *Applied Geochemistry*, *19*(7), 1011–1037.

De Carlo, E.H., Hoover, D.J., Young, C.W., Hoover, R.S., Mackenzie, F.T. (2007). Impact of storm runoff from tropical watersheds on coastal water quality and productivity. *Applied Geochemistry*, *22*(8 SPEC. ISS.), 1777–1797.

Dimova, N.T., Swarzenski, P.W., Dulaiova, H., Glenn, C.R. (2012). Utilizing multichannel electrical resistivity methods to examine the dynamics of the fresh water-seawater interface in two Hawaiian groundwater systems. *Journal of Geophysical Research: Ocean*, *117*(2), 1–12. doi: 10.1029/2011JC007509.

Dulai, H., Kleven, A., Ruttenberg, K., Briggs, R., Thomas, F. (2016) Evaluation of submarine groundwater discharge as coastal nutrient source and its role in coastal groundwater quality and quantity. In: Fares A, editor. Emerging issues in groundwater resources, Advances in Water Security. doi: 10.1007/978-3-319-32008-3_8.

Dulaiova, H., Burnett, W., Chanton, J., Moore, W., Bokuniewicz, H., Charette, M., & Sholkovitz, E. (2006). Assessment of groundwater discharges into West Neck Bay, New York, via natural tracers. *Continental Shelf Research*, *26*(16), 1971–1983. doi: 10.1016/j.csr.2006.07.011

Dulaiova, H., Burnett, W.C., Wattayakorn, G., Sojisuporn, P. (2006). Are groundwater inputs into river-dominated areas important? The Chao Phraya River, Gulf of Thailand. *Limnolology and Oceanography*, *51*(5), 2232–2247.

Dulaiova, H., Camilli, R., Henderson, P. B., & Charette, M. A. (2010). Coupled radon, methane and nitrate sensors for large-scale assessment of groundwater discharge and non-point source pollution to coastal waters. *Journal of Environmental Radioactivity*, *101*(7), 553–563. doi: 10.1016/j.jenvrad.2009.12.004

Elmir, S., (2018). Septic systems vulnerable to sea level rise. Final Report in support of Resolution No. R-911-16.

European Commission, (2003). European Commission Technical Guidance Document in Support of Commission Directive 93//67/EEC on Risk Assessment for New Notified Substances and Commission Regulation (EC) No. 1488/94 on Risk Assessment for Existing Substance, Part II.

Feng, H., Cochran, J. K., Lwiza, H., Brownawell, B. J., & Hirschberg, D. J. (1998). Distribution of heavy metal and PCB contaminants in the sediments of an urban estuary: The Hudson River. *Marine Environmental Research*, *45*(1), 69–88. doi: 10.1016/s0141-1136(97)00025-1

Ferrari, B., Mons, R., Vollat, B., Fraysse, B., Paxéus, N., Giudice, R. L., … Garric, J. (2004). Environmental Risk Assessment of Six Human Pharmaceuticals: Are the Current Environmental Risk Assessment Procedures Sufficient For The Protection Of The Aquatic Environment? *Environmental Toxicology and Chemistry*, *23*(5), 1344. doi: 10.1897/03-246

Finstick, S. A. (1996). Subsurface geology and hydrogeology of downtown Honolulu with engineering and environmental implications. Water Resources Research Center, University of Hawaii at Manoa-

Freeze, R. A., & Cherry, J. A. (1982). *Groundwater*. Englewood Cliffs, NJ: Prentice-Hall.

Garcia-Solsona, E., Masqué, P., Garcia-Orellana, J., Rapaglia, J., Beck, A., Cochran, J., … Collavini, F. (2008). Estimating submarine groundwater discharge around Isola La Cura, northern Venice Lagoon (Italy), by using the radium quartet. *Marine Chemistry*, *109*(3-4), 292–306. doi: 10.1016/j.marchem.2008.02.007

Giambelluca, T.W., Chen, Q., Frazier, A.G., Price, J.P., Chen, Y.L., et al. (2013). Online rainfall atlas of Hawai‘i. *Bulletin of the American Meteorological Society, 94*, 313-316. doi: 10.1175/BAMS-D-11-00228.1.

Gingerich, S.B., Oki, D.S., (2000). Ground water in Hawai‘i Fact Sheet 126-00. US Geological Survey.
Gonneea, M. E., Morris, P. J., Dulaiova, H., & Charette, M. A. (2008). New perspectives on radium behavior within a subterranean estuary. *Marine Chemistry*, *109*(3-4), 250–267. doi: 10.1016/j.marchem.2007.12.002

Gonneea, M.E., Mulligan, A.E., Charette, M.A. (2013). Climate-driven sea level anomalies modulate coastal groundwater dynamics and discharge. *Geophysical Research Letters, 40*(1): 2701–2706.

Gonzalez, F.I., (1971). Descriptive study of the physical oceanography of the Ala Wai Canal. Master’s Thesis, Univ. of Hawai‘i at Mānoa.

Habel, S. L., Fletcher, C. H., Rotzoll, K., & El-Kadi, A. (2017). Development of a model to simulate groundwater inundation induced by sea-level rise and high tides in Honolulu, Hawaii. *Water Research, 114*, 122-134. doi: 10.1016/j.watres.2017.02.0350043-1354

Habel, S., Fletcher, C. H., Anderson, T. R., & Thompson, P. R. (2020). Sea-Level Rise Induced Multi-Mechanism Flooding and Contribution to Urban Infrastructure Failure. *Scientific Reports, 10*(1). doi: 10.1038/s41598-020-60762-4

Han, G. H., Hur, H. G., & Kim, S. D. (2006). Ecotoxicological Risk Of Pharmaceuticals From Wastewater Treatment Plants In Korea: Occurrence And Toxicity To Daphnia Magna. *Environmental Toxicology and Chemistry, 25*(1), 265. doi: 10.1897/05-193r.1

Hawai’i Climate Change Mitigation and Adaptation Commission. (2017). Hawai’i Sea Level Rise Vulnerability and Adaptation Report. *Prepared by Tetra Tech, Inc. and the State of Hawai’i Department of Land and Natural Resources*, Office of Conservation and Coastal Lands, under the State of Hawai’i Department of Land and Natural Resources.

Hawaii Coastal Geology Group. DEM Imagery for Oahu. (2013). Available from: https://www.soest.hawaii.edu/coasts/data/oahu/dem.html.

Hernando, M., Mezcua, M., Fernandezalba, A., & Barcelo, D. (2006). Environmental risk assessment of pharmaceutical residues in wastewater effluents, surface waters and sediments. *Talanta, 69*(2), 334–342. doi: 10.1016/j.talanta.2005.09.037

Ho, D.T., De Carlo, E.H., Schlosser, P. (2018). Air-Sea Gas Exchange and CO2 Fluxes in a Tropical Coral Reef Lagoon. *Journal of Geophysical Research: Oceans*, *123*, 8701-8713.

Hoover, D.J. (2002). Fluvial nitrogen and phosphorus in Hawaii: storm runoff, land use, and impacts on coastal waters [dissertation]. Honolulu (HI): University of Hawai‘i at Mānoa.

Hoover, D.J., MacKenzie, F.T. (2009). Fluvial fluxes of water, suspended particulate matter, and nutrients and potential impacts on tropical coastal water Biogeochemistry: Oahu, Hawai’i. *Aquatic Geochemistry, 15*(4), 547–570.

Hunt Jr., C.D. (1996). Geohydrology of the Island of Oahu, Hawaii. U.S. Geological Survey Professional Paper 1412-B. p. B1-B54.

Izuka, S.K., Hill, B.R., Shade, P.J., Tribble, G.W. (1993). Geohydrology and possible transport routes of polychlorinated biphenyls in Haiku Valley, Oahu, Hawaii: U.S. Geological Survey Water-Resources Investigations Report. 92-4168, 48 p.

James, C. A., Miller-Schulze, J. P., Ultican, S., Gipe, A. D., & Baker, J. E. (2016). Evaluating Contaminants of Emerging Concern as tracers of wastewater from septic systems. *Water Research*, *101*, 241–251. doi: 10.1016/j.watres.2016.05.046

Jickells, T. D. (1998). Nutrient Biogeochemistry of the Coastal Zone. *Science*, *281*(5374), 217–222. doi: 10.1126/science.281.5374.217

Johnston, E. L., Mayer-Pinto, M., Hutchings, P. A., Marzinelli, E. M., Ahyong, S. T., Birch, G., … Hedge, L. H. (2015). Sydney Harbour: what we do and do not know about a highly diverse estuary. *Marine and Freshwater Research*, *66*(12), 1073. doi: 10.1071/mf15159

Jokiel PL. Illustrated Scientific Guide to Kāneʻohe Bay, Oahu. (1991). Hawaii Institute of Marine Biology: 1–65.

Kelly, J. L., Dulai, H., Glenn, C. R., & Lucey, P. G. (2018). Integration of aerial infrared thermography and in situ radon-222 to investigate submarine groundwater discharge to Pearl Harbor, Hawaii, USA. *Limnology and Oceanography*, *64*(1), 238–257. doi: 10.1002/lno.11033

Kim, G., & Hwang, D.-W. (2002). Tidal pumping of groundwater into the coastal ocean revealed from submarine 222Rn and CH4 monitoring. *Geophysical Research Letters*, *29*(14). doi: 10.1029/2002gl015093

Kim, G., Kim, J.S., Hwang, D.W. (2011). Submarine groundwater discharge from oceanic islands standing in oligotrophic oceans: Implications for global biological production and organic carbon fluxes. *Limnology and Oceanography, 56*(2), 673–682.

Kolpin, D. W., Furlong, E. T., Meyer, M. T., Thurman, E. M., Zaugg, S. D., Barber, L. B., & Buxton, H. T. (2002). Pharmaceuticals, Hormones, and Other Organic Wastewater Contaminants in U.S. Streams, 1999−2000: A National Reconnaissance. *Environmental Science & Technology*, *36*(6), 1202–1211. doi: 10.1021/es011055j

Knee, K. L., Gossett, R., Boehm, A. B., & Paytan, A. (2010). Caffeine and agricultural pesticide concentrations in surface water and groundwater on the north shore of Kauai (Hawaii, USA). *Marine Pollution Bulletin, 60*(8), 1376-1382. doi:10.1016/j.marpolbul.2010.04.019

Knee K., Street, J.H., Grossman, E.G., Paytan, A. (2010). Nutrient inputs to the coastal ocean from submarine groundwater discharge in a groundwater-dominated system: Relation to land use (Kona coast, Hawaii, U.S.A.). *Limnology and Oceanography, 55*(3), 1105–22. doi: 10.4319/lo.2010.55.3.1105a.

Knee, K., and Paytan, A. (2011). 4.08 submarine groundwater discharge: a source of nutrients, metals, and pollutants to the Coastal Ocean. Treat. Estuar. Coast. Sci. 4, 205–234. doi: 10.1016/B978-0-12-374711-2.00410-1

Kroeger, K.D., Swarzenski, P.W., Greenwood, W.J., Reich, C. (2007). Submarine groundwater discharge to Tampa Bay: Nutrient fluxes and biogeochemistry of the coastal aquifer. *Marine Chemistry, 104(*1–2), 85–97.

Kroeger, K. D., and Charette, M. A. (2008). Nitrogen biogeochemistry of submarine groundwater discharge. *Limnol. Oceanogr. 53*, 1025–1039. doi: 10.4319/lo.2008.53.3.1025

Kwon, E. Y., Kim, G., Primeau, F., Moore, W. S., Cho, H-M, DeVries, T., et al. (2014). Global estimate of submarine groundwater discharge based on na observationally constrained radium isotope model. *Geophys. Res. Lett. 42*, 8438–8444. doi: 10.1002/2014GL061574

Land Use Land Cover of Hawaii. Accessed from the Hawaii Statewide GIS Program (geodata.hawaii.gov)

Lange, A., Katsu, Y., Ichikawa, R., Paull, G. C., Chidgey, L. L., Coe, T. S., … Tyler, C. R. (2008). Altered Sexual Development in Roach (Rutilus rutilus) Exposed to Environmental Concentrations of the Pharmaceutical 17α-Ethinylestradiol and Associated Expression Dynamics of Aromatases and Estrogen Receptors. *Toxicological Sciences*, *106*(1), 113–123. doi: 10.1093/toxsci/kfn151

Lapworth, D., Baran, N., Stuart, M., & Ward, R. (2012). Emerging organic contaminants in groundwater: A review of sources, fate and occurrence. *Environmental Pollution, 163*, 287–303. doi: 10.1016/j.envpol.2011.12.034

Lau, L.S., Mink, J.F. (2006). Hydrology of the Hawaiian Islands. University of Hawaii Press. 274 p.

LaValle, F.F. (2018). The effects of submarine groundwater discharge on tropical reef benthic community composition, structure, and primary productivity [dissertation]. Honolulu (HI): University of Hawai‘i at Mānoa.

Laws, E.A., Redalje, D.G. (1979). Effect of sewage enrichment on the phytoplankton population of a subtropical estuary. *Pac Sci,. 33*(2), 129–44.

Leta, O.T., El-Kadi, A.I., Dulai, H., Ghazal, K.A. (2016). Assessment of climate change impacts on water balance components of Heeia watershed in Hawaii. *Journal of Hydrology: Regional Studies*, *8*, 182–197. doi: 10.1016/j.ejrh.2016.09.006

Lin, A. Y.-C., Yu, T.-H., & Lin, C.-F. (2008). Pharmaceutical contamination in residential, industrial, and agricultural waste streams: Risk to aqueous environments in Taiwan. *Chemosphere, 74*(1), 131–141. doi: 10.1016/j.chemosphere.2008.08.027

Lubarsky, K.A., Silbiger, N.J., Donahue, M.J. (2018). Effects of submarine groundwater discharge on coral accretion and bioerosion on two shallow reef flats. *Limnol Oceanogr, 63*(4), 1660-1676. doi: 10.1002/lno.10799.

Luijendijk, E., Gleeson, T., & Moosdorf, N. (2020). Fresh groundwater discharge insignificant for the world's oceans but important for coastal ecosystems. *Nature Communications*, *11*(1). doi: 10.1038/s41467-020-15064-8

MacDonald, G.A., Abbott, A.T., Peterson, F.L., (1983). Volcanoes in the sea: the geology of Hawai'i. University of Hawai'i Press.

Macintyre, S., Wannikhof, R., Chanton, J.P. (1995). Trace gas exchanges across the air-water interface in freshwater and coastal marine environments. In: Matson, P.A.; Harriss, R.C.; eds. Biogenic Trace Gases: Measuring Emissions from Soil and Water. Cambridge, MA: Blackwell; 52–97.

Manuel, J. (2014). Nutrient Pollution: A Persistent Threat to Waterways. *Environmental Health Perspectives*, *122*(11), 3139-3150. doi: 10.1289/ehp.122-A304

Martin, C.E.A., Galy, A., Hovius, N., Bickle, M., Lin, I.T., et al. (2013). The sources and fluxes of dissolved chemistry in a semi-confined, sandy coastal aquifer: the Pingtung Plain, Taiwan. *Applied Geochemistry*, 33, 222–36.

Martínez-Hernández, V., Meffe, R., Herrera, S., Arranz, E., & Bustamante, I. D. (2014). Sorption/desorption of non-hydrophobic and ionisable pharmaceutical and personal care products from reclaimed water onto/from a natural sediment. *Science of The Total Environment*, *472*, 273–281. doi: 10.1016/j.scitotenv.2013.11.036

Mathioudakis, M.R. (2018). Hydrology of contaminant flow regimes to groundwater, streams, and the ocean waters of Kāne'ohe Bay, O'ahu [thesis]. Honolulu (HI): University of Hawai'i at Mānoa.

Mayer-Pinto, M., Johnston, E. L., Hutchings, P. A., Marzinelli, E. M., Ahyong, S. T., Birch, G., … Hedge, L. H. (2015). Sydney Harbour: a review of anthropogenic impacts on the biodiversity and ecosystem function of one of the world. *Marine and Freshwater Research*, *66*(12), 1088. doi: 10.1071/mf15157

McCance, W., Jones, O., Edwards, M., Surapaneni, A., Chadalavada, S., & Currell, M. (2018). Contaminants of Emerging Concern as novel groundwater tracers for delineating wastewater impacts in urban and peri-urban areas. *Water Research*, *146*, 118–133. doi: 10.1016/j.watres.2018.09.013

McGowan, M.P. (2004). Submarine groundwater discharge: freshwater and nutrient input into Hawaii's coastal zone [thesis]. Honolulu (HI): University of Hawai'i at Mānoa.

McKenzie, T., Dulai, H., Chang, J. (2019). Parallels between stream and coastal water quality associated with groundwater discharge. *PLoS ONE, 14*(10), e0224513. doi: 10.1371/journal.pone.0224513

McKenzie, T., Holloway, C., Dulai, H., Tucker, J. P., Sugimoto, R., Nakajima, T., … Santos, I. R. (2020). Submarine groundwater discharge: A previously undocumented source of contaminants of emerging concern to the coastal ocean (Sydney, Australia). *Marine Pollution Bulletin, 160,* 111519. doi: 10.1016/j.marpolbul.2020.111519

Mehrle, P. M., Buckler, D. R., Little, E. E., Smith, L. M., Petty, J. D., Peterman, P. H., … Adams, W. J. (1988). Toxicity and bioconcentration of 2,3,7,8-tetrachlorodibenzodioxin and 2,3,7,8-tetrachlorodibenzofuran in rainbow trout. *Environmental Toxicology and Chemistry*, *7*(1), 47–62. doi: 10.1002/etc.5620070108

Mendoza, A., Aceña, J., Pérez, S., Alda, M. L. D., Barceló, D., Gil, A., & Valcárcel, Y. (2015). Pharmaceuticals and iodinated contrast media in a hospital wastewater: A case study to analyse their presence and characterise their environmental risk and hazard. *Environmental Research, 140,* 225–241. doi: 10.1016/j.envres.2015.04.003

Michael, H. A., Mulligan, A. E., & Harvey, C. F. (2005). Seasonal oscillations in water exchange between aquifers and the coastal ocean. *Nature*, *436*(7054), 1145–1148. doi: 10.1038/nature03935

Middleton, J. H., Cox, D., & Tate, P. (1996). The oceanography of the Sydney region. *Marine Pollution Bulletin*, *33*(7-12), 124–131. doi: 10.1016/s0025-326x(96)00170-1

Milliman, J. D. (2001). River inputs, in *Encyclopedia of Ocean Sciences*, edited by J. H. Steele, S. A. Thorpe, and K. K. Turekian, pp. 2419– 2427, Academic Press, doi: 10.1006/rwos.2001.0074

Montoya, D., (2015). Pollution in Sydney Harbour: sewage, toxic chemicals and microplastics. Briefing Paper No 03/2015.

Moore, W. S. (1996). Large groundwater inputs to coastal waters revealed by 226Ra enrichments. *Nature*, *380*(6575), 612–614. doi: 10.1038/380612a0

Moore, W. S., & Arnold, R. (1996). Measurement of223Ra and224Ra in coastal waters using a delayed coincidence counter. *Journal of Geophysical Research: Oceans*, *101*(C1), 1321–1329. doi: 10.1029/95jc03139

Moore, W. S. (1999). The subterranean estuary: a reaction zone of ground water and sea water. *Marine Chemistry*, *65*(1-2), 111–125. doi: 10.1016/s0304-4203(99)00014-6

Moore, W. S. (2000). Ages of continental shelf waters determined from 223Ra and 224Ra. *Journal of Geophysical Research: Oceans*, *105*(C9), 22117–22122. doi: 10.1029/1999jc000289

Moore, W. S. (2003). Sources and fluxes of submarine groundwater discharge delineated by radium isotopes. *Biogeochemistry*, *66*(1/2), 75–93. doi: 10.1023/b:biog.0000006065.77764.a0

Moore, W. S., Blanton, J. O., & Joye, S. B. (2006). Estimates of flushing times, submarine groundwater discharge, and nutrient fluxes to Okatee Estuary, South Carolina. *Journal of Geophysical Research*, *111*(C9). doi: 10.1029/2005jc003041

Moore, W. S. (2010). The Effect of Submarine Groundwater Discharge on the Ocean. *Annual Review of Marine Science*, *2*(1), 59–88. https://doi.org/10.1146/annurev-marine-120308-081019

Moosdorf, N., Stieglitz, T., Waska, H., Dürr, H.H., Hartmann, J. (2015). Submarine groundwater discharge from tropical islands: a review. *Grundwasser*, *20*(1), 53–67. doi: 10.1007/s00767-014-0275-3.

National Health and Medical Research Council (NHMRC), (2008). Guidelines for Managing Risks in Recreational Waters, Canberra. Office of Environment and Heritage, New South Wales. Beachwatch Programs. Protocol for assessment and management of microbial risks in recreational waters.

NRC [National Research Council Committee on Wastewater Management for Coastal Urban Areas, Water Science and Technology Board]. (1993). Managing wastewater in coasta lurban areas. National Research Council, Washington, D.C., USA.

National Weather Service (NWS) Climate Prediction Center (CPC). Cold & Warm Episodes by Season. (2018). Available from: https://origin.cpc.ncep.noaa.gov/products/analysis_monitoring/ensostuff/ONI_v5.php.

National Weather Service (NWS) Hydronet Data. (2018). Available from: https://www.weather.gov/hfo/hydronet-data.

Nelson, S.T., Tingey, D.G., Selck, B. (2013). The denudation of ocean islands by ground and surface waters: The effects of climate, soil thickness, and water contact times on Oahu, Hawaii. *Geochimica et Cosmochimica Acta*, 103, 276–94.

New South Wales (NSW) Legistlation. (2015). Local Environmental Plan. https://legislation.nsw.gov.au/#/view/EPI/2015/20/full

New South Wales (NSW) Department of Plannning, Industry, and Environment. (2018). Botany Bay. https://www.environment.nsw.gov.au/Topics/Water/Estuaries/Estuaries-of-NSW/Botany-Bay

New South Wales (NSW) Environmental Protection Agency (EPA) Botany Bay area. https://www.epa.nsw.gov.au/your-environment/contaminated-land/pfas-investigation-program/pfas-investigation-sites/botany-bay-area

NSW Office of Environment and Heritage (2018). Botany Bay. https://www.environment.nsw.gov.au/topics/water/estuaries/estuaries-of-nsw/botany-bay

Nödler, K., Voutsa, D., & Licha, T. (2014). Polar organic micropollutants in the coastal environment of different marine systems. *Marine Pollution Bulletin*, *85*(1), 50–59. doi: 10.1016/j.marpolbul.2014.06.024

Patel, M., Kumar, R., Kishor, K., Mlsna, T., Pittman, C. U., & Mohan, D. (2019). Pharmaceuticals of Emerging Concern in Aquatic Systems: Chemistry, Occurrence, Effects, and Removal Methods. *Chemical Reviews*, *119*(6), 3510–3673. doi: 10.1021/acs.chemrev.8b00299

Petermann, E., Schubert, M. (2015). Quantification of the response delay of mobile radon-in-air detectors applied for detecting short-term fluctuations of radon-in-water concentrations. *Eur Phys J Spec Top*, 707, 697–707. doi: 10.1140/epjst/e2015-02400-5.

Peterson, R. N., Burnett, W. C., Taniguchi, M., Chen, J., Santos, I. R., & Ishitobi, T. (2008). Radon and radium isotope assessment of submarine groundwater discharge in the Yellow River delta, China. *Journal of Geophysical Research*, *113*(C9). doi: 10.1029/2008jc004776

Pires, A., Almeida, Â., Correia, J., Calisto, V., Schneider, R.J., Esteves, V.I., Soares, A.M.V.M., Figueira, E., Freitas, R. (2016). Long-term exposure to caffeine and carbamazepine: Impacts on the regenerative capacity of the polychaete Diopatra neapolitana. *Chemosphere, 146*, 565-573. doi: 10.1016/j.chemosphere.2015.12.035

Porder, S., Ramachandran, S. (2012). The phosphorus concentration of common rocks—a potential driver of ecosystem P status. *Plant and Soil*. *367*(1-2), 41–55.

Pubchem Database – National Library of Medicine. https://pubchem.ncbi.nlm.nih.gov/

Rapaglia, J., Beck, A., Stieglitz, T., Bokuniewicz, H., Kontar, E. (2006). Submarine groundwater discharge patterns through volcanic fractured rock. Submarine Groundwater Discharge Assessment Intercomparison Experiment, Mauritius; Report to UNESCO.

Rapaglia, J., Ferrarin, C., Zaggia, L., Moore, W. S., Umgiesser, G., Garcia-Solsona, E., … Masqué, P. (2010). Investigation of residence time and groundwater flux in Venice Lagoon: comparing radium isotope and hydrodynamical models. *Journal of Environmental Radioactivity*, *101*(7), 571–581. doi.org/10.1016/j.jenvrad.2009.08.010

Redfield, A.C., Ketchum, B.H., Richards, F.A. (1963). The influence of organisms on the composition of seawater. In M. N. Hill, editor. The sea, v2. Interscience. p 26-77.

Richardson, C. M., Dulai, H., Popp, B. N., Ruttenberg, K., & Fackrell, J. K. (2017). Submarine groundwater discharge drives biogeochemistry in two Hawaiian reefs. *Limnology and Oceanography*, *62*(S1). doi: 10.1002/lno.10654

Rodellas, V., Garcia-Orellana, J., Trezzi, G., Masqué, P., Stieglitz, T. C., Bokuniewicz, H., … Berdalet, E. (2017). Using the radium quartet to quantify submarine groundwater discharge and porewater exchange. *Geochimica Et Cosmochimica Acta*, *196*, 58–73. doi: 10.1016/j.gca.2016.09.016

Rodríguez-Eugenio, N., McLaughlin, M. J., & Pennock, D. (2018). *Soil pollution: a hidden reality*. Rome: Food and Agriculture Organization of the United Nations.

Rosenberry, D.O., Labaugh, J.W. (2008). Field techniques for estimating water fluxes between surface water and ground water. Techniques and Methods.

Rotzoll, K., & Fletcher, C. H. (2012). Assessment of groundwater inundation as a consequence of sea-level rise. *Nature Climate Change*, *3*(5), 477–481. doi: 10.1038/nclimate1725

Roy, P.S. (1981). Geology of the Sydney Basin. Geological Survey of New South Wales Quarterly Notes, 41–91.

Ringuet, S., MacKenzie, F.T. (2005). Controls on Nutrient and Phytoplankton Dynamics during Normal Flow and Storm Runoff Conditions, Southern Kaneohe Bay, Hawaii. *Estuaries*, *28*(3), 327–37.

Sadat-Noori, M., Tait, D. R., Maher, D. T., Holloway, C., & Santos, I. R. (2018). Greenhouse gases and submarine groundwater discharge in a Sydney Harbour embayment (Australia). *Estuarine, Coastal and Shelf Science*, *207*, 499–509. doi: 10.1016/j.ecss.2017.05.020

Santos, I. R., Burnett, W. C., Dittmar, T., Suryaputra, I. G., & Chanton, J. (2009). Tidal pumping drives nutrient and dissolved organic matter dynamics in a Gulf of Mexico subterranean estuary. *Geochimica Et Cosmochimica Acta*, *73*(5), 1325–1339. doi: 10.1016/j.gca.2008.11.029

Safeeq, M., Mair, A., Fares, A. (2013). Temporal and spatial trends in air temperature on the Island of Oahu, *Hawaii. Int J Climatol*. *33*(13), 2816–2835.

Seitzinger, S.P., Harrison, J.A., Dumont, E., Beusen, A.H.W., Bouwman, A.F. (2005). Sources and delivery of carbon, nitrogen, and phosphorus to the coastal zone: An overview of Global Nutrient Export from Watersheds (NEWS) models and their application. *Global Biogeochem Cycles*, *19*(4).

Shade, P.J., Nichols, W.D. (1996). Water Budget and the Effects of Land-Use Changes on Ground-Water Recharge, Oahu, Hawaii, Issue 1412, Part 3. U.S. Geological Survey Professional Paper 1412-C. 38 p.

Sherrod, D.R., Sinton, J.M., Watkins, S.E., Brunt, K.M. (2007). Geologic Map of the State of Hawai‘i, Sheet 3 – Island of O‘ahu.

Siegener, R., & Chen, R. (2002). Caffeine in Boston Harbor seawater. *Marine Pollution Bulletin*, *44*(5), 383–387. doi: 10.1016/s0025-326x(00)00176-4

Singer, A. C., Xu, Q., & Keller, V. D. (2019). Translating antibiotic prescribing into antimicrobial resistance in the environment: a hazard characterisation case study. *PLoS One*, 14(9): e0221568. doi: 10.1101/539536

Slangen, A.B.A., Carson, M., Katsman, C.A., Van De Wal, R. S. W., Köhl, A., Vermeersen, L.L.A., et al. (2014). Projecting twenty-first century regional sea-level changes. *Climatic Change*, *124*(1-2), 317–332.

Slomp, C.P., Van Cappellen, P. (2004). Nutrient inputs to the coastal ocean through submarine groundwater discharge: Controls and potential impact. *J Hydrol. 295*(1–4), 64–86.

Smith, S.V., Kimmerer, W.J., Laws, E.A., Brock, R.E., Walsh, T.W. (1981). Kaneohe Bay sewage diversion experiment: perspectives on ecosystem responses to nutritional perturbation. *Pacific Sci. 35*(4), 279–395.

Spirandelli, D., Babcock, R., Shen, S. (2018). Assessing the Vulnerability of Coastal Wastewater Infrastructure to Climate Change. University of Hawai‘i Sea Grant Publication.

State of Hawaii. Hawaii Administrative Rules Title 11, Chapter 54. (2014). Available from: https://health.hawaii.gov/cwb/files/2013/04/Clean_Water_Branch_HAR_11-54_20141115.pdf.

State of Hawaii Office of Planning and Permitting. Hawaii Statewide GIS Program: Download GIS Data. (2018). Available from: http://planning.hawaii.gov/gis/download-gis-data.

Stearns, H.T., (1935). Pleistocene shore lines on the islands of O‘ahu and Maui, Hawai‘i. *Geol. Soc. Am. Bull. 46*, 1927–1956.

Stearns, H.T., Vaksvik, K. (1935) Geology and ground-water resources of the island of Oahu, Hawaii.

Street, J.H., Knee, K.L., Grossman, E.E., Paytan, A. (2008). Submarine groundwater discharge and nutrient addition to the coastal zone and coral reefs of leeward Hawaii. *Marine Chemistry*, *109*(3-4), 355–76. doi: 10.1016/j.marchem.2007.08.009.

Suh, J.-Y., Brown, P. L., & Birch, G. F. (2003). Hydrogeochemical characteristics and importance of natural and anthropogenic influences on soil and groundwater in reclaimed land adjacent to Port Jackson, Sydney, Australia. *Marine and Freshwater Research*, *54*(6), 767. doi: 10.1071/mf02075

Suh, J.-Y., Birch, G. F., Hughes, K., & Matthai, C. (2004). Spatial distribution and source of heavy metals in reclaimed lands of Homebush Bay: the venue of the 2000 Olympic Games, Sydney, New South Wales. *Australian Journal of Earth Sciences*, *51*(1), 53–67. doi: 10.1046/j.1400-0952.2003.01043.x

Swarzenski, P.W., Reich, C.D., Spechler, R.M., Kindinger, J.L., Moore, W.S. (2001). Using multiple geochemical tracers to characterize the hydrogeology of the submarine spring off Crescent Beach, Florida. *Chem Geol, 179*, 187–202.

Swarzenski, P.W. & Kindinger, J.L. (2003). Leaky coastal margins: examples of enhanced coastal groundwater/ surface water exchange from Tampa Bay and Crescent Beach submarine spring, Florida, USA. CH5 in *Coastal Aquifer Management, Monitoring and Modeling Case Studies*, pp 93-112.

Sweet, W. V., J. Park, J. J. Marra, C. Zervas, and S. Gill (2014). Sea level rise and nuisance flood frequency changes around the United States, NOAA Tech. Rep. NOS CO-OPS 73, 53 pp.

Sweet, W.V., Dusek, G., Carbin, G., Marra, J., Marcy, D., Simon, S. (2020). 2019 State of U.S. High Tide Flooding with a 2020 Outlook, NOAA Tech. Rep. NOS CO-OPS 092, 17 pp.

Sydney Water. (2010). Sewage Treatment System Impact Monitoring Program.

Szymczycha, B., Borecka, M., Białk-Bielińska, A., Siedlewicz, G., & Pazdro, K. (2020). Submarine groundwater discharge as a source of pharmaceutical and caffeine residues in coastal ecosystem: Bay of Puck, southern Baltic Sea case study. *Science of The Total Environment*, 136522. doi: 10.1016/j.scitotenv.2020.136522

Takasaki, K.J., Hirashima, G.T., Lubke, E.R. (1969). Water resources of windward Oahu, Hawaii. U.S. Geological Survey Water Supply Pap 1894. 119 p.; 3 pls. in pocket.

Takasaki, K.J., Mink, J.F. (1985). Evaluation of major dike-impounded ground-water reservoirs, Island of Oahu. United States Geological Survey Water Supply Pap 2217. 77 p.

Tamborski, J., Cochran, J., Bokuniewicz, H., Heilbrun, C., Garcia-Orella, J., Rodellas, V., Wilson, R. (2020). Radium mass balance sensitivity analysis for submarine groundwater discharge estimation in semi-enclosed basins: The case study of Long Island Sound. *Frontiers in Environmental Science* (in press). doi: 10.3389/fenvs.2020.00108

Taniguchi, M., Burnett, W.C., Cable, J.E., Turner, J.V. (2002). Investigation of submarine groundwater discharge. *Hydrol Process, 16*(11), 2115–2129.

Taniguchi, M., Burnett, W.C., Dulaiova, H., Siringan, F., Foronda, J., et al. (2008). Groundwater discharge as an important land-sea pathway into Manila Bay, Philippines. *J Coast Res, 24*, 15–24.

Taniguchi, M., Dulai, H., Burnett, K. M., Santos, I. R., Sugimoto, R., Stieglitz, T., … Burnett, W. C. (2019). Submarine Groundwater Discharge: Updates on Its Measurement Techniques, Geophysical Drivers, Magnitudes, and Effects. *Frontiers in Environmental Science*, *7*. doi: 10.3389/fenvs.2019.00141

Thompson, P. R., Widlansky, M. J., Merrifield, M. A., Becker, J. M., & Marra, J. J. (2019). A Statistical Model for Frequency of Coastal Flooding in Honolulu, Hawaii, During the 21st Century. *Journal of Geophysical Research: Oceans*, *124*(4), 2787–2802. doi: 10.1029/2018jc014741

Townscape, Inc. Ko‘olaupoku Watershed Management Plan. (2012). Available from: https://www.boardofwatersupply.com/bws/media/files/koolau-poko-wmp-final-2012.pdf.

Tran, N.H., Li, J., Hu, J., Ong, S.L., 2014. Occurrence and suitability of pharmaceuticals and personal care products as molecular markers for raw wastewater contamination in surface water and groundwater. Environ. Sci. Pollut. Res. 21, 4727–4740.

United Nations (2017). Factsheet: People and Oceans. Accessed from: https://www.un.org/sustainabledevelopment/wp-content/uploads/2017/05/Ocean-fact-sheet-package.pdf

United Nations. Atlas of the Oceans. Accessed from: http://www.oceansatlas.org/subtopic/en/c/114/

USEPA. 2002a. The Clean Water and Drinking Water Gap Analysis; United States Environmental Protection Agency: Washington, DC, USA.

USEPA. 2002b. Onsite Wastewater Treatment Systems Manual [Internet]. pp. 1–367. Available from: http://www.epa.gov/ORD/NRMRL/Pubs/625180012/625180012.htm.

U.S. Geological Survey. (2018) National Water Information System data available on the World Wide Web (USGS Water Data for the Nation). Available from: https://waterdata.usgs.gov/nwis/.

University of Hawai’i Sea Grant College Program. (2017) Hawai’i and Pacific Islands King Tides Project. Available from: http://seagrant.soest.hawaii.edu/coastal-and-climate-science-and-resilience/ccs-projects/hawaii-pacific-islands-king-tides-project/

University of Hawai’i at Mānoa College of Tropical Agriculture and Human Resources (CTAHR). (2014). Hawaii Soil Atlas. Available from: http://gis.ctahr.hawaii.edu/SoilAtlas.

Valiela, I., Costa, J., Foreman, K., Teal, J. M., Howes, B., & Aubrey, D. (1990). Transport of groundwater-borne nutrients from watersheds and their effects on coastal waters. *Biogeochemistry*, *10*(3), 177–197. doi: 10.1007/bf00003143

Verlicchi, P., Aukidy, M. A., & Zambello, E. (2012). Occurrence of pharmaceutical compounds in urban wastewater: Removal, mass load and environmental risk after a secondary treatment—A review. *Science of The Total Environment*, *429*, 123–155.

Vitousek, P.M., Aber, J.D., Howarth, R.W., Likens, G.E., Matson, P.A., Schindler, D.W., et al. (1997). Human alteration of the global nitrogen cycle: sources and consequences.

Vitousek, P.M., Ladefoged, T.N., Kirch, P.V., Hartshorn, A.S., Graves, M.W., et al. (2004). Soils, Agriculture, and Society in Precontact Hawai`i. *Science, 304*(5677), 1665-1669. doi: 10.1126/science.1099619.

Vystavna, Y., Huneau, F., Grynenko, V., Vergeles, Y., Celle-Jeanton, H., Tapie, N., … Coustumer, P. L. (2012). Pharmaceuticals in Rivers of Two Regions with Contrasted Socio-Economic Conditions: Occurrence, Accumulation, and Comparison for Ukraine and France. *Water, Air, & Soil Pollution*, *223*(5), 2111–2124. doi: 10.1007/s11270-011-1008-1

Walsh, C.J., Roy, A.H., Feminella, J.W., Cottingham, P.D., Groffman, P.M., Morgan, I.I., RP. (2005). The urban stream syndrome: current knowledge and the search for a cure. J. N. *Am. Benthol. Soc.*, *24*(3), 706-23. doi: 10.1899/0887-3593(2005)024\[0706:TUSSCK\]2.0.CO;2.

Walters, E., Mcclellan, K., & Halden, R. U. (2010). Occurrence and loss over three years of 72 pharmaceuticals and personal care products from biosolids–soil mixtures in outdoor mesocosms. *Water Research*, *44*(20), 6011–6020. doi: 10.1016/j.watres.2010.07.051

Webster, I.T., Hancock, G.J., Murray, A.S., (1995). Modelling the effect of salinity on radium desorption from sediments. Geochimica et Cosmochimica Acta 59, 2469–2476.
Welch, E. M., Dulai, H., El-Kadi, A., & Shuler, C. K. (2019). Submarine Groundwater Discharge and Stream Baseflow Sustain Pesticide and Nutrient Fluxes in Fagaalu Bay, American Samoa. *Frontiers in Environmental Science, 7*. doi: 10.3389/fenvs.2019.00162

Wentworth, C.K. (1951). The problem of safe yield in insular Ghyben-Herzberg systems. Eos.
White, D.S. (1993). Perspectives on defining and delineating hyporheic zones. *J North Am Benthol Soc*, 12, 61-69.

White, D., Lapworth, D. J., Civil, W., & Williams, P. (2019). Tracking changes in the occurrence and source of pharmaceuticals within the River Thames, UK; from source to sea. *Environmental Pollution*, *249*, 257–266. doi: 10.1016/j.envpol.2019.03.015

Whittier, R.B., El-Kadi, A.I. (2009). Human and Environmental Risk Ranking of Onsite Sewage Disposal Systems: Final Report. Honolulu, Hawai‘i: State of Hawai’i Department of Health, Safe Drinking Water Branch; 142 p.

Wiegel, R.I. (2008). Waikiki Beach, Oahu, Hawaii: History of its transformation from a natural to an urban shore. *Shore & Beach, 76*(2), 3-30.

Winter, T.C., Harvey, J.W., Franke, O.L., Alley, W.M. (1998). Ground water and surface water; a single resource. U.S. Geological Survey Circular 1139. 79. Available from: http://pubs.usgs.gov/circ/circ1139/pdf/circ1139.pdf.

Wong, P.P., I.J. Losada, J.-P. Gattuso, J. Hinkel, A. Khattabi, K.L. McInnes, Y. Saito, and A. Sallenger, (2014). Coastal systems and low-lying areas. In: Climate Change 2014: Impacts, Adaptation, and Vulnerability. Part A: Global and Sectoral Aspects. Contribution of Working Group II to the Fifth Assessment Report of the Intergovernmental Panel on Climate Change

[Field, C.B., V.R. Barros, D.J. Dokken, K.J. Mach, M.D. Mastrandrea, T.E. Bilir, M. Chatterjee, K.L. Ebi, Y.O. Estrada, R.C. Genova, B. Girma, E.S. Kissel, A.N. Levy, S. MacCracken, P.R. Mastrandrea, and L.L.White (eds.)]. Cambridge University Press, Cambridge, United Kingdom and New York, NY, USA, pp. 361-409.

WWAP (United Nations World Water Assessment Programme). (2017). The United Nations World Water Development Report 2017. Wastewater: The Untapped Resource. Paris, UNESCO.

Xing, Y., Chen, X., Zhuang, J., & Chen, X. (2015). What happens when pharmaceuticals meet colloids. *Ecotoxicology*, *24*(10), 2100–2114. https://doi.org/10.1007/s10646-015-1557-y

Yang, J.-F., Ying, G.-G., Zhao, J.-L., Tao, R., Su, H.-C., & Liu, Y.-S. (2011). Spatial and seasonal distribution of selected antibiotics in surface waters of the Pearl Rivers, China. *Journal of Environmental Science and Health, Part B*, *46*(3), 272–280. doi: 10.1080/03601234.2011.540540

Yoon, Y., Ryu, J., Oh, J., Choi, B.-G., & Snyder, S. A. (2010). Occurrence of endocrine disrupting compounds, pharmaceuticals, and personal care products in the Han River (Seoul, South Korea). *Science of The Total Environment*, *408*(3), 636–643. doi: 10.1016/j.scitotenv.2009.10.049

Zekster, I.S. (2000). Groundwater and the environment: applications for the global community. Boca Raton: Lewis Publishers.

Zhang, Y. & Li, W. (2019) Blending antibiotic resistance into environmental risk assessment of antibiotics: A case study in coastal waters of the Bohai Bay, China, *Human and Ecological Risk Assessment: An International Journal*, *25*(6), 1406-1421. doi: 10.1080/10807039.2018.1464381